Synthesis and characterization of a novel sulphur-reduced graphene oxide/metal oxides composite for supercapacitor applications

by

Delvina Japhet Tarimo

A thesis submitted in partial fulfillment of the requirements for the degree of

DOCTOR OF PHILOSOPHY (Ph.D.) IN PHYSICS

Faculty of Natural and Agricultural Sciences

University of Pretoria

Hatfield Pretoria

August 2020

Supervisor/promoter: **Prof. Ncholu. I. Manyala**

DECLARATION

I, **Delvina Japhet Tarimo** declare that this thesis, entitled *"**Synthesis and characterization of a novel sulphur-reduced graphene oxide/metal oxides composite for supercapacitor applications**"* which I hereby submit for the degree **Doctor of Philosophy (Ph.D.)** in the Department of Physics, University of Pretoria, South Africa has not previously been submitted by me for a degree at any other tertiary institution.

Signature …….. Date …….

DEDICATION

To the Glory of Almighty God, thank you for giving me strength to stand above all and achieve this.

To my late, mother and brother.

To my family members for their unending love.

ACKNOWLEDGEMENTS

My foremost goes to my Creator, the Almighty God through his son Jesus Christ, who gave me the spiritual, mental strength, good health, knowledge, ability and opportunity to undertake and accomplish this research work successfully. I may not be able to mention all individuals and organizations that have their support to the accomplishment of this work, but their contribution remains worth in my life.

I would like to express my special gratitude to my supervisor/promoter Prof. Ncholu Manyala for giving me the opportunity through SARChI chair in Carbon Technology and Materials to join his group and undertake this research work. I acknowledge his cooperation, motivation, material support, valued guidance and supervision, insightful comments and direction throughout the period of my Ph.D. studies. I am grateful for his hard comments and questions which build and encourage me to broaden my research knowledge from different outlooks.

I would also like to express my thanks to Prof. C. Theron, head of Physics Department, University of Pretoria for his great support towards the achievement of this program. My deepest appreciation goes to South African Research Chairs Initiative of the Department of Science and Technology (DST) and National Research Foundation (NRF) of South Africa (Grant No. 61056) for financial support.

I wish to express my warmest thanks to Mrs Suzette Seymore at the Institute of Applied Materials, South Campus for her everlasting help in procurement and laboratory work. I acknowledge Ms Charity Maepa, Mrs Erna van Wilpe, Mr Coenraad Snyman and Ms Irine Jiyane in the microscopy unity for their technical assistance during SEM, TEM and EDX measurements; Prof. Melanie Rademeyer and Dr. Frikkie Malan for technical assistance during XRD measurements as well as Mr. Adetola Henry Adewole and Kapambwe P. Kabwe from Chemistry Department for assistance in FTIR measurements.

My special thanks go to Dr. Kabir Oyeduton and Dr. Abdulmajid Mirghin of the Carbon and Advanced Nanomaterials group for their support, advice, encouragement and self-sacrificing during the course of study. Correspondingly, Dr. Bridget Mutuma and Dr. Maty Ndeye Ndiaye are very much appreciated for their advice, encouragement and support. Also, I would like to extend my thanks to the rest of my colleagues in the Carbon and Advanced Nanomaterials group, Ms. P Murovhi, Miss Fatou Ndeye Sylla, Mr. Samba Sarr, Mr. Vianney Kitenge, Mr. Badr Mohammed, Dr. O. Fasakini, Mr. Tjatji Tjebane, Mr. Vusane Maphwiri, Mr. Gift Rutavi, Ms. Abigail Phori, Miss Nkyasi Rantho, Mrs Melba Rambau and Mrs. Daba Bakhoum for their reliable assistance when required and a pleasant working environment. I love you all.

Special thanks go to Dr. Margaret E. Samiji, Dr. Nuru R. Mlyuka, Mr. Justine Nyarige, Prof. Justus Simiyu and Mr. Pannan Kyesmen for their assistance of all kinds before, during and towards the success of this program. I am also grateful to the friends and colleagues I made here at the Department of Physics, Chemistry and Biology, University of Pretoria, students and staff who together we made a friendly environment throughout my stay during the course of study.

A special and unending gratitude to my son, brother, twin and forever friend, Derick D. Mtui, my father, Japhet K. Tarimo, my aunt Maria K. Tarimo, my cousins Jaqueline and Mary Tarimo, my uncle Godson Tarimo, my grand-mother Ndefisiyo Sumary, my brother Bryson Tarimo and all other family members for their endless prayers and support towards the completion of this study. Finally, I would like to acknowledge my friends Mr. Kelvin Ndai, Mr. Erick Gwakisa, Mr. Reuben Maghembe and Miss. Dorice Seif for their encouragement throughout the accomplishment of this research work.

I thank you all who cheered me on to complete this study. May God bless you!

TABLE OF CONTENTS

DECLARATION I

DEDICATION II

ACKNOWLEDGEMENTS III

TABLE OF CONTENTS V

LIST OF FIGURES IX

LIST OF EQUATIONS XI

ABSTRACT XIII

CHAPTER 1 1

1.0 INTRODUCTION 1

1.1 Background and motivation of the study 1

1.2 Objective of the Study 5

1.3 Arrangement of the thesis 6

REFERENCES 8

CHAPTER 2 36

2.0 LITERATURE REVIEW 36

2.1 Theory of Electrochemical Energy Storage (EES) 36

2.2 Supercapacitors 38

2.2.1 Electric double-layer capacitors (EDLCs) 38

2.2.2 Pseudocapacitors 41

2.2.3 Hybrid supercapacitors 42

2.4 Electrode materials for supercapacitors 43

2.4.1 Carbon electrode materials 43

2.4.2 Transition metals oxides/hydroxides (TMOs/TMOHs) 46

2.4.3 Conducting polymers (CPs) 48
2.4.4 Composites 48
2.5 Electrolytes *49*
2.5.1 Aqueous electrolytes (AEs) 50
2.5.2 Ionic liquid electrolytes (ILEs) 51
2.5.3 Organic electrolytes (OEs) 51
2.6 Electrode fabrication and testing *52*
2.6.1 Three-electrode measurements 52
2.6.2 Two-electrode measurements 53
2.7 Electrochemical evaluation *56*
2.7.1 Cyclic voltammetry (CV) 57
2.7.2 Galvanostatic charge/discharge (GCD) 58
2.7.3 Electrochemical impedance spectroscopy (EIS) 60
2.7.4 Stability test (charge/discharge cycling, voltage holding, and self-discharge) ... 64
REFERENCES 66
CHAPTER 3 94
3.0 EXPERIMENTAL DETAILS AND CHARACTERIZATION TECHNIQUES 94
3.1 Preparation of the materials *94*
3.1.1 Production of graphene oxide by Hummer's method 94
3.1.2 Freeze-drying technique 95
3.1.3 Preparation of graphene oxide (GO) and reduced graphene oxide (RGO) samples 96
3.1.4 Synthesis of sulphur-reduced graphene oxide (RGO-S) composite 98
3.1.5 Hydrothermal process 99
3.1.6 Synthesis of manganese dioxide (MnO_2) 100

3.1.7 Synthesis RGO-S/MnO_2 composite sample....101
3.1.8 Precipitation method....102
3.1.9 Synthesis of cobalt oxide (Co_3O_4) sample....103
3.1.10 Synthesis of RGO-S/Co_3O_4 composite sample....104
3.1.11 Synthesis of polyaniline (PANI)....105
3.1.12 Synthesis of Carbonized Iron Cations Adsorbed onto PANI (C-FP) Material..
....105
3.1.13 Synthesis of activated carbon from peanut shell waste (AC-PS) 106
3.2 Characterization of the materials....106
3.2.1 X-ray Photoelectron Spectroscopy (XPS) 106
3.2.2 X-ray diffraction (XRD) 108
3.2.3 Raman spectroscopy 110
3.2.4 Fourier transform infrared (FTIR) spectroscopy 112
3.2.5 Scanning electron microscope (SEM) 113
3.2.6 Transmission electron microscopy (TEM) 116
3.3 Electrochemical characterization....119
REFERENCES....121
CHAPTER 4....149
4.0 RESULTS AND DISCUSSION....149
4.1 Introduction....149
4.2: Sulphur-reduced graphene oxide composite with improved electrochemical performance for supercapacitor applications 150
4.2.1: Summary of the study....150
4.2.2: Concluding remarks....164

4.3: High energy and excellent stability asymmetric supercapacitor derived from sulphur-reduced graphene oxide/manganese dioxide composite and activated carbon from peanut shell.....*165*

4.3.1: Summary of the study.....165

4.3.2: Concluding remarks.....178

4.4: Enhanced electrochemical performance of supercapattery derived from sulphur-reduced graphene oxide/cobalt oxide composite and activated carbon from peanut shells.....*179*

4.4.1: Summary of the study.....179

4.4.2: Concluding remarks.....198

REFERENCES.....199

CHAPTER 5.....226

5.0 GENERAL CONCLUSION AND FUTURE WORK.....226

5.1 General conclusion.....*226*

5.2 Future work.....*231*

LIST OF FIGURES

Figure 2.1: Charge separation of EDLC supercapacitor 39

Figure 2.2: Double-layer model showing the (a) Helmholtz model, (b) Gouy-Chapman model and (c) Stern layer..... 41

Figure 2.3: Ragone plot for different energy storage system..... 43

Figure 2.4: Structure of graphene (a) single layer graphene and (b) graphene doped with sulfur..... 45

Figure 2.5: Schematic illustration of a three-electrode set-up with a working electrode (WE), counter electrode (CE) and reference electrode (RE) 53

Figure 2.6: Schematic design of a two-electrode set-up 56

Figure 2.7: Schematic sketch of CV curves for (a) EDLC, (b) Pseudo-capacitor and (c) Faradic material..... 58

Figure 2.8: Schematic sketch of GCD curves for (a) EDLC, (b) Pseudo-capacitor and (c) Faradic material..... 60

Figure 2.8: Schematic illustration of imaginary impedance (Z'') versus real impedance (Z')..... 61

Figure 2.9: Schematic drawing of an equivalent circuit model for EIS analysis..... 63

Figure 3.1: Representation design of a freeze-drying process 96

Figure 3.2: Synthesis procedure of RGO sample..... 98

Figure 3.3: Schematic diagram of the synthesis of RGO-S. 99

Figure 3.4: Schematic design of a Teflon-lined stainless-steel autoclave. 100

Figure 3.5: Synthesis route of MnO_2 sample..... 101

Figure 3.6: Schematic figure of the synthesis of RGO-S/MnO_2 composite sample. 101

Figure 3.7: The APCVD system used for annealing in this thesis..... 103

Figure 3.8: Schematic of the synthesis process of Co_3O_4 sample..... 104

Figure 3.9: Synthesis procedure of RGO-S/Co_3O_4 composite.....105

Figure 3.10: Schematic design of the synthesis of carbonized iron cations adsorbed onto... 106

PANI (C-FP) sample……..106

Figure 3.11: Schematic representation of the working principle of XPS 108

Figure 3.12: Representation of the working principle of X-ray diffraction.....109

Figure 3.13: Raman spectrum of sulphur……...111

Figure 3.14: A WITec alpha 300 RAS+Confocal micro-Raman microscope (Ulm, Germany) employed for samples characterization in this thesis.....112

Figure 3.15: A schematic design of FTIR spectrometer 113

Figure 3.16: High-resolution field emission scanning electron microscope (SEM-Zeiss Ultra Plus 55)……...116

Figure 3.17: High-resolution transmission electron microscope (HRTEM FEI Tecnai-F30 JEOL 2100F)……..117

Figure 3.18: (a) The IUPAC classification of adsorption/desorption isotherms for gas-solid equilibria and (b) the adsorption/desorption hysteresis 119

Figure 3.19: A Biologic VMP300 potentiostat used in this thesis.....120

Figure 5.1: Capacity/capacitance retention of RGO-S//C-FP, RGO-S/100 mg MnO_2//AC-PS and RGO-S/200 mg Co_3O_4//AC-PS devices……..229

Figure 5.2: Ragone plot for RGO-S//C-FP, RGO-S/100 mg MnO_2//AC-PS and RGO-S/200 mg Co_3O_4//AC-PS devices……...230

LIST OF EQUATIONS

$\frac{1}{C_T} = \frac{1}{C_H} + \frac{1}{C_G}$ (1) ..... (17)

$Q_s = \frac{\Delta t \times I_d}{3.6}$ [mAh g^{-1}] (2)..... (31)

$C_s = \frac{\Delta t \times I_d}{\Delta V}$ [F g-1] (3) ……..(31)

$E_d = \frac{1}{2} C_s \Delta V^2 = \frac{C_s \times \Delta V^2}{7.2}$ [Wh kg^{-1}] (4) …… ..... (31)

$E_d = \frac{I}{3.6 * m} \int V dt$ [Wh kg^{-1}] (5)..... (31)

$P_d = \frac{E_d}{\Delta t} \times 3600$ [W kg^{-1}] (6)..... (32)

$Q = C_s \times m\, \Delta V$ (7)..... (32)

$\frac{m_+}{m_-} = \frac{C_{s-}\ \Delta V_-}{C_{s+}\ \Delta V_+}$ (8)..... (32)

$Q_+ = Q_- \Longrightarrow m_+ \times 3.6 Q_{s+} = m_- \times \Delta V_- \times C_{s-} \Longrightarrow \frac{m_-}{m_+} = \frac{3.6 \times Q_{s+}}{\Delta V_- \times C_{s-}}$ (9)..... (32)

$C_s = \frac{\int (I_D \times dV)}{\nu \times \Delta V}$ [F g^{-1}] (10)..... (35)

$C_{DL} = \frac{1}{R_{CT} 2\pi f_{max}}$ (11)..... (39)

$C = \frac{1}{2\pi f |Z''|}$ (12)..... (40)

$C_E = \frac{t_D}{t_c} \times 100\ \%$ (13)..... (41)

$\eta_E = \frac{E_d}{E_c}$ x 100 % (14)..... (41)

$$Co(NO_3)_{2(s)} + 2NaOH_{(l)} + H_2O_{(l)} \rightarrow Co(OH)_{2(s)} + 2NaNO_{3(aq)} + H_2O_{(l)} \quad (15) \ldots\ldots (68)$$

$$3Co(OH)_{2(s)} \xrightarrow{annealed\ in\ air} Co_3O_{4(s)} + 2H_2O_{(g)} + H_{2(g)} \quad (16) \ldots\ldots (68)$$

$$B.E = h\nu - E_{k.e} - W_f \quad (17) \ldots\ldots (104)$$

$$n\lambda = 2d\ sin\theta \quad (18) \ldots\ldots (72)$$

$$D = \frac{k\lambda}{\beta cos\theta} \quad (19) \ldots\ldots (106)$$

ABSTRACT

This study is focussed on synthesis and characterization of a novel sulphur-reduced graphene oxide/metal oxides composite for supercapacitor applications. Carbon-based materials have validated its capability in various applications, especially as electrode materials for energy storage devices hence become an attention-grabbing to the researchers, however, they suffer from low specific energy. Thus, further modification is still required for commercial level applications. Specifically, graphene-based composites materials have displayed immeasurable feasibility since they can be chemically combined with other carbon-based/metal oxides materials and with a range of different elements to form strong covalent bonds which improve their electrochemical properties. Hence, it is essential to study and produce different carbon-based/metal oxides composites materials by optimizing their morphology and surface functionalities so as to enhance their electrochemical performance. This study has established synthesis of sulphur-reduced graphene oxide composites materials which are discussed in different sections in chapter four. The composite materials were synthesized by Hummers, hydrothermal and precipitation methods. Some of the composite materials have gone through freeze drying and annealing process to complete their synthesis. Morphology, structure, elemental mapping/composition and specific surface area/pore size distribution were analysed by field emission scanning electron microscope (FESEM), transmission electron microscope (TEM), energy-dispersive X-ray spectroscopy (EDX), X-ray powder diffraction (XRD), Raman spectroscopy, X-ray photoelectron spectroscopy (XPS), Fourier transform infrared spectroscopy (FTIR) and Brunauer-Emmett-Teller (BET) techniques. The electrochemical performance was evaluated using cyclic voltammetry (CV), galvanostatic charge-discharge (GCD) and electrochemical impedance spectroscopy (EIS) in three and two electrode configurations.

The specific capacity of 113.8 mAh g^{-1} was obtained for RGO-S at 0.5 A g^{-1} which is much higher compared to RGO with a specific capacity of 12.5 mAh g^{-1} at the same specific current. The fabricated hybrid device (RGO-S//C-FP) presented a high specific energy and specific power of 35.2 Wh kg^{-1} and 375 W kg^{-1} at 0.5 A g^{-1} in an working voltage of 1.5 V, respectively. A good cycling stability performance with an energy efficiency of 99% was recorded for the hybrid device for up to 10,000 cycling at 3 A g^{-1}.

Also, an optimization was done by varying mass loading of MnO_2 (50, 100 and 150 mg) into the pristine sample (RGO-S) and the 100 mg MnO_2 was studied as the optimal amount to have good synergy between the RGO-S and MnO_2 due to the higher electrochemical performance demonstrated by RGO-S/100 mg MnO_2 composite. The RGO-S/100 mg MnO_2 composite presented a specific capacitance of 180. 4 F g^{-1} at 1 A g^{-1}. The assembled device (RGO-S/MnO_2//AC-PS) presented an outstanding specific energy of 71.7 Wh kg^{-1} with its corresponding specific power of 850 W kg^{-1} at 1 A g^{-1}. An outstanding performance was noted when the device was able to withstand a specific energy of 55.3 Wh kg^{-1} at a high specific current of 5 A g^{-1}. The capacitance retention of 94.5 % and columbic efficiency of 99.6 % up to 10,000 cycles at 5 A g^{-1} was recorded. A voltage holding of up to 90 h was attained with an efficiency of 70.5 %. An exceptional self-discharge of about 1.45 V was recorded within the first 10 h, and 1.00 V after 72 h out of the initial potential of 1.7 V.

Additionally, an optimized RGO-S/200 mg Co_3O_4 composite material showed the uppermost specific capacity of 171.8 mAh g^{-1} at 1 A g^{-1} and an excellent stability of 99.7 % for over 5000 cycles at 5 A g^{-1} in three-electrode configuration. The assembled supercapattery device (RGO-S/200 mg Co_3O_4//AC-PS) demonstrated high specific energy of 45.8 Wh kg^{-1} and specific power of 725 W kg^{-1} at 1 A g^{-1} in an operating potential of 1.45 V. The constructed device retained 83.4 % of its initial capacitance for over 10,000 cycles, with a columbic efficiency of 99.5 % at 8 A g^{-1}. The device maintained an efficiency of 71.6 % over an outstanding floating

time of 150 h at 10 A g^{-1}. The outcomes of this study has established an impressive capability of sulphur-reduced graphene oxides composites as a novel electrode materials for supercapacitor applications.

1.0 INTRODUCTION

In this chapter, a detailed information about the background, motivation and objectives of the study and arrangement of thesis will be discussed.

1.1 Background and motivation of the study

The increase in technology, change in climate and high consumption of fossil fuel which result into environmental pollution have countless influence on the ecology and world economy [1]. This has increased the attention to explore and expand renewable energy sources like wind, hydropower, solar and geothermal [2]. Nevertheless, the energy supplied by these sources is not always available during the demand since its production varies with occasion and atmospheric conditions. For example, solar energy can only be produced throughout the daytime and wind does not blow all the time thus, to have sufficient energy for our daily deeds, energy storage devices are required. However, the requirement remains on the amount of energy to be stored by these devices and how fast can be delivered [3].

For decade, batteries (traditional energy storage) with massive weight and larger volume have been employed as the electrochemical energy storage devices due to their capability to deliver high specific energy ~ 30 – 300 Wh kg^{-1}. However, toxicity, high maintenance cost, low specific power and short life span remain as weakness particularly, in the application demanding high instantaneous power like elevators, airplane emergency doors, and engine car start [4]. Additionally, the development of high-performance devices like electric vehicles, portable electronic devices and smart grid also remained as the main need for an alternative power resources than the traditional energy resources [5].

Thus, recently, supercapacitor has been considered as a supplement for traditional energy storage like battery hence, become a fundamental matter for many researchers all over the world. This is due to its unique properties like high cycle life, low maintenance cost, easy portability, light weight, and high specific power as compared to batteries [6]. However, its practical applications are limited by low specific energy [7]. In practice, supercapacitor's specific energy is the result of half of capacitance and squared working voltage of the electrolyte ($E = \frac{1}{2}CV^2$), thus the approach of increasing energy is mostly emphasis on increasing both capacitance and voltage [8]. This drives researchers to produce and design novel electrode materials and optimize an electrolyte which owe wider operating potential so as to increase supercapacitor's specific energy. Moreover, this can be achieved through finding new available electrode material with good corrosion resistance, high conductivity, high intrinsic capacitance or pseudo-capacitance, fairly low cost, high specific surface area (greater than 2000 $m^2\ g^{-1}$), controlled pore structure and high energy storage efficiency [9].

Through charge storage mechanism, supercapacitor is categorized into two forms: Electric double layer capacitor (EDLC) and Faradaic capacitor [10]. The main difference between these two mechanisms depends on where and how the charge is being stored. In electric double layer capacitor (EDLC), charges are absorbed physically on the surface of the electrode without any charge transfer, thus prevent the structure of EDLC from disintegration through insertion and de-insertion of electrolyte ions during charging/discharging process [11]. This results into higher stability however they suffer from low specific capacitance which limits their practical applications [12]. Usually, graphene, activated carbon, carbon nanotube and its forms are the main materials employed in the fabrication of EDLC electrodes [13][14]. In principal, when storage of charges appears at the interface between the electrode and electrolyte, the storage is two dimensional in nature, though when electrode is sufficiently porous and has suggestive

portion of a well distributed micro-pores, the storage is converted to three dimensional. Thus, once studied at molecular level the storage still remains two dimensional [15]. On the other hand, Faradaic capacitor stores charge by means of charge transfer which occurs through redox reaction between the electrode and electrolyte [16]. A particular example of Faradaic capacitor involve pseudocapacitive materials in which redox reaction occurs and storage mechanism is silent capacitive. Pseudocapacitor employs transition metal oxides/hydroxides and conducting polymers as the electrode materials where the redox process occurs within the material and is fundamentally three dimensional at both macroscopic and molecular levels resulting into higher specific capacity/capacitance than EDLC materials but still they are faced with low conductivity and stability [17].

Graphene has brought attention in different applications including EES due to larger specific surface area, low cost, good electrical conductivity, high corrosion resistance, good mechanical and chemical stability [18]. However, the synthesis method which involves chemicals that comprises of oxidation/reduction routes affect the chemical structure of the resulting graphene (graphene oxide - GO) thus, lower its electrochemical performance [19][20]. This challenge can be resolved by modifying the surface chemistry via optimizing the oxygen-containing surface functionalities which results into reduced graphene oxide (RGO) [21]. Furthermore, the electrochemical performance can be improved by changing morphological properties and through heteroatom dopants/agents such as boron (B), phosphorus (P), oxygen (O), nitrogen (N) and sulphur (S) [22][23]. In particular, incorporation of sulphur into reduced graphene oxide by interstitials or substitutions has great impact due to its ability to create redox active sites which changes its physical and chemical properties by attracting a greater number of electrons due to small electronegativity variation of 0.03 (carbon (2.55) and S (2.58)). This will

improve surface properties, wettability, and decrease charge transfer resistance of reduced graphene oxide [24][25].

Furthermore, the electrochemical performance of reduced graphene oxide can be improved by producing metal oxide/S-reduced graphene oxide composites. Typically, due to various oxidation states, different transition metal oxides, namely; manganese (Mn), cobalt (Co), iron (Fe), tin (Tn) and nickel (Ni) oxides have been explored as electrode materials for supercapacitors [26][27]. Precisely, manganese dioxide (MnO_2) and cobalt oxide (Co_3O_4) have been studied as a promising electrode material due to their high theoretical capacity/capacitance, high redox reactivity, pseudocapacitive performance, easily tunable surface properties, abundance in nature, different oxidation state, cost-effectiveness and environmentally friendly in terms of easy preparation procedure [28][29]. The storage mechanism can be attained by either eletrosorption or reversible redox reactions in which the change of valence state might be complemented with charge-discharge process [30]. However, they suffer from low ionic/electrical conductivity, narrow operating potential and poor dissolution and aggregation during redox reaction which hold back their capacitive behavior, particularly at high scan rate consequently result into rapid reduction of specific energy at high specific power [17][31]. Therefore, to reduce the overall limitations brought by carbon-based material and metal oxide, formation of composites through integration of the two materials has been seen as the unique approach to improve their electrochemical performance. This is because the bond formed by the interaction between carbon-based materials and transition metal oxides can ease diffusion rate and ionic mobility and hence improve the overall electrochemical properties of supercapacitors [32].

Therefore, this study emphases on advanced transformations in EES knowledge through investigation and its progress. It focusses on producing sulphur-reduced graphene oxide composite material for supercapacitor applications. The important approach is the demonstration of various hybrid devices formed by making a composite that combines both either EDLCs materials, EDLCs and pseudocapacitors materials or battery-type into one device. In this study the following has been explored in detail: The electrochemical performance of carbon-based material (reduced graphene oxide) has been enhanced by incorporation of sulphur as heteroatom agent with high redox-active sites. Carbon-based material (reduced graphene oxide) with high conductivity and long cycling but low capacitance has been combined with pseudocapacitor material (MnO_2) which offer high specific capacity/capacitance but poor conductivity and cycling and integrate the behavior of the two materials into one device with improved electrochemical performance. Also, battery-type material (cobalt oxide) with low conductivity has been joined with supercapacitor materials and produce a supercapattery device resulted in a performance comparable to that of a supercapacitor with extended cycling stability and higher specific energy without comprising its specific power.

1.2 Objective of the study

The general aim of this study is to develop sulphur-reduced graphene oxide composite materials with high improvement on the general supercapacitor's performance. The following are the specific objectives of this study:

i. Synthesis of sulphur-reduced graphene oxide (RGO-S) by an improved Hummers' method.

ii. Synthesis of sulphur-reduced graphene oxide/manganese dioxide composite (RGO-S/MnO_2) by an improved Hummers' method followed by freeze drying process and hydrothermal method.

iii. Synthesis of sulphur-reduced graphene oxide/cobalt oxide composite (RGO-S/Co_3O_4) by annealing process followed by hydrothermal method.

iv. Analysis of the elemental composition, micrographs, structural and specific surface area/pore size distribution of the materials using energy-dispersive X-ray spectroscopy (EDX), scanning electron microscope (SEM), transmission electron microscope (TEM), X-ray photoelectron spectroscopy (XPS), X-ray powdered diffraction (XRD), Fourie transform infrared (FTIR) spectroscopy, Raman spectroscopy and Brunauer-Emmett-Teller (BET) techniques.

v. Assessment of the electrochemical performance in terms of conductivity, working potential window and mechanism behavior of the synthesized material in a three-electrode configuration using cyclic voltammetry (CV), galvanostatic charge-discharge (GCD) and electrochemical impedance spectroscopy (EIS) techniques.

vi. Fabrication of the full device in order to evaluate the practical applications of the materials in terms of specific energy and specific power produced.

1.3 Arrangement of the thesis

This thesis is divided into five (5) chapters as summarized below:

Chapter 1

Introduction: This chapter provides a detailed information about the background and motivation, objectives of the study and arrangement of thesis.

Chapter 2

Literature review: This chapter describes a comprehensive review of energy storage in terms of theory of the electrochemical energy storage (EES), mechanism behavior, electrode materials, electrolytes, electrode fabrication, testing and evaluation.

Chapter 3

Synthesis methods and characterization techniques: This chapter explains the experimental procedures employed during synthesis of the materials, and the associated characterization techniques applied in evaluation of the performance of the materials.

Chapter 4

Results and discussion: This chapter describes the achieved results after synthesis, characterization and electrochemical evaluation of sulphur-reduced graphene oxide composite materials.

Chapter 5

Conclusion and suggestion for further study: This chapter presents the overall conclusion resulting from this study and suggestion for future work.

REFERENCES

[1] J.W. Lund, 100 Years of Geothermal Power Product, Proceedings. (2005) 1–10.

[2] T. Ma, H. Yang, L. Lu, Development of hybrid battery-supercapacitor energy storage for remote area renewable energy systems, Applied Energy. 153 (2015) 56–62. https://doi.org/10.1016/j.apenergy.2014.12.008.

[3] G. Kayakutlu, E. Mercier-Laurent, 3 - Intelligence for Energy, in: G. Kayakutlu, E. Mercier-Laurent (Eds.), Intelligence in Energy, Elsevier, 2017: pp. 79–116. https://doi.org/https://doi.org/10.1016/B978-1-78548-039-3.50003-1.

[4] A.R. Dehghani-Sanij, E. Tharumalingam, M.B. Dusseault, R. Fraser, Study of energy storage systems and environmental challenges of batteries, Renewable and Sustainable Energy Reviews. 104 (2019) 192–208. https://doi.org/10.1016/j.rser.2019.01.023.

[5] X. Zhang, L. Hou, A. Ciesielski, P. Samorì, 2D Materials Beyond Graphene for High-Performance Energy Storage Applications, Advanced Energy Materials. 6 (2016) 21. https://doi.org/10.1002/aenm.201600671.

[6] R.B. Rakhi, H.N. Alshareef, Enhancement of the energy storage properties of supercapacitors using graphene nanosheets dispersed with metal oxide-loaded carbon nanotubes, Journal of Power Sources. 196 (2011) 8858–8865. https://doi.org/10.1016/j.jpowsour.2011.06.038.

[7] A. Eftekhari, Metrics for Fast Supercapacitors as Energy Storage Devices, ACS Sustainable Chemistry and Engineering. 7 (2019) 3688–3691. https://doi.org/10.1021/acssuschemeng.7b04532.

[8] K.W. Nam, C.W. Lee, X.Q. Yang, B.W. Cho, W.S. Yoon, K.B. Kim, Electrodeposited manganese oxides on three-dimensional carbon nanotube substrate: Supercapacitive behaviour in aqueous and organic electrolytes, Journal of Power Sources. 188 (2009) 323–331. https://doi.org/10.1016/j.jpowsour.2008.11.133.

[9] P. Simon, Y. Gogotsi, P. Simon, Y. Gogotsi, N. Materials, Materials for electrochemical capacitors To cite this version : HAL Id : hal-02417326, 7 (2019) 845–854.

[10] M. Vangari, T. Pryor, L. Jiang, Supercapacitors: Review of materials and fabrication methods, Journal of Energy Engineering. 139 (2013) 72–79. https://doi.org/10.1061/(ASCE)EY.1943-7897.0000102.

[11] M. Hahn, O. Barbieri, R. Gallay, R. Kötz, A dilatometric study of the voltage limitation of carbonaceous electrodes in aprotic EDLC type electrolytes by charge-induced strain, Carbon. 44 (2006) 2523–2533. https://doi.org/10.1016/j.carbon.2006.05.002.

[12] M. Jayalakshmi, K. Balasubramanian, Simple capacitors to supercapacitors - An overview, International Journal of Electrochemical Science. 3 (2008) 1196–1217.

[13] Xian Jian, Shiyu Liu, Yuqi Gao, Wei Tian, Zhicheng Jiang, Xiangyun Xiao, Hui Tang, Liangjun Yin, Carbon-Based Electrode Materials for Supercapacitor: Progress, Challenges and Prospective Solutions, J. of Electrical Engineering. 4 (2016) 75–87. https://doi.org/10.17265/2328-2223/2016.02.004.

[14] S. Najib, E. Erdem, Current progress achieved in novel materials for supercapacitor electrodes: Mini review, Nanoscale Advances. 1 (2019) 2817–2827. https://doi.org/10.1039/c9na00345b.

[15] A. Noori, M.F. El-Kady, M.S. Rahmanifar, R.B. Kaner, M.F. Mousavi, Towards establishing standard performance metrics for batteries, supercapacitors and beyond, Chemical Society Reviews. 48 (2019) 1272–1341. https://doi.org/10.1039/c8cs00581h.

[16] B. Viswanathan, Chapter 13 - Supercapacitors, in: B. Viswanathan (Ed.), Energy Sources, Elsevier, Amsterdam, 2017: pp. 315–328. https://doi.org/https://doi.org/10.1016/B978-0-444-56353-8.00013-7.

[17] G.Z. Chen, Supercapacitor and supercapattery as emerging electrochemical energy stores, International Materials Reviews. 62 (2017) 173–202. https://doi.org/10.1080/09506608.2016.1240914.

[18] A.S. Lemine, M.M. Zagho, T.M. Altahtamouni, N. Bensalah, Graphene a promising electrode material for supercapacitors—A review, International Journal of Energy Research. 42 (2018) 4284–4300. https://doi.org/10.1002/er.4170.

[19] M.E. Uddin, T. Kuila, G.C. Nayak, N.H. Kim, B.C. Ku, J.H. Lee, Effects of various surfactants on the dispersion stability and electrical conductivity of surface modified graphene, Journal of Alloys and Compounds. 562 (2013) 134–142. https://doi.org/10.1016/j.jallcom.2013.01.127.

[20] Y. Bai, L. Lu, J. Bao, G. Sun, B. Zhang, J. Zeng, S. Chen, The preparation and electrochemical performance of nitrogen-doped graphene/Co(OH)2 composite, International Journal of Electrochemical Science. 14 (2019) 606–617. https://doi.org/10.20964/2019.01.48.

[21] Z. Lin, Y. Liu, Y. Yao, O.J. Hildreth, Z. Li, K. Moon, C.P. Wong, Superior capacitance of functionalized graphene, Journal of Physical Chemistry C. 115 (2011) 7120–7125. https://doi.org/10.1021/jp2007073.

[22] N.A. Kumar, J.B. Baek, Doped graphene supercapacitors, Nanotechnology. 26 (2015). https://doi.org/10.1088/0957-4484/26/49/492001.

[23] S. Verma, B. Verma, Synthesis of sulfur / phosphorous-doped graphene aerogel as a modified super capacitor electrode, (2018).

[24] S. Yaglikci, Y. Gokce, E. Yagmur, Z. Aktas, The performance of sulphur doped activated carbon supercapacitors prepared from waste tea, Environmental Technology. 0 (2019) 1–13. https://doi.org/10.1080/09593330.2019.1575480.

[25] X. Yu, S.K. Park, S.H. Yeon, H.S. Park, Three-dimensional, sulfur-incorporated

graphene aerogels for the enhanced performances of pseudocapacitive electrodes, Journal of Power Sources. 278 (2015) 484–489. https://doi.org/10.1016/j.jpowsour.2014.12.102.

[26] W. Zhang, F. Liu, Q. Li, Q. Shou, J. Cheng, L. Zhang, B.J. Nelson, X. Zhang, Transition metal oxide and graphene nanocomposites for high-performance electrochemical capacitors, Physical Chemistry Chemical Physics. 14 (2012) 16331–16337. https://doi.org/10.1039/c2cp43673f.

[27] Y. Wang, J. Guo, T. Wang, J. Shao, D. Wang, Y.W. Yang, Mesoporous transition metal oxides for supercapacitors, Nanomaterials. 5 (2015) 1667–1689. https://doi.org/10.3390/nano5041667.

[28] Y.T. Wang, A.H. Lu, H.L. Zhang, W.C. Li, Synthesis of Nanostructured mesoporous manganese oxides with three-dimensional frameworks and their application in supercapacitors, Journal of Physical Chemistry C. 115 (2011) 5413–5421. https://doi.org/10.1021/jp110938x.

[29] M. Pang, G. Long, S. Jiang, Y. Ji, W. Han, B. Wang, X. Liu, Y. Xi, D. Wang, F. Xu, Ethanol-assisted solvothermal synthesis of porous nanostructured cobalt oxides (CoO/Co3O4) for high-performance supercapacitors, Chemical Engineering Journal. 280 (2015) 377–384. https://doi.org/10.1016/j.cej.2015.06.053.

[30] P. Simon, Y. Gogotsi, Materials for electrochemical capacitors, Materials for Sustainable Energy: A Collection of Peer-Reviewed Research and Review Articles from Nature Publishing Group. (2010) 138–147. https://doi.org/10.1142/9789814317665_0021.

[31] Z. Song, Y. Zhang, W. Liu, S. Zhang, G. Liu, H. Chen, J. Qiu, Hydrothermal synthesis and electrochemical performance of Co 3O4/reduced graphene oxide nanosheet composites for supercapacitors, Electrochimica Acta. 112 (2013) 120–126.

https://doi.org/10.1016/j.electacta.2013.08.155.

[32] Q. Yang, Z. Li, R. Zhang, L. Zhou, M. Shao, M. Wei, Carbon modified transition metal oxides/hydroxides nanoarrays toward high-performance flexible all-solid-state supercapacitors, Nano Energy. 41 (2017) 408–416. https://doi.org/10.1016/j.nanoen.2017.09.049.

[33] Y. Chiang, Electrochemical Energy Storage for the Grid, World. (2010).

[34] M.S. Whittingham, History, evolution, and future status of energy storage, Proceedings of the IEEE. 100 (2012) 1518–1534. https://doi.org/10.1109/JPROC.2012.2190170.

[35] O. Razbani, M. Assadi, Artificial neural network model of a short stack solid oxide fuel cell based on experimental data, Journal of Power Sources. 246 (2014) 581–586. https://doi.org/10.1016/j.jpowsour.2013.08.018.

[36] P.N. Kanani, The Parthian Battery: Electric current 2000 years ago?, Fachzeitschrift Des VINI. (2004) 38.

[37] D.S. Ginley, D. Cahen, Fundamentals of materials for energy and environmental sustainability, Fundamentals of Materials for Energy and Environmental Sustainability. (2011) 1–753. https://doi.org/10.1017/CBO9780511718786.

[38] J. Ho, T.R. Jow, S. Boggs, Historical introduction to capacitor technology, IEEE Electrical Insulation Magazine. 26 (2010) 20–25. https://doi.org/10.1109/MEI.2010.5383924.

[39] J. Hedesan, J. Tendler, The structure of scientific revolutions, 2017. https://doi.org/10.4324/9781912281589.

[40] M.J. Ratcliff, Abraham Trembley's strategy of generosity and the scope of celebrity in the mid-eighteenth century., Isis; an International Review Devoted to the History of Science and Its Cultural Influences. 95 (2004) 555–575. https://doi.org/10.1086/430649.

[41] A. Allerhand, Who Invented the Earliest Capacitor Bank ("Battery" of Leyden Jars)? It's Complicated, Proceedings of the IEEE. 106 (2018) 496–503. https://doi.org/10.1109/JPROC.2018.2795846.

[42] J. Both, Electrolytic capacitors, 1890 to 1925: Early history and basic principle, IEEE Electrical Insulation Magazine. 31 (2015) 22–29. https://doi.org/10.1109/MEI.2015.6996675.

[43] M. Yassine, D. Fabris, Performance of commercially available supercapacitors, Energies. 10 (2017). https://doi.org/10.3390/en10091340.

[44] M. Hepel, High Energy-Density Electric Double-Layer and Hybrid Supercapacitors Based on Graphene Composites, Encyclopedia of Surface and Colloid Science, Third Edition. 1 (2015) 1–22. https://doi.org/10.1081/e-escs3-120051485.

[45] L. Zhang, High-Power Energy Storage: Ultracapacitors, Elsevier Inc., 2018. https://doi.org/10.1016/B978-0-12-812786-5.00002-1.

[46] H. Ji, X. Zhao, Z. Qiao, J. Jung, Y. Zhu, Y. Lu, L.L. Zhang, A.H. MacDonald, R.S. Ruoff, Capacitance of carbon-based electrical double-layer capacitors, Nature Communications. 5 (2014). https://doi.org/10.1038/ncomms4317.

[47] A. González, E. Goikolea, J.A. Barrena, R. Mysyk, Review on supercapacitors: Technologies and materials, Renewable and Sustainable Energy Reviews. 58 (2016) 1189–1206. https://doi.org/10.1016/j.rser.2015.12.249.

[48] M.M.M. Ahmed, T. Imae, Graphene-Based Nanolayers Toward Energy Storage Device, Elsevier B.V., 2017. https://doi.org/10.1016/B978-0-444-63739-0.00010-4.

[49] K.B. Oldham, A Gouy-Chapman-Stern model of the double layer at a (metal)/(ionic liquid) interface, Journal of Electroanalytical Chemistry. 613 (2008) 131–138. https://doi.org/10.1016/j.jelechem.2007.10.017.

[50] V.L. Shapovalov, G. Brezesinski, Breakdown of the Gouy - Chapman model for

highly charged Langmuir monolayers: Counterion size effect, Journal of Physical Chemistry B. 110 (2006) 10032–10040. https://doi.org/10.1021/jp056801b.

[51] M.A. Brown, G.V. Bossa, S. May, Emergence of a Stern Layer from the Incorporation of Hydration Interactions into the Gouy-Chapman Model of the Electrical Double Layer, Langmuir. 31 (2015) 11477–11483. https://doi.org/10.1021/acs.langmuir.5b02389.

[52] Y. Jiang, J. Liu, Definitions of Pseudocapacitive Materials: A Brief Review, Energy & Environmental Materials. 2 (2019) 30–37. https://doi.org/10.1002/eem2.12028.

[53] D. Majumdar, M. Mandal, S.K. Bhattacharya, Journey from supercapacitors to supercapatteries: recent advancements in electrochemical energy storage systems, Emergent Materials. (2020). https://doi.org/10.1007/s42247-020-00090-5.

[54] A. Muzaffar, M.B. Ahamed, K. Deshmukh, J. Thirumalai, A review on recent advances in hybrid supercapacitors: Design, fabrication and applications, Renewable and Sustainable Energy Reviews. 101 (2019) 123–145. https://doi.org/10.1016/j.rser.2018.10.026.

[55] X. Li, B. Wei, Supercapacitors based on nanostructured carbon, Nano Energy. 2 (2013) 159–173. https://doi.org/10.1016/j.nanoen.2012.09.008.

[56] J.P. Cheng, J. Zhang, F. Liu, Recent development of metal hydroxides as electrode material of electrochemical capacitors, RSC Advances. 4 (2014) 38893–38917. https://doi.org/10.1039/c4ra06738j.

[57] G.A. Snook, P. Kao, A.S. Best, Conducting-polymer-based supercapacitor devices and electrodes, Journal of Power Sources. 196 (2011) 1–12. https://doi.org/10.1016/j.jpowsour.2010.06.084.

[58] Y. Lu, G. Long, L. Zhang, T. Zhang, M. Zhang, F. Zhang, Y. Yang, Y. Ma, Y. Chen, What are the practical limits for the specific surface area and capacitance of bulk sp2

carbon materials?, Science China Chemistry. 59 (2016) 225–230. https://doi.org/10.1007/s11426-015-5474-y.

[59] A. Bianco, H.M. Cheng, T. Enoki, Y. Gogotsi, R.H. Hurt, N. Koratkar, T. Kyotani, M. Monthioux, C.R. Park, J.M.D. Tascon, J. Zhang, All in the graphene family - A recommended nomenclature for two-dimensional carbon materials, Carbon. 65 (2013) 1–6. https://doi.org/10.1016/j.carbon.2013.08.038.

[60] A. Benítez, A. Caballero, J. Morales, J. Hassoun, E. Rodríguez-Castellón, J. Canales-Vázquez, Physical activation of graphene: An effective, simple and clean procedure for obtaining microporous graphene for high-performance Li/S batteries, Nano Research. 12 (2019) 759–766. https://doi.org/10.1007/s12274-019-2282-2.

[61] H. Nguyen Bich, H. Nguyen Van, Promising applications of graphene and graphene-based nanostructures, Advances in Natural Sciences: Nanoscience and Nanotechnology. 7 (2016). https://doi.org/10.1088/2043-6262/7/2/023002.

[62] J. Yang, S. Gunasekaran, Electrochemically reduced graphene oxide sheets for use in high performance supercapacitors, Carbon. 51 (2013) 36–44. https://doi.org/10.1016/j.carbon.2012.08.003.

[63] W.S. Hummers, R.E. Offeman, Preparation of Graphitic Oxide, Journal of the American Chemical Society. 80 (1958) 1339. https://doi.org/10.1021/ja01539a017.

[64] P.L. Chiu, D.D.T. Mastrogiovanni, D. Wei, C. Louis, M. Jeong, G. Yu, P. Saad, C.R. Flach, R. Mendelsohn, E. Garfunkel, H. He, Microwave- and nitronium ion-enabled rapid and direct production of highly conductive low-oxygen graphene, Journal of the American Chemical Society. 134 (2012) 5850–5856. https://doi.org/10.1021/ja210725p.

[65] C.N.R. Rao, K.S. Subrahmanyam, H.S.S.R. Matte, B. Abdulhakeem, A. Govindaraj, B. Das, P. Kumar, A. Ghosh, D.J. Late, A study of the synthetic methods and

properties of graphenes, Science and Technology of Advanced Materials. 11 (2010). https://doi.org/10.1088/1468-6996/11/5/054502.

[66] F. Bonaccorso, A. Lombardo, T. Hasan, Z. Sun, L. Colombo, A.C. Ferrari, Production and processing of graphene and 2d crystals, Materials Today. 15 (2012) 564–589. https://doi.org/10.1016/S1369-7021(13)70014-2.

[67] K. Parvez, S. Yang, X. Feng, K. Müllen, Exfoliation of graphene via wet chemical routes, Synthetic Metals. 210 (2015) 123–132. https://doi.org/10.1016/j.synthmet.2015.07.014.

[68] M.J. Yoo, H.B. Park, Effect of hydrogen peroxide on properties of graphene oxide in Hummers method, Carbon. 141 (2019) 515–522. https://doi.org/10.1016/j.carbon.2018.10.009.

[69] Z. Tian, J. Li, G. Zhu, J. Lu, Y. Wang, Z. Shi, C. Xu, Facile synthesis of highly conductive sulfur-doped reduced graphene oxide sheets, Physical Chemistry Chemical Physics. 18 (2015) 1125–1130. https://doi.org/10.1039/c5cp05475c.

[70] Y. Li, G. Wang, T. Wei, Z. Fan, P. Yan, Nitrogen and sulfur co-doped porous carbon nanosheets derived from willow catkin for supercapacitors, Nano Energy. 19 (2016) 165–175. https://doi.org/10.1016/j.nanoen.2015.10.038.

[71] J. Han, L.L. Zhang, S. Lee, J. Oh, K.S. Lee, J.R. Potts, J. Ji, X. Zhao, R.S. Ruoff, S. Park, Generation of B-doped graphene nanoplatelets using a solution process and their supercapacitor applications, ACS Nano. 7 (2013) 19–26. https://doi.org/10.1021/nn3034309.

[72] F. Alvi, M.K. Ram, P.A. Basnayaka, E. Stefanakos, Y. Goswami, A. Kumar, Graphene-polyethylenedioxythiophene conducting polymer nanocomposite based supercapacitor, Electrochimica Acta. 56 (2011) 9406–9412. https://doi.org/10.1016/j.electacta.2011.08.024.

[73] M. Duraivel, S. Nagappan, B. Balamuralitharan, S. Selvam, S.N. Karthick, K. Prabakar, C.S. Ha, H.J. Kim, Superior one-pot synthesis of a doped graphene oxide electrode for a high power density supercapacitor, New Journal of Chemistry. 42 (2018) 11093–11101. https://doi.org/10.1039/c8nj01672k.

[74] A.K. Geim, K.S. Novoselov, The rise of graphene, Nature Materials. 6 (2007) 183–191. https://doi.org/10.1038/nmat1849.

[75] B. Quan, S.H. Yu, D.Y. Chung, A. Jin, J.H. Park, Y.E. Sung, Y. Piao, Single source precursor-based solvothermal synthesis of heteroatom-doped graphene and its energy storage and conversion applications, Scientific Reports. 4 (2014) 23–25. https://doi.org/10.1038/srep05639.

[76] P.Z. Guo, Q.Q. Ji, L.L. Zhang, S.Y. Zhao, X.S. Zhao, Preparation and characterization of peanut shell-based microporous carbons as electrode materials for supercapacitors, Wuli Huaxue Xuebao/ Acta Physico - Chimica Sinica. 27 (2011) 2836–2840. https://doi.org/10.3866/PKU.WHXB20112836.

[77] N.F. Sylla, N.M. Ndiaye, B.D. Ngom, D. Momodu, M.J. Madito, B.K. Mutuma, N. Manyala, Effect of porosity enhancing agents on the electrochemical performance of high-energy ultracapacitor electrodes derived from peanut shell waste, Scientific Reports. 9 (2019) 1–15. https://doi.org/10.1038/s41598-019-50189-x.

[78] K. Yang, J. Peng, C. Srinivasakannan, L. Zhang, H. Xia, X. Duan, Preparation of high surface area activated carbon from coconut shells using microwave heating, Bioresource Technology. 101 (2010) 6163–6169. https://doi.org/10.1016/j.biortech.2010.03.001.

[79] L. Khezami, A. Chetouani, B. Taouk, R. Capart, Production and characterisation of activated carbon from wood components in powder: Cellulose, lignin, xylan, Powder Technology. 157 (2005) 48–56. https://doi.org/10.1016/j.powtec.2005.05.009.

[80] I.I.G. Inal, S.M. Holmes, A. Banford, Z. Aktas, The performance of supercapacitor electrodes developed from chemically activated carbon produced from waste tea, Applied Surface Science. 357 (2015) 696–703. https://doi.org/10.1016/j.apsusc.2015.09.067.

[81] H. Pan, J. Li, Y.P. Feng, Carbon nanotubes for supercapacitor, Nanoscale Research Letters. 5 (2010) 654–668. https://doi.org/10.1007/s11671-009-9508-2.

[82] J. Kong, A.M. Cassell, H. Dai, Chemical vapor deposition of methane for single-walled carbon nanotubes, Chemical Physics Letters. 292 (1998) 567–574. https://doi.org/10.1016/S0009-2614(98)00745-3.

[83] C.D. Scott, S. Arepalli, P. Nikolaev, R.E. Smalley, Growth mechanisms for single-wall carbon nanotubes in a laser-ablation process, Applied Physics A: Materials Science and Processing. 72 (2001) 573–580. https://doi.org/10.1007/s003390100761.

[84] J.L. Hutchison, N.A. Kiselev, E.P. Krinichnaya, A. V. Krestinin, R.O. Loutfy, A.P. Morawsky, V.E. Muradyan, E.D. Obraztsova, J. Sloan, S. V. Terekhov, D.N. Zakharov, Double-walled carbon nanotubes fabricated by a hydrogen arc discharge method, Carbon. 39 (2001) 761–770. https://doi.org/10.1016/S0008-6223(00)00187-1.

[85] C. qi YI, J. peng ZOU, H. zhi YANG, X. LENG, Recent advances in pseudocapacitor electrode materials: Transition metal oxides and nitrides, Transactions of Nonferrous Metals Society of China (English Edition). 28 (2018) 1980–2001. https://doi.org/10.1016/S1003-6326(18)64843-5.

[86] A.N. Naveen, P. Manimaran, S. Selladurai, Cobalt oxide (Co3O4)/graphene nanosheets (GNS) composite prepared by novel route for supercapacitor application, Journal of Materials Science: Materials in Electronics. 26 (2015) 8988–9000. https://doi.org/10.1007/s10854-015-3582-2.

[87] M. Toupin, T. Brousse, D. Bélanger, Charge storage mechanism of MnO2 electrode

used in aqueous electrochemical capacitor, Chemistry of Materials. 16 (2004) 3184–3190. https://doi.org/10.1021/cm049649j.

[88] L.-B. Kong, M. Liu, J.-W. Lang, Y.-C. Luo, L. Kang, Asymmetric Supercapacitor Based on Loose-Packed Cobalt Hydroxide Nanoflake Materials and Activated Carbon, Journal of The Electrochemical Society. 156 (2009) A1000. https://doi.org/10.1149/1.3236500.

[89] A. Bello, K. Makgopa, M. Fabiane, D. Dodoo-Ahrin, K.I. Ozoemena, N. Manyala, Chemical adsorption of NiO nanostructures on nickel foam-graphene for supercapacitor applications, Journal of Materials Science. 48 (2013) 6707–6712. https://doi.org/10.1007/s10853-013-7471-x.

[90] H. Kelly-Holmes, Principles and applications of electrochemical capacitors, Electrochimica Acta 45. 45 (2000) 2483–2498. https://doi.org/10.1057/9780230503014.

[91] F. Zhang, D. Zhu, X. Chen, X. Xu, Z. Yang, C. Zou, K. Yang, S. Huang, A nickel hydroxide-coated 3D porous graphene hollow sphere framework as a high performance electrode material for supercapacitors, Physical Chemistry Chemical Physics. 16 (2014) 4186–4192. https://doi.org/10.1039/c3cp54334j.

[92] F. Li, J. Song, H. Yang, S. Gan, Q. Zhang, D. Han, A. Ivaska, L. Niu, One-step synthesis of graphene/{SnO}2nanocomposites and its application in electrochemical supercapacitors, Nanotechnology. 20 (2009) 455602. https://doi.org/10.1088/0957-4484/20/45/455602.

[93] H. Wang, Q. Fu, C. Pan, Green mass synthesis of graphene oxide and its MnO2 composite for high performance supercapacitor, Electrochimica Acta. 312 (2019) 11–21. https://doi.org/10.1016/j.electacta.2019.04.178.

[94] A. Numan, N. Duraisamy, F. Saiha Omar, Y.K. Mahipal, K. Ramesh, S. Ramesh,

Enhanced electrochemical performance of cobalt oxide nanocube intercalated reduced graphene oxide for supercapacitor application, RSC Advances. 6 (2016) 34894–34902. https://doi.org/10.1039/c6ra00160b.

[95] S. Park, S. Kim, Effect of carbon blacks filler addition on electrochemical behaviors of Co3O4/graphene nanosheets as a supercapacitor electrodes, Electrochimica Acta. 89 (2013) 516–522. https://doi.org/10.1016/j.electacta.2012.11.075.

[96] H.J. Ahonen, J. Lukkari, J. Kankare, n- and p-doped poly(3,4-ethylenedioxythiophene): Two electronically conducting states of the polymer, Macromolecules. 33 (2000) 6787–6793. https://doi.org/10.1021/ma0004312.

[97] Y. Huang, H. Li, Z. Wang, M. Zhu, Z. Pei, Q. Xue, Y. Huang, C. Zhi, Nanostructured Polypyrrole as a flexible electrode material of supercapacitor, Nano Energy. 22 (2016) 422–438. https://doi.org/10.1016/j.nanoen.2016.02.047.

[98] K.S. Ryu, Y.G. Lee, Y.S. Hong, Y.J. Park, X. Wu, K.M. Kim, M.G. Kang, N.G. Park, S.H. Chang, Poly(ethylenedioxythiophene) (PEDOT) as polymer electrode in redox supercapacitor, Electrochimica Acta. 50 (2004) 843–847. https://doi.org/10.1016/j.electacta.2004.02.055.

[99] A. Laforgue, P. Simon, C. Sarrazin, J.F. Fauvarque, Polythiophene-based supercapacitors, Journal of Power Sources. 80 (1999) 142–148. https://doi.org/10.1016/S0378-7753(98)00258-4.

[100] X. Cao, H.Y. Zeng, S. Xu, J. Yuan, J. Han, G.F. Xiao, Facile fabrication of the polyaniline/layered double hydroxide nanosheet composite for supercapacitors, Applied Clay Science. 168 (2019) 175–183. https://doi.org/10.1016/j.clay.2018.11.011.

[101] M.A.A. Mohd Abdah, N.H.N. Azman, S. Kulandaivalu, Y. Sulaiman, Review of the use of transition-metal-oxide and conducting polymer-based fibres for high-

performance supercapacitors, Materials and Design. 186 (2020) 108199. https://doi.org/10.1016/j.matdes.2019.108199.

[102] H.W. Wang, Z.A. Hu, Y.Q. Chang, Y.L. Chen, Z.Y. Zhang, Y.Y. Yang, H.Y. Wu, Preparation of reduced graphene oxide/cobalt oxide composites and their enhanced capacitive behaviors by homogeneous incorporation of reduced graphene oxide sheets in cobalt oxide matrix, Materials Chemistry and Physics. 130 (2011) 672–679. https://doi.org/10.1016/j.matchemphys.2011.07.043.

[103] C. Zhong, Y. Deng, W. Hu, D. Sun, X. Han, J. Qiao, J. Zhang, Electrolytes for electrochemical supercapacitors, 2016. https://doi.org/10.1201/b21497-3.

[104] C. Zhong, Y. Deng, W. Hu, J. Qiao, L. Zhang, J. Zhang, A review of electrolyte materials and compositions for electrochemical supercapacitors, Chemical Society Reviews. 44 (2015) 7484–7539. https://doi.org/10.1039/c5cs00303b.

[105] L. Demarconnay, E. Raymundo-Piñero, F. Béguin, A symmetric carbon/carbon supercapacitor operating at 1.6 v by using a neutral aqueous solution, Electrochemistry Communications. 12 (2010) 1275–1278. https://doi.org/10.1016/j.elecom.2010.06.036.

[106] D. Jiménez-Cordero, F. Heras, M.A. Gilarranz, E. Raymundo-Piñero, Grape seed carbons for studying the influence of texture on supercapacitor behaviour in aqueous electrolytes, Carbon. 71 (2014) 127–138. https://doi.org/10.1016/j.carbon.2014.01.021.

[107] H. Wu, X. Wang, L. Jiang, C. Wu, Q. Zhao, X. Liu, B. Hu, L. Yi, The effects of electrolyte on the supercapacitive performance of activated calcium carbide-derived carbon, Journal of Power Sources. 226 (2013) 202–209. https://doi.org/10.1016/j.jpowsour.2012.11.014.

[108] K. Fic, G. Lota, M. Meller, E. Frackowiak, Novel insight into neutral medium as electrolyte for high-voltage supercapacitors, Energy and Environmental Science. 5 (2012) 5842–5850. https://doi.org/10.1039/c1ee02262h.

[109] K. Fic, G. Lota, E. Frackowiak, Effect of surfactants on capacitance properties of carbon electrodes, Electrochimica Acta. 60 (2012) 206–212. https://doi.org/10.1016/j.electacta.2011.11.059.

[110] P. Sun, Z. Li, L. Zhang, C. Dong, Z. Li, H. Yao, J. Wang, G. Li, Synthesis of cobalt-nickel pyrophosphates/N-doped graphene composites with high rate capability for asymmetric supercapacitor, Journal of Alloys and Compounds. 750 (2018) 607–616. https://doi.org/10.1016/j.jallcom.2018.04.024.

[111] A. Brandt, S. Pohlmann, A. Varzi, A. Balducci, S. Passerini, Ionic liquids in supercapacitors, MRS Bulletin. 38 (2013) 554–559. https://doi.org/10.1557/mrs.2013.151.

[112] J.S. Skyler, Ionic-liquid materials for the electrochemical challenges of the future, Endocrinologist. 3 (1993) 233–238. https://doi.org/10.1097/00019616-199307000-00001.

[113] P.W. Ruch, D. Cericola, A. Foelske-Schmitz, R. Kötz, A. Wokaun, Aging of electrochemical double layer capacitors with acetonitrile-based electrolyte at elevated voltages, Electrochimica Acta. 55 (2010) 4412–4420. https://doi.org/10.1016/j.electacta.2010.02.064.

[114] S. Vaquero, R. Díaz, M. Anderson, J. Palma, R. Marcilla, Insights into the influence of pore size distribution and surface functionalities in the behaviour of carbon supercapacitors, Electrochimica Acta. 86 (2012) 241–247. https://doi.org/10.1016/j.electacta.2012.08.006.

[115] E. Raymundo-Piñero, K. Kierzek, J. Machnikowski, F. Béguin, Relationship between the nanoporous texture of activated carbons and their capacitance properties in different electrolytes, Carbon. 44 (2006) 2498–2507. https://doi.org/10.1016/j.carbon.2006.05.022.

[116] Y.T. Pi, Y.T. Li, S.S. Xu, X.Y. Xing, H.K. Ma, Z.B. He, T.Z. Ren, Is the conductive agent useful in electrodes of graphitized activated carbon?, RSC Advances. 6 (2016) 100708–100712. https://doi.org/10.1039/c6ra18246a.

[117] S. Priyono, T.D. Sari, Ramlan, A. Subhan, B. Prihandoko, Effect of polymer binders on the electrochemical Performance of Al-doped lithium titanate electrode, Journal of Physics: Conference Series. 1282 (2019). https://doi.org/10.1088/1742-6596/1282/1/012056.

[118] M.D. Stoller, R.S. Ruoff, Best practice methods for determining an electrode material's performance for ultracapacitors, Energy and Environmental Science. 3 (2010) 1294–1301. https://doi.org/10.1039/c0ee00074d.

[119] N. Elgrishi, K.J. Rountree, B.D. McCarthy, E.S. Rountree, T.T. Eisenhart, J.L. Dempsey, A Practical Beginner's Guide to Cyclic Voltammetry, Journal of Chemical Education. 95 (2018) 197–206. https://doi.org/10.1021/acs.jchemed.7b00361.

[120] S. Zhang, N. Pan, Supercapacitors Performance Evaluation - Zhang - 2015 - Advanced Energy Materials - Wiley Online Library, Advanced Energy Materials. (2015). https://onlinelibrary.wiley.com/doi/pdf/10.1002/aenm.201401401.

[121] D.J. Tarimo, K.O. Oyedotun, A.A. Mirghni, N. Manyala, Sulphur-reduced graphene oxide composite with improved electrochemical performance for supercapacitor applications, International Journal of Hydrogen Energy. 45 (2020). https://doi.org/10.1016/j.ijhydene.2020.03.059.

[122] M. Lu, F. Beguin, E. Frackowiak, Supercapacitors : Materials, Systems, and Applications, Wiley VCH, Weinheim, 2013.

[123] D.J. Tarimo, K.O. Oyedotun, A.A. Mirghni, N.F. Sylla, N. Manyala, High energy and excellent stability asymmetric supercapacitor derived from sulphur-reduced graphene oxide/manganese dioxide composite and activated carbon from peanut shell,

Electrochimica Acta. 353 (2020) 136498. https://doi.org/10.1016/j.electacta.2020.136498.

[124] A.A. Mirghni, K.O. Oyedotun, B.A. Mahmoud, A. Bello, S.C. Ray, N. Manyala, Nickel-cobalt phosphate/graphene foam as enhanced electrode for hybrid supercapacitor, Composites Part B: Engineering. 174 (2019) 106953. https://doi.org/10.1016/j.compositesb.2019.106953.

[125] J.H. Chae, G.Z. Chen, 1.9 V Aqueous Carbon-Carbon Supercapacitors With Unequal Electrode Capacitances, Electrochimica Acta. 86 (2012) 248–254. https://doi.org/10.1016/j.electacta.2012.07.033.

[126] F. Ochai-Ejeh, M.J. Madito, K. Makgopa, M.N. Rantho, O. Olaniyan, N. Manyala, Electrochemical performance of hybrid supercapacitor device based on birnessite-type manganese oxide decorated on uncapped carbon nanotubes and porous activated carbon nanostructures, Electrochimica Acta. 289 (2018) 363–375. https://doi.org/10.1016/j.electacta.2018.09.032.

[127] N. Aristov, A. Habekost, Cyclic Voltammetry - A Versatile Electrochemical Method Investigating Electron Transfer Processes, World Journal of Chemical Education, Vol. 3, 2015, Pages 115-119. 3 (2015) 115–119. https://doi.org/10.12691/WJCE-3-5-2.

[128] T.S. Mathis, N. Kurra, X. Wang, D. Pinto, P. Simon, Y. Gogotsi, Energy Storage Data Reporting in Perspective—Guidelines for Interpreting the Performance of Electrochemical Energy Storage Systems, Advanced Energy Materials. 9 (2019) 1–13. https://doi.org/10.1002/aenm.201902007.

[129] S. Alehashem, F. Chambers, J.W. Strojek, G.M. Swain, R. Ramesham, Cyclic Voltammetric Studies of Charge Transfer Reactions at Highly Boron-Doped Polycrystalline Diamond Thin-Film Electrodes, Analytical Chemistry. 67 (1995) 2812–2821. https://doi.org/10.1021/ac00113a014.

[130] W. Zhang, C. Ma, J. Fang, J. Cheng, X. Zhang, S. Dong, L. Zhang, Asymmetric electrochemical capacitors with high energy and power density based on graphene/CoAl-LDH and activated carbon electrodes, RSC Advances. 3 (2013) 2483–2490. https://doi.org/10.1039/c2ra23283a.

[131] Allen J. Bard and Larry R. Faulkner, Electrochemical Methods: Fundamentals and Applications, New York: Wiley, 2001, 2nd ed., Russian Journal of Electrochemistry. 38 (2002) 1364–1365. https://doi.org/10.1023/A:1021637209564.

[132] B. Akinwolemiwa, C. Peng, G.Z. Chen, Redox Electrolytes in Supercapacitors, Journal of The Electrochemical Society. 162 (2015) A5054–A5059. https://doi.org/10.1149/2.0111505jes.

[133] A.S. Ambrozevich, S.A. Ambrozevich, R.T. Sibatov, V. V. Uchaikin, Features of Charging–Discharging of Supercapacitors, Russian Electrical Engineering. 89 (2018) 64–70. https://doi.org/10.3103/S1068371218010029.

[134] S. Ban, J. Zhang, L. Zhang, K. Tsay, D. Song, X. Zou, Charging and discharging electrochemical supercapacitors in the presence of both parallel leakage process and electrochemical decomposition of solvent, Electrochimica Acta. 90 (2013) 542–549. https://doi.org/10.1016/j.electacta.2012.12.056.

[135] P.L. Taberna, P. Simon, J.F. Fauvarque, Electrochemical Characteristics and Impedance Spectroscopy Studies of Carbon-Carbon Supercapacitors, Journal of The Electrochemical Society. 150 (2003) A292. https://doi.org/10.1149/1.1543948.

[136] K. Hara, H. Arakawa, C. Dssc, S. Cell, D. Physics, K.M. Jeerage, R.D. Noble, C.A. Koval, M. Kouhnavard, N. Ahmad, L. Babak, V. Ghaffari, N. Chandra, D. Nath, H. Joon, W. Choi, J. Lee, Impedance Spectroscopy Theory, Experiment, and Applications, 2013. https://doi.org/10.1016/j.snb.2007.02.003.

[137] R. Negroiu, P. Svasta, C. Ionescu, A. Vasile, Investigation of Supercapacitor's

Impedance Based on Spectroscopic Measurements, (n.d.).

[138] F. Mansfeld, Analysis and Interpretation of EIS Data for Metals and Alloys - An Introduction to Electrochemical Impedance Measurement, (1999) 1–77.

[139] D.Y. Momodu, Investigation of metal hydroxides graphene composites as electrode materials for supercapacitor applications, (2015) 185. http://repository.up.ac.za/handle/2263/50281.

[140] B.A. Mei, O. Munteshari, J. Lau, B. Dunn, L. Pilon, Physical Interpretations of Nyquist Plots for EDLC Electrodes and Devices, Journal of Physical Chemistry C. 122 (2018) 194–206. https://doi.org/10.1021/acs.jpcc.7b10582.

[141] A. Allison, H.A. Andreas, Minimizing the Nyquist-plot semi-circle of pseudocapacitive manganese oxides through modification of the oxide-substrate interface resistance, Journal of Power Sources. 426 (2019) 93–96. https://doi.org/10.1016/j.jpowsour.2019.04.029.

[142] J. Bisquert, G. Garcia-Belmonte, P. Bueno, E. Longo, L.O.S. Bulhões, Impedance of constant phase element (CPE)-blocked diffusion in film electrodes, Journal of Electroanalytical Chemistry. 452 (1998) 229–234. https://doi.org/10.1016/S0022-0728(98)00115-6.

[143] H. Liu, M.G. George, N. Ge, D. Muirhead, P. Shrestha, J. Lee, R. Banerjee, R. Zeis, M. Messerschmidt, J. Scholta, P. Krolla, A. Bazylak, Microporous Layer Degradation in Polymer Electrolyte Membrane Fuel Cells, Journal of The Electrochemical Society. 165 (2018) F3271–F3280. https://doi.org/10.1149/2.0291806jes.

[144] A. Khosrozadeh, G. Singh, Q. Wang, G. Luo, M. Xing, Supercapacitor with extraordinary cycling stability and high rate from nano-architectured polyaniline/graphene on Janus nanofibrous film with shape memory, Journal of Materials Chemistry A. 6 (2018) 21064–21077. https://doi.org/10.1039/C8TA07426G.

[145] A. Laheäär, P. Przygocki, Q. Abbas, F. Béguin, Appropriate methods for evaluating the efficiency and capacitive behavior of different types of supercapacitors, Electrochemistry Communications. 60 (2015) 21–25. https://doi.org/10.1016/j.elecom.2015.07.022.

[146] A. Bello, F. Barzegar, M.J. Madito, D.Y. Momodu, A.A. Khaleed, T.M. Masikhwa, J.K. Dangbegnon, N. Manyala, Stability studies of polypyrole- derived carbon based symmetric supercapacitor via potentiostatic floating test, Electrochimica Acta. 213 (2016) 107–114. https://doi.org/10.1016/j.electacta.2016.06.151.

[147] D. Weingarth, A. Foelske-Schmitz, R. Kötz, Cycle versus voltage hold - Which is the better stability test for electrochemical double layer capacitors?, Journal of Power Sources. 225 (2013) 84–88. https://doi.org/10.1016/j.jpowsour.2012.10.019.

[148] J. Kowal, E. Avaroglu, F. Chamekh, A. Šenfelds, T. Thien, D. Wijaya, D.U. Sauer, Detailed analysis of the self-discharge of supercapacitors, Journal of Power Sources. 196 (2011) 573–579. https://doi.org/10.1016/j.jpowsour.2009.12.028.

[149] J. Niu, B.E. Conway, W.G. Pell, Comparative studies of self-discharge by potential decay and float-current measurements at C double-layer capacitor and battery electrodes, Journal of Power Sources. 135 (2004) 332–343. https://doi.org/10.1016/j.jpowsour.2004.03.068.

[150] L. Staudenmaier, Verfahren zur darstellung der graphitsäure, Berichte Der Deutschen Chemischen Gesellschaft. 31 (1898) 1481–1487.

[151] J. Chen, B. Yao, C. Li, G. Shi, An improved Hummers method for eco-friendly synthesis of graphene oxide, Carbon. 64 (2013) 225–229. https://doi.org/10.1016/j.carbon.2013.07.055.

[152] D.C. Marcano, D. V. Kosynkin, J.M. Berlin, A. Sinitskii, Z. Sun, A. Slesarev, L.B. Alemany, W. Lu, J.M. Tour, Improved synthesis of graphene oxide, ACS Nano. 4

(2010) 4806–4814. https://doi.org/10.1021/nn1006368.

[153] I.V.G. and A.A.F. K. S. Novoselov, A. K. Geim, S. V. Morozov, D. Jiang, Y. Zhang, S. V. Dubonos, Electric Field Effect in Atomically Thin Carbon Films, 306 (2016) 666–669.

[154] S.C. Tsinontides, P. Rajniak, D. Pham, W.A. Hunke, J. Placek, S.D. Reynolds, Freeze drying - Principles and practice for successful scale-up to manufacturing, International Journal of Pharmaceutics. 280 (2004) 1–16. https://doi.org/10.1016/j.ijpharm.2004.04.018.

[155] Lyophilization/Freeze Drying - An Review 7, (n.d.) 2700.

[156] Z. Ling, C. Yu, X. Fan, S. Liu, J. Yang, M. Zhang, G. Wang, N. Xiao, J. Qiu, Freeze-drying for sustainable synthesis of nitrogen doped porous carbon cryogel with enhanced supercapacitor and lithium ion storage performance, Nanotechnology. 26 (2015). https://doi.org/10.1088/0957-4484/26/37/374003.

[157] S. Singh, Lyophilization/Freeze drying - A review, Age. 20 (2015) 60yrs.

[158] J. Zhang, Z. Yang, X. Wang, T. Ren, Q. Qiao, Homogeneous sulphur-doped composites: Porous carbon materials with unique hierarchical porous nanostructure for super-capacitor application, RSC Advances. 6 (2016) 84847–84853. https://doi.org/10.1039/c6ra17231h.

[159] J. Li, Q. Wu, J. Wu, T.S. Division, O. Ridge, O. Ridge, C. Sciences, E. Division, Handbook of Nanoparticles, Handbook of Nanoparticles. (2015). https://doi.org/10.1007/978-3-319-13188-7.

[160] D. Rickard, G.W. Luther, Chemistry of iron sulfides, 2007. https://doi.org/10.1021/cr0503658.

[161] A.E. Lewis, Review of metal sulphide precipitation, Hydrometallurgy. 104 (2010) 222–234. https://doi.org/10.1016/j.hydromet.2010.06.010.

[162] J. Grandgirard, D. Poinsot, L. Krespi, J.P. Nénon, A.M. Cortesero, Conventional and Microwave Hydrothermal Synthesis and Application of Functional Materials: A Review, Entomologia Experimentalis et Applicata. 103 (2002) 239–248. https://doi.org/10.1023/A.

[163] Y.X. Gan, A.H. Jayatissa, Z. Yu, X. Chen, M. Li, Hydrothermal Synthesis of Nanomaterials, Journal of Nanomaterials. 2020 (2020). https://doi.org/10.1155/2020/8917013.

[164] G. Sharma, A. Kumar, S. Sharma, M. Naushad, R. Prakash Dwivedi, Z.A. ALOthman, G.T. Mola, Novel development of nanoparticles to bimetallic nanoparticles and their composites: A review, Journal of King Saud University - Science. 31 (2019) 257–269. https://doi.org/10.1016/j.jksus.2017.06.012.

[165] Y. Dahman, Chapter 6 - Nanopolymers**By Yaser Dahman, Kevin Deonanan, Timothy Dontsos, and Andrew Iammatteo., in: Y. Dahman (Ed.), Nanotechnology and Functional Materials for Engineers, Elsevier, 2017: pp. 121–144. https://doi.org/https://doi.org/10.1016/B978-0-323-51256-5.00006-X.

[166] B. Akturk, A.B. Kizilkanat, Improvement of durability and drying shrinkage of sodium carbonate activated slag through the incorporation of calcium hydroxide and sodium hydroxide, Construction and Building Materials. 243 (2020) 118260. https://doi.org/10.1016/j.conbuildmat.2020.118260.

[167] S. Barzgar, B. Lothenbach, M. Tarik, A. Di Giacomo, C. Ludwig, The effect of sodium hydroxide on Al uptake by calcium silicate hydrates (C[sbnd]S[sbnd]H), Journal of Colloid and Interface Science. 572 (2020) 246–256. https://doi.org/10.1016/j.jcis.2020.03.057.

[168] H.D. Alvarenga, T. Van De Putte, N. Van Steenberge, J. Sietsma, H. Terryn, Influence of Carbide Morphology and Microstructure on the Kinetics of Superficial

Decarburization of C-Mn Steels, Metallurgical and Materials Transactions A: Physical Metallurgy and Materials Science. 46 (2015) 123–133. https://doi.org/10.1007/s11661-014-2600-y.

[169] K. Xiao, H. Wu, H. Lv, X. Wu, H. Qian, The study of the effects of cooling conditions on high quality graphene growth by the APCVD method, Nanoscale. 5 (2013) 5524–5529. https://doi.org/10.1039/c3nr00524k.

[170] K.O. Oyedotun, M.J. Madito, D.Y. Momodu, A.A. Mirghni, T.M. Masikhwa, N. Manyala, Synthesis of ternary NiCo-MnO2 nanocomposite and its application as a novel high energy supercapattery device, Chemical Engineering Journal. 335 (2018) 416–433. https://doi.org/10.1016/j.cej.2017.10.169.

[171] J.D. Andrade, X-ray photoelectron spectroscopy (XPS), in: Surface and Interfacial Aspects of Biomedical Polymers, Springer, 1985: pp. 105–195.

[172] G. Greczynski, L. Hultman, X-ray photoelectron spectroscopy: Towards reliable binding energy referencing, Progress in Materials Science. 107 (2020) 100591. https://doi.org/10.1016/j.pmatsci.2019.100591.

[173] R. Kohli, K.L. Mittal, eds., Chapter 3 - Methods for Assessing Surface Cleanliness, in: Developments in Surface Contamination and Cleaning, Volume 12, Elsevier, 2019: pp. 23–105. https://doi.org/https://doi.org/10.1016/B978-0-12-816081-7.00003-6.

[174] J. Epp, X-ray diffraction (XRD) techniques for materials characterization, in: Materials Characterization Using Nondestructive Evaluation (NDE) Methods, Elsevier, 2016: pp. 81–124.

[175] J.P. Patel, P.H. Parsania, 3 - Characterization, testing, and reinforcing materials of biodegradable composites, in: N.G. Shimpi (Ed.), Biodegradable and Biocompatible Polymer Composites, Woodhead Publishing, 2018: pp. 55–79. https://doi.org/https://doi.org/10.1016/B978-0-08-100970-3.00003-1.

[176] O.I. Olubiyi, F.-K. Lu, D. Calligaris, F.A. Jolesz, N.Y. Agar, Advances in molecular imaging for surgery, in: Image-Guided Neurosurgery, Elsevier, 2015: pp. 407–439.

[177] P. Vandenabeele, Practical Raman spectroscopy: an introduction, John Wiley & Sons, 2013.

[178] K.S. Joya, X. Sala, In situ Raman and surface-enhanced Raman spectroscopy on working electrodes: Spectroelectrochemical characterization of water oxidation electrocatalysts, Physical Chemistry Chemical Physics. 17 (2015) 21094–21103. https://doi.org/10.1039/c4cp05053c.

[179] K. Kneipp, H. Kneipp, P. Corio, S.D.M. Brown, K. Shafer, J. Motz, L.T. Perelman, E.B. Hanlon, A. Marucci, G. Dresselhaus, M.S. Dresselhaus, Surface-enhanced and normal stokes and anti-stokes raman spectroscopy of single-walled carbon nanotubes, Physical Review Letters. 84 (2000) 3470–3473. https://doi.org/10.1103/PhysRevLett.84.3470.

[180] A.T. Ward, Raman spectroscopy of sulfur, sulfur-selenium, and sulfur-arsenic mixtures, Journal of Physical Chemistry. 72 (1968) 4133–4139. https://doi.org/10.1021/j100858a031.

[181] C. Nims, B. Cron, M. Wetherington, J. Macalady, J. Cosmidis, Low frequency Raman Spectroscopy for micron-scale and in vivo characterization of elemental sulfur in microbial samples, Scientific Reports. 9 (2019) 1–12. https://doi.org/10.1038/s41598-019-44353-6.

[182] G. Guimbretière, S. Duraipandian, T. Ricci, Field remote Stokes/anti-Stokes Raman characterization of sulfur in hydrothermal vents, Journal of Raman Spectroscopy. 49 (2018) 1385–1394. https://doi.org/10.1002/jrs.5378.

[183] G.S. Allan, Fourier Transform Infrared Spectroscopy (FTIR), Encyclopedia of Earth Sciences Series. (2017) 1046. https://doi.org/10.1007/978-1-4020-4409-0.

[184] P.M. Shameer, P.M. Nishath, Exploration and enhancement on fuel stability of biodiesel: A step forward in the track of global commercialization, in: Advanced Biofuels, Elsevier, 2019: pp. 181–213.

[185] D. Titus, E.J.J. Samuel, S.M. Roopan, Nanoparticle characterization techniques, in: Green Synthesis, Characterization and Applications of Nanoparticles, Elsevier, 2019: pp. 303–319.

[186] N.J. and D.R. Vij, FOURIER TRANSFORM INFRARED SPECTROSCOPY, 2006. https://doi.org/10.1007/0-387-37590-2.

[187] M. Salouti, F.K. Derakhshan, Chapter 3 - Phytosynthesis of Nanoscale Materials, in: M. Ghorbanpour, S.H. Wani (Eds.), Advances in Phytonanotechnology, Academic Press, 2019: pp. 45–121. https://doi.org/https://doi.org/10.1016/B978-0-12-815322-2.00003-1.

[188] J.I. Goldstein, D.E. Newbury, J.R. Michael, N.W.M. Ritchie, J.H.J. Scott, D.C. Joy, Scanning electron microscopy and X-ray microanalysis, Springer, 2017.

[189] A.K. Singh, Chapter 4 - Experimental Methodologies for the Characterization of Nanoparticles, in: A.K. Singh (Ed.), Engineered Nanoparticles, Academic Press, Boston, 2016: pp. 125–170. https://doi.org/https://doi.org/10.1016/B978-0-12-801406-6.00004-2.

[190] J. Telegdi, A. Shaban, G. Vastag, Biocorrosion-steel, in: Encyclopedia of Interfacial Chemistry: Surface Science and Electrochemistry, Elsevier, 2018: pp. 28–42.

[191] O.D. Neikov, N.A. Yefimov, Chapter 1 - Powder Characterization and Testing, in: O.D. Neikov, S.S. Naboychenko, N.A. Yefimov (Eds.), Handbook of Non-Ferrous Metal Powders (Second Edition), Second Edi, Elsevier, Oxford, 2019: pp. 3–62. https://doi.org/https://doi.org/10.1016/B978-0-08-100543-9.00001-4.

[192] J. Bergström, 2 - Experimental Characterization Techniques, in: J. Bergström (Ed.),

Mechanics of Solid Polymers, William Andrew Publishing, 2015: pp. 19–114. https://doi.org/https://doi.org/10.1016/B978-0-323-31150-2.00002-9.

[193] T. Walther, Chapter 4 - Transmission Electron Microscopy of Nanostructures, in: S. Thomas, R. Thomas, A.K. Zachariah, R.K. Mishra (Eds.), Microscopy Methods in Nanomaterials Characterization, Elsevier, 2017: pp. 105–134. https://doi.org/https://doi.org/10.1016/B978-0-323-46141-2.00004-3.

[194] C. Escalante, E. Sierra, Fundamentals of transmission electron microscopy, the technique with the best resolution in the world, (2019) 0–6.

[195] R.T. G, A.B. R, Review Article TRANSMISSION ELECTRON MICROSCOPY-AN OVERVIEW ISSN Online : - 2321-7855 International Research Journal for Inventions in TRANSMISSION ELECTRON MICROSCOPY- AN OVERVIEW, (2019).

[196] S. Brunauer, L.S. Deming, W.E. Deming, E. Teller, On a Theory of the van der Waals Adsorption of Gases, Journal of the American Chemical Society. 62 (1940) 1723–1732. https://doi.org/10.1021/ja01864a025.

[197] M. Thommes, K. Kaneko, A. V. Neimark, J.P. Olivier, F. Rodriguez-Reinoso, J. Rouquerol, K.S.W. Sing, Physisorption of gases, with special reference to the evaluation of surface area and pore size distribution (IUPAC Technical Report), Pure and Applied Chemistry. 87 (2015) 1051–1069. https://doi.org/10.1515/pac-2014-1117.

[198] C.D.H.E. (UK); R.A.W.H. (FRG); L.M. (Netherlands); R.A.P. (USA); J.R. (France); T.S. (Poland) K. S. W. SING (UK, *Membership, REPORTING PHYSISORPTION DATA FOR GAS/SOLID SYSTEMS with Special Reference to the Determination of Surface Area and Porosity, 81 (1998) 420–430.

[199] Bio-Logic, EC-Lab Software: Techniques and Applications, (2009) 1–175.

[200] F.-B. Wu, B. Yang, J.-L. Ye, eds., Chapter 2 - Technologies of energy storage systems, in: Grid-Scale Energy Storage Systems and Applications, Academic Press, 2019: pp.

17–56. https://doi.org/https://doi.org/10.1016/B978-0-12-815292-8.00002-2.

[201] L. Zhou, W. Utetiwabo, R. Chen, W. Yang, Layer by Layer Assemble of Colloid Nanomaterial and Functional Multilayer Films for Energy Storage and Conversion, (2019).

[202] E.Z. Kurmaev, A. V. Galakhov, A. Moewes, S. Moehlecke, Y. Kopelevich, Interlayer conduction band states in graphite-sulfur composites, Physical Review B - Condensed Matter and Materials Physics. 66 (2002) 1–3. https://doi.org/10.1103/PhysRevB.66.193402.

[203] Q. Cheng, J. Tang, J. Ma, H. Zhang, N. Shinya, L.C. Qin, Graphene and nanostructured MnO2 composite electrodes for supercapacitors, Carbon. 49 (2011) 2917–2925. https://doi.org/10.1016/j.carbon.2011.02.068.

[204] T. Chen, Y. Tang, Y. Qiao, Z. Liu, W. Guo, J. Song, S. Mu, S. Yu, Y. Zhao, F. Gao, All-solid-state high performance asymmetric supercapacitors based on novel MnS nanocrystal and activated carbon materials, Scientific Reports. 6 (2016) 1–9. https://doi.org/10.1038/srep23289.

[205] X. Zhao, H. Wang, G. Zhai, G. Wang, Facile Assembly of 3D Porous Reduced Graphene Oxide/Ultrathin MnO 2 Nanosheets-S Aerogels as Efficient Polysulfide Adsorption Sites for High-Performance Lithium–Sulfur Batteries, Chemistry - A European Journal. 23 (2017) 7037–7045. https://doi.org/10.1002/chem.201604828.

[206] C.W. Jones, Applications of hydrogen peroxide and derivatives, Royal Society of Chemistry, 2007.

[207] T.T. Nguyen, V.H. Nguyen, R.K. Deivasigamani, D. Kharismadewi, Y. Iwai, J.J. Shim, Facile synthesis of cobalt oxide/reduced graphene oxide composites for electrochemical capacitor and sensor applications, Solid State Sciences. 53 (2016) 71–77. https://doi.org/10.1016/j.solidstatesciences.2016.01.006.

[208] C. A reduced graphene oxide/Co3O4 composite for supercapacitor electrodeXiang, M. Li, M. Zhi, A. Manivannan, N. Wu, A reduced graphene oxide/Co3O4 composite for supercapacitor electrode, Journal of Power Sources. 226 (2013) 65–70. https://doi.org/10.1016/j.jpowsour.2012.10.064.

2.0 LITERATURE REVIEW

This chapter presents theory of electrochemical energy storage, classification of electrochemical energy storage, supercapacitors, electrode materials for supercapacitor, electrolytes, electrode fabrication, testing and electrochemical evaluation.

2.1 Theory of Electrochemical Energy Storage (EES)

Electrochemical energy storage (EES) is a technique which store electricity by chemical form in which chemical and electrical energy share electron as a carrier [33]. The history of EES started from Parthian battery/the Bagdad battery which was discovered by Austrian painter and director of the Bagdad Museum [34] [35]. It consists of copper tube, ceramic pot and iron rod in which it was hypothesized by researchers that the object functioned as a galvanic cell. The iron rod enclosed by a cylinder built of a rolled copper sheet was inserted in the clay jar which was filled with a vinegar solution. The electricity was generated from the jar and it was about 1.1 to 2.0 V for the purpose of electroplating, pain relief and religious tingle. The real battery was inverted for the first time by Alessandro Volta in 1800s using alternating discs of copper (Cu) and zinc (Zn) separated by a cardboard with a brine solution as the electrolyte, and wires connected to the end to produce a continuous stable electricity [36]. This developed into the two-electrolyte Daniel cell in 1836 comprising of copper pot full of a copper sulfate solution in which it was dipped in a porous clay container filled with sulfuric acid and used zinc as anode and copper pot as cathode [37]. The porous clay pot permits the passage of ions without allowing the solution to mix, consequently protecting the battery life. The following ground-breaking was the growth of Leclanche cell in 1866 using zinc as anode and carbon as cathode. The breakthrough invention was development of rechargeable batteries: Nickel-cadmium (1899), nickel-metal hydride (1986) and Li-ion batteries (1972) which was commercialized in

1990s due to advancement in technology through the use of portable electronic devices accompanied by its light weight and high energy storage [34].

A capacitor is an electric device which store small amount of energy compared to batteries in the electric field between a pair of closely spaced conductors [12]. Usually, the voltage is applied to the capacitor and an electric charge of equal magnitude, but opposite polarity builds on each plate. The invention of capacitor was commenced by Ewald Georg von Kleist in 1745, by which he invented a glass jar containing a conducting fluid and iron nail inserted inside. The glass jar was found to preserve charge after being electrified with the friction machine [38] [39]. It was followed by another discovery from Pieter van Musschenbroek in 1746 who came up with the glass jar, which was wrapped inside and outside by a thin metal foil and named as Leyden jar [40]. In 1876, another capacitor made up by sandwiching of aluminum and tantalum paper with electrolyte in-between the two metal foils and rolled up tightly into a cylinder was discovered. It was observed that the current was able to flow in one direction and hence formation of oxide dielectrics in the opposite direction. This was the first electrolytic capacitor which was patented in 1896 [41]. It was followed by discovery of other capacitors which were named based on the source of fabrication, these are; mica dielectric capacitor developed in 1909, the capacitor constructed by polyethylene terephthalate and patented in 1941, and plastic dielectric capacitors established in the beginning of 1959 [42]. The first capacitor describing the concept of charge storage through electric double-layer using porous carbon coated on a metallic current collector in a sulfuric acid solution was discovered by General Electric in 1957 and it was unpractical [38]. In 1971, Nippon Electric Corporation introduced the first commercialized electric double-layer capacitor (EDLC) filled by a standard oil which was capable of producing 5.5 V, and hence, it was the beginning of using electrochemical capacitors in commercial devices [15]. The earliest commercialized EDLC was named as ‘supercapacitor’

by NEC, Incorporation of Tokyo, Japan and 'ultracapacitor' by Pinnacle Research Institute (USA) though, currently the electrochemical capacitors are mostly denoted as supercapacitors or ultracapacitors.

2.2 Supercapacitors

Supercapacitor is an electrochemical capacitor that has high specific energy compared to traditional capacitor. It contains two electrodes separated by a dielectric material (separator) with sufficient porosity which allow the movement of ions from the electrolyte. The supercapacitor is charged once the ions are drawn over the electrical double-layer by applying voltage to the electrodes. However, when discharging the capacitor, they move away from the layer [43].

Supercapacitors are classified into three types depending on their charge storage mechanisms. Namely, electric double-layer capacitors (EDLCs), pseudocapacitors and hybrid capacitors [44].

2.2.1 Electric double-layer capacitors (EDLCs)

EDLCs store charge on the surface of the electrode through physical adsorption and desorption of ions within the interface of the electrode/electrolyte when a voltage bias is applied as shown in Figure 2.1 [45]. This means that the electrode materials do not participate in chemical reaction throughout the process of charge/discharge. Normally, the whole process of carrying ions, followed by adsorption/desorption, strike in a second, hence compromising EDLCs with the fast charge/discharge capability. This permits energy to be stored and delivered at very high power due to the very low and almost negligible of resistances linked by the charge transfer reaction existing in batteries [46]. Therefore, the concept of EDLCs relies on the electric double layer presents at the boundary between the electrodes and its connecting electrolyte medium.

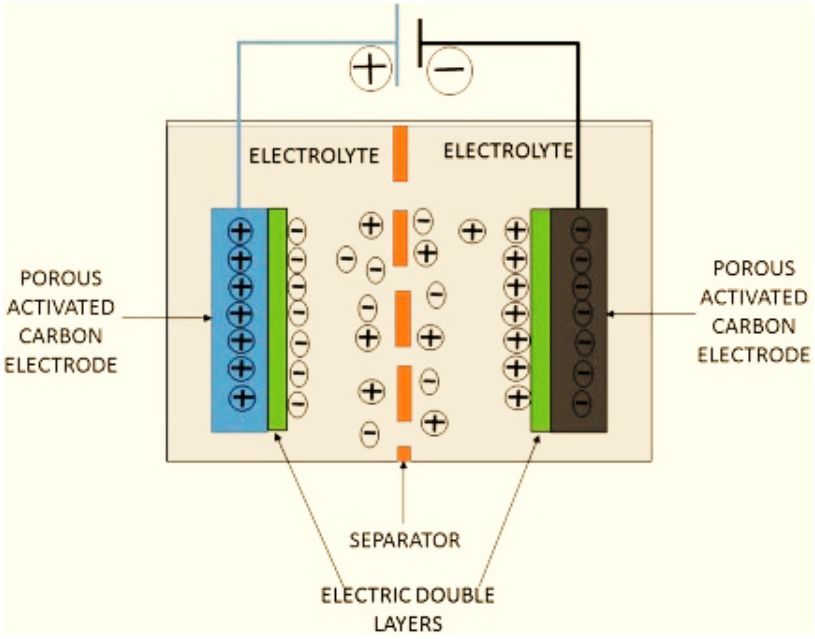

Figure 2.1: Charge separation of EDLC supercapacitor [45].

The phenomenon of EDLCs was originally revealed by Hermann von Helmholtz and later enhanced by Gouy-Chapman and Stern as demonstrated in Figure 2.2 [47]. Initially, Helmholtz gathered the information that when two layers of opposite polarity form at the interface between electrode and electrolyte, the charged electrodes immersed in the electrolyte medium repel the co-ions of the charge while attracting counterions to their surfaces. The model describes the EDLCs as a molecular dielectric which stores charge electrostatically in which, the stored charges are linearly dependent on the voltage applied, when it's below the electrolyte decomposition voltage. Furthermore, this model estimated that a constant capacitance is independent from the charge density but dependent on the dielectric constant of the electrolyte solvent and the thickness of the double layer. Helmholtz model considered entirely charges to be adsorbed at the surface of the electrode without taking into account incorporation/diffusion of ions in the solution and the interaction between solvent dipole movements and the electrode [48].

The second EDLCs phenomenon was made by Gouy and Chapman who developed Gouy-Chapman model which spotted capacitance being reliant on the applied voltage and ionic concentration, and not constant as suggested by Helmholtz [49]. The Gouy-Chapman model modified the Helmholtz model by taking into consideration the mobility of ions in the electrolyte medium as a mark of diffusion and electrostatic forces. The charge distribution of ions versus distance from the metal surface permits Maxwell-Boltzmann statistics to be used with the electric potential being noted to decrease exponentially away from the surface of the bulk liquid [50]. The drawback of this model occurs when the idea of ion-ion interaction in the liquid was ignored, while it plays an important role at higher ionic concentration. Also, the model fails to account for the extremely charged diffusive layers due to the assumption made, including, the dielectric constant at the interface between the electrode and the bulk liquid.

The limitations above provided a room to the Stein to modify the Gouy-Chapman model through joining the Helmholtz model (absorption of ions at the interface of the electrode) and Gouy-Chapman model (integration of diffusive layer) [51], with their total double layer capacitance being written as the series combination of the two, which can be expressed as;

$$\frac{\mathbf{1}}{\boldsymbol{C_T}} = \frac{\mathbf{1}}{\boldsymbol{C_H}} + \frac{\mathbf{1}}{\boldsymbol{C_G}} \quad (1)$$

Where; C_T is the total capacitance, C_H represent Helmholtz capacitance and C_G stands for Gouy-Chapman capacitance.

This shows that near the electrodes the Helmholtz model leads while for the bulk liquid the Gouy-Chapman model dominates. Therefore, Stern model estimated no interaction of ions from the electrolyte and electrodes, hence properties and concentration of the electrolyte should remain constant throughout the charge/discharge process which is also applied for an ideal EDLCs system.

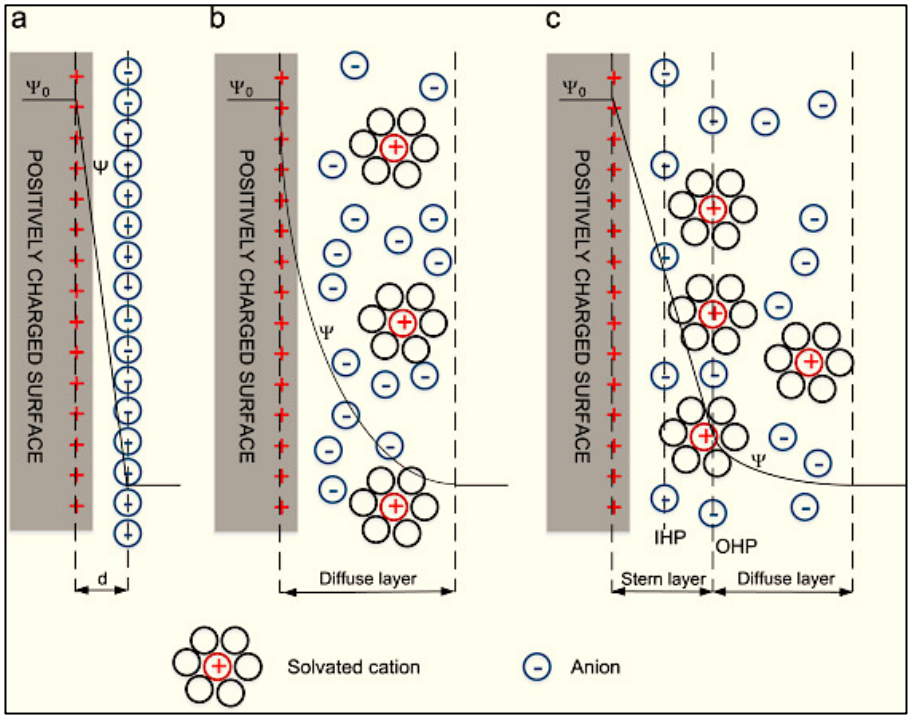

Figure 2.2: Double-layer model showing the (a) Helmholtz model, (b) Gouy-Chapman model and (c) Stern layer [47].

2.2.2 Pseudocapacitors

Pseudocapacitors store energy Faradically through electron charge transfer which occur between the surface of the electrode and electrolyte. This is accomplished by fast and reversible redox reactions, intercalation process and eletrosorption [52]. The redox reactions in pseudocapacitors result from the chemical reaction that contains electrons transfer and occur on the surface of the electrode between two species, while intercalation occurs when ions are inserted into the pores of the bulk redox material guided by a Faradaic charge transfer with no transformation of crystallographic. Eletrosorption in pseudocapacitors appear at the surface of the electrodes, when ions are detached from the electrolyte medium by the imposed electric field and adsorbed onto the surface of the electrodes following polarization of the electrodes.

The Faradaic behavior at the surface of the electrode has supported the energy stored in a pseudocapacitors by increasing the specific energy at the cost of specific power and cycle life compared to EDLCs [53].

2.2.3 Hybrid supercapacitors

Hybrid supercapacitors are electrochemical energy storage with high capacitance and high energy storage ability which resulted from the combined characteristics of EDLCs and pseudocapacitors. Since the goal of electrochemical energy storage is to fabricate a capacitor with high specific energy without compromising its specific power, then, the prospect of this combination creates strong attention to the researchers due to enhanced additional characters conveyed by the hybrid device (Figure 2.3) [54]. As spotted in Ragone plot (Figure 2.3), the hybrid supercapacitor fulfils the region of specific energy and specific power compared to other supercapacitors. Normally, for hybrid device, one half of hybrid supercapacitor perform as EDLCs while the other half perform as a pseudocapacitors. However, if the final device revealed mostly EDLCs characteristics than Faradaic behavior then this type of hybrid device is named as supercapattery while the one with more Faradaic behavior than EDLCs is termed as supercabattery [17]. These types of device have an improved electrochemical performance due to incorporation of supercapacitor and battery-type characteristics.

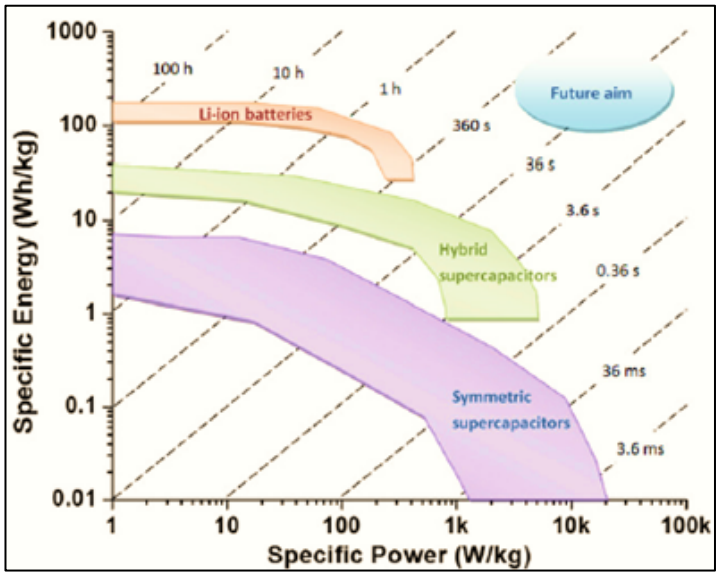

Figure 2.3: Ragone plot for different energy storage system [55].

2.4 Electrode materials for supercapacitors

Beside the other components of the device, electrochemical performance of supercapacitor is mostly influenced by the choice of electrode material which determine electrical properties of the fabricated device. The following properties remain crucial for the electrode material selection: low cost and environmentally friendly, low ohmic and internal resistance, small pore size, short diffusion length and high specific surface area, and low volume and weight [56]. Generally, the electrode material for supercapacitors are classified into four: carbon electrode materials, transition metal oxides/hydroxides, conducting polymers and composites.

2.4.1 Carbon electrode materials

EDLCs materials has displayed a distinctive property which significantly influence the performance of the device. Generally, carbon-based material comprising of graphene, activated carbon, carbon nanotubes and so on have been studied as the electrode material for EDLCs due to their existence in varying forms (nanofibers, nanosheets, aerogels, and powders), broad working temperature, high chemical stability, high conductivity, availability, cost-

effectiveness, non-toxicity and high specific surface area [57]. Since, the charge storage mechanism of EDLCs device occur at the surface of the electrode, the surface property of the electrode material and pore size adapted from appropriate type of electrolyte plays a significant role to improve the capacitance of the material. The specific surface area of the carbon materials can go up to ~ 3500 $m^2 g^{-1}$ [58].

Graphene is an allotrope of carbon arranged in a single layer of atoms (Figure 2.4 (a)) in two-dimensional hexagonal pattern in which one atom forms each vertex and is considered as an elementary foundation element of all other two-dimensional allotropes of carbon [59]. Graphene hold exceptional features like good chemical and mechanical stability, highly tunable surface area, (~ 2675 $m^2 g^{-1}$), good conductivity, and structural flexibility. These properties have made graphene to be used in different applications like energy storage devices, chemical, industrial and medical processes, sensors, and water purification [60]. For a while, more attention has been given by researchers on the use of graphene for energy storage because of its tunable surface functional groups, shorter diffusion length and small pore size which is influenced by the synthesis method, and an extended potential window resulted from the type of electrolyte used [61]. Graphene has been synthesized by different methods including; Hummer's method [62][63], microwave method [64], chemical vapor deposition (CVD) [65], dispersion method [66] and chemical exfoliation [67]. In fact, the properties of graphene displayed using these methods does not favor the material to be used for practical application due to restacking of graphene sheets, high inter-sheet contact resistance and formation of large number of radical generations [68]. Thus, most researchers have focused on increasing the electrochemical performance of graphene by doping using heteroatom dopants/agents like sulphur (S) [25][69], nitrogen (N) [70], boron (B) [71], phosphorus (P) [23] or through composite formation using oxide/hydroxide [26] or conducting polymer materials [72].

Between these heteroatom dopants/agents, S has drawn major interest to the researchers due to lower electronegativity (S - 2.58) which offers ability to form additional redox active sites as shown in Figure 2.4 (b), which increases capacitance of the graphene. Integration of S into graphene improve surface properties, conductivity, enhance wettability, and decrease charge transfer resistance [73].

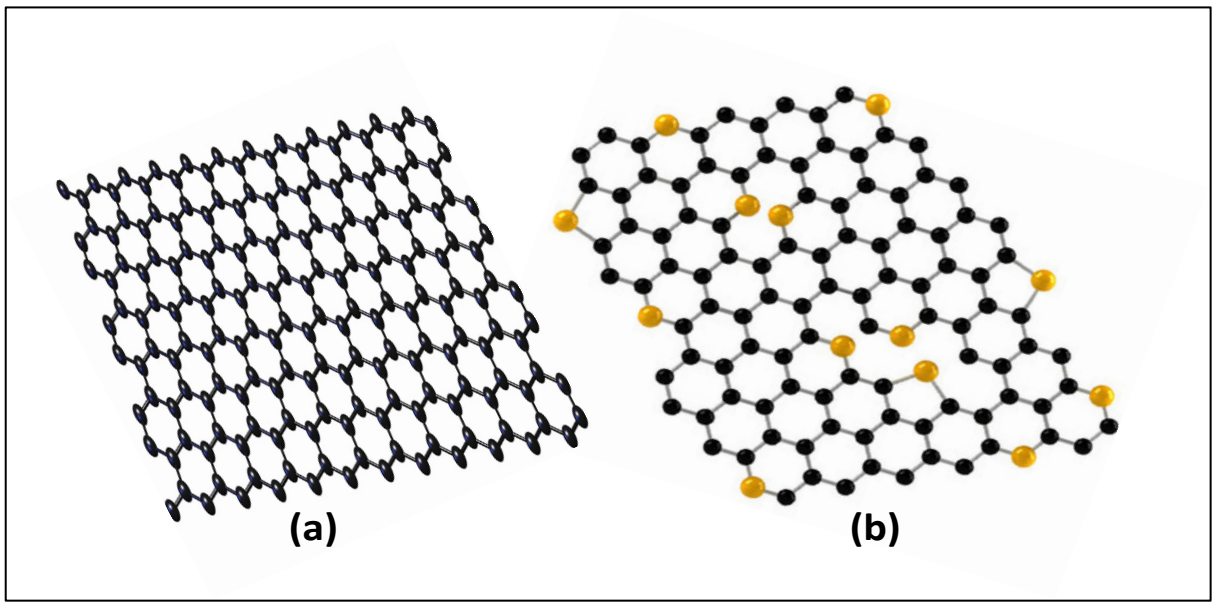

Figure 2.4: Structure of graphene (a) single layer graphene [74] and (b) graphene doped with sulfur [75].

Activated carbons are forms of carbon derived from carbon-based raw materials such as peanut shells [76][77], coconut shells [78], wood [79], waste tea leaves [80], and so on through activations. Thermal or chemical treatment is applied to produce a carbon material with small, low-volume pores which increase the surface area available for adsorption or chemical reactions. The activation procedure is classified into two parts namely; thermal activation and chemical activation. Thermal activation involves pyrolysis of carbon-based material using oxidizing gases like carbon dioxide, steam, air, ammonia or mixture of these gases at high temperature range of 500 to 1200 ^{o}C. The chemical activation involves the use of activating

agents like phosphoric acid, sulfuric acid, potassium hydroxide, zinc chloride and sodium hydroxide at a temperature range of 400 to 850 ^{o}C [9]. Surface area, porosity and pore-size distribution of the resulting carbon material can be controlled by variation of time, temperature, activating agent and gas environment during activation. These parameters have an influence on the performance of the produced carbon material.

Carbon nanotube (CNT) is an additional allotrope of carbon achieved by disintegration of a certain hydrocarbon through chemical reactions by varying synthesis conditions. They have been studied as a unique electrode material for supercapacitor applications owing to its great potential contributed by the readily available surface area [81]. CVD [82], laser ablation [83], arc discharge [84] are some of the approaches used to produce CNTs with good chemical and mechanical stability, distinctive pore structure and excellent conductivity. CNTs can be labelled as a single-walled carbon nanotubes (SWCNTs) and multi-walled carbon nanotubes (MWCNTs). The former is originated from one dimensional, cylindrical shaped allotropes of carbon with an approximate dimeter of 1 nm while the latter is derived as a hollow, cylindrically shaped allotropes of carbon with high length to diameter ratio made by multiple one-atom-thick sheets of carbon [81]. They can be fabricated directly on the conductive substrates to be used as electrodes and hence improve the electrochemical performance due to the available surface area which allow the passage of the electrolyte's ions.

2.4.2 Transition metals oxides/hydroxides (TMOs/TMOHs)

Transition metals oxides/hydroxides are studied as a potential material for supercapacitor fabrication due to high theoretical specific capacity/capacitance from fast redox reactions occur between the electrode and electrolyte [85]. These materials are considered as a possible pseudocapacitive due to their very fast reversible reaction with electron transfer without phase

transformation of the molecules within the electrode material which do not engage in creating or breaking of chemical bonds. Basically, the de-solvated ions which provides the pseudo-capacitance in TMOs/TMOHs hold on to the atomic structure of the electrode, and changes are spread on the surface of the electrode material by adsorption processes. The redox process in TMOs/TMOHs is faster and more stable over time, however, it leaves traces of reaction products which produce capacity/capacitance degradation. The pseudocapacitive behavior of a TMOs/TMOHs result into the charge-dependent and linear capacitive behavior unlike TMOs/TMOHs in Faradic (batteries) which have charge independent behavior. The reversibility of these material can be shown by the cyclic voltammetry (CV) curves, which indicates that symmetric redox peaks are considerably different from the rectangular CV curves in EDLCs. Different TMOs/TMOHs have been investigated as the electrode material for supercapacitors applications. These include; cobalt oxide (Co_3O_4) [86], manganese oxide (MnO_2) [87], cobalt hydroxide ($Co(OH)_2$) [88], nickel oxide (NiO) [89], ruthenium oxide (RuO_2) [90], nickel hydroxide ($Ni(OH)_2$ [91] and tin oxide (SnO_2) [92]. Precisely, MnO_2 and Co_3O_4 as a TMOs has been well-established as the electrode material for supercapacitor applications due to several oxidation states, high redox reactivity, high specific capacitance/capacity, high stability, easily tunable surface properties, readily available/cost-effectiveness, and non-toxicity [93][94]. Conversely, they are encountered with low conductivity, poor cycling, mechanical degradation and agglomeration of particles at high mass loading [95]. These drawbacks can be solved by combining the TMOs with highly conductive EDLCs material like graphene so as to enhance their electrochemical properties by the synergy effect between the two materials.

2.4.3 Conducting polymers (CPs)

Conducting polymers are organic polymers that used as electrode material for supercapacitors and charges are stored and released by redox process. In CPs charges are stored under fast and reversible redox reactions at the surface and bulk of the electrodes from which ions are transferred to the polymer by oxidation (p-doping) and released back into the solution by reduction (n-doping). The electron transfer from polymer to dopants classified as a p-doping is stronger than n-doping due to high stability which prevent it from degradation [96]. These materials can be synthesized by chemical polymerization or electropolymerisation of the corresponding monomers. For supercapacitor applications, the main studied CPs are polypyrrole (PPy) [97], poly(3,4 ethylenedioxythiophene) (PEDOT) [98], polythiophene (PT) [99], and polyaniline (PANI) [100][101]. These materials are characterized by high porosity, high conductivity, wide potential window, environmentally friendly and low equivalent series resistance compared to EDLCs materials. These exceptional properties make CPs as a great potential material which deliver high capacitance consequently high specific energy and specific power. However, their application in supercapacitor is limited by mechanical stress experienced during redox reactions and lack of efficient n-doped which results into poor rate capability and poor cycling stability [101]. Thus, researchers have suggested the addition of carbon-based materials as the means to retain the stability of the CPs. Beside other CPs, PANI is the best candidate due to an outstanding conductivity, facile synthesis procedure, easy control of redox states, and high theoretical capacitance of up to 2000 F g^{-1} [100].

2.4.4 Composites

EDLCs material has high conductivity and store charges on the surface of the electrode at a constant potential, although they are plagued with low specific capacitance [102]. On the other hand, redox reactions facilitate the storage mechanism in pseudocapacitive material which

results into high specific capacitance, however, they are limited with poor charge transfer ability [94]. Therefore, a composite material is produced by integrating the properties of two materials being either EDLCs and/or pseudocapacitive in order to make the resulting material with superior properties. Composites material has several essential features like extended potential window, high specific surface area, and high conductivity which occur as the result of the combined synergy effect of the two materials. Among the EDLCs material for instance conductive graphene can perform as means for charge transfer in pseudocapacitive materials like TMOs (MnO_2 and Co_3O_4) and enhance the whole conductivity as a result of improved electrochemical properties. An introduction of highly conductive and stable matrix like graphene has been established in the literature as potential materials to enhance the electrochemical performance of the electrode materials. The incorporation of GF into TMOs results in a synergistic effect, which facilitates the dispersion of TMOs and serves as extensive transport platform for electrolyte ions. This in turn robust three-dimensional network, eliminates particles aggregation and minimizes ion diffusion resistance and adequate electrode/electrolyte contact [10].

2.5 Electrolytes

Electrolyte is considered as one of the most essential components which influence the electrochemical performance of supercapacitors. The interaction between electrode and electrolyte, interaction between ion concentration and solvent, ion type and size play a significant role on the formation of EDLCs or PCs nature [103]. The selection of electrolytes depends on the following requirements; high ionic conductivity, wide-ranging working temperature, low viscosity, wide operating potential window, volatility, accessibility at high purity, environmentally friendly, cost effectiveness, and high chemical and electrochemical stability [104]. Each requirement contributes in one way or another on the performance of

supercapacitor. For example, high ionic conductivity contributes to low equivalent series resistance (ESR) which strongly influence specific power. Additionally, the highest working potential window is controlled by the electrochemical stability of the electrolytes, which in turn limits the specific energy and specific power stored in supercapacitors [105]. So far, the frequently liquid electrolytes used in supercapacitors are; aqueous, ionic and organic liquid electrolytes, however, researchers have reported new electrolytes named as solid state and gel electrolytes [103]. Up to now, there is no perfect electrolyte that meets all the requirements; hence each has its own advantages and disadvantages as described below.

2.5.1 Aqueous electrolytes (AEs)

Aqueous electrolytes are formed by dissociating solute into water to form ions which results into a solution with ionic conductivity. They consist of basic (eg. KOH), acidic (eg. H_2SO_4) and neutral electrolytes (eg. Na_2SO_4) which are; easy to prepare, non-corrosive, less expensive, environmentally friendly and non-flammable. Furthermore, they have high ionic conductivity which is influenced by pressure, molar concentration and temperature of the solute [106][107]. For example, AEs with high molar concentration consequently will have high ionic conductivity which supports low ESR, which in turn increases specific power. Generally, the specific capacitance of EDLCs material is higher in AEs due to high dielectric constant and small solvated ions. However, the working potential window is limited by electrolysis of water which results into hydrogen evolution reaction (HER) at low potential (0 V) and oxygen evolution reaction (OER) at high potential (~ 1.23 V), hence restricts the specific energy. Additionally, the working temperature range of AEs is limited due to freezing of electrolyte at low temperature [108]. The AEs can be improved by adding low concentration of surfactant like tetrapropylammonium (TPAB). This reduces viscosity in the interface of the electrode and electrolyte, thus allow electrolyte ions to penetrate easily into the pores of the material [109].

2.5.2 Ionic liquid electrolytes (ILEs)

Ionic liquid electrolytes are molten salt constitute of cations and anions whose melting point is below 100 ^{o}C [110]. These molten salts (like aliphatic ammonium salts, quaternary ammonium salts) have distinctive ion size due to lack of solvent and related solvation shells. They are characterized by high electrochemical and thermal stability, non-volatile, wide potential window (~ 6 V) and low vapor pressure [111]. However, they are limited by high viscosity at low temperature which reduces its conductivity and then specific capacitance. Furthermore, ILEs has low ionic conductivity which results into high ESR, thus, affects power output. On the other hand, due to large variation of anions and cations, ILEs are non-flammable and allow easily tunable physical and chemical properties. This provides an important improvement so as to meet certain requirements like working temperature, operating potential window and low ESR which has influences on the electrochemical performance of supercapacitor [112].

2.5.3 Organic electrolytes (OEs)

Organic electrolytes are formed when conducting salts is dissolved into organic solvents like butylene carbonate (BC), propylene carbonate (PC) or acetonitrile (ACN) in order to produce highly conductive electrolytes. They are usually used in commercial applications due to large working potential window of about ~ 3.5 V normally, water content should be less than 3 – 5 ppm so as to maintain large working potential window [113]. The performance of supercapacitor in OEs is influenced by the nature of salts and solvents like high conductivity, electrochemical stability, ion size, low viscosity, and interaction between ions and solvents [114]. However, toxicity, high flammability, volatility and environmental instability limits their application in supercapacitor as they require special precautions during operation so as to avoid explosion and poisoning [115].

2.6 Electrode fabrication and testing

Electrode fabrication in supercapacitor is done by mixing together active material, conducting agent and binder using a determined mass ratio of either 8:1:1 or 7:1.5:1.5 or 8:1.5:0.5 for the three materials. Conducting agent (carbon acetylene black - CAB or carbon black - CB) is used to enhance conductivity of the active material [116] while binder (polyvinylidene fluoride – PVDF or polytetrafluoroethylene - PTFE) is used to bind the active material into the current collector [117]. Then, a small amount of solvent (N-methyl-2-pyrrolidone - NMP) is added to the mixture to form a homogenous slurry which is pasted onto a nickel foam/carbon paper which act as a current collector and exposed to drying process. The choice of current collector depends on the type of the electrolyte used in a specific measurement. Specifically, carbon paper is usually used with acidic electrolyte like H_2SO_4, while nickel foam is used with basic and neutral electrolyte such as KOH, Na_2SO_4, and KNO_3. Thereafter, the electrochemical evaluation of the working electrode is achieved using three (half-cell) or two-electrode (full cell) configuration.

2.6.1 Three-electrode measurements

Principally, the three-electrode set-up is used to establish the primary electrochemical properties of the working electrode. Specifically, an equivalent series resistance, operating potential window, specific capacity/capacitance and cycling performance are the main properties reviewed by three-electrode set-up [118]. The set-up comprises of counter electrode (CE), reference electrode (RE), working electrode (WE) and electrolyte as displayed in figure 2.5 [119]. Counter electrode is normally from inert materials, like graphite, glassy carbon or platinum which are very conductive and have very high surface area. CE offers a means of applying voltage to the working electrode and allow the generated current to flow through without passing it to the reference electrode. Normally, CE does not participate in the

electrochemical reaction. Reference electrode is made up by silver/silver chloride (Ag/AgCl) or saturated calomel electrode (SCE) or mercury/mercury oxide, which are stable with a well-known electrode potential. The function of RE is to allow measuring of potential of the working electrode without passing current through it. Working electrode is the electrode of concern fabricated from either carbon-based material, metal oxide or conducting polymer, and which the evaluation is done.

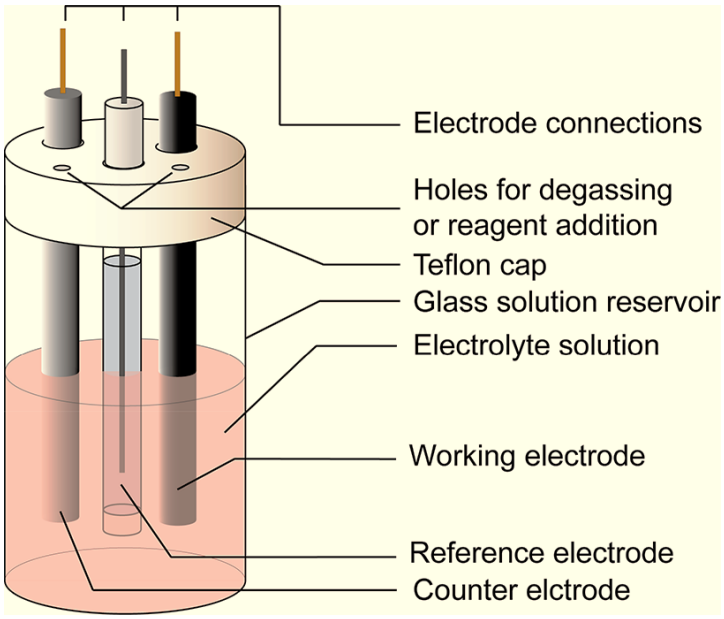

Figure 2.5: Schematic illustration of a three-electrode set-up with a working electrode (WE), counter electrode (CE) and reference electrode (RE) [119].

2.6.2 Two-electrode measurements

Two-electrode set-up is used to evaluate the electrochemical properties of the working material for practical applications in supercapacitor. Some of the properties evaluated are specific energy, specific power and cycling stability [120]. The set-up consists of positive and negative electrode, separator, electrolyte, spring, spacer, and positive and negative case as shown in

Figure 2.6. The positive and negative electrode are sandwiched by a separator and electrolyte in between, then, squeezed by spring and spacer to maintain a tight contact of the device. The positive and negative electrodes might be of the same materials which results into symmetric device or different materials hence asymmetric device [15][54].

The symmetric device is made up by the same material in both negative and positive electrodes whereby both electrodes have the same capacity/capacitance. The specific capacity and capacitance are calculated from the following expressions respectively [121] [122]:

$$Q_s = \frac{\Delta t \times I_d}{3.6} \text{ [mAh g}^{-1}\text{]} \quad (2)$$

$$C_s = \frac{\Delta t \times I_d}{\Delta V} \text{ [F g}^{-1}\text{]} \quad (3)$$

where; I_d indicates the applied specific currents (A g^{-1}), Δt signifies the discharge time (s), ΔV stands for operating potential (V), Q_s represents specific capacity and C_s presents specific capacitance.

For a linear charge/discharge profile, the specific energy (E_d) can be evaluated using the following equation [123]:

$$E_d = \frac{1}{2} C_s \Delta V^2 = \frac{C_s \times \Delta V^2}{7.2} \text{ [Wh kg}^{-1}\text{]} \quad (4)$$

Whereas, for non-linear charge/discharge profile, the specific energy (E_d) can be estimated as [124]:

$$E_d = \frac{I}{3.6 * m} \int V dt \text{ [Wh kg}^{-1}\text{]} \quad (5)$$

where, I is the applied current (mA), $\int V dt$ is the area under discharge curve, m (mg) is the total mass of the active electrode and E_d is the specific energy.

The following expression can be applied to evaluate the specific power (P_d) of the device as shown below:

$$P_d = \frac{E_d}{\Delta t} \times 3600 \ \text{[W kg}^{-1}\text{]} \quad (6)$$

where, E_d is the specific energy and Δt presents the discharge time.

For the asymmetric device, the negative and positive electrodes have same/different materials hence both electrodes demonstrate different capacity/capacitance, whereby one of them is higher than the other. Since the working voltage window of the asymmetric device depend on the capacity/capacitance of the working material in each electrode, then the mass balance plays an important role so as to balance the charge of each electrode. For the asymmetric device with one electrode displaying linear charge/discharge curve, and the other electrode displaying non-linear charge/discharge curve, the mass balance on each electrode should be evaluated differently [125].

For both positive and negative electrodes with linear charge/discharge curve, the charge balance equation, $Q_+ = Q_-$ can be used to balance the mass of each electrode with the charge stored on each electrode being stated as [126]:

$$Q = C_s \times m\,\Delta V \quad (7)$$

From the above, the mass balance of each electrode can be determined as

$$\frac{m_+}{m_-} = \frac{C_{s-}\ \Delta V_-}{C_{s+}\ \Delta V_+} \quad (8)$$

For positive electrode with non-linear charge/discharge profile and negative electrode with linear charge/discharge profile, the mass on each electrode can be evaluated using the charge balance equation, as described below [15]:

$$Q_+ = Q_- \Longrightarrow m_+ \times 3.6Q_{s+} = m_- \times \Delta V_- \times C_{s-} \Longrightarrow \frac{m_-}{m_+} = \frac{3.6 \times Q_{s+}}{\Delta V_- \times C_{s-}} \quad (9)$$

where; Q_+ and Q_-: charge stored on the positive and negative electrode, respectively, Q_{s+}: specific capacity for positive electrode, C_{s-} specific capacitance for the negative electrode, ΔV_-: potential window for the negative electrode, m_+ and m_- stands for masses (mg) for the positive and negative electrodes.

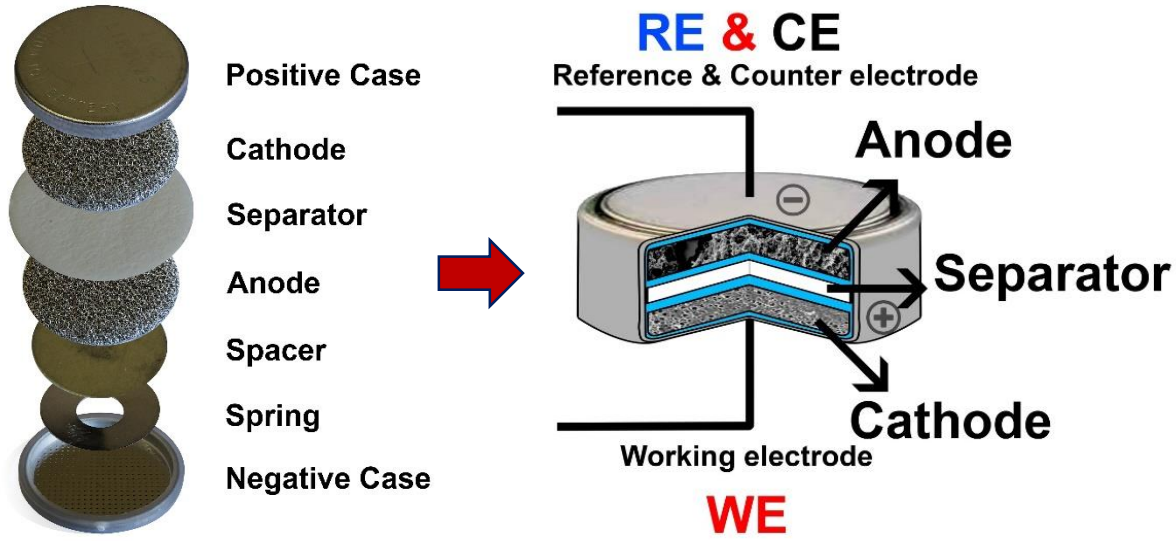

Figure 2.6: Schematic design of a two-electrode set-up

2.7 Electrochemical evaluation

The cyclic voltammetry (CV), galvanostatic charge/discharge (GCD), and electrochemical impedance spectroscopy (EIS) are the main test techniques frequently used to evaluate the electrochemical performance of the working electrode in supercapacitors. Additionally, another test known as stability test which involves charge/discharge cycling, voltage holding, and self-discharge is used to provide more understanding on the performance of supercapacitor [120]. On the other hand, current, voltage and time are the basic essential parameters measured by these techniques regardless of either the measurement is done in three or two electrode configurations.

2.7.1 Cyclic voltammetry (CV)

Cyclic voltammetry (CV) is the most unique technique applied in electrochemical measurements to evaluate the performance of the working electrode in three and two electrodes set up. It offers the description about the reversibility of the electrode and the reaction mechanism (adsorption-controlled or diffusion-controlled process) occurring at the surface of the working electrode [127]. For example, Figure 2.7 [128], illustrate the mechanism behavior displayed by the working electrode, through which the EDLCs materials are presented by the rectangular shape (Figure 2.7 (a) - red line) without redox peak indicating the ideal capacitive behavior. However, the twist of the rectangular shape to parallelogram (Figure 2.7 (a) - black line) indicates the resistivity of the material. The pseudocapacitive materials are presented by either rectangular CV curve, quasi-rectangular CV curve or CV curve with highly reversible and significantly broadened peaks (Figure 2.7 (b)). Hybrid materials presents the CV shape indicating combination of either one or both the EDLCs, pseudocapacitive or battery type behavior. Normally, the hybrid device with EDLCs behavior displays rectangular shape, while the one with combination of supercapacitive and battery-like behavior shows a moderately quasi-rectangular CV with hump for the redox peaks. The CV curve (Figure 2.7 (c)) of the battery type material is demonstrated by the distinct redox peaks signifying the Faradic behavior of the material. The CV curve measures the current of the working electrode as the function of the applied potential/voltage and the resulting current response can be plotted as a function of potential/voltage. This is performed at different scan rates (rate of change of potential/voltage with time) so as to explore the behavior of the working electrode from low to high scan rate [129]. Additionally, the CV measurement is commonly applied for EDLCs material to investigate the stability of the working potential/voltage window in a specific electrolyte. The resulting capacitance from the CV curve is known as gravimetric specific capacitance, and is estimated using the following equation [130]:

$$C_s = \frac{\int(I_D \times dV)}{\nu \times \Delta V} \text{ [F g}^{-1}\text{]} \quad (10)$$

where; I_D – gravimetric specific current (A g^{-1}), ν – scan rate (mV s^{-1}) and ΔV – working potential (V).

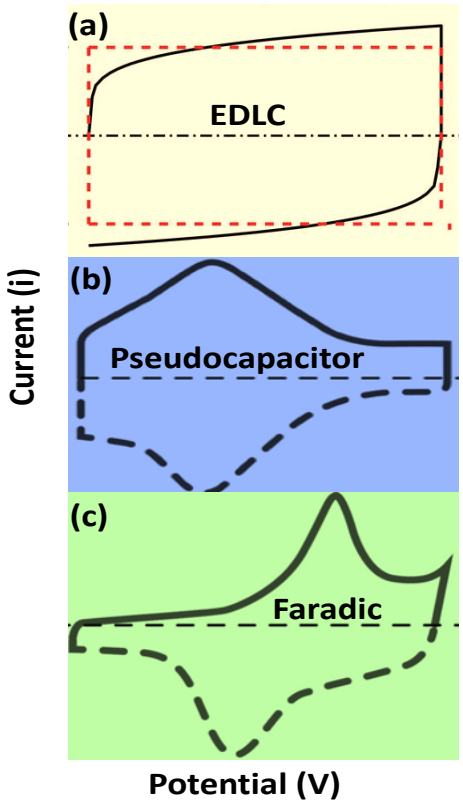

Figure 2.7: Schematic sketch of CV curves for (a) EDLC, (b) Pseudo-capacitor and (c) Faradic material [128].

2.7.2 Galvanostatic charge/discharge (GCD)

The galvanostatic charge/discharge is the best technique used to evaluate and predict the working conditions of the practical supercapacitor. The variation of potential/voltage as function of time is recorded from the GCD curve when a constant current is applied to the working electrode, and the electrode is charged and discharged between the boundaries of the two potential/voltage [131]. Furthermore, normally the outer surface of the working electrode

contributes to the charge/discharge process at high current while at low current both outer and inner sites will be accessed by the electrolyte ions. Corresponding to CV curve, EDLCs, pseudocapacitive, hybrid and battery systems present a distinctive response in a GCD curve (Figure 2.8) [132], with voltage increasing and decreasing linearly as the current flows for EDLCs and some pseudocapacitive materials (Figure 2.8 (a)). On the other hand, certain pseudocapacitive and hybrid materials present non-linear GCD curve with one or more small slanted potential/voltage plateau regions (Figure 2.8 (b)) while battery material reveal prolonged potential/voltage plateau with a clear redox peak on the GCD curve (Figure 2.8 (c)). Besides, the GCD measurement is used to assess the working potential/voltage, stability limit of the electrode and electrolyte, specific capacitance, specific capacity, specific energy, specific power, rate capability and efficiency of the working electrode [133]. For example, the working potential/voltage can be established by increasing the potential/voltage gradually (charging process) till a spike is spotted then change to discharging process so as to conserve the stability of the working electrode. This is because during charging process, the plateau observed at high potential/voltage indicates that the current is consumed by the decomposition of solvent. Therefore, the optimum working potential/voltage is an essential component in determining the electrochemical performance of the working electrode and reducing the negative impact of the decomposition of electrode and/or electrolyte [134].

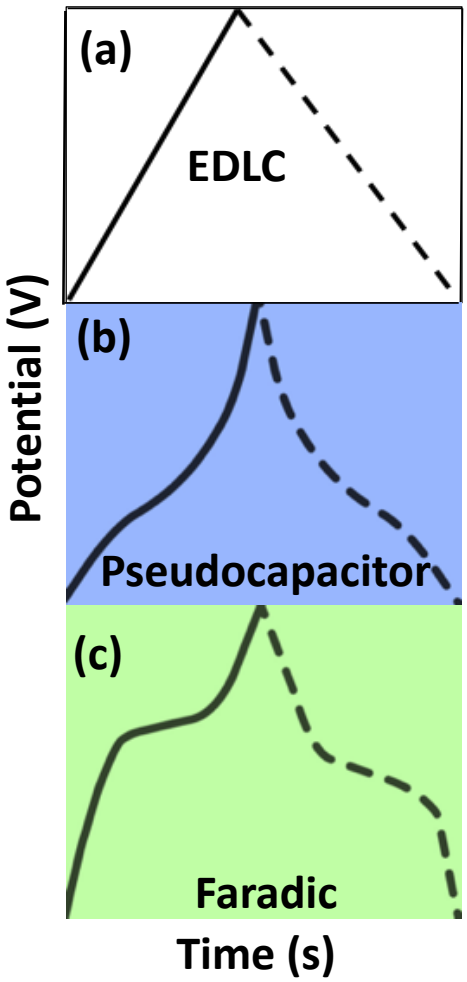

Figure 2.8: Schematic sketch of GCD curves for (a) EDLC, (b) Pseudo-capacitor and (c) Faradic material [128] [132].

2.7.3 Electrochemical impedance spectroscopy (EIS)

Electrochemical impedance spectroscopy is a fundamental technique for evaluating the impedance of a working electrode in dependency of the AC potentials frequency or open circuit potential. It measures the impedance of a working electrode as a function of frequency at a set potential/voltage. EIS response provides information about the structure, interface and reaction taking place within the working electrode [128] [135]. Generally, a small amplitude sinusoidal potential (mV) superimposed is initiated over a broad range of frequency (mHz to kHz) and the resultant impedance is recorded as a function of modulation frequency. The displayed

signals of an EIS report is properly denoted as a Nyquist plot (imaginary versus real part of the impedance) or Bode plot (magnitude and phase response versus frequency). The report can be applied to evaluate the solution resistance (R_Ω)/equivalent series resistance (ESR), charge transfer resistance (R_{CT}), and double layer capacitor (C_{DL}) of the working electrode [136].

The Nyquist plot is normally represented as the imaginary part (Z (ω)'') versus real part (Z (ω)') of the impedance and is classified into three sections which are; low, medium and high-frequency regions as shown in Figure 2.8 [137][138].

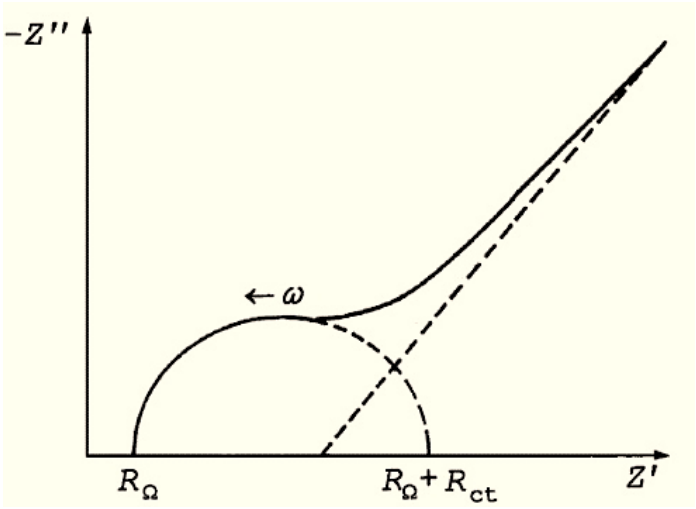

Figure 2.8: Schematic illustration of imaginary impedance (Z'') versus real impedance (Z') [139].

At low frequency region (< 1 Hz), the impedance plot signifies features of a pure capacitive behavior in which a straight line parallel to the imaginary (Z') x-axis is noticed (i.e. double layer capacitor (C_{DL}) has very high impedance). However, this is not always the case as the performance of the working electrode is influenced by other factors like ion diffusion process which make the straight line to shift slightly about 45^o to 90^o. Therefore, the impedance contribution at the point where the right end of the semi-circle would hit the 0 of the y-axis is

a solution resistance (R_Ω) plus charge transfer resistance (R_{CT}) ($R_\Omega + R_{CT}$). Hence, R_Ω and R_{CT} can be easily obtained by reading the value from semicircle. Moreover, the double layer capacitor (C_{DL}) can be estimated from the frequency at the maximum point of semi-circle as follows [140]:

$$C_{DL} = \frac{1}{R_{CT} 2\pi f_{max}} \tag{11}$$

The medium frequency region (10 Hz – 1 Hz) displays charge transfer resistance linked to the porosity of the working electrode in pseudocapacitive material. At high frequency region (> 10^4 Hz), the intercept of the real (Z') x-axis in the impedance plot provides information about equivalent series resistance (ESR)/solution resistance (R_Ω). Normally, the presence of small semicircle at high-frequency region is contributed by the charge transfer resistance (R_{CT}) and mass transport within the working electrode [141].

Furthermore, by varying frequency in the EIS, it generates sufficient performance on different conduction pathways in an equivalent circuit. This implies that physical and chemical properties of the working electrode can be modified by varying frequency so that, it can perform like pure capacitor or resistor. This analysis can be done by fitting the experimental data to an appropriate equivalent circuit model (see Figure 2.9 as an example). The equivalent circuit should be simple to provide the best corresponding impedance model and experimental impedance. Frequently circuit elements used in equivalent circuit models are capacitance (C), resistance (R), constant phase element (CPE) and Warburg coefficient (W) [142]. Usually, capacitance involve double layer capacitance (C_{DL}) which appear as ions from the electrolyte stick between the surface of the working electrode and electrolyte. Furthermore, the resistance consists of charge transfer resistance (R_{CT}) which appear on the surface of the electrode in the electrochemical double layer; polarization resistance (R_P) which results from an open-circuit

when the potential of an electrode is forced away from its value; ohmic resistance (R_Ω) occur as a result of a potential drop between working electrode and reference electrode; and equivalent series resistance (ESR)/solution resistance (R_Ω) which comprises of contact resistance between the working electrode and the current collector, and the interface resistance of the working electrode and ions from the electrolyte [123]. Constant phase element (CPE) is used to model the double layer behavior, and it arises when the capacitor behaves as a pure capacitor or pure resistor or Warburg element. The Warburg coefficient (W) is connected with CPE which describes the diffusion element that can be applied to model semi-infinite linear diffusion.

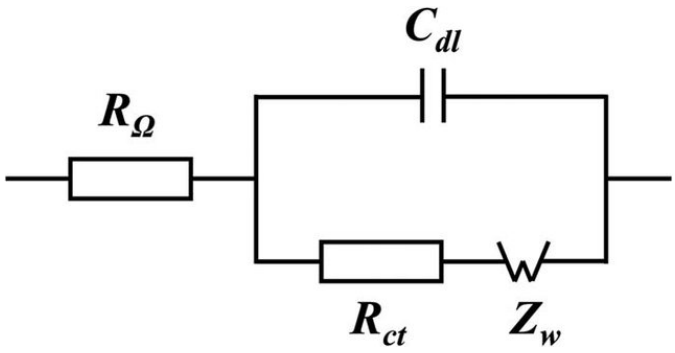

Figure 2.9: Schematic drawing of an equivalent circuit model for EIS analysis [143].

The Bode plot displays the magnitude and phase response versus frequency of the working electrode [138]. In a Bode plot, the capacitor in parallel to a resistor is noted easily as the peak in the phase shift. The ion diffusion mechanism between the ideal capacitive ion diffusion and Warburg diffusion has developed a Bode plot with a crooked line with regard to the real x-axis with the angle of $45^o \leq \theta \leq 90^o$. The capacitance can be evaluated from the linear part of Bode plot as shown below [138]:

$$C = \frac{1}{2\pi f|Z''|} \quad (12)$$

2.7.4 Stability test (charge/discharge cycling, voltage holding, and self-discharge)

The galvanostatic charge/discharge cycling (GCDC) is a regular technique employed to evaluate the electrochemical performance and cycle life of the working electrode in a three- and two-electrode configurations. Normally, the working electrode is exposed to a number of charged/discharge cycles, whereby the cycling performance relies on the working potential/voltage boundary, electrolyte, current applied, and temperature [144]. For EDLCs, the discharge time of each cycle divided by the charging time multiply by 100 % present the columbic efficiency (C_E - %) as shown in the equation below:

$$C_E = \frac{t_D}{t_c} \times 100\ \% \quad (13)$$

where; t_c, t_D, and C_E (%) are times for charging and discharging times with the same current, as well as the columbic efficiency, respectively.

Usually, the columbic efficiency of the ideal supercapacitor remains at 100 %, however it's not always the case for normal supercapacitor due to different factors like conductivity and decomposition of the electrode and electrolyte. For pseudo-capacitor and/or Faradic efficiency (η_E - %) is applied to study the cycling performance of the device as indicated below [145]:

$$\eta_E = \frac{E_d}{E_c} \text{ x } 100\ \% \quad (14)$$

E_c, E_d and η_E are charge energy, discharge energy and energy efficiency, respectively.

Voltage holding/floating test (VH/FT) is the best technique compared to normal stability test as it provides more information about the decomposition of the material which might occur during stability test [146]. Usually, the device is charged and discharged for few cycles and the specific capacitance is monitored. Thereafter, the device is held at a maximum voltage for a specified interval of time, then subjected to charge and discharge again for few cycles and left

at that fixed potential for the next specified interval of time. The process is repeated until the device shows dissimilar performance within the specified period [147].

Self-discharge (SD) is the voltage drop of a fully charged device without load after a certain period of time in an open circuit. This behavior is caused by an efficient thermodynamic driving force which manages to move charges into the equilibrium state. SD is used to assess the energy loss in the device over a certain period of testing and measure the reduction in capacitance and voltage. Normally, the device is charged for several hours to a maximum voltage, and then left to discharge in an open circuit in without of load connection [148]. Generally, SD process occurs under one/combination of these mechanisms; charge redistribution, parasitic Faradic reaction and ohmic leakage of current between the electrodes [149].

REFERENCES

[1] J.W. Lund, 100 Years of Geothermal Power Product, Proceedings. (2005) 1–10.

[2] T. Ma, H. Yang, L. Lu, Development of hybrid battery-supercapacitor energy storage for remote area renewable energy systems, Applied Energy. 153 (2015) 56–62. https://doi.org/10.1016/j.apenergy.2014.12.008.

[3] G. Kayakutlu, E. Mercier-Laurent, 3 - Intelligence for Energy, in: G. Kayakutlu, E. Mercier-Laurent (Eds.), Intelligence in Energy, Elsevier, 2017: pp. 79–116. https://doi.org/https://doi.org/10.1016/B978-1-78548-039-3.50003-1.

[4] A.R. Dehghani-Sanij, E. Tharumalingam, M.B. Dusseault, R. Fraser, Study of energy storage systems and environmental challenges of batteries, Renewable and Sustainable Energy Reviews. 104 (2019) 192–208. https://doi.org/10.1016/j.rser.2019.01.023.

[5] X. Zhang, L. Hou, A. Ciesielski, P. Samorì, 2D Materials Beyond Graphene for High-Performance Energy Storage Applications, Advanced Energy Materials. 6 (2016) 21. https://doi.org/10.1002/aenm.201600671.

[6] R.B. Rakhi, H.N. Alshareef, Enhancement of the energy storage properties of supercapacitors using graphene nanosheets dispersed with metal oxide-loaded carbon nanotubes, Journal of Power Sources. 196 (2011) 8858–8865. https://doi.org/10.1016/j.jpowsour.2011.06.038.

[7] A. Eftekhari, Metrics for Fast Supercapacitors as Energy Storage Devices, ACS Sustainable Chemistry and Engineering. 7 (2019) 3688–3691. https://doi.org/10.1021/acssuschemeng.7b04532.

[8] K.W. Nam, C.W. Lee, X.Q. Yang, B.W. Cho, W.S. Yoon, K.B. Kim, Electrodeposited manganese oxides on three-dimensional carbon nanotube substrate: Supercapacitive behaviour in aqueous and organic electrolytes, Journal of Power Sources. 188 (2009) 323–331. https://doi.org/10.1016/j.jpowsour.2008.11.133.

[9] P. Simon, Y. Gogotsi, P. Simon, Y. Gogotsi, N. Materials, Materials for electrochemical capacitors To cite this version : HAL Id : hal-02417326, 7 (2019) 845–854.

[10] M. Vangari, T. Pryor, L. Jiang, Supercapacitors: Review of materials and fabrication methods, Journal of Energy Engineering. 139 (2013) 72–79. https://doi.org/10.1061/(ASCE)EY.1943-7897.0000102.

[11] M. Hahn, O. Barbieri, R. Gallay, R. Kötz, A dilatometric study of the voltage limitation of carbonaceous electrodes in aprotic EDLC type electrolytes by charge-induced strain, Carbon. 44 (2006) 2523–2533. https://doi.org/10.1016/j.carbon.2006.05.002.

[12] M. Jayalakshmi, K. Balasubramanian, Simple capacitors to supercapacitors - An overview, International Journal of Electrochemical Science. 3 (2008) 1196–1217.

[13] Xian Jian, Shiyu Liu, Yuqi Gao, Wei Tian, Zhicheng Jiang, Xiangyun Xiao, Hui Tang, Liangjun Yin, Carbon-Based Electrode Materials for Supercapacitor: Progress, Challenges and Prospective Solutions, J. of Electrical Engineering. 4 (2016) 75–87. https://doi.org/10.17265/2328-2223/2016.02.004.

[14] S. Najib, E. Erdem, Current progress achieved in novel materials for supercapacitor electrodes: Mini review, Nanoscale Advances. 1 (2019) 2817–2827. https://doi.org/10.1039/c9na00345b.

[15] A. Noori, M.F. El-Kady, M.S. Rahmanifar, R.B. Kaner, M.F. Mousavi, Towards establishing standard performance metrics for batteries, supercapacitors and beyond, Chemical Society Reviews. 48 (2019) 1272–1341. https://doi.org/10.1039/c8cs00581h.

[16] B. Viswanathan, Chapter 13 - Supercapacitors, in: B. Viswanathan (Ed.), Energy Sources, Elsevier, Amsterdam, 2017: pp. 315–328. https://doi.org/https://doi.org/10.1016/B978-0-444-56353-8.00013-7.

[17] G.Z. Chen, Supercapacitor and supercapattery as emerging electrochemical energy stores, International Materials Reviews. 62 (2017) 173–202. https://doi.org/10.1080/09506608.2016.1240914.

[18] A.S. Lemine, M.M. Zagho, T.M. Altahtamouni, N. Bensalah, Graphene a promising electrode material for supercapacitors—A review, International Journal of Energy Research. 42 (2018) 4284–4300. https://doi.org/10.1002/er.4170.

[19] M.E. Uddin, T. Kuila, G.C. Nayak, N.H. Kim, B.C. Ku, J.H. Lee, Effects of various surfactants on the dispersion stability and electrical conductivity of surface modified graphene, Journal of Alloys and Compounds. 562 (2013) 134–142. https://doi.org/10.1016/j.jallcom.2013.01.127.

[20] Y. Bai, L. Lu, J. Bao, G. Sun, B. Zhang, J. Zeng, S. Chen, The preparation and electrochemical performance of nitrogen-doped graphene/Co(OH)2 composite, International Journal of Electrochemical Science. 14 (2019) 606–617. https://doi.org/10.20964/2019.01.48.

[21] Z. Lin, Y. Liu, Y. Yao, O.J. Hildreth, Z. Li, K. Moon, C.P. Wong, Superior capacitance of functionalized graphene, Journal of Physical Chemistry C. 115 (2011) 7120–7125. https://doi.org/10.1021/jp2007073.

[22] N.A. Kumar, J.B. Baek, Doped graphene supercapacitors, Nanotechnology. 26 (2015). https://doi.org/10.1088/0957-4484/26/49/492001.

[23] S. Verma, B. Verma, Synthesis of sulfur / phosphorous-doped graphene aerogel as a modified super capacitor electrode, (2018).

[24] S. Yaglikci, Y. Gokce, E. Yagmur, Z. Aktas, The performance of sulphur doped activated carbon supercapacitors prepared from waste tea, Environmental Technology. 0 (2019) 1–13. https://doi.org/10.1080/09593330.2019.1575480.

[25] X. Yu, S.K. Park, S.H. Yeon, H.S. Park, Three-dimensional, sulfur-incorporated

graphene aerogels for the enhanced performances of pseudocapacitive electrodes, Journal of Power Sources. 278 (2015) 484–489. https://doi.org/10.1016/j.jpowsour.2014.12.102.

[26] W. Zhang, F. Liu, Q. Li, Q. Shou, J. Cheng, L. Zhang, B.J. Nelson, X. Zhang, Transition metal oxide and graphene nanocomposites for high-performance electrochemical capacitors, Physical Chemistry Chemical Physics. 14 (2012) 16331–16337. https://doi.org/10.1039/c2cp43673f.

[27] Y. Wang, J. Guo, T. Wang, J. Shao, D. Wang, Y.W. Yang, Mesoporous transition metal oxides for supercapacitors, Nanomaterials. 5 (2015) 1667–1689. https://doi.org/10.3390/nano5041667.

[28] Y.T. Wang, A.H. Lu, H.L. Zhang, W.C. Li, Synthesis of Nanostructured mesoporous manganese oxides with three-dimensional frameworks and their application in supercapacitors, Journal of Physical Chemistry C. 115 (2011) 5413–5421. https://doi.org/10.1021/jp110938x.

[29] M. Pang, G. Long, S. Jiang, Y. Ji, W. Han, B. Wang, X. Liu, Y. Xi, D. Wang, F. Xu, Ethanol-assisted solvothermal synthesis of porous nanostructured cobalt oxides (CoO/Co3O4) for high-performance supercapacitors, Chemical Engineering Journal. 280 (2015) 377–384. https://doi.org/10.1016/j.cej.2015.06.053.

[30] P. Simon, Y. Gogotsi, Materials for electrochemical capacitors, Materials for Sustainable Energy: A Collection of Peer-Reviewed Research and Review Articles from Nature Publishing Group. (2010) 138–147. https://doi.org/10.1142/9789814317665_0021.

[31] Z. Song, Y. Zhang, W. Liu, S. Zhang, G. Liu, H. Chen, J. Qiu, Hydrothermal synthesis and electrochemical performance of Co 3O4/reduced graphene oxide nanosheet composites for supercapacitors, Electrochimica Acta. 112 (2013) 120–126.

https://doi.org/10.1016/j.electacta.2013.08.155.

[32] Q. Yang, Z. Li, R. Zhang, L. Zhou, M. Shao, M. Wei, Carbon modified transition metal oxides/hydroxides nanoarrays toward high-performance flexible all-solid-state supercapacitors, Nano Energy. 41 (2017) 408–416. https://doi.org/10.1016/j.nanoen.2017.09.049.

[33] Y. Chiang, Electrochemical Energy Storage for the Grid, World. (2010).

[34] M.S. Whittingham, History, evolution, and future status of energy storage, Proceedings of the IEEE. 100 (2012) 1518–1534. https://doi.org/10.1109/JPROC.2012.2190170.

[35] O. Razbani, M. Assadi, Artificial neural network model of a short stack solid oxide fuel cell based on experimental data, Journal of Power Sources. 246 (2014) 581–586. https://doi.org/10.1016/j.jpowsour.2013.08.018.

[36] P.N. Kanani, The Parthian Battery: Electric current 2000 years ago?, Fachzeitschrift Des VINI. (2004) 38.

[37] D.S. Ginley, D. Cahen, Fundamentals of materials for energy and environmental sustainability, Fundamentals of Materials for Energy and Environmental Sustainability. (2011) 1–753. https://doi.org/10.1017/CBO9780511718786.

[38] J. Ho, T.R. Jow, S. Boggs, Historical introduction to capacitor technology, IEEE Electrical Insulation Magazine. 26 (2010) 20–25. https://doi.org/10.1109/MEI.2010.5383924.

[39] J. Hedesan, J. Tendler, The structure of scientific revolutions, 2017. https://doi.org/10.4324/9781912281589.

[40] M.J. Ratcliff, Abraham Trembley's strategy of generosity and the scope of celebrity in the mid-eighteenth century., Isis; an International Review Devoted to the History of Science and Its Cultural Influences. 95 (2004) 555–575. https://doi.org/10.1086/430649.

[41] A. Allerhand, Who Invented the Earliest Capacitor Bank ("Battery" of Leyden Jars)? It's Complicated, Proceedings of the IEEE. 106 (2018) 496–503. https://doi.org/10.1109/JPROC.2018.2795846.

[42] J. Both, Electrolytic capacitors, 1890 to 1925: Early history and basic principle, IEEE Electrical Insulation Magazine. 31 (2015) 22–29. https://doi.org/10.1109/MEI.2015.6996675.

[43] M. Yassine, D. Fabris, Performance of commercially available supercapacitors, Energies. 10 (2017). https://doi.org/10.3390/en10091340.

[44] M. Hepel, High Energy-Density Electric Double-Layer and Hybrid Supercapacitors Based on Graphene Composites, Encyclopedia of Surface and Colloid Science, Third Edition. 1 (2015) 1–22. https://doi.org/10.1081/e-escs3-120051485.

[45] L. Zhang, High-Power Energy Storage: Ultracapacitors, Elsevier Inc., 2018. https://doi.org/10.1016/B978-0-12-812786-5.00002-1.

[46] H. Ji, X. Zhao, Z. Qiao, J. Jung, Y. Zhu, Y. Lu, L.L. Zhang, A.H. MacDonald, R.S. Ruoff, Capacitance of carbon-based electrical double-layer capacitors, Nature Communications. 5 (2014). https://doi.org/10.1038/ncomms4317.

[47] A. González, E. Goikolea, J.A. Barrena, R. Mysyk, Review on supercapacitors: Technologies and materials, Renewable and Sustainable Energy Reviews. 58 (2016) 1189–1206. https://doi.org/10.1016/j.rser.2015.12.249.

[48] M.M.M. Ahmed, T. Imae, Graphene-Based Nanolayers Toward Energy Storage Device, Elsevier B.V., 2017. https://doi.org/10.1016/B978-0-444-63739-0.00010-4.

[49] K.B. Oldham, A Gouy-Chapman-Stern model of the double layer at a (metal)/(ionic liquid) interface, Journal of Electroanalytical Chemistry. 613 (2008) 131–138. https://doi.org/10.1016/j.jelechem.2007.10.017.

[50] V.L. Shapovalov, G. Brezesinski, Breakdown of the Gouy - Chapman model for

highly charged Langmuir monolayers: Counterion size effect, Journal of Physical Chemistry B. 110 (2006) 10032–10040. https://doi.org/10.1021/jp056801b.

[51] M.A. Brown, G.V. Bossa, S. May, Emergence of a Stern Layer from the Incorporation of Hydration Interactions into the Gouy-Chapman Model of the Electrical Double Layer, Langmuir. 31 (2015) 11477–11483. https://doi.org/10.1021/acs.langmuir.5b02389.

[52] Y. Jiang, J. Liu, Definitions of Pseudocapacitive Materials: A Brief Review, Energy & Environmental Materials. 2 (2019) 30–37. https://doi.org/10.1002/eem2.12028.

[53] D. Majumdar, M. Mandal, S.K. Bhattacharya, Journey from supercapacitors to supercapatteries: recent advancements in electrochemical energy storage systems, Emergent Materials. (2020). https://doi.org/10.1007/s42247-020-00090-5.

[54] A. Muzaffar, M.B. Ahamed, K. Deshmukh, J. Thirumalai, A review on recent advances in hybrid supercapacitors: Design, fabrication and applications, Renewable and Sustainable Energy Reviews. 101 (2019) 123–145. https://doi.org/10.1016/j.rser.2018.10.026.

[55] X. Li, B. Wei, Supercapacitors based on nanostructured carbon, Nano Energy. 2 (2013) 159–173. https://doi.org/10.1016/j.nanoen.2012.09.008.

[56] J.P. Cheng, J. Zhang, F. Liu, Recent development of metal hydroxides as electrode material of electrochemical capacitors, RSC Advances. 4 (2014) 38893–38917. https://doi.org/10.1039/c4ra06738j.

[57] G.A. Snook, P. Kao, A.S. Best, Conducting-polymer-based supercapacitor devices and electrodes, Journal of Power Sources. 196 (2011) 1–12. https://doi.org/10.1016/j.jpowsour.2010.06.084.

[58] Y. Lu, G. Long, L. Zhang, T. Zhang, M. Zhang, F. Zhang, Y. Yang, Y. Ma, Y. Chen, What are the practical limits for the specific surface area and capacitance of bulk sp2

carbon materials?, Science China Chemistry. 59 (2016) 225–230. https://doi.org/10.1007/s11426-015-5474-y.

[59] A. Bianco, H.M. Cheng, T. Enoki, Y. Gogotsi, R.H. Hurt, N. Koratkar, T. Kyotani, M. Monthioux, C.R. Park, J.M.D. Tascon, J. Zhang, All in the graphene family - A recommended nomenclature for two-dimensional carbon materials, Carbon. 65 (2013) 1–6. https://doi.org/10.1016/j.carbon.2013.08.038.

[60] A. Benítez, A. Caballero, J. Morales, J. Hassoun, E. Rodríguez-Castellón, J. Canales-Vázquez, Physical activation of graphene: An effective, simple and clean procedure for obtaining microporous graphene for high-performance Li/S batteries, Nano Research. 12 (2019) 759–766. https://doi.org/10.1007/s12274-019-2282-2.

[61] H. Nguyen Bich, H. Nguyen Van, Promising applications of graphene and graphene-based nanostructures, Advances in Natural Sciences: Nanoscience and Nanotechnology. 7 (2016). https://doi.org/10.1088/2043-6262/7/2/023002.

[62] J. Yang, S. Gunasekaran, Electrochemically reduced graphene oxide sheets for use in high performance supercapacitors, Carbon. 51 (2013) 36–44. https://doi.org/10.1016/j.carbon.2012.08.003.

[63] W.S. Hummers, R.E. Offeman, Preparation of Graphitic Oxide, Journal of the American Chemical Society. 80 (1958) 1339. https://doi.org/10.1021/ja01539a017.

[64] P.L. Chiu, D.D.T. Mastrogiovanni, D. Wei, C. Louis, M. Jeong, G. Yu, P. Saad, C.R. Flach, R. Mendelsohn, E. Garfunkel, H. He, Microwave- and nitronium ion-enabled rapid and direct production of highly conductive low-oxygen graphene, Journal of the American Chemical Society. 134 (2012) 5850–5856. https://doi.org/10.1021/ja210725p.

[65] C.N.R. Rao, K.S. Subrahmanyam, H.S.S.R. Matte, B. Abdulhakeem, A. Govindaraj, B. Das, P. Kumar, A. Ghosh, D.J. Late, A study of the synthetic methods and

properties of graphenes, Science and Technology of Advanced Materials. 11 (2010). https://doi.org/10.1088/1468-6996/11/5/054502.

[66] F. Bonaccorso, A. Lombardo, T. Hasan, Z. Sun, L. Colombo, A.C. Ferrari, Production and processing of graphene and 2d crystals, Materials Today. 15 (2012) 564–589. https://doi.org/10.1016/S1369-7021(13)70014-2.

[67] K. Parvez, S. Yang, X. Feng, K. Müllen, Exfoliation of graphene via wet chemical routes, Synthetic Metals. 210 (2015) 123–132. https://doi.org/10.1016/j.synthmet.2015.07.014.

[68] M.J. Yoo, H.B. Park, Effect of hydrogen peroxide on properties of graphene oxide in Hummers method, Carbon. 141 (2019) 515–522. https://doi.org/10.1016/j.carbon.2018.10.009.

[69] Z. Tian, J. Li, G. Zhu, J. Lu, Y. Wang, Z. Shi, C. Xu, Facile synthesis of highly conductive sulfur-doped reduced graphene oxide sheets, Physical Chemistry Chemical Physics. 18 (2015) 1125–1130. https://doi.org/10.1039/c5cp05475c.

[70] Y. Li, G. Wang, T. Wei, Z. Fan, P. Yan, Nitrogen and sulfur co-doped porous carbon nanosheets derived from willow catkin for supercapacitors, Nano Energy. 19 (2016) 165–175. https://doi.org/10.1016/j.nanoen.2015.10.038.

[71] J. Han, L.L. Zhang, S. Lee, J. Oh, K.S. Lee, J.R. Potts, J. Ji, X. Zhao, R.S. Ruoff, S. Park, Generation of B-doped graphene nanoplatelets using a solution process and their supercapacitor applications, ACS Nano. 7 (2013) 19–26. https://doi.org/10.1021/nn3034309.

[72] F. Alvi, M.K. Ram, P.A. Basnayaka, E. Stefanakos, Y. Goswami, A. Kumar, Graphene-polyethylenedioxythiophene conducting polymer nanocomposite based supercapacitor, Electrochimica Acta. 56 (2011) 9406–9412. https://doi.org/10.1016/j.electacta.2011.08.024.

[73] M. Duraivel, S. Nagappan, B. Balamuralitharan, S. Selvam, S.N. Karthick, K. Prabakar, C.S. Ha, H.J. Kim, Superior one-pot synthesis of a doped graphene oxide electrode for a high power density supercapacitor, New Journal of Chemistry. 42 (2018) 11093–11101. https://doi.org/10.1039/c8nj01672k.

[74] A.K. Geim, K.S. Novoselov, The rise of graphene, Nature Materials. 6 (2007) 183–191. https://doi.org/10.1038/nmat1849.

[75] B. Quan, S.H. Yu, D.Y. Chung, A. Jin, J.H. Park, Y.E. Sung, Y. Piao, Single source precursor-based solvothermal synthesis of heteroatom-doped graphene and its energy storage and conversion applications, Scientific Reports. 4 (2014) 23–25. https://doi.org/10.1038/srep05639.

[76] P.Z. Guo, Q.Q. Ji, L.L. Zhang, S.Y. Zhao, X.S. Zhao, Preparation and characterization of peanut shell-based microporous carbons as electrode materials for supercapacitors, Wuli Huaxue Xuebao/ Acta Physico - Chimica Sinica. 27 (2011) 2836–2840. https://doi.org/10.3866/PKU.WHXB20112836.

[77] N.F. Sylla, N.M. Ndiaye, B.D. Ngom, D. Momodu, M.J. Madito, B.K. Mutuma, N. Manyala, Effect of porosity enhancing agents on the electrochemical performance of high-energy ultracapacitor electrodes derived from peanut shell waste, Scientific Reports. 9 (2019) 1–15. https://doi.org/10.1038/s41598-019-50189-x.

[78] K. Yang, J. Peng, C. Srinivasakannan, L. Zhang, H. Xia, X. Duan, Preparation of high surface area activated carbon from coconut shells using microwave heating, Bioresource Technology. 101 (2010) 6163–6169. https://doi.org/10.1016/j.biortech.2010.03.001.

[79] L. Khezami, A. Chetouani, B. Taouk, R. Capart, Production and characterisation of activated carbon from wood components in powder: Cellulose, lignin, xylan, Powder Technology. 157 (2005) 48–56. https://doi.org/10.1016/j.powtec.2005.05.009.

[80] I.I.G. Inal, S.M. Holmes, A. Banford, Z. Aktas, The performance of supercapacitor electrodes developed from chemically activated carbon produced from waste tea, Applied Surface Science. 357 (2015) 696–703. https://doi.org/10.1016/j.apsusc.2015.09.067.

[81] H. Pan, J. Li, Y.P. Feng, Carbon nanotubes for supercapacitor, Nanoscale Research Letters. 5 (2010) 654–668. https://doi.org/10.1007/s11671-009-9508-2.

[82] J. Kong, A.M. Cassell, H. Dai, Chemical vapor deposition of methane for single-walled carbon nanotubes, Chemical Physics Letters. 292 (1998) 567–574. https://doi.org/10.1016/S0009-2614(98)00745-3.

[83] C.D. Scott, S. Arepalli, P. Nikolaev, R.E. Smalley, Growth mechanisms for single-wall carbon nanotubes in a laser-ablation process, Applied Physics A: Materials Science and Processing. 72 (2001) 573–580. https://doi.org/10.1007/s003390100761.

[84] J.L. Hutchison, N.A. Kiselev, E.P. Krinichnaya, A. V. Krestinin, R.O. Loutfy, A.P. Morawsky, V.E. Muradyan, E.D. Obraztsova, J. Sloan, S. V. Terekhov, D.N. Zakharov, Double-walled carbon nanotubes fabricated by a hydrogen arc discharge method, Carbon. 39 (2001) 761–770. https://doi.org/10.1016/S0008-6223(00)00187-1.

[85] C. qi YI, J. peng ZOU, H. zhi YANG, X. LENG, Recent advances in pseudocapacitor electrode materials: Transition metal oxides and nitrides, Transactions of Nonferrous Metals Society of China (English Edition). 28 (2018) 1980–2001. https://doi.org/10.1016/S1003-6326(18)64843-5.

[86] A.N. Naveen, P. Manimaran, S. Selladurai, Cobalt oxide (Co3O4)/graphene nanosheets (GNS) composite prepared by novel route for supercapacitor application, Journal of Materials Science: Materials in Electronics. 26 (2015) 8988–9000. https://doi.org/10.1007/s10854-015-3582-2.

[87] M. Toupin, T. Brousse, D. Bélanger, Charge storage mechanism of MnO2 electrode

used in aqueous electrochemical capacitor, Chemistry of Materials. 16 (2004) 3184–3190. https://doi.org/10.1021/cm049649j.

[88] L.-B. Kong, M. Liu, J.-W. Lang, Y.-C. Luo, L. Kang, Asymmetric Supercapacitor Based on Loose-Packed Cobalt Hydroxide Nanoflake Materials and Activated Carbon, Journal of The Electrochemical Society. 156 (2009) A1000. https://doi.org/10.1149/1.3236500.

[89] A. Bello, K. Makgopa, M. Fabiane, D. Dodoo-Ahrin, K.I. Ozoemena, N. Manyala, Chemical adsorption of NiO nanostructures on nickel foam-graphene for supercapacitor applications, Journal of Materials Science. 48 (2013) 6707–6712. https://doi.org/10.1007/s10853-013-7471-x.

[90] H. Kelly-Holmes, Principles and applications of electrochemical capacitors, Electrochimica Acta 45. 45 (2000) 2483–2498. https://doi.org/10.1057/9780230503014.

[91] F. Zhang, D. Zhu, X. Chen, X. Xu, Z. Yang, C. Zou, K. Yang, S. Huang, A nickel hydroxide-coated 3D porous graphene hollow sphere framework as a high performance electrode material for supercapacitors, Physical Chemistry Chemical Physics. 16 (2014) 4186–4192. https://doi.org/10.1039/c3cp54334j.

[92] F. Li, J. Song, H. Yang, S. Gan, Q. Zhang, D. Han, A. Ivaska, L. Niu, One-step synthesis of graphene/{SnO}2nanocomposites and its application in electrochemical supercapacitors, Nanotechnology. 20 (2009) 455602. https://doi.org/10.1088/0957-4484/20/45/455602.

[93] H. Wang, Q. Fu, C. Pan, Green mass synthesis of graphene oxide and its MnO2 composite for high performance supercapacitor, Electrochimica Acta. 312 (2019) 11–21. https://doi.org/10.1016/j.electacta.2019.04.178.

[94] A. Numan, N. Duraisamy, F. Saiha Omar, Y.K. Mahipal, K. Ramesh, S. Ramesh,

Enhanced electrochemical performance of cobalt oxide nanocube intercalated reduced graphene oxide for supercapacitor application, RSC Advances. 6 (2016) 34894–34902. https://doi.org/10.1039/c6ra00160b.

[95] S. Park, S. Kim, Effect of carbon blacks filler addition on electrochemical behaviors of Co3O4/graphene nanosheets as a supercapacitor electrodes, Electrochimica Acta. 89 (2013) 516–522. https://doi.org/10.1016/j.electacta.2012.11.075.

[96] H.J. Ahonen, J. Lukkari, J. Kankare, n- and p-doped poly(3,4-ethylenedioxythiophene): Two electronically conducting states of the polymer, Macromolecules. 33 (2000) 6787–6793. https://doi.org/10.1021/ma0004312.

[97] Y. Huang, H. Li, Z. Wang, M. Zhu, Z. Pei, Q. Xue, Y. Huang, C. Zhi, Nanostructured Polypyrrole as a flexible electrode material of supercapacitor, Nano Energy. 22 (2016) 422–438. https://doi.org/10.1016/j.nanoen.2016.02.047.

[98] K.S. Ryu, Y.G. Lee, Y.S. Hong, Y.J. Park, X. Wu, K.M. Kim, M.G. Kang, N.G. Park, S.H. Chang, Poly(ethylenedioxythiophene) (PEDOT) as polymer electrode in redox supercapacitor, Electrochimica Acta. 50 (2004) 843–847. https://doi.org/10.1016/j.electacta.2004.02.055.

[99] A. Laforgue, P. Simon, C. Sarrazin, J.F. Fauvarque, Polythiophene-based supercapacitors, Journal of Power Sources. 80 (1999) 142–148. https://doi.org/10.1016/S0378-7753(98)00258-4.

[100] X. Cao, H.Y. Zeng, S. Xu, J. Yuan, J. Han, G.F. Xiao, Facile fabrication of the polyaniline/layered double hydroxide nanosheet composite for supercapacitors, Applied Clay Science. 168 (2019) 175–183. https://doi.org/10.1016/j.clay.2018.11.011.

[101] M.A.A. Mohd Abdah, N.H.N. Azman, S. Kulandaivalu, Y. Sulaiman, Review of the use of transition-metal-oxide and conducting polymer-based fibres for high-

performance supercapacitors, Materials and Design. 186 (2020) 108199. https://doi.org/10.1016/j.matdes.2019.108199.

[102] H.W. Wang, Z.A. Hu, Y.Q. Chang, Y.L. Chen, Z.Y. Zhang, Y.Y. Yang, H.Y. Wu, Preparation of reduced graphene oxide/cobalt oxide composites and their enhanced capacitive behaviors by homogeneous incorporation of reduced graphene oxide sheets in cobalt oxide matrix, Materials Chemistry and Physics. 130 (2011) 672–679. https://doi.org/10.1016/j.matchemphys.2011.07.043.

[103] C. Zhong, Y. Deng, W. Hu, D. Sun, X. Han, J. Qiao, J. Zhang, Electrolytes for electrochemical supercapacitors, 2016. https://doi.org/10.1201/b21497-3.

[104] C. Zhong, Y. Deng, W. Hu, J. Qiao, L. Zhang, J. Zhang, A review of electrolyte materials and compositions for electrochemical supercapacitors, Chemical Society Reviews. 44 (2015) 7484–7539. https://doi.org/10.1039/c5cs00303b.

[105] L. Demarconnay, E. Raymundo-Piñero, F. Béguin, A symmetric carbon/carbon supercapacitor operating at 1.6 v by using a neutral aqueous solution, Electrochemistry Communications. 12 (2010) 1275–1278. https://doi.org/10.1016/j.elecom.2010.06.036.

[106] D. Jiménez-Cordero, F. Heras, M.A. Gilarranz, E. Raymundo-Piñero, Grape seed carbons for studying the influence of texture on supercapacitor behaviour in aqueous electrolytes, Carbon. 71 (2014) 127–138. https://doi.org/10.1016/j.carbon.2014.01.021.

[107] H. Wu, X. Wang, L. Jiang, C. Wu, Q. Zhao, X. Liu, B. Hu, L. Yi, The effects of electrolyte on the supercapacitive performance of activated calcium carbide-derived carbon, Journal of Power Sources. 226 (2013) 202–209. https://doi.org/10.1016/j.jpowsour.2012.11.014.

[108] K. Fic, G. Lota, M. Meller, E. Frackowiak, Novel insight into neutral medium as electrolyte for high-voltage supercapacitors, Energy and Environmental Science. 5 (2012) 5842–5850. https://doi.org/10.1039/c1ee02262h.

[109] K. Fic, G. Lota, E. Frackowiak, Effect of surfactants on capacitance properties of carbon electrodes, Electrochimica Acta. 60 (2012) 206–212. https://doi.org/10.1016/j.electacta.2011.11.059.

[110] P. Sun, Z. Li, L. Zhang, C. Dong, Z. Li, H. Yao, J. Wang, G. Li, Synthesis of cobalt-nickel pyrophosphates/N-doped graphene composites with high rate capability for asymmetric supercapacitor, Journal of Alloys and Compounds. 750 (2018) 607–616. https://doi.org/10.1016/j.jallcom.2018.04.024.

[111] A. Brandt, S. Pohlmann, A. Varzi, A. Balducci, S. Passerini, Ionic liquids in supercapacitors, MRS Bulletin. 38 (2013) 554–559. https://doi.org/10.1557/mrs.2013.151.

[112] J.S. Skyler, Ionic-liquid materials for the electrochemical challenges of the future, Endocrinologist. 3 (1993) 233–238. https://doi.org/10.1097/00019616-199307000-00001.

[113] P.W. Ruch, D. Cericola, A. Foelske-Schmitz, R. Kötz, A. Wokaun, Aging of electrochemical double layer capacitors with acetonitrile-based electrolyte at elevated voltages, Electrochimica Acta. 55 (2010) 4412–4420. https://doi.org/10.1016/j.electacta.2010.02.064.

[114] S. Vaquero, R. Díaz, M. Anderson, J. Palma, R. Marcilla, Insights into the influence of pore size distribution and surface functionalities in the behaviour of carbon supercapacitors, Electrochimica Acta. 86 (2012) 241–247. https://doi.org/10.1016/j.electacta.2012.08.006.

[115] E. Raymundo-Piñero, K. Kierzek, J. Machnikowski, F. Béguin, Relationship between the nanoporous texture of activated carbons and their capacitance properties in different electrolytes, Carbon. 44 (2006) 2498–2507. https://doi.org/10.1016/j.carbon.2006.05.022.

[116] Y.T. Pi, Y.T. Li, S.S. Xu, X.Y. Xing, H.K. Ma, Z.B. He, T.Z. Ren, Is the conductive agent useful in electrodes of graphitized activated carbon?, RSC Advances. 6 (2016) 100708–100712. https://doi.org/10.1039/c6ra18246a.

[117] S. Priyono, T.D. Sari, Ramlan, A. Subhan, B. Prihandoko, Effect of polymer binders on the electrochemical Performance of Al-doped lithium titanate electrode, Journal of Physics: Conference Series. 1282 (2019). https://doi.org/10.1088/1742-6596/1282/1/012056.

[118] M.D. Stoller, R.S. Ruoff, Best practice methods for determining an electrode material's performance for ultracapacitors, Energy and Environmental Science. 3 (2010) 1294–1301. https://doi.org/10.1039/c0ee00074d.

[119] N. Elgrishi, K.J. Rountree, B.D. McCarthy, E.S. Rountree, T.T. Eisenhart, J.L. Dempsey, A Practical Beginner's Guide to Cyclic Voltammetry, Journal of Chemical Education. 95 (2018) 197–206. https://doi.org/10.1021/acs.jchemed.7b00361.

[120] S. Zhang, N. Pan, Supercapacitors Performance Evaluation - Zhang - 2015 - Advanced Energy Materials - Wiley Online Library, Advanced Energy Materials. (2015). https://onlinelibrary.wiley.com/doi/pdf/10.1002/aenm.201401401.

[121] D.J. Tarimo, K.O. Oyedotun, A.A. Mirghni, N. Manyala, Sulphur-reduced graphene oxide composite with improved electrochemical performance for supercapacitor applications, International Journal of Hydrogen Energy. 45 (2020). https://doi.org/10.1016/j.ijhydene.2020.03.059.

[122] M. Lu, F. Beguin, E. Frackowiak, Supercapacitors : Materials, Systems, and Applications, Wiley VCH, Weinheim, 2013.

[123] D.J. Tarimo, K.O. Oyedotun, A.A. Mirghni, N.F. Sylla, N. Manyala, High energy and excellent stability asymmetric supercapacitor derived from sulphur-reduced graphene oxide/manganese dioxide composite and activated carbon from peanut shell,

Electrochimica Acta. 353 (2020) 136498. https://doi.org/10.1016/j.electacta.2020.136498.

[124] A.A. Mirghni, K.O. Oyedotun, B.A. Mahmoud, A. Bello, S.C. Ray, N. Manyala, Nickel-cobalt phosphate/graphene foam as enhanced electrode for hybrid supercapacitor, Composites Part B: Engineering. 174 (2019) 106953. https://doi.org/10.1016/j.compositesb.2019.106953.

[125] J.H. Chae, G.Z. Chen, 1.9 V Aqueous Carbon-Carbon Supercapacitors With Unequal Electrode Capacitances, Electrochimica Acta. 86 (2012) 248–254. https://doi.org/10.1016/j.electacta.2012.07.033.

[126] F. Ochai-Ejeh, M.J. Madito, K. Makgopa, M.N. Rantho, O. Olaniyan, N. Manyala, Electrochemical performance of hybrid supercapacitor device based on birnessite-type manganese oxide decorated on uncapped carbon nanotubes and porous activated carbon nanostructures, Electrochimica Acta. 289 (2018) 363–375. https://doi.org/10.1016/j.electacta.2018.09.032.

[127] N. Aristov, A. Habekost, Cyclic Voltammetry - A Versatile Electrochemical Method Investigating Electron Transfer Processes, World Journal of Chemical Education, Vol. 3, 2015, Pages 115-119. 3 (2015) 115–119. https://doi.org/10.12691/WJCE-3-5-2.

[128] T.S. Mathis, N. Kurra, X. Wang, D. Pinto, P. Simon, Y. Gogotsi, Energy Storage Data Reporting in Perspective—Guidelines for Interpreting the Performance of Electrochemical Energy Storage Systems, Advanced Energy Materials. 9 (2019) 1–13. https://doi.org/10.1002/aenm.201902007.

[129] S. Alehashem, F. Chambers, J.W. Strojek, G.M. Swain, R. Ramesham, Cyclic Voltammetric Studies of Charge Transfer Reactions at Highly Boron-Doped Polycrystalline Diamond Thin-Film Electrodes, Analytical Chemistry. 67 (1995) 2812–2821. https://doi.org/10.1021/ac00113a014.

[130] W. Zhang, C. Ma, J. Fang, J. Cheng, X. Zhang, S. Dong, L. Zhang, Asymmetric electrochemical capacitors with high energy and power density based on graphene/CoAl-LDH and activated carbon electrodes, RSC Advances. 3 (2013) 2483–2490. https://doi.org/10.1039/c2ra23283a.

[131] Allen J. Bard and Larry R. Faulkner, Electrochemical Methods: Fundamentals and Applications, New York: Wiley, 2001, 2nd ed., Russian Journal of Electrochemistry. 38 (2002) 1364–1365. https://doi.org/10.1023/A:1021637209564.

[132] B. Akinwolemiwa, C. Peng, G.Z. Chen, Redox Electrolytes in Supercapacitors, Journal of The Electrochemical Society. 162 (2015) A5054–A5059. https://doi.org/10.1149/2.0111505jes.

[133] A.S. Ambrozevich, S.A. Ambrozevich, R.T. Sibatov, V. V. Uchaikin, Features of Charging–Discharging of Supercapacitors, Russian Electrical Engineering. 89 (2018) 64–70. https://doi.org/10.3103/S1068371218010029.

[134] S. Ban, J. Zhang, L. Zhang, K. Tsay, D. Song, X. Zou, Charging and discharging electrochemical supercapacitors in the presence of both parallel leakage process and electrochemical decomposition of solvent, Electrochimica Acta. 90 (2013) 542–549. https://doi.org/10.1016/j.electacta.2012.12.056.

[135] P.L. Taberna, P. Simon, J.F. Fauvarque, Electrochemical Characteristics and Impedance Spectroscopy Studies of Carbon-Carbon Supercapacitors, Journal of The Electrochemical Society. 150 (2003) A292. https://doi.org/10.1149/1.1543948.

[136] K. Hara, H. Arakawa, C. Dssc, S. Cell, D. Physics, K.M. Jeerage, R.D. Noble, C.A. Koval, M. Kouhnavard, N. Ahmad, L. Babak, V. Ghaffari, N. Chandra, D. Nath, H. Joon, W. Choi, J. Lee, Impedance Spectroscopy Theory, Experiment, and Applications, 2013. https://doi.org/10.1016/j.snb.2007.02.003.

[137] R. Negroiu, P. Svasta, C. Ionescu, A. Vasile, Investigation of Supercapacitor's

Impedance Based on Spectroscopic Measurements, (n.d.).

[138] F. Mansfeld, Analysis and Interpretation of EIS Data for Metals and Alloys - An Introduction to Electrochemical Impedance Measurement, (1999) 1–77.

[139] D.Y. Momodu, Investigation of metal hydroxides graphene composites as electrode materials for supercapacitor applications, (2015) 185. http://repository.up.ac.za/handle/2263/50281.

[140] B.A. Mei, O. Munteshari, J. Lau, B. Dunn, L. Pilon, Physical Interpretations of Nyquist Plots for EDLC Electrodes and Devices, Journal of Physical Chemistry C. 122 (2018) 194–206. https://doi.org/10.1021/acs.jpcc.7b10582.

[141] A. Allison, H.A. Andreas, Minimizing the Nyquist-plot semi-circle of pseudocapacitive manganese oxides through modification of the oxide-substrate interface resistance, Journal of Power Sources. 426 (2019) 93–96. https://doi.org/10.1016/j.jpowsour.2019.04.029.

[142] J. Bisquert, G. Garcia-Belmonte, P. Bueno, E. Longo, L.O.S. Bulhões, Impedance of constant phase element (CPE)-blocked diffusion in film electrodes, Journal of Electroanalytical Chemistry. 452 (1998) 229–234. https://doi.org/10.1016/S0022-0728(98)00115-6.

[143] H. Liu, M.G. George, N. Ge, D. Muirhead, P. Shrestha, J. Lee, R. Banerjee, R. Zeis, M. Messerschmidt, J. Scholta, P. Krolla, A. Bazylak, Microporous Layer Degradation in Polymer Electrolyte Membrane Fuel Cells, Journal of The Electrochemical Society. 165 (2018) F3271–F3280. https://doi.org/10.1149/2.0291806jes.

[144] A. Khosrozadeh, G. Singh, Q. Wang, G. Luo, M. Xing, Supercapacitor with extraordinary cycling stability and high rate from nano-architectured polyaniline/graphene on Janus nanofibrous film with shape memory, Journal of Materials Chemistry A. 6 (2018) 21064–21077. https://doi.org/10.1039/C8TA07426G.

[145] A. Laheäär, P. Przygocki, Q. Abbas, F. Béguin, Appropriate methods for evaluating the efficiency and capacitive behavior of different types of supercapacitors, Electrochemistry Communications. 60 (2015) 21–25. https://doi.org/10.1016/j.elecom.2015.07.022.

[146] A. Bello, F. Barzegar, M.J. Madito, D.Y. Momodu, A.A. Khaleed, T.M. Masikhwa, J.K. Dangbegnon, N. Manyala, Stability studies of polypyrole- derived carbon based symmetric supercapacitor via potentiostatic floating test, Electrochimica Acta. 213 (2016) 107–114. https://doi.org/10.1016/j.electacta.2016.06.151.

[147] D. Weingarth, A. Foelske-Schmitz, R. Kötz, Cycle versus voltage hold - Which is the better stability test for electrochemical double layer capacitors?, Journal of Power Sources. 225 (2013) 84–88. https://doi.org/10.1016/j.jpowsour.2012.10.019.

[148] J. Kowal, E. Avaroglu, F. Chamekh, A. Šenfelds, T. Thien, D. Wijaya, D.U. Sauer, Detailed analysis of the self-discharge of supercapacitors, Journal of Power Sources. 196 (2011) 573–579. https://doi.org/10.1016/j.jpowsour.2009.12.028.

[149] J. Niu, B.E. Conway, W.G. Pell, Comparative studies of self-discharge by potential decay and float-current measurements at C double-layer capacitor and battery electrodes, Journal of Power Sources. 135 (2004) 332–343. https://doi.org/10.1016/j.jpowsour.2004.03.068.

[150] L. Staudenmaier, Verfahren zur darstellung der graphitsäure, Berichte Der Deutschen Chemischen Gesellschaft. 31 (1898) 1481–1487.

[151] J. Chen, B. Yao, C. Li, G. Shi, An improved Hummers method for eco-friendly synthesis of graphene oxide, Carbon. 64 (2013) 225–229. https://doi.org/10.1016/j.carbon.2013.07.055.

[152] D.C. Marcano, D. V. Kosynkin, J.M. Berlin, A. Sinitskii, Z. Sun, A. Slesarev, L.B. Alemany, W. Lu, J.M. Tour, Improved synthesis of graphene oxide, ACS Nano. 4

(2010) 4806–4814. https://doi.org/10.1021/nn1006368.

[153] I.V.G. and A.A.F. K. S. Novoselov, A. K. Geim, S. V. Morozov, D. Jiang, Y. Zhang, S. V. Dubonos, Electric Field Effect in Atomically Thin Carbon Films, 306 (2016) 666–669.

[154] S.C. Tsinontides, P. Rajniak, D. Pham, W.A. Hunke, J. Placek, S.D. Reynolds, Freeze drying - Principles and practice for successful scale-up to manufacturing, International Journal of Pharmaceutics. 280 (2004) 1–16. https://doi.org/10.1016/j.ijpharm.2004.04.018.

[155] Lyophilization/Freeze Drying - An Review 7, (n.d.) 2700.

[156] Z. Ling, C. Yu, X. Fan, S. Liu, J. Yang, M. Zhang, G. Wang, N. Xiao, J. Qiu, Freeze-drying for sustainable synthesis of nitrogen doped porous carbon cryogel with enhanced supercapacitor and lithium ion storage performance, Nanotechnology. 26 (2015). https://doi.org/10.1088/0957-4484/26/37/374003.

[157] S. Singh, Lyophilization/Freeze drying - A review, Age. 20 (2015) 60yrs.

[158] J. Zhang, Z. Yang, X. Wang, T. Ren, Q. Qiao, Homogeneous sulphur-doped composites: Porous carbon materials with unique hierarchical porous nanostructure for super-capacitor application, RSC Advances. 6 (2016) 84847–84853. https://doi.org/10.1039/c6ra17231h.

[159] J. Li, Q. Wu, J. Wu, T.S. Division, O. Ridge, O. Ridge, C. Sciences, E. Division, Handbook of Nanoparticles, Handbook of Nanoparticles. (2015). https://doi.org/10.1007/978-3-319-13188-7.

[160] D. Rickard, G.W. Luther, Chemistry of iron sulfides, 2007. https://doi.org/10.1021/cr0503658.

[161] A.E. Lewis, Review of metal sulphide precipitation, Hydrometallurgy. 104 (2010) 222–234. https://doi.org/10.1016/j.hydromet.2010.06.010.

[162] J. Grandgirard, D. Poinsot, L. Krespi, J.P. Nénon, A.M. Cortesero, Conventional and Microwave Hydrothermal Synthesis and Application of Functional Materials: A Review, Entomologia Experimentalis et Applicata. 103 (2002) 239–248. https://doi.org/10.1023/A.

[163] Y.X. Gan, A.H. Jayatissa, Z. Yu, X. Chen, M. Li, Hydrothermal Synthesis of Nanomaterials, Journal of Nanomaterials. 2020 (2020). https://doi.org/10.1155/2020/8917013.

[164] G. Sharma, A. Kumar, S. Sharma, M. Naushad, R. Prakash Dwivedi, Z.A. ALOthman, G.T. Mola, Novel development of nanoparticles to bimetallic nanoparticles and their composites: A review, Journal of King Saud University - Science. 31 (2019) 257–269. https://doi.org/10.1016/j.jksus.2017.06.012.

[165] Y. Dahman, Chapter 6 - Nanopolymers**By Yaser Dahman, Kevin Deonanan, Timothy Dontsos, and Andrew Iammatteo., in: Y. Dahman (Ed.), Nanotechnology and Functional Materials for Engineers, Elsevier, 2017: pp. 121–144. https://doi.org/https://doi.org/10.1016/B978-0-323-51256-5.00006-X.

[166] B. Akturk, A.B. Kizilkanat, Improvement of durability and drying shrinkage of sodium carbonate activated slag through the incorporation of calcium hydroxide and sodium hydroxide, Construction and Building Materials. 243 (2020) 118260. https://doi.org/10.1016/j.conbuildmat.2020.118260.

[167] S. Barzgar, B. Lothenbach, M. Tarik, A. Di Giacomo, C. Ludwig, The effect of sodium hydroxide on Al uptake by calcium silicate hydrates (C[sbnd]S[sbnd]H), Journal of Colloid and Interface Science. 572 (2020) 246–256. https://doi.org/10.1016/j.jcis.2020.03.057.

[168] H.D. Alvarenga, T. Van De Putte, N. Van Steenberge, J. Sietsma, H. Terryn, Influence of Carbide Morphology and Microstructure on the Kinetics of Superficial

Decarburization of C-Mn Steels, Metallurgical and Materials Transactions A: Physical Metallurgy and Materials Science. 46 (2015) 123–133. https://doi.org/10.1007/s11661-014-2600-y.

[169] K. Xiao, H. Wu, H. Lv, X. Wu, H. Qian, The study of the effects of cooling conditions on high quality graphene growth by the APCVD method, Nanoscale. 5 (2013) 5524–5529. https://doi.org/10.1039/c3nr00524k.

[170] K.O. Oyedotun, M.J. Madito, D.Y. Momodu, A.A. Mirghni, T.M. Masikhwa, N. Manyala, Synthesis of ternary NiCo-MnO2 nanocomposite and its application as a novel high energy supercapattery device, Chemical Engineering Journal. 335 (2018) 416–433. https://doi.org/10.1016/j.cej.2017.10.169.

[171] J.D. Andrade, X-ray photoelectron spectroscopy (XPS), in: Surface and Interfacial Aspects of Biomedical Polymers, Springer, 1985: pp. 105–195.

[172] G. Greczynski, L. Hultman, X-ray photoelectron spectroscopy: Towards reliable binding energy referencing, Progress in Materials Science. 107 (2020) 100591. https://doi.org/10.1016/j.pmatsci.2019.100591.

[173] R. Kohli, K.L. Mittal, eds., Chapter 3 - Methods for Assessing Surface Cleanliness, in: Developments in Surface Contamination and Cleaning, Volume 12, Elsevier, 2019: pp. 23–105. https://doi.org/https://doi.org/10.1016/B978-0-12-816081-7.00003-6.

[174] J. Epp, X-ray diffraction (XRD) techniques for materials characterization, in: Materials Characterization Using Nondestructive Evaluation (NDE) Methods, Elsevier, 2016: pp. 81–124.

[175] J.P. Patel, P.H. Parsania, 3 - Characterization, testing, and reinforcing materials of biodegradable composites, in: N.G. Shimpi (Ed.), Biodegradable and Biocompatible Polymer Composites, Woodhead Publishing, 2018: pp. 55–79. https://doi.org/https://doi.org/10.1016/B978-0-08-100970-3.00003-1.

[176] O.I. Olubiyi, F.-K. Lu, D. Calligaris, F.A. Jolesz, N.Y. Agar, Advances in molecular imaging for surgery, in: Image-Guided Neurosurgery, Elsevier, 2015: pp. 407–439.

[177] P. Vandenabeele, Practical Raman spectroscopy: an introduction, John Wiley & Sons, 2013.

[178] K.S. Joya, X. Sala, In situ Raman and surface-enhanced Raman spectroscopy on working electrodes: Spectroelectrochemical characterization of water oxidation electrocatalysts, Physical Chemistry Chemical Physics. 17 (2015) 21094–21103. https://doi.org/10.1039/c4cp05053c.

[179] K. Kneipp, H. Kneipp, P. Corio, S.D.M. Brown, K. Shafer, J. Motz, L.T. Perelman, E.B. Hanlon, A. Marucci, G. Dresselhaus, M.S. Dresselhaus, Surface-enhanced and normal stokes and anti-stokes raman spectroscopy of single-walled carbon nanotubes, Physical Review Letters. 84 (2000) 3470–3473. https://doi.org/10.1103/PhysRevLett.84.3470.

[180] A.T. Ward, Raman spectroscopy of sulfur, sulfur-selenium, and sulfur-arsenic mixtures, Journal of Physical Chemistry. 72 (1968) 4133–4139. https://doi.org/10.1021/j100858a031.

[181] C. Nims, B. Cron, M. Wetherington, J. Macalady, J. Cosmidis, Low frequency Raman Spectroscopy for micron-scale and in vivo characterization of elemental sulfur in microbial samples, Scientific Reports. 9 (2019) 1–12. https://doi.org/10.1038/s41598-019-44353-6.

[182] G. Guimbretière, S. Duraipandian, T. Ricci, Field remote Stokes/anti-Stokes Raman characterization of sulfur in hydrothermal vents, Journal of Raman Spectroscopy. 49 (2018) 1385–1394. https://doi.org/10.1002/jrs.5378.

[183] G.S. Allan, Fourier Transform Infrared Spectroscopy (FTIR), Encyclopedia of Earth Sciences Series. (2017) 1046. https://doi.org/10.1007/978-1-4020-4409-0.

[184] P.M. Shameer, P.M. Nishath, Exploration and enhancement on fuel stability of biodiesel: A step forward in the track of global commercialization, in: Advanced Biofuels, Elsevier, 2019: pp. 181–213.

[185] D. Titus, E.J.J. Samuel, S.M. Roopan, Nanoparticle characterization techniques, in: Green Synthesis, Characterization and Applications of Nanoparticles, Elsevier, 2019: pp. 303–319.

[186] N.J. and D.R. Vij, FOURIER TRANSFORM INFRARED SPECTROSCOPY, 2006. https://doi.org/10.1007/0-387-37590-2.

[187] M. Salouti, F.K. Derakhshan, Chapter 3 - Phytosynthesis of Nanoscale Materials, in: M. Ghorbanpour, S.H. Wani (Eds.), Advances in Phytonanotechnology, Academic Press, 2019: pp. 45–121. https://doi.org/https://doi.org/10.1016/B978-0-12-815322-2.00003-1.

[188] J.I. Goldstein, D.E. Newbury, J.R. Michael, N.W.M. Ritchie, J.H.J. Scott, D.C. Joy, Scanning electron microscopy and X-ray microanalysis, Springer, 2017.

[189] A.K. Singh, Chapter 4 - Experimental Methodologies for the Characterization of Nanoparticles, in: A.K. Singh (Ed.), Engineered Nanoparticles, Academic Press, Boston, 2016: pp. 125–170. https://doi.org/https://doi.org/10.1016/B978-0-12-801406-6.00004-2.

[190] J. Telegdi, A. Shaban, G. Vastag, Biocorrosion-steel, in: Encyclopedia of Interfacial Chemistry: Surface Science and Electrochemistry, Elsevier, 2018: pp. 28–42.

[191] O.D. Neikov, N.A. Yefimov, Chapter 1 - Powder Characterization and Testing, in: O.D. Neikov, S.S. Naboychenko, N.A. Yefimov (Eds.), Handbook of Non-Ferrous Metal Powders (Second Edition), Second Edi, Elsevier, Oxford, 2019: pp. 3–62. https://doi.org/https://doi.org/10.1016/B978-0-08-100543-9.00001-4.

[192] J. Bergström, 2 - Experimental Characterization Techniques, in: J. Bergström (Ed.),

Mechanics of Solid Polymers, William Andrew Publishing, 2015: pp. 19–114. https://doi.org/https://doi.org/10.1016/B978-0-323-31150-2.00002-9.

[193] T. Walther, Chapter 4 - Transmission Electron Microscopy of Nanostructures, in: S. Thomas, R. Thomas, A.K. Zachariah, R.K. Mishra (Eds.), Microscopy Methods in Nanomaterials Characterization, Elsevier, 2017: pp. 105–134. https://doi.org/https://doi.org/10.1016/B978-0-323-46141-2.00004-3.

[194] C. Escalante, E. Sierra, Fundamentals of transmission electron microscopy, the technique with the best resolution in the world, (2019) 0–6.

[195] R.T. G, A.B. R, Review Article TRANSMISSION ELECTRON MICROSCOPY-AN OVERVIEW ISSN Online : - 2321-7855 International Research Journal for Inventions in TRANSMISSION ELECTRON MICROSCOPY- AN OVERVIEW, (2019).

[196] S. Brunauer, L.S. Deming, W.E. Deming, E. Teller, On a Theory of the van der Waals Adsorption of Gases, Journal of the American Chemical Society. 62 (1940) 1723–1732. https://doi.org/10.1021/ja01864a025.

[197] M. Thommes, K. Kaneko, A. V. Neimark, J.P. Olivier, F. Rodriguez-Reinoso, J. Rouquerol, K.S.W. Sing, Physisorption of gases, with special reference to the evaluation of surface area and pore size distribution (IUPAC Technical Report), Pure and Applied Chemistry. 87 (2015) 1051–1069. https://doi.org/10.1515/pac-2014-1117.

[198] C.D.H.E. (UK); R.A.W.H. (FRG); L.M. (Netherlands); R.A.P. (USA); J.R. (France); T.S. (Poland) K. S. W. SING (UK, *Membership, REPORTING PHYSISORPTION DATA FOR GAS/SOLID SYSTEMS with Special Reference to the Determination of Surface Area and Porosity, 81 (1998) 420–430.

[199] Bio-Logic, EC-Lab Software: Techniques and Applications, (2009) 1–175.

[200] F.-B. Wu, B. Yang, J.-L. Ye, eds., Chapter 2 - Technologies of energy storage systems, in: Grid-Scale Energy Storage Systems and Applications, Academic Press, 2019: pp.

17–56. https://doi.org/https://doi.org/10.1016/B978-0-12-815292-8.00002-2.

[201] L. Zhou, W. Utetiwabo, R. Chen, W. Yang, Layer by Layer Assemble of Colloid Nanomaterial and Functional Multilayer Films for Energy Storage and Conversion, (2019).

[202] E.Z. Kurmaev, A. V. Galakhov, A. Moewes, S. Moehlecke, Y. Kopelevich, Interlayer conduction band states in graphite-sulfur composites, Physical Review B - Condensed Matter and Materials Physics. 66 (2002) 1–3. https://doi.org/10.1103/PhysRevB.66.193402.

[203] Q. Cheng, J. Tang, J. Ma, H. Zhang, N. Shinya, L.C. Qin, Graphene and nanostructured MnO2 composite electrodes for supercapacitors, Carbon. 49 (2011) 2917–2925. https://doi.org/10.1016/j.carbon.2011.02.068.

[204] T. Chen, Y. Tang, Y. Qiao, Z. Liu, W. Guo, J. Song, S. Mu, S. Yu, Y. Zhao, F. Gao, All-solid-state high performance asymmetric supercapacitors based on novel MnS nanocrystal and activated carbon materials, Scientific Reports. 6 (2016) 1–9. https://doi.org/10.1038/srep23289.

[205] X. Zhao, H. Wang, G. Zhai, G. Wang, Facile Assembly of 3D Porous Reduced Graphene Oxide/Ultrathin MnO 2 Nanosheets-S Aerogels as Efficient Polysulfide Adsorption Sites for High-Performance Lithium–Sulfur Batteries, Chemistry - A European Journal. 23 (2017) 7037–7045. https://doi.org/10.1002/chem.201604828.

[206] C.W. Jones, Applications of hydrogen peroxide and derivatives, Royal Society of Chemistry, 2007.

[207] T.T. Nguyen, V.H. Nguyen, R.K. Deivasigamani, D. Kharismadewi, Y. Iwai, J.J. Shim, Facile synthesis of cobalt oxide/reduced graphene oxide composites for electrochemical capacitor and sensor applications, Solid State Sciences. 53 (2016) 71–77. https://doi.org/10.1016/j.solidstatesciences.2016.01.006.

[208] C. A reduced graphene oxide/Co3O4 composite for supercapacitor electrodeXiang, M. Li, M. Zhi, A. Manivannan, N. Wu, A reduced graphene oxide/Co3O4 composite for supercapacitor electrode, Journal of Power Sources. 226 (2013) 65–70. https://doi.org/10.1016/j.jpowsour.2012.10.064.

3.0 EXPERIMENTAL DETAILS AND CHARACTERIZATION TECHNIQUES

This chapter provides a detailed explanation about the experimental methods and procedures applied throughout the preparation of the material and the associated techniques used for characterization. Also, the description of some instruments used for preparation and characterization of the material are presented.

3.1 Preparation of the materials

3.1.1 Production of graphene oxide by Hummer's method

The Hummer's method is the chemical route which was developed in 1958 by Hummers and Offeman as a risk-free, quicker, and more effective way of making graphene oxide [63]. The method was introduced to combat the problems of Staudenmaier-Hofmann-Hamdi method which includes adding potassium chlorate to the combination of concentrated sulphuric acid, nitric acid and graphite at a temperature above 98 ^{o}C for one week. The resultant was hazardous due to the explosion developing from the mixture, time consuming and produced very little amount of graphene oxide [150]. Thus, Hummers method appeared as a substitute to suppress the hazardous caused by the Staudenmaier-Hofmann-Hamdi method. Hummer's method is completed by adding potassium permanganate into the solution of concentrated sulphuric acid, sodium nitrate and graphite which is less hazardous. The whole process is completed under 45 ^{o}C with less than two hours and more quantity of graphene oxide is produced [151][152]. The method appeared to be distinctive following the invention of graphene in 2004 [153]. Since then, a high quantity of graphene oxide with high quality has been produced by many researchers through modification of the Hummers method. In this thesis, the graphene oxide and reduced graphene oxide was produced from graphite powder as the basic precursor via a modified Hummers method.

3.1.2 Freeze-drying technique

Freeze-drying is the procedure which use sublimation technique to remove water or other solvent from a frozen material which are placed under vacuum. Sublimation develops once a frozen liquid changes to the gaseous state without passing through the liquid phase. Therefore, freeze drying works by freezing the material, subsequently decreasing the pressure and adding heat to allow the frozen water in the material to sublimate [154]. It involves three stages, namely; freezing (pre-freezing), sublimation (primary drying) and adsorption (secondary drying) [155]. Freezing of the material is done rapidly using large ice crystals which can be produced by slow freezing or annealing, then increasing the material temperature which allow crystals to grow. Annealing is applied for the materials which tend to precipitate. Thereafter, it is followed by a slow process which involves lowering of pressure and adding heat for water to sublimate from the material. The last stage is the adsorption whereby the bonds between the material and water molecule are broken and removed by raising temperature above the sublimation phase. This technique produces high quality material because of the low processing temperature and maintains the porous structure of the material. The technique has been reported to produce various energy storage materials including carbon and metal oxides [156]. Figure 3.1 presents an illustration of freeze-drying process.

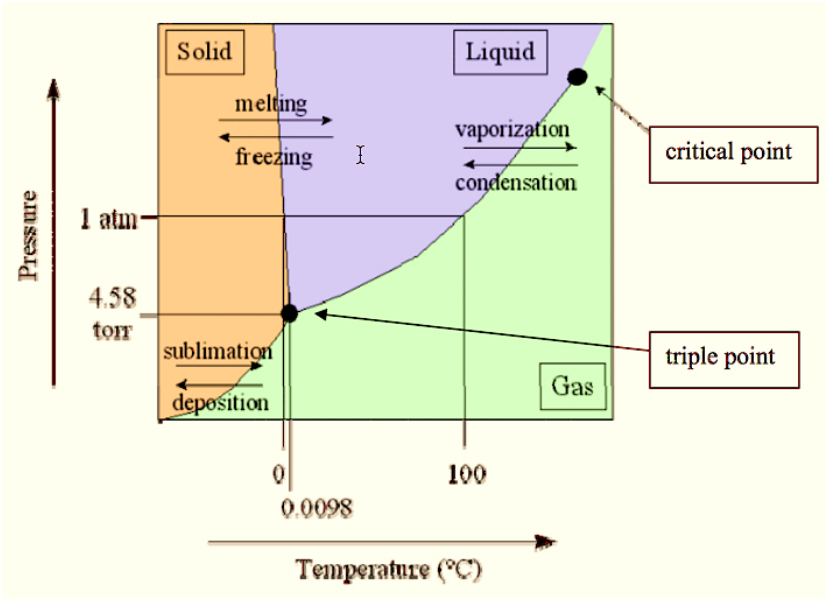

Figure 3.1: Representation design of a freeze-drying process [157].

3.1.3 Preparation of graphene oxide (GO) and reduced graphene oxide (RGO) samples

A modified Hummer's method was applied to produce graphene oxide by utilizing graphite powder as the starting precursor [62][158]. Briefly, 5 g of graphite powder was added slowly to 100 mL of sulphuric acid (H_2SO_4) which works as an intercalated molecules for the penetrating oxidation of bulk graphite in an ice bath to cool the acid. Thereafter, 2.5 g each of potassium hydrogen sulphate ($KHSO_4$) and calcium chloride ($CaCl_2$) were added subsequently upon stirring. $KHSO_4$ was used to start up the reaction while $CaCl_2$ used as a water remover. Effervescence was noticed upon additional of $CaCl_2$. The resulting mixture was stirred at 400 rev/min for 40 min. at 60 ^oC, followed by a further addition of 10 g of potassium permanganate ($KMnO_4$) as an oxidizing agent and 50 mL of H_2SO_4. The solution was further stirred (250 rev/min) for 2 hours at 60 ^oC for homogeneity. The dark-grey resulting mixture was removed from the heating plate and left to cool down to room temperature. Thereafter, 20 mL of hydrogen peroxide (H_2O_2 - 30 %) alongside 120 mL of deionized water (DI water) were added to stop the reaction, which caused a vigorous rise in temperature of the mixture and bore great potential hazard. Therefore, great cautions must be taken during the synthesis of the material.

The resulting mixture called graphene oxide (GO) was allowed to cool down naturally to room temperature, and thereafter was re-dispersed into a 100 mL of DI water and sonicated for 2 hours for further reduction of GO. Sonication uses sound energy to agitate atoms in a solution whereby it converts an electrical signal into a physical vibration to break materials apart. These disturbances can mix solutions, accelerate the dissolution of GO into a liquid and remove dissolved gas from liquids. The mixture was left to settle down for 12 hours, washed several times with DI water and then centrifuge and freeze dried for 12 hours to obtain the final sample named as reduced graphene oxide (RGO), as shown in figure 3.2.

In brief it can be noted that: in concentrated H_2SO_4, $KMnO_4$ reacts to form manganese heptoxide (Mn_2O_7), where a strong oxidant and permanganate ion participate in graphene oxidation. The oxidant mixture has access to the spaces between the graphene layers due to the intercalation of graphite with H_2SO_4. In that case, it will react with graphene and enhancing the functional groups such as hydroxyl (–OH), epoxide (–O–), and carboxylic acids (–COOH) to form GO. Through various situations the oxidation process might not result into a full transformation of graphite to graphite oxide, thus a pre-oxidation phase can be included prior to the common oxidation (e.g. through utilizing $KHSO_4$ in H_2SO_4). An essential process was observed when the reaction was stimulated with water and H_2O_2 in which $HMnO_4$ was formed by the reactions between water and potassium heptoxide, and efficiently stopping the oxidation reaction. Furthermore, the H_2O_2 reacts with manganese oxides in the mixture and reduce them to manganese ions. It follows that, manganese ions, under oxidized graphite, unoxidized graphite and other ions in the mixture were removed and the recovered mixture was named as graphene oxide (GO). Next, the graphene oxide was exfoliated to single-layered or few-layered of GO. Generally, it was achieved by mechanical process through sonication and resulted into reduced graphene oxide (RGO).

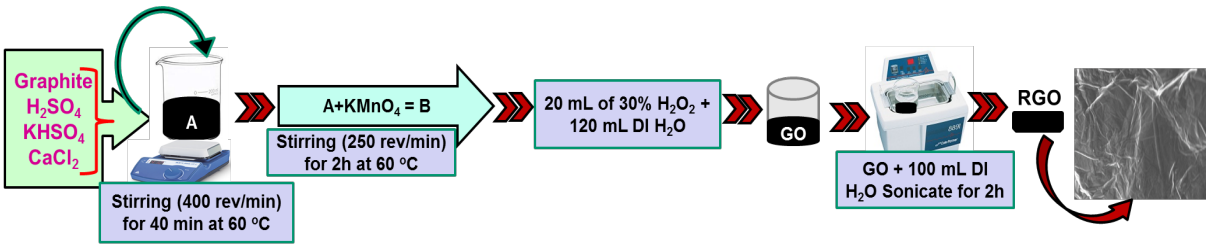

Figure 3.2: Synthesis procedure of RGO sample.

3.1.4 Synthesis of sulphur-reduced graphene oxide (RGO-S) composite

The synthesis of RGO-S composite sample was done as follow: A homogenous solution labelled 'A' was formed by mixing 1 g of sulphur powder and 3 g of sodium sulphide (Na_2S) (act as a sulphur source) into 100 mL of DI water and sonicated. Next, a solution marked 'B' was formed by dissolving 50 g of L-Ascorbic acid in 12 g of DI water. Afterward, 3 g of as-synthesized RGO was mixed into mixture of solutions 'A' and 'B' and the resultant mixture was named 'C'. Subsequently, 2 mL of HCl was added to solution 'C' and then stirred for 5 min. The purpose of adding a small volume of HCl is to enhance the ion exchange and modifying the pH of the mixture, which give rise to an effective polarity. Furthermore, addition of HCl might produce H_2S which is not anticipated to be part of the sulphur in the RGO matrix since it is soluble in water. The mixture was sonicated for 2 h and then stirred (400 revs/min.) for 1 h at 40 °C, centrifuged for 10 min. at 5000 rpm and freeze-dried for 12 h. The as-synthesized sample was named as sulphur doped reduced graphene oxide (RGO-S). Figure 3.3 below is the representation of the synthesis of RGO-S composite sample.

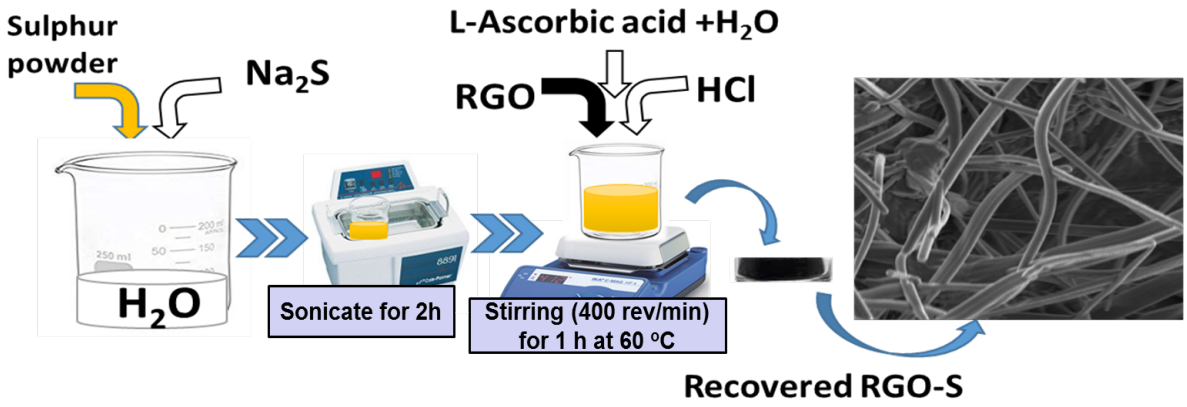

Figure 3.3: Schematic diagram of the synthesis of RGO-S.

3.1.5 Hydrothermal process

Hydrothermal/solvothermal method is the chemical reaction method based on solution which used to produce several chemical compounds and it operates in a closed system. During synthesis, the precursors are dissolved in either water-based medium (hydrothermal method) or nonaqueous/organic compounds medium (solvothermal method) [159]. Under normal conditions some materials like sulphides, silicates, among others, are basically insoluble in water or nonaqueous medium, thus the method provides ability to dilute them at high temperature and pressure [160][161]. Normally, the reaction medium is carried out into an airtight Teflon-lined stainless-steel autoclave or glass autoclaves or quartz autoclaves which is subjected under different conditions. Teflon-lined (Figure 3.4) is one of the mostly used autoclaves due to its ability to sustain higher temperature and pressure. Besides, it's easy to regulate properties of the resulting materials like morphology, structure and size of the nanoparticles through hydrothermal/solvothermal method. This can be done by varying reaction conditions like temperature, concentration, time, and initial pH of the medium [162]. The benefit of hydrothermal/solvothermal method over others is that; it can produce nanomaterials which are not stable at higher temperatures; nanomaterials with high vapor pressures can be produced with minimum loss of the materials, it is also capable of making

high purity and homogeneous product; and the composition can be controlled well through liquid phase or multiphase chemical reactions. However, it is limited by high cost equipment like autoclave and inability to control crystals during growth process [163]. In this study, manganese dioxide and sulphur-reduced graphene oxide/manganese dioxide composite were produced by a hydrothermal method.

Figure 3.4: Schematic design of a Teflon-lined stainless-steel autoclave.

3.1.6 Synthesis of manganese dioxide (MnO_2)

0.5 g of $KMnO_4$ (source of manganese) was dissolved into 60 mL of DI water and stirred at 150 revs/min for 10 min. Afterward, 2 mL of HCl was added dropwise and stirred for 10 min in air. HCl act as a mild reducing agent to reduce $KMnO_4$ to form MnO_2 whereby it is oxidised to free chlorine gas when heated with permanganate salt. The solution was transferred into 100 mL autoclave and heated in the oven at 130 ^oC for 1 h. The processes were repeated at different dwell times of 2 h, 5 h, 8 h and 11 h respectively. The solution was left to cool down naturally and then washed several times with the mixture of DI water and ethanol to remove the

impurities. The sample was dried in the oven for 12 h at 60 ºC. Figure 3.5 shows the synthesis route used to produce the MnO_2 sample.

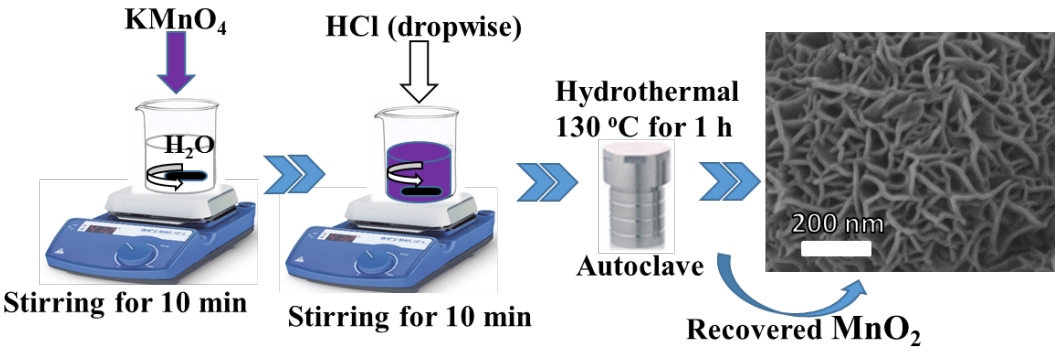

Figure 3.5: Synthesis route of MnO_2 sample.

3.1.7 Synthesis RGO-S/MnO_2 composite sample

1 g of RGO-S was dispersed into 80 mL of DI water to form a solution which was stirred at 200 revs/min for 10 min for homogeneity. Thereafter, 50 mg of MnO_2 prepared for 1 h was added into the solution and then stirred for 5 min. The process was repeated by varying masses of MnO_2 synthesized for 1 h (100 mg and 150 mg). The suspension was transferred into the autoclave and then heated in the oven at 150 ºC for 1 h. The solution was left to cool down to room temperature, washed several times with DI water and then dried in the oven for 12 h. Figure 3.6 displays a representation design of the experimental process for synthesizing sulphur-reduced graphene oxide/manganese dioxide composite.

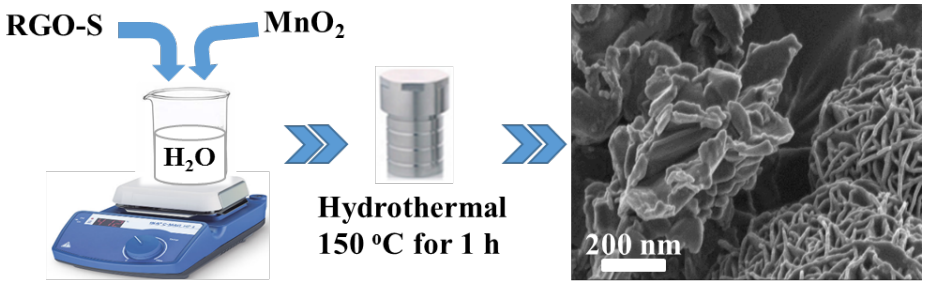

Figure 3.6: Schematic figure of the synthesis of RGO-S/MnO_2 composite sample.

3.1.8 Precipitation method

Precipitation method is the procedure of transforming solution into solid by converting the substance into insoluble form. The chemical reaction that occurs between the soluble metal compounds and the precipitating reagent converts the ionic metals to an insoluble particle, whereby, settling and decantation is applied to remove the particle produced by this reaction [164]. Precipitation is influenced by precipitant, concentration and type of ionic metals existing in the solution, reaction conditions like pH of the mixture, and existence of additional components which might prevent the precipitation reaction [165]. For example, the commonly attained chemical precipitation is the hydroxide precipitation (OH precipitation) through a precipitant known as sodium hydroxide or calcium hydroxide which is applied to form metal hydroxides. Normally, metal hydroxides progressively soluble equally at low and high pH values. Thus, the optimal pH for precipitation of some metal might trigger other metal to soluble or start going back into solution because every liquefied metal contains a unique pH value through which the targeted hydroxide precipitation develops. Compared to other method, precipitation has an elevated degree of refinement due to its option of removing a specific component without removing other materials. However, this method results into agglomeration and randomness of particle size [166][167].

In this study, precipitation was applied to produce cobalt hydroxide from cobalt nitrate precursor then followed by annealing to complete the reaction (cobalt oxide). Annealing is the heat controlling procedure which modifies the microstructure of the materials by changing its physical or chemical properties. Generally, the physical development in the material can be accomplished by a steady cooling. This process can be attained after exposing the material to a temperature over its recrystallization temperature, and then retained at a particular temperature for a certain period for uniformity [168]. This activity can be achieved with the

support of atmospheric pressure chemical vapor deposition system (APCVD). The materials to be annealed are positioned at the central part of the reactor chamber in air, constant gas or combination of gases run at a certain temperature. The technique is simple, economical and consistent hence, appropriate for making uniform, good quality, and significant mass production of the materials [169]. Figure 3.7 displays the APCVD system applied in this thesis for annealing cobalt hydroxide in air in order to produce cobalt oxide.

Figure 3.7: The APCVD system used for annealing in this thesis.

3.1.9 Synthesis of cobalt oxide (Co_3O_4) sample

Co_3O_4 sample was produced by precipitation method and then followed by annealing as displays in figure 3.8 below. 8 g of $CoNO_3$ was dissolved into 400 mL of DI water and stirred for 15 min, then 56 mL of 1 M NaOH was added dropwise into the mixture which changed the color from pink to dark greenish color. $CoNO_3$ precursor was used as a source of cobalt while 1 M NaOH was used for polymerization and to maintain the pH of 10 of the mixture while

stirring for 2 h. The achieved mixture of cobalt hydroxide was decanted, and then DI water was used to wash the sample several times before centrifuging at 10,000 revs/min for 10 min following drying in the oven at 60 °C for 12 h. The dried sample was later annealed in air for 2 h at 800 °C (5 °C/min) using APCVD to remove the OH group and any possible impurities. Equation 15 and 16 below show a complete reaction to obtain Co_3O_4.

$$Co(NO_3)_{2(s)} + 2NaOH_{(l)} + H_2O_{(l)} \rightarrow Co(OH)_{2(s)} + 2NaNO_{3(aq)} + H_2O_{(l)} \quad (15)$$

$$3Co(OH)_{2(s)} \xrightarrow{annealed\ in\ air} Co_3O_{4(s)} + 2H_2O_{(g)} + H_{2(g)} \quad (16)$$

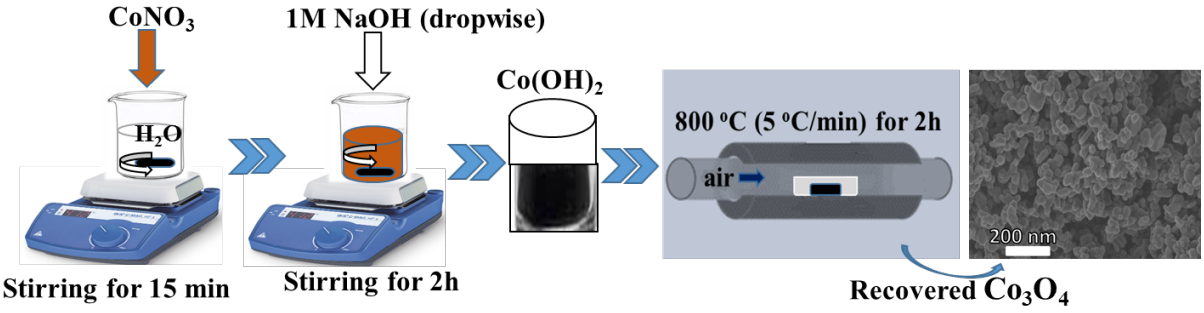

Figure 3.8: Schematic of the synthesis process of Co_3O_4 sample.

3.1.10 Synthesis of RGO-S/Co_3O_4 composite sample

The RGO-S/Co_3O_4 composite sample was prepared through adding 1 g of RGO-S and 100 mg of Co_3O_4 into 100 mL of DI water and sonicated in 1 h for homogeneity (Figure 3.9). Afterward, the mixture was transferred into a Teflon-lined autoclave and heated in the oven at 150 °C for 1 h. The process was repeated by altering the mass of Co_3O_4 between 200 mg and 300 mg. Thereafter, the mixture was let to settle down for easy separation and then washed several times with DI water. Afterward, an oven set at 60 °C was used to dry the sample for 12 h.

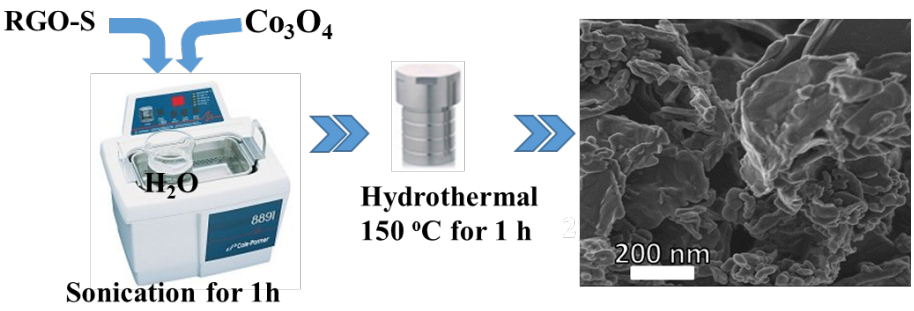

Figure 3.9: Synthesis procedure of RGO-S/Co_3O_4 composite

3.1.11 Synthesis of polyaniline (PANI)

In this thesis, the utilized PANI material was produced as explained in our previously published work [170]. Briefly, 0.2 M aniline hydrochloride was added to 0.25 M of ammonium peroxydisulfate. The mixture was stirred for 10 minutes, and then left to stand overnight for polymerization. The supernatant was decanted away and the collected precipitate was washed several times with deionized water. The resulting sample was dried overnight in an electric oven at 60 °C under ambient condition.

3.1.12 Synthesis of Carbonized Iron Cations Adsorbed onto PANI (C-FP) Material

0.5 g of polyaniline (PANI), 0.4 g iron (II) nitrate nonahydrate, 0.25 g of polyvinylidene fluoride (PVDF) and carbon acetylene black (CAB) were mixed together and then completely dissolved into 20 mL of 99.9 % ethanol (Figure 3.10). The mixture was stirred for 5 minutes and then sonicated until a slurry was formed. The slurry was then pasted into a nickel foam and annealed at a ramping rate of 17 °C/min until 850 °C in nitrogen (500 ccm flow rate) gas environment at a dwell time of 2 h to obtain iron cations (Fe^{2+}) adsorbed onto the PANI film (C-FP) directly grown onto the nickel foam. At this temperature of 850 °C, the PANI film decomposed into the nickel foam template on which the material was coated. The precursors'

masses were carefully selected to ensure an approximate weight ratio of 80:10:10 for iron (II) nitrate salt and PANI, CAB and PVDF, respectively.

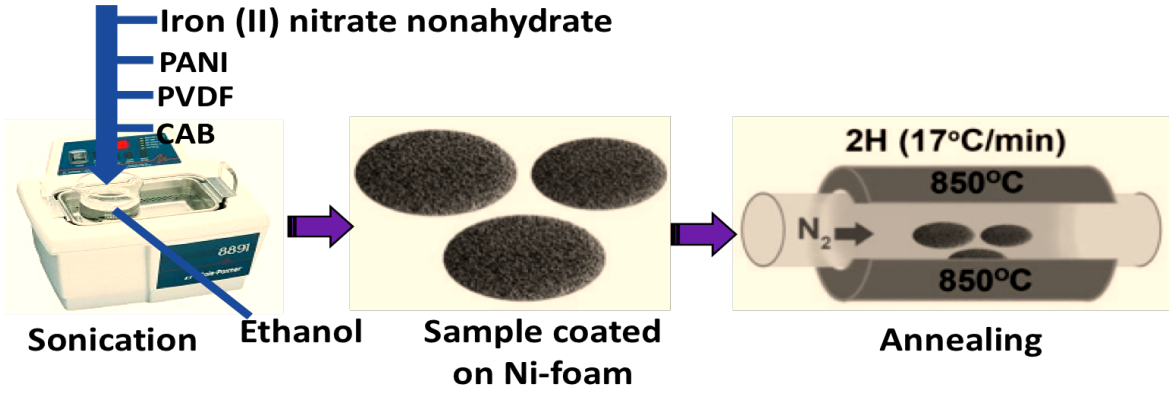

Figure 3.10: Schematic design of the synthesis of carbonized iron cations adsorbed onto PANI (C-FP) sample.

3.1.13 Synthesis of activated carbon from peanut shell waste (AC-PS)

The activated carbon nanostructure applied in this thesis was prepared as reported in our previous work [77]. In brief, two steps at high temperature were followed in the preparation of the material. First, the raw material from peanut shell waste (source of carbon) was pyrolyzed using argon gas at 600 ºC for 2 h. After that, a mass ratio of 1:4 corresponding to peanut shell waste and potassium hydroxide (KOH) as a raw material and activating agent, respectively were mixed together and then activated at 850 ºC for 1 h. The attained sample was labelled as activated carbon from peanut shell waste **(**AC-PS).

3.2 Characterization of the materials

3.2.1 X-ray Photoelectron Spectroscopy (XPS)

X-ray Photoelectron Spectroscopy (XPS) is an instrument utilized to analyse the elemental compositions covering the surface of the material and how they bonded to each other, their

chemical states, electronic structure and density of the electronic states present within the material through the application of photoelectric effect [171]. XPS is affiliated to the group of photoemission spectroscope where a beam of X-rays are irradiated into the material in order to acquire the electron occupant's spectra. The process is achieved by exciting a sample surface with mono-energetic X-rays generating photoelectrons to be emitted from the sample surface and the energy of the emitted photoelectrons (Figure 3.11) is evaluated by the electron energy analyser. The spectrum of the photoelectrons produced can be plotted as the number of electrons emitted against a specific binding energy of the electron detected. A set of distinctive peaks which matches with the arrangement of the electron in the materials (ie. 1s, 2s, 2p, 3s, etc) are generated by each element [172]. A characteristic set of XPS peaks are produced by each element at a particular binding energy values which classify each element that occurs on the surface of the material being analysed. The binding energy can be evaluated by the work of Ernest Rutherford as follows:

$$B.E = h\nu - E_{k.e} - W_f \quad (17)$$

where, $B.E$ is the energy of emitted electron, $h\nu$ present the energy of the X-ray photons being used, $E_{k.e}$ stands for kinetic energy of the emitted electron as measured by the instrument and W_f is the work function of the material.

In this thesis, the electronic states of the surface elements existing within the composite sample was analysed by a Versa Probe 5000 spectrometer XPS analyser activated with a 100 μm monochromatic Al-Kα exciting source.

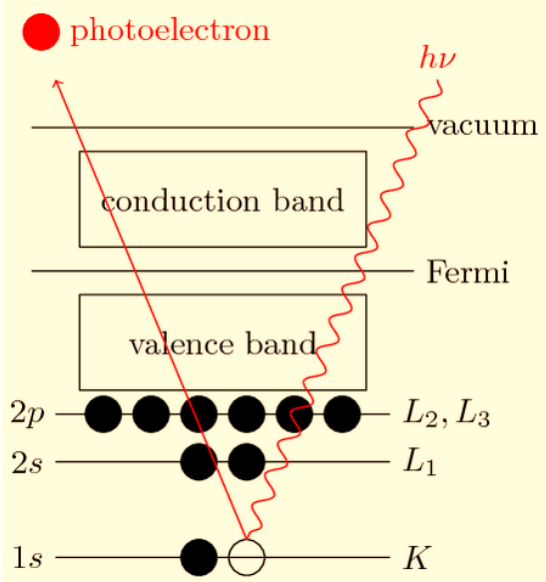

Figure 3.11: Schematic representation of the working principle of XPS

3.2.2 X-ray diffraction (XRD)

X-ray diffraction (XRD) is a non-destructive method that offers comprehensive details concerning phases of the materials, crystallographic structure and preferred orientations, and other structural parameters like crystallinity, grain size, crystal defects and strain [173]. The XRD technique comprises of X-ray detector, X-ray tube and sample holder. XRD spectra are produced in a cathode ray tube by heating a filament to generate electrons, then the electrons are accelerated towards the target (constructed by copper or cobalt) by employing voltage and bombarding the target material with electrons. Therefore, the spectra are generated once the electrons gain sufficient energy to remove inner shell electrons of the target material. These spectra contains several components filtered to produce a monochromatic beam of X-rays through a constructive interference. Therefore, from each set of the lattice planes, the X-rays scattered at a definite angles within the material and fulfill the Bragg's law [174]:

$$n\lambda = 2d\ sin\theta \quad (18)$$

where, λ presents the incident ray wavelength, d represents the spacing among the planes in the atomic lattice, θ shows the incident angle and n is an integer value (1, 2, 3, 4, ….).

The angle between the projection of the x-ray source and the detector is 2θ (Figure 3.12) which shows that the law correlates with the wavelength of the electromagnetic radiation to the diffraction angle and the lattice spacing in a crystalline sample. Due to random orientation of the powder materials, the diffraction directions of the lattice can be achieved by scanning the material in the range of 2θ angles. Thus, X-ray characteristics spectra of various wavelengths are generated based on the target used (Co-λ = 1.7890 Å or Cu- λ = 1.5406 Å) in which the peak intensities are determined by the atomic positions inside the lattice planes [175].

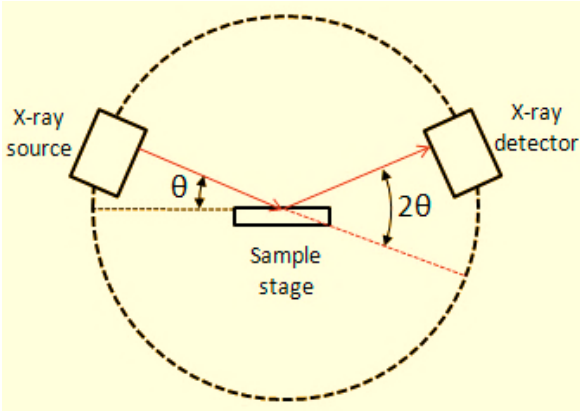

Figure 3.12: Representation of the working principle of X-ray diffraction.

From the XRD peak, the crystallite sizes of the materials can be evaluated by utilizing Scherer's formula as follows:

$$D = \frac{k\lambda}{\beta cos\theta} \tag{19}$$

where, D presents average crystallite size in nanometer, k is the Scherer's constant and equivalent to 0.89, λ is the X-ray wavelength, β is full width half maximum (FWHM) of XRD peak in radian and θ is XRD peak position (one half of 2θ). However, this equation is applicable only for spherical particles.

In this thesis, the phase structures of the material was analysed by X-ray diffraction (XRD - Bruker BV 2D PHASER Best Benchtop); (PANalytical BV, Amsterdam, Netherland) with

reflection geometry at 2θ values (5 - 90°) using Cu K_{α_1} radiation source ($\lambda = 0.15406\ nm$) in a step size of 0.005° at 30 mA and 50 kV.

3.2.3 Raman spectroscopy

Raman spectroscopy is a non-destructive method employed to detect the rotational, vibrational, low frequency modes and chemical structure of the molecular system within the material by using the interaction of light with material [176]. Raman spectroscopy is built on the Raman effect that involves light scattering procedure. When light interacts with the molecules in solid, liquid or gas it includes both; elastic (Rayleigh) scattering with similar wavelength to incident light, and inelastic (Raman) scattering at different wavelengths, due to molecular vibrations [177]. A Raman spectra can be evaluated when a particle scatters incident light of a laser light source at a high intensity. The polarization of the molecular electron cloud is induced by the oscillating electromagnetic field of the photon. This transfers the energy of the photon to the molecule and make it to stay in a higher energy density state. The number of peaks features by the Raman spectrum is indicated by the Raman scattering light showing its intensity and the wavelength position. Distinct peak matches a particular molecular vibration comprising of individual bonds and/or groups of bonds. The energy variation linking the incident light and scattered light is known as Raman shift which is displayed by the resultant spectrum representing the intensity of the scattered light versus wavelength of the Raman shift (cm^{-1}). The shift at wavelength higher and lower than that of the incident light is characterized as Stokes and ant-Stokes scattering, respectively. The former develops when the molecule acquires energy from the photon during scattering, and the scattered photon loses energy which increases the wavelength, while the latter occurs when the molecule loses energy by resting at the lower vibrational level, and the scattered photons get the matching energy which decreases the wavelength [178]. Mostly, higher-intensity Stokes scattering peaks are utilized for analysis,

in spite of anti-Stokes peaks which are rarely used. This is because quantum mechanically, Stokes and ant-Stokes are correspondingly possible processes, through an ensemble of molecules the bulk of molecules will be in the ground vibrational level (Boltzmann distribution). Thus, Stokes scatter is statistically more likely process [179]. For example, Figure 3.13 illustrates the Raman spectrum of sulphur measured using the excitation wavelength of 532 nm (green laser) in which the Stokes scattering is noticed in the lower wavenumber (longer wavelength) region and anti-Stokes scattering in the higher wavenumber (shorter wavelength) region [180][181].

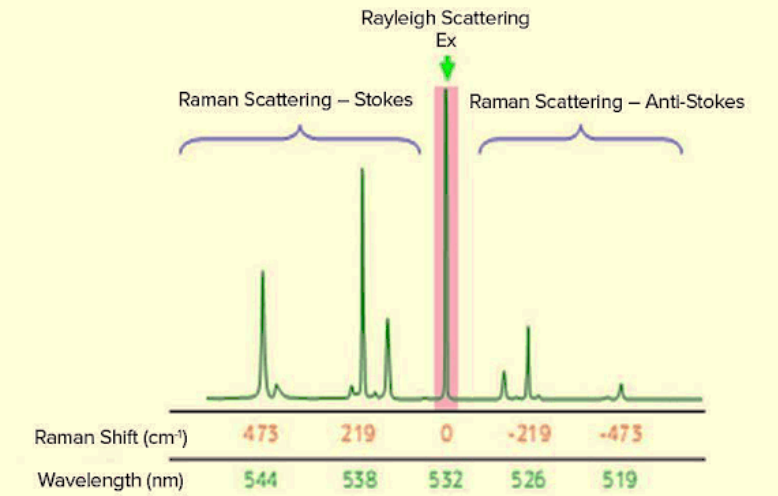

Figure 3.13: Raman spectrum of sulphur [182].

In this thesis, A WITec alpha 300 RAS+Confocal micro-Raman microscope (Ulm, Germany) displayed in Figure 3.14 was utilized to analyse the synthesized samples. To avoid sample heating, the system was operated at laser power of 5 mW and wavelength of 532 nm in a spectral acquisition time of 150 s.

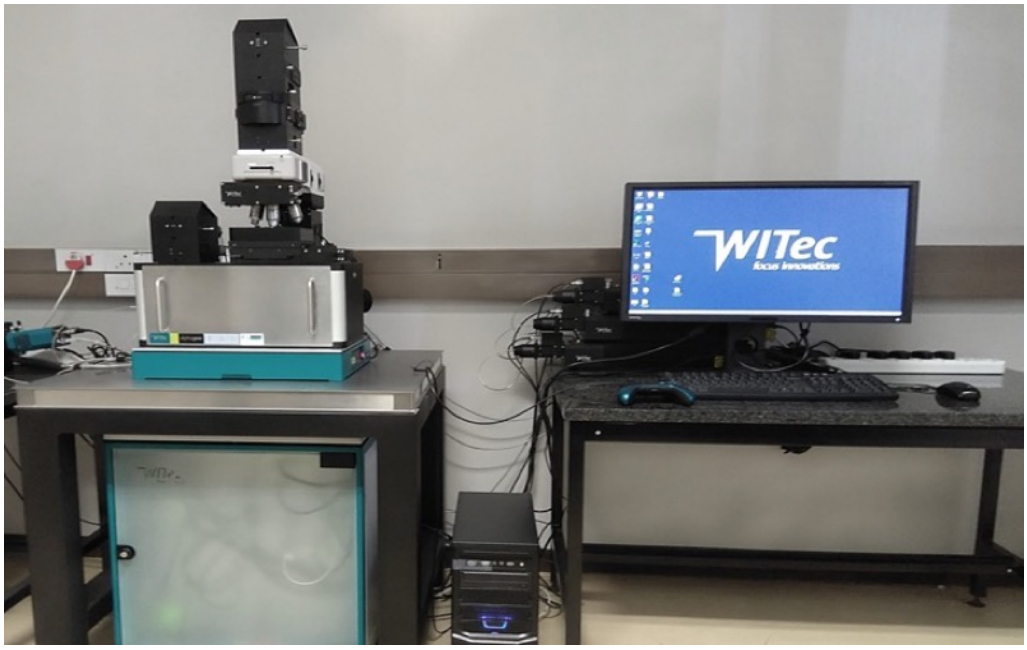

Figure 3.14: A WITec alpha 300 RAS+Confocal micro-Raman microscope (Ulm, Germany) employed for samples characterization in this thesis.

3.2.4 Fourier transform infrared (FTIR) spectroscopy

The FTIR spectroscopy is a technique developed to attain an infrared spectrum of transmission, absorption or emission of solid, liquid or gas molecules by assembling the high-spectral resolution data through a broad spectral range [183]. It employs the mathematical process (Fourier) to interpret the raw data (interferogram) into the actual spectrum. FTIR spectroscopy is acquired to identify different functional groups within the materials. Usually, the bonds between various elements absorb lights at different frequency and then, the light is measured using an infrared spectrometer which creates the output of an infrared spectrum. The vibration characteristics of the chemical functional groups in the sample are detected by Infrared spectroscopy. Once the infrared light interacts with the material, it makes the chemical bonds to stretch, contract and bend. Consequently, it allows the chemical functional group to adsorb infrared radiation in a particular wavenumber range irrespective of the structure of the rest of the molecule. Therefore, the relationship between the band wavenumber location and the

chemical structure is applied to determine the functional group within the material. The specific molecular groups dominant in the materials will be established via a spectrum data in the automated software of spectroscopy subject on the infrared absorption frequency range (4000 – 400 cm^{-1}) which will be presented as the infrared light absorbance/reflectance/transmittance versus frequency (wavelength) [184]. The standard FTIR spectrometer (Figure 3.15) consists of detector, sample cell, amplifier, A/D convertor, computer and source of radiation. The radiation from the source passes via interferometer to get to the detector in which the signal is magnified and changed to a digital signal by the A/D convertor and amplifier, thereafter, the signal is communicated to the computer [185]. The FTIR attained via a Varian FTIR spectroscopy ranging 400 - 4000 cm^{-1} in wavenumber was employed to determine the functional group of the material in this thesis.

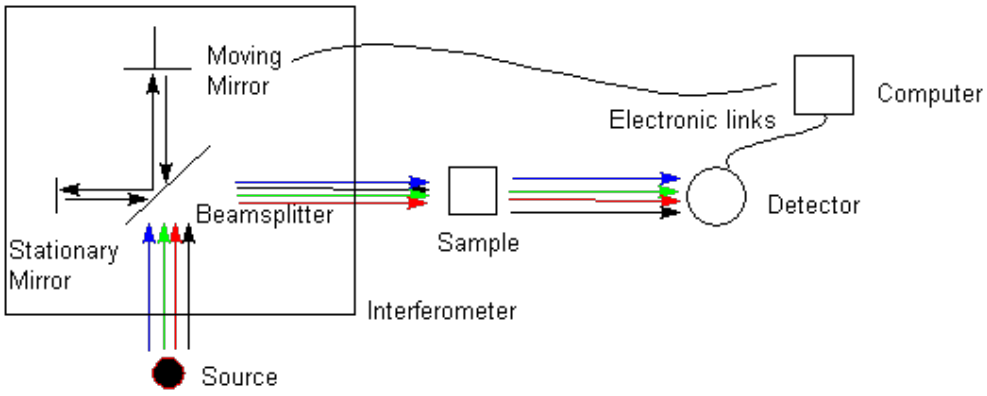

Figure 3.15: A schematic design of FTIR spectrometer [186].

3.2.5 Scanning electron microscope (SEM)

The scanning electron microscope (SEM) is an instrument utilizing a high-energy beam of electrons to scan the surface of a material in order to produce a high-resolution image which display information about topography and materials surface composition [187]. When electrons interact with the materials, they generate variety of signals such as: Secondary

electrons (SE – which produce SEM images), backscattered electrons (BSE), photons (characteristics X-rays applied for EDS analysis), diffracted backscattered electrons (EBSD – utilized to determine crystallographic structures and orientations), visible light and bremsstrahlung which are collected by one or more detectors to form images displayed on the computer screen [188]. SE and BSE are normally used for imaging the material whereby, the former is applied for presenting morphology and topography on the samples while the latter is used to demonstrate rapid discrimination of phases in multiphase samples based on mean atomic number. X-ray production is generated by electron rearrangement in the energy levels of the electronic structure in different shells in which characteristics X-rays are applied to classify composition and elements presents within the material. Generally, SEM consists of an electron gun/source, anode (accelerator), electron beam, magnetic lenses, detector and sample holder [189]. When an electron gun releases electrons, they become accelerated by the applied voltage where the magnetic lenses converge the stream of electrons into a focused beam which then hits the sample surface in a particular spot. The electron beam then scans the surface of the material in a rectangular raster and magnification can be amplified by decreasing the size of the scanned area on the sample. The equivalent signals are measured, and the values are mapped as variations in brightness on the image display. The SE are more frequently used as the read-out signal.

Energy dispersive X-ray spectroscopy (EDS) is the standard method applied to recognize and quantify the elemental compositions and/or chemical characterization present within the material [190]. The EDS set-up is linked with SEM system whereby the analysis is performed concurrently. In EDS, the atom within the material are determined by SEM's high-energy beam of charged particles like protons or electrons that hits the material and excite the emission of characteristics X-rays from an inner shell. This shows that, the developed electron vacancies

are occupied by electrons from higher-energy shell, and the emitted X-ray is used to balance the difference in energy between the higher energy shell and the lower energy shell of the electron. Therefore, the atoms on the surface of the materials are excited by the electron beam which emits specific wavelengths of X-rays energy which are representative of the atomic structure of the elements [191]. The X-ray emission can be evaluated by utilizing energy dispersive detector which distinguishes among X-ray energies via spectrum. The characteristic spectrum attained permits the elemental identification through matching with the reference spectra. Hence, relevant elements are allocated revealing the composition of the atoms on the materials surface [192]. Figure 3.16 display the scanning electron microscope (SEM-Zeiss Ultra Plus 55 field emission scanning electron microscopes; Akishima-shi, Japan) run at 2.0 kV and fitted out with an energy dispersive X-ray spectroscopy (EDS) functioned at 20 kV which was employed to study the morphology and elemental composition of the synthesized samples.

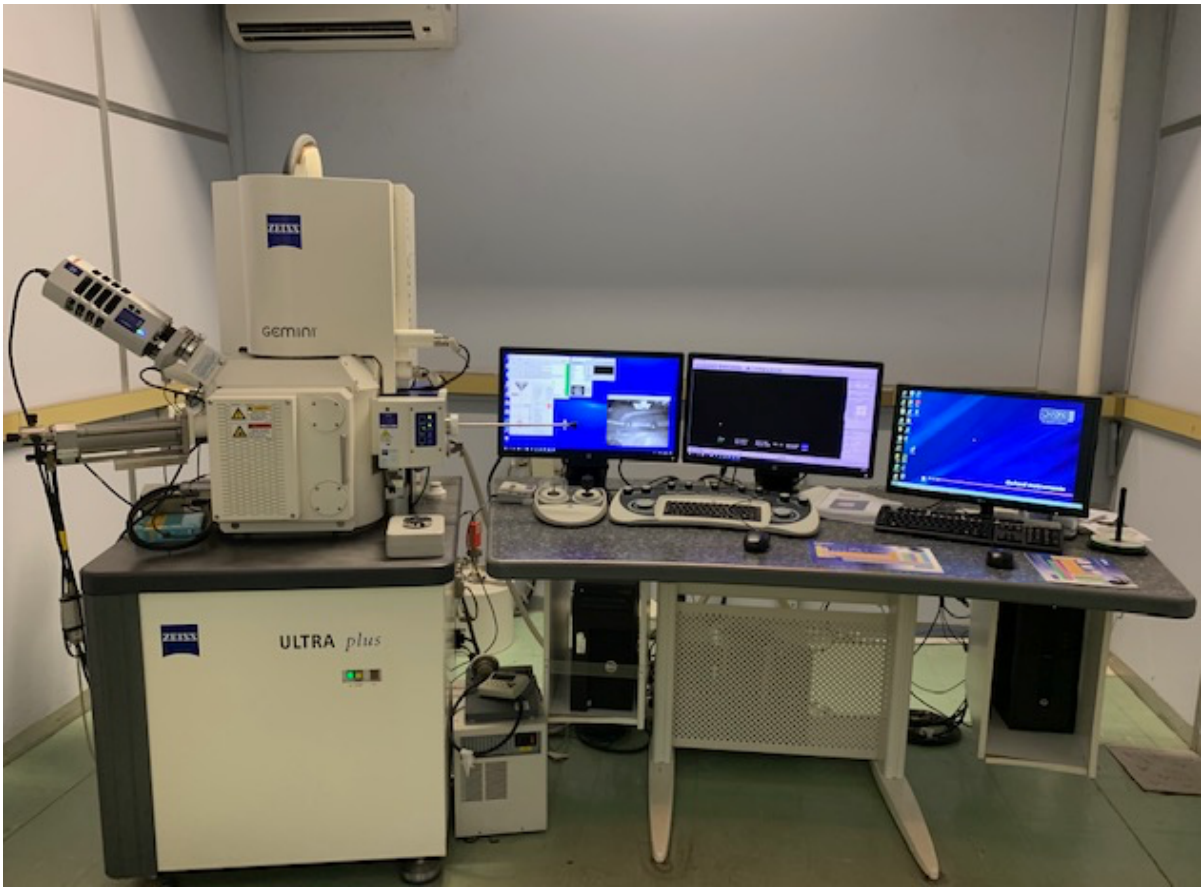

Figure 3.16: High-resolution field emission scanning electron microscope (SEM-Zeiss Ultra Plus 55).

3.2.6 Transmission electron microscopy (TEM)

A transmission electron microscope (TEM) is a method employed to study the sample morphology in transmission mode by giving much higher resolution of the material than SEM through using electron magnification [193]. The electron gun which is a part of a TEM accelerate electrons to pass through the material and drawn toward one end of the anode. After the electrons leave the electron gun, they enter the condenser scheme that comprises of one or two electromagnetic lenses which produce a magnetic field that narrows the electrons into a thin beam. Next, the electron beam enter the image generating scheme where at the start of the scheme is the sample being imaged. When electron beam is transmitted through the sample some electrons are detained or bounced as they try to pass through the sample. The transmitted

ones then become focused as an enlarged image onto a fluorescent screen, which emit light when knocked by these charged particles to create image [194]. Thus, the way image is produced in TEM shows the difference between TEM and SEM, where SEM images are created by electrons that are emitted from the surface which gives surface image of the sample unlike TEM which acquires image of the internal composition of the material. TEM display various features of the sample, such as high magnification image of the internal structure like morphology and crystallization and stress. Most TEM systems have a resolution of less than 0.05 nm, thus, the specimen has a very thin tube less than 100 nm in order to allow the electrons to pass through [195]. Figure 3.17 shows a high-resolution transmission electron microscope (HRTEM FEI Tecnai-F30 JEOL 2100F; built-in with LaB6 filament, a Gartan U1000 camera of 2028 x 2028 pixels; Akishima-shi, Japan) functioned at 200 kV which was applied to study the internal structure of the synthesized samples in this thesis.

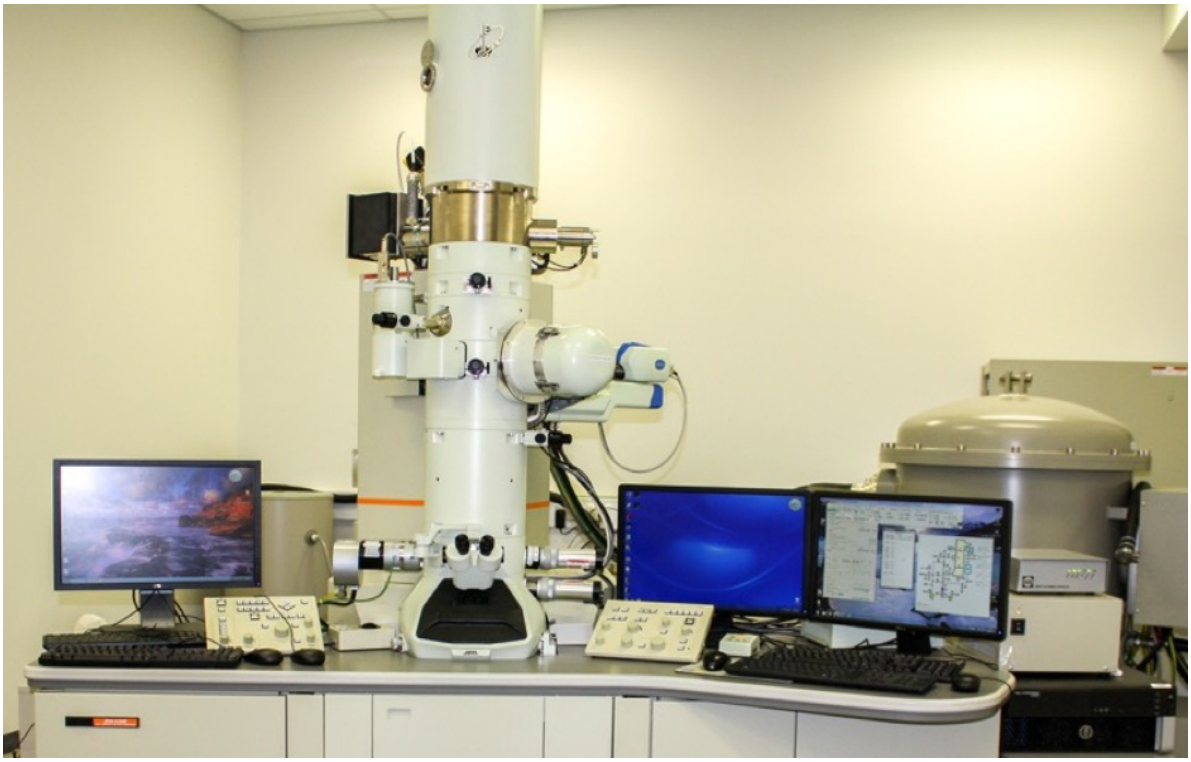

Figure 3.17: High-resolution transmission electron microscope (HRTEM FEI Tecnai-F30 JEOL 2100F).

3.2.7 The N_2 gas adsorption/desorption analysis

The gas adsorption/desorption technique is grounded on the gas adsorption theory on solid surfaces. The varying curve of equilibrium adsorption under a certain pressure is named as adsorption isotherm. The specific surface area (SSA), pore size distribution and average pore volume can be evaluated by analyzing the adsorption isotherm. The nitrogen adsorption on solid surface depends on the nitrogen-relative pressure (P/Po; 0.05 – 0.1) where P is the partial pressure of the nitrogen and Po is the saturated vapor pressure of nitrogen under temperature of liquid nitrogen. In this thesis, the N_2 adsorption/desorption isotherms were measured by NOVA Touch LX^6 version equipped with a quanta-chrome Touch-Win software analyzer. The specific surface area was calculated using Brunauer-Emmett-Teller (BET) method from the adsorption/desorption curve while pore size distribution was evaluated by using DFT method. All samples were degassed at 80 ^oC for 10 h under high vacuum environment in order to remove the remaining moistures. Thereafter, the samples were loaded into analysis chamber under liquid nitrogen at a low temperature (77 K) and pressure. It was monitored by treating the samples with a certain amount of gas and followed by evacuation of the gas to obtain the amount of gas adsorbed by the samples over a relative pressure range (P/Po; $0.01 < P/Po < 0.2$).

The adsorption isotherms are categorized depending on the molecular interactions between the gas and the adsorbed surface. The five types of isotherm were firstly reported by Brunauer et al. (1940) [196] followed by six isotherm types reported by International Union of Pure and Applied Chemistry (IUPAC) (1985) [197]. Later, Gregg and Sing provided details on the differences among the classifications of isotherms with additional adsorption and desorption hysteresis [198]. Figure 3.18 (a) presents different types of isotherms. The adsorption on the microporous structure is presented by type I isotherm which is termed as Langmuir type. The strong and weak interactions correspond to microporous showing type II and III, respectively.

The weak interactions of mesoporous structure are characterized by type V. Type VI is a typical stepwise of layer-by-layer adsorption on the microporous surface. The adsorption/desorption hysteresis loop is categorized into four classes specifically, H1, H2, H3 and H4 as displayed in figure 3.18 (b). H1 is ascribed to the small distribution of related cylindrical-like pores, H2 indicates a complex pore structure, while H3 and H4 matching the collections of slit-shaped pores, and complex materials comprising of both microporous and mesoporous structures, respectively.

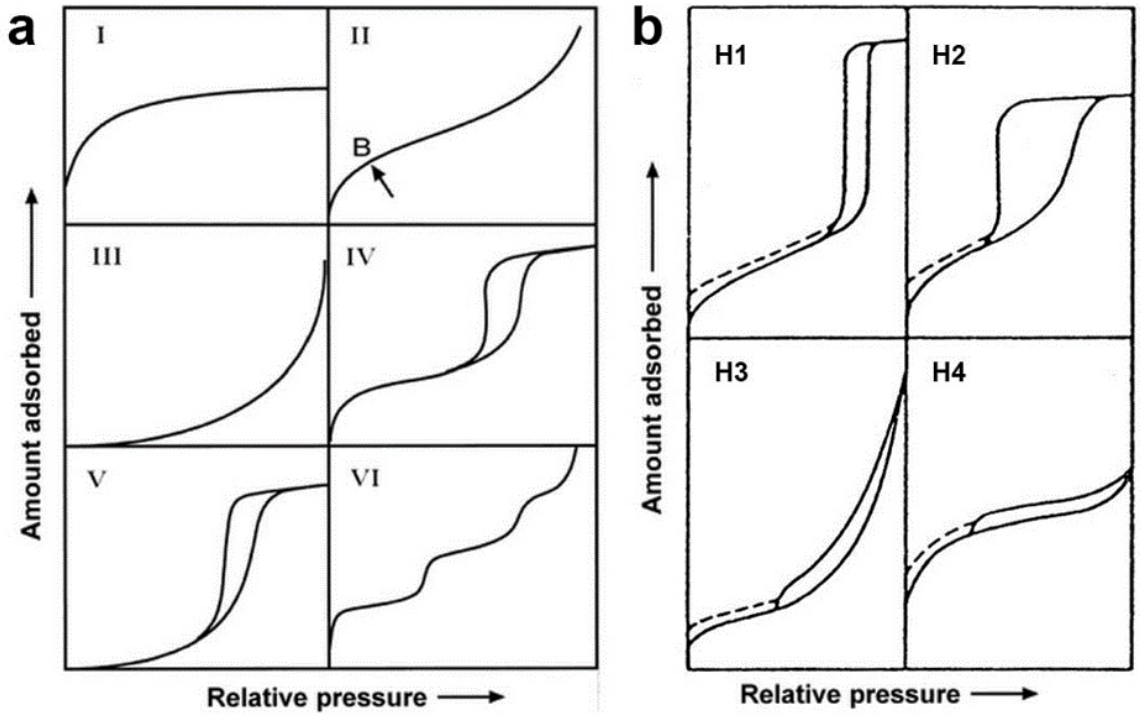

Figure 3.18: (a) The IUPAC classification of adsorption/desorption isotherms for gas-solid equilibria and (b) the adsorption/desorption hysteresis [197].

3.4 Electrochemical characterization

The electrochemical characterization of the synthesized sample in this thesis was conducted by a Biologic VMP300 potentiostat (Knoxville TN 37930, USA) controlled by EC-Lab V1.40 software as shown in Figure 3.19 [199]. The working electrode was prepared by adding few

drops of 1-methyl 2-pyrollidone (NMP) in a mixture contains 80 % of the active material and 10 % each of conductive carbon acetylene black (CB) and Polyvinylidene fluoride (PVDF) to make a slurry. The slurry was pasted onto a clean nickel foam used as a current collector and then dried in an oven at 60 ^{o}C for 12 h. The capacitive performance of the electrodes was conducted in the three- and two-electrode measurements systems. The electrochemical measurements in three electrode configuration were carried out using synthesized sample as the working electrode, Ag/AgCl as a reference electrode and glassy carbon as a counter electrode in aqueous electrolytes. For two-electrode, the device was fabricated by sand witching the synthesized material with a filter paper as a separator in a coin cell configuration. The cyclic voltammetry (CV), galvanostatic charge-discharge (GCD) and electrochemical impedance spectroscopy (EIS) in a frequency range of 0.01 Hz to 100 kHz at open circuit potential were measured in both configurations.

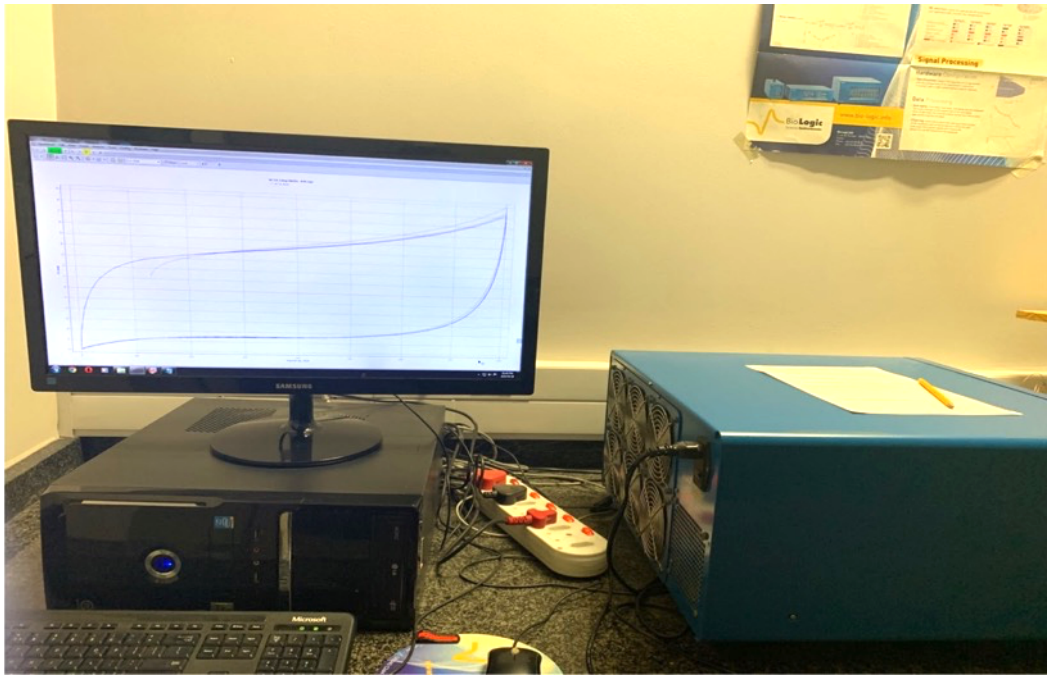

Figure 3.19: A Biologic VMP300 potentiostat used in this thesis.

REFERENCES

[1] J.W. Lund, 100 Years of Geothermal Power Product, Proceedings. (2005) 1–10.

[2] T. Ma, H. Yang, L. Lu, Development of hybrid battery-supercapacitor energy storage for remote area renewable energy systems, Applied Energy. 153 (2015) 56–62. https://doi.org/10.1016/j.apenergy.2014.12.008.

[3] G. Kayakutlu, E. Mercier-Laurent, 3 - Intelligence for Energy, in: G. Kayakutlu, E. Mercier-Laurent (Eds.), Intelligence in Energy, Elsevier, 2017: pp. 79–116. https://doi.org/https://doi.org/10.1016/B978-1-78548-039-3.50003-1.

[4] A.R. Dehghani-Sanij, E. Tharumalingam, M.B. Dusseault, R. Fraser, Study of energy storage systems and environmental challenges of batteries, Renewable and Sustainable Energy Reviews. 104 (2019) 192–208. https://doi.org/10.1016/j.rser.2019.01.023.

[5] X. Zhang, L. Hou, A. Ciesielski, P. Samorì, 2D Materials Beyond Graphene for High-Performance Energy Storage Applications, Advanced Energy Materials. 6 (2016) 21. https://doi.org/10.1002/aenm.201600671.

[6] R.B. Rakhi, H.N. Alshareef, Enhancement of the energy storage properties of supercapacitors using graphene nanosheets dispersed with metal oxide-loaded carbon nanotubes, Journal of Power Sources. 196 (2011) 8858–8865. https://doi.org/10.1016/j.jpowsour.2011.06.038.

[7] A. Eftekhari, Metrics for Fast Supercapacitors as Energy Storage Devices, ACS Sustainable Chemistry and Engineering. 7 (2019) 3688–3691. https://doi.org/10.1021/acssuschemeng.7b04532.

[8] K.W. Nam, C.W. Lee, X.Q. Yang, B.W. Cho, W.S. Yoon, K.B. Kim, Electrodeposited manganese oxides on three-dimensional carbon nanotube substrate: Supercapacitive behaviour in aqueous and organic electrolytes, Journal of Power Sources. 188 (2009) 323–331. https://doi.org/10.1016/j.jpowsour.2008.11.133.

[9] P. Simon, Y. Gogotsi, P. Simon, Y. Gogotsi, N. Materials, Materials for electrochemical capacitors To cite this version : HAL Id : hal-02417326, 7 (2019) 845–854.

[10] M. Vangari, T. Pryor, L. Jiang, Supercapacitors: Review of materials and fabrication methods, Journal of Energy Engineering. 139 (2013) 72–79. https://doi.org/10.1061/(ASCE)EY.1943-7897.0000102.

[11] M. Hahn, O. Barbieri, R. Gallay, R. Kötz, A dilatometric study of the voltage limitation of carbonaceous electrodes in aprotic EDLC type electrolytes by charge-induced strain, Carbon. 44 (2006) 2523–2533. https://doi.org/10.1016/j.carbon.2006.05.002.

[12] M. Jayalakshmi, K. Balasubramanian, Simple capacitors to supercapacitors - An overview, International Journal of Electrochemical Science. 3 (2008) 1196–1217.

[13] Xian Jian, Shiyu Liu, Yuqi Gao, Wei Tian, Zhicheng Jiang, Xiangyun Xiao, Hui Tang, Liangjun Yin, Carbon-Based Electrode Materials for Supercapacitor: Progress, Challenges and Prospective Solutions, J. of Electrical Engineering. 4 (2016) 75–87. https://doi.org/10.17265/2328-2223/2016.02.004.

[14] S. Najib, E. Erdem, Current progress achieved in novel materials for supercapacitor electrodes: Mini review, Nanoscale Advances. 1 (2019) 2817–2827. https://doi.org/10.1039/c9na00345b.

[15] A. Noori, M.F. El-Kady, M.S. Rahmanifar, R.B. Kaner, M.F. Mousavi, Towards establishing standard performance metrics for batteries, supercapacitors and beyond, Chemical Society Reviews. 48 (2019) 1272–1341. https://doi.org/10.1039/c8cs00581h.

[16] B. Viswanathan, Chapter 13 - Supercapacitors, in: B. Viswanathan (Ed.), Energy Sources, Elsevier, Amsterdam, 2017: pp. 315–328. https://doi.org/https://doi.org/10.1016/B978-0-444-56353-8.00013-7.

[17] G.Z. Chen, Supercapacitor and supercapattery as emerging electrochemical energy stores, International Materials Reviews. 62 (2017) 173–202. https://doi.org/10.1080/09506608.2016.1240914.

[18] A.S. Lemine, M.M. Zagho, T.M. Altahtamouni, N. Bensalah, Graphene a promising electrode material for supercapacitors—A review, International Journal of Energy Research. 42 (2018) 4284–4300. https://doi.org/10.1002/er.4170.

[19] M.E. Uddin, T. Kuila, G.C. Nayak, N.H. Kim, B.C. Ku, J.H. Lee, Effects of various surfactants on the dispersion stability and electrical conductivity of surface modified graphene, Journal of Alloys and Compounds. 562 (2013) 134–142. https://doi.org/10.1016/j.jallcom.2013.01.127.

[20] Y. Bai, L. Lu, J. Bao, G. Sun, B. Zhang, J. Zeng, S. Chen, The preparation and electrochemical performance of nitrogen-doped graphene/Co(OH)2 composite, International Journal of Electrochemical Science. 14 (2019) 606–617. https://doi.org/10.20964/2019.01.48.

[21] Z. Lin, Y. Liu, Y. Yao, O.J. Hildreth, Z. Li, K. Moon, C.P. Wong, Superior capacitance of functionalized graphene, Journal of Physical Chemistry C. 115 (2011) 7120–7125. https://doi.org/10.1021/jp2007073.

[22] N.A. Kumar, J.B. Baek, Doped graphene supercapacitors, Nanotechnology. 26 (2015). https://doi.org/10.1088/0957-4484/26/49/492001.

[23] S. Verma, B. Verma, Synthesis of sulfur / phosphorous-doped graphene aerogel as a modified super capacitor electrode, (2018).

[24] S. Yaglikci, Y. Gokce, E. Yagmur, Z. Aktas, The performance of sulphur doped activated carbon supercapacitors prepared from waste tea, Environmental Technology. 0 (2019) 1–13. https://doi.org/10.1080/09593330.2019.1575480.

[25] X. Yu, S.K. Park, S.H. Yeon, H.S. Park, Three-dimensional, sulfur-incorporated

graphene aerogels for the enhanced performances of pseudocapacitive electrodes, Journal of Power Sources. 278 (2015) 484–489. https://doi.org/10.1016/j.jpowsour.2014.12.102.

[26] W. Zhang, F. Liu, Q. Li, Q. Shou, J. Cheng, L. Zhang, B.J. Nelson, X. Zhang, Transition metal oxide and graphene nanocomposites for high-performance electrochemical capacitors, Physical Chemistry Chemical Physics. 14 (2012) 16331–16337. https://doi.org/10.1039/c2cp43673f.

[27] Y. Wang, J. Guo, T. Wang, J. Shao, D. Wang, Y.W. Yang, Mesoporous transition metal oxides for supercapacitors, Nanomaterials. 5 (2015) 1667–1689. https://doi.org/10.3390/nano5041667.

[28] Y.T. Wang, A.H. Lu, H.L. Zhang, W.C. Li, Synthesis of Nanostructured mesoporous manganese oxides with three-dimensional frameworks and their application in supercapacitors, Journal of Physical Chemistry C. 115 (2011) 5413–5421. https://doi.org/10.1021/jp110938x.

[29] M. Pang, G. Long, S. Jiang, Y. Ji, W. Han, B. Wang, X. Liu, Y. Xi, D. Wang, F. Xu, Ethanol-assisted solvothermal synthesis of porous nanostructured cobalt oxides (CoO/Co3O4) for high-performance supercapacitors, Chemical Engineering Journal. 280 (2015) 377–384. https://doi.org/10.1016/j.cej.2015.06.053.

[30] P. Simon, Y. Gogotsi, Materials for electrochemical capacitors, Materials for Sustainable Energy: A Collection of Peer-Reviewed Research and Review Articles from Nature Publishing Group. (2010) 138–147. https://doi.org/10.1142/9789814317665_0021.

[31] Z. Song, Y. Zhang, W. Liu, S. Zhang, G. Liu, H. Chen, J. Qiu, Hydrothermal synthesis and electrochemical performance of Co 3O4/reduced graphene oxide nanosheet composites for supercapacitors, Electrochimica Acta. 112 (2013) 120–126.

https://doi.org/10.1016/j.electacta.2013.08.155.

[32] Q. Yang, Z. Li, R. Zhang, L. Zhou, M. Shao, M. Wei, Carbon modified transition metal oxides/hydroxides nanoarrays toward high-performance flexible all-solid-state supercapacitors, Nano Energy. 41 (2017) 408–416. https://doi.org/10.1016/j.nanoen.2017.09.049.

[33] Y. Chiang, Electrochemical Energy Storage for the Grid, World. (2010).

[34] M.S. Whittingham, History, evolution, and future status of energy storage, Proceedings of the IEEE. 100 (2012) 1518–1534. https://doi.org/10.1109/JPROC.2012.2190170.

[35] O. Razbani, M. Assadi, Artificial neural network model of a short stack solid oxide fuel cell based on experimental data, Journal of Power Sources. 246 (2014) 581–586. https://doi.org/10.1016/j.jpowsour.2013.08.018.

[36] P.N. Kanani, The Parthian Battery: Electric current 2000 years ago?, Fachzeitschrift Des VINI. (2004) 38.

[37] D.S. Ginley, D. Cahen, Fundamentals of materials for energy and environmental sustainability, Fundamentals of Materials for Energy and Environmental Sustainability. (2011) 1–753. https://doi.org/10.1017/CBO9780511718786.

[38] J. Ho, T.R. Jow, S. Boggs, Historical introduction to capacitor technology, IEEE Electrical Insulation Magazine. 26 (2010) 20–25. https://doi.org/10.1109/MEI.2010.5383924.

[39] J. Hedesan, J. Tendler, The structure of scientific revolutions, 2017. https://doi.org/10.4324/9781912281589.

[40] M.J. Ratcliff, Abraham Trembley's strategy of generosity and the scope of celebrity in the mid-eighteenth century., Isis; an International Review Devoted to the History of Science and Its Cultural Influences. 95 (2004) 555–575. https://doi.org/10.1086/430649.

[41] A. Allerhand, Who Invented the Earliest Capacitor Bank (“Battery” of Leyden Jars)? It’s Complicated, Proceedings of the IEEE. 106 (2018) 496–503. https://doi.org/10.1109/JPROC.2018.2795846.

[42] J. Both, Electrolytic capacitors, 1890 to 1925: Early history and basic principle, IEEE Electrical Insulation Magazine. 31 (2015) 22–29. https://doi.org/10.1109/MEI.2015.6996675.

[43] M. Yassine, D. Fabris, Performance of commercially available supercapacitors, Energies. 10 (2017). https://doi.org/10.3390/en10091340.

[44] M. Hepel, High Energy-Density Electric Double-Layer and Hybrid Supercapacitors Based on Graphene Composites, Encyclopedia of Surface and Colloid Science, Third Edition. 1 (2015) 1–22. https://doi.org/10.1081/e-escs3-120051485.

[45] L. Zhang, High-Power Energy Storage: Ultracapacitors, Elsevier Inc., 2018. https://doi.org/10.1016/B978-0-12-812786-5.00002-1.

[46] H. Ji, X. Zhao, Z. Qiao, J. Jung, Y. Zhu, Y. Lu, L.L. Zhang, A.H. MacDonald, R.S. Ruoff, Capacitance of carbon-based electrical double-layer capacitors, Nature Communications. 5 (2014). https://doi.org/10.1038/ncomms4317.

[47] A. González, E. Goikolea, J.A. Barrena, R. Mysyk, Review on supercapacitors: Technologies and materials, Renewable and Sustainable Energy Reviews. 58 (2016) 1189–1206. https://doi.org/10.1016/j.rser.2015.12.249.

[48] M.M.M. Ahmed, T. Imae, Graphene-Based Nanolayers Toward Energy Storage Device, Elsevier B.V., 2017. https://doi.org/10.1016/B978-0-444-63739-0.00010-4.

[49] K.B. Oldham, A Gouy-Chapman-Stern model of the double layer at a (metal)/(ionic liquid) interface, Journal of Electroanalytical Chemistry. 613 (2008) 131–138. https://doi.org/10.1016/j.jelechem.2007.10.017.

[50] V.L. Shapovalov, G. Brezesinski, Breakdown of the Gouy - Chapman model for

highly charged Langmuir monolayers: Counterion size effect, Journal of Physical Chemistry B. 110 (2006) 10032–10040. https://doi.org/10.1021/jp056801b.

[51] M.A. Brown, G.V. Bossa, S. May, Emergence of a Stern Layer from the Incorporation of Hydration Interactions into the Gouy-Chapman Model of the Electrical Double Layer, Langmuir. 31 (2015) 11477–11483. https://doi.org/10.1021/acs.langmuir.5b02389.

[52] Y. Jiang, J. Liu, Definitions of Pseudocapacitive Materials: A Brief Review, Energy & Environmental Materials. 2 (2019) 30–37. https://doi.org/10.1002/eem2.12028.

[53] D. Majumdar, M. Mandal, S.K. Bhattacharya, Journey from supercapacitors to supercapatteries: recent advancements in electrochemical energy storage systems, Emergent Materials. (2020). https://doi.org/10.1007/s42247-020-00090-5.

[54] A. Muzaffar, M.B. Ahamed, K. Deshmukh, J. Thirumalai, A review on recent advances in hybrid supercapacitors: Design, fabrication and applications, Renewable and Sustainable Energy Reviews. 101 (2019) 123–145. https://doi.org/10.1016/j.rser.2018.10.026.

[55] X. Li, B. Wei, Supercapacitors based on nanostructured carbon, Nano Energy. 2 (2013) 159–173. https://doi.org/10.1016/j.nanoen.2012.09.008.

[56] J.P. Cheng, J. Zhang, F. Liu, Recent development of metal hydroxides as electrode material of electrochemical capacitors, RSC Advances. 4 (2014) 38893–38917. https://doi.org/10.1039/c4ra06738j.

[57] G.A. Snook, P. Kao, A.S. Best, Conducting-polymer-based supercapacitor devices and electrodes, Journal of Power Sources. 196 (2011) 1–12. https://doi.org/10.1016/j.jpowsour.2010.06.084.

[58] Y. Lu, G. Long, L. Zhang, T. Zhang, M. Zhang, F. Zhang, Y. Yang, Y. Ma, Y. Chen, What are the practical limits for the specific surface area and capacitance of bulk sp2

carbon materials?, Science China Chemistry. 59 (2016) 225–230. https://doi.org/10.1007/s11426-015-5474-y.

[59] A. Bianco, H.M. Cheng, T. Enoki, Y. Gogotsi, R.H. Hurt, N. Koratkar, T. Kyotani, M. Monthioux, C.R. Park, J.M.D. Tascon, J. Zhang, All in the graphene family - A recommended nomenclature for two-dimensional carbon materials, Carbon. 65 (2013) 1–6. https://doi.org/10.1016/j.carbon.2013.08.038.

[60] A. Benítez, A. Caballero, J. Morales, J. Hassoun, E. Rodríguez-Castellón, J. Canales-Vázquez, Physical activation of graphene: An effective, simple and clean procedure for obtaining microporous graphene for high-performance Li/S batteries, Nano Research. 12 (2019) 759–766. https://doi.org/10.1007/s12274-019-2282-2.

[61] H. Nguyen Bich, H. Nguyen Van, Promising applications of graphene and graphene-based nanostructures, Advances in Natural Sciences: Nanoscience and Nanotechnology. 7 (2016). https://doi.org/10.1088/2043-6262/7/2/023002.

[62] J. Yang, S. Gunasekaran, Electrochemically reduced graphene oxide sheets for use in high performance supercapacitors, Carbon. 51 (2013) 36–44. https://doi.org/10.1016/j.carbon.2012.08.003.

[63] W.S. Hummers, R.E. Offeman, Preparation of Graphitic Oxide, Journal of the American Chemical Society. 80 (1958) 1339. https://doi.org/10.1021/ja01539a017.

[64] P.L. Chiu, D.D.T. Mastrogiovanni, D. Wei, C. Louis, M. Jeong, G. Yu, P. Saad, C.R. Flach, R. Mendelsohn, E. Garfunkel, H. He, Microwave- and nitronium ion-enabled rapid and direct production of highly conductive low-oxygen graphene, Journal of the American Chemical Society. 134 (2012) 5850–5856. https://doi.org/10.1021/ja210725p.

[65] C.N.R. Rao, K.S. Subrahmanyam, H.S.S.R. Matte, B. Abdulhakeem, A. Govindaraj, B. Das, P. Kumar, A. Ghosh, D.J. Late, A study of the synthetic methods and

properties of graphenes, Science and Technology of Advanced Materials. 11 (2010). https://doi.org/10.1088/1468-6996/11/5/054502.

[66] F. Bonaccorso, A. Lombardo, T. Hasan, Z. Sun, L. Colombo, A.C. Ferrari, Production and processing of graphene and 2d crystals, Materials Today. 15 (2012) 564–589. https://doi.org/10.1016/S1369-7021(13)70014-2.

[67] K. Parvez, S. Yang, X. Feng, K. Müllen, Exfoliation of graphene via wet chemical routes, Synthetic Metals. 210 (2015) 123–132. https://doi.org/10.1016/j.synthmet.2015.07.014.

[68] M.J. Yoo, H.B. Park, Effect of hydrogen peroxide on properties of graphene oxide in Hummers method, Carbon. 141 (2019) 515–522. https://doi.org/10.1016/j.carbon.2018.10.009.

[69] Z. Tian, J. Li, G. Zhu, J. Lu, Y. Wang, Z. Shi, C. Xu, Facile synthesis of highly conductive sulfur-doped reduced graphene oxide sheets, Physical Chemistry Chemical Physics. 18 (2015) 1125–1130. https://doi.org/10.1039/c5cp05475c.

[70] Y. Li, G. Wang, T. Wei, Z. Fan, P. Yan, Nitrogen and sulfur co-doped porous carbon nanosheets derived from willow catkin for supercapacitors, Nano Energy. 19 (2016) 165–175. https://doi.org/10.1016/j.nanoen.2015.10.038.

[71] J. Han, L.L. Zhang, S. Lee, J. Oh, K.S. Lee, J.R. Potts, J. Ji, X. Zhao, R.S. Ruoff, S. Park, Generation of B-doped graphene nanoplatelets using a solution process and their supercapacitor applications, ACS Nano. 7 (2013) 19–26. https://doi.org/10.1021/nn3034309.

[72] F. Alvi, M.K. Ram, P.A. Basnayaka, E. Stefanakos, Y. Goswami, A. Kumar, Graphene-polyethylenedioxythiophene conducting polymer nanocomposite based supercapacitor, Electrochimica Acta. 56 (2011) 9406–9412. https://doi.org/10.1016/j.electacta.2011.08.024.

[73] M. Duraivel, S. Nagappan, B. Balamuralitharan, S. Selvam, S.N. Karthick, K. Prabakar, C.S. Ha, H.J. Kim, Superior one-pot synthesis of a doped graphene oxide electrode for a high power density supercapacitor, New Journal of Chemistry. 42 (2018) 11093–11101. https://doi.org/10.1039/c8nj01672k.

[74] A.K. Geim, K.S. Novoselov, The rise of graphene, Nature Materials. 6 (2007) 183–191. https://doi.org/10.1038/nmat1849.

[75] B. Quan, S.H. Yu, D.Y. Chung, A. Jin, J.H. Park, Y.E. Sung, Y. Piao, Single source precursor-based solvothermal synthesis of heteroatom-doped graphene and its energy storage and conversion applications, Scientific Reports. 4 (2014) 23–25. https://doi.org/10.1038/srep05639.

[76] P.Z. Guo, Q.Q. Ji, L.L. Zhang, S.Y. Zhao, X.S. Zhao, Preparation and characterization of peanut shell-based microporous carbons as electrode materials for supercapacitors, Wuli Huaxue Xuebao/ Acta Physico - Chimica Sinica. 27 (2011) 2836–2840. https://doi.org/10.3866/PKU.WHXB20112836.

[77] N.F. Sylla, N.M. Ndiaye, B.D. Ngom, D. Momodu, M.J. Madito, B.K. Mutuma, N. Manyala, Effect of porosity enhancing agents on the electrochemical performance of high-energy ultracapacitor electrodes derived from peanut shell waste, Scientific Reports. 9 (2019) 1–15. https://doi.org/10.1038/s41598-019-50189-x.

[78] K. Yang, J. Peng, C. Srinivasakannan, L. Zhang, H. Xia, X. Duan, Preparation of high surface area activated carbon from coconut shells using microwave heating, Bioresource Technology. 101 (2010) 6163–6169. https://doi.org/10.1016/j.biortech.2010.03.001.

[79] L. Khezami, A. Chetouani, B. Taouk, R. Capart, Production and characterisation of activated carbon from wood components in powder: Cellulose, lignin, xylan, Powder Technology. 157 (2005) 48–56. https://doi.org/10.1016/j.powtec.2005.05.009.

[80] I.I.G. Inal, S.M. Holmes, A. Banford, Z. Aktas, The performance of supercapacitor electrodes developed from chemically activated carbon produced from waste tea, Applied Surface Science. 357 (2015) 696–703. https://doi.org/10.1016/j.apsusc.2015.09.067.

[81] H. Pan, J. Li, Y.P. Feng, Carbon nanotubes for supercapacitor, Nanoscale Research Letters. 5 (2010) 654–668. https://doi.org/10.1007/s11671-009-9508-2.

[82] J. Kong, A.M. Cassell, H. Dai, Chemical vapor deposition of methane for single-walled carbon nanotubes, Chemical Physics Letters. 292 (1998) 567–574. https://doi.org/10.1016/S0009-2614(98)00745-3.

[83] C.D. Scott, S. Arepalli, P. Nikolaev, R.E. Smalley, Growth mechanisms for single-wall carbon nanotubes in a laser-ablation process, Applied Physics A: Materials Science and Processing. 72 (2001) 573–580. https://doi.org/10.1007/s003390100761.

[84] J.L. Hutchison, N.A. Kiselev, E.P. Krinichnaya, A. V. Krestinin, R.O. Loutfy, A.P. Morawsky, V.E. Muradyan, E.D. Obraztsova, J. Sloan, S. V. Terekhov, D.N. Zakharov, Double-walled carbon nanotubes fabricated by a hydrogen arc discharge method, Carbon. 39 (2001) 761–770. https://doi.org/10.1016/S0008-6223(00)00187-1.

[85] C. qi YI, J. peng ZOU, H. zhi YANG, X. LENG, Recent advances in pseudocapacitor electrode materials: Transition metal oxides and nitrides, Transactions of Nonferrous Metals Society of China (English Edition). 28 (2018) 1980–2001. https://doi.org/10.1016/S1003-6326(18)64843-5.

[86] A.N. Naveen, P. Manimaran, S. Selladurai, Cobalt oxide (Co3O4)/graphene nanosheets (GNS) composite prepared by novel route for supercapacitor application, Journal of Materials Science: Materials in Electronics. 26 (2015) 8988–9000. https://doi.org/10.1007/s10854-015-3582-2.

[87] M. Toupin, T. Brousse, D. Bélanger, Charge storage mechanism of MnO2 electrode

used in aqueous electrochemical capacitor, Chemistry of Materials. 16 (2004) 3184–3190. https://doi.org/10.1021/cm049649j.

[88] L.-B. Kong, M. Liu, J.-W. Lang, Y.-C. Luo, L. Kang, Asymmetric Supercapacitor Based on Loose-Packed Cobalt Hydroxide Nanoflake Materials and Activated Carbon, Journal of The Electrochemical Society. 156 (2009) A1000. https://doi.org/10.1149/1.3236500.

[89] A. Bello, K. Makgopa, M. Fabiane, D. Dodoo-Ahrin, K.I. Ozoemena, N. Manyala, Chemical adsorption of NiO nanostructures on nickel foam-graphene for supercapacitor applications, Journal of Materials Science. 48 (2013) 6707–6712. https://doi.org/10.1007/s10853-013-7471-x.

[90] H. Kelly-Holmes, Principles and applications of electrochemical capacitors, Electrochimica Acta 45. 45 (2000) 2483–2498. https://doi.org/10.1057/9780230503014.

[91] F. Zhang, D. Zhu, X. Chen, X. Xu, Z. Yang, C. Zou, K. Yang, S. Huang, A nickel hydroxide-coated 3D porous graphene hollow sphere framework as a high performance electrode material for supercapacitors, Physical Chemistry Chemical Physics. 16 (2014) 4186–4192. https://doi.org/10.1039/c3cp54334j.

[92] F. Li, J. Song, H. Yang, S. Gan, Q. Zhang, D. Han, A. Ivaska, L. Niu, One-step synthesis of graphene/{SnO}2nanocomposites and its application in electrochemical supercapacitors, Nanotechnology. 20 (2009) 455602. https://doi.org/10.1088/0957-4484/20/45/455602.

[93] H. Wang, Q. Fu, C. Pan, Green mass synthesis of graphene oxide and its MnO2 composite for high performance supercapacitor, Electrochimica Acta. 312 (2019) 11–21. https://doi.org/10.1016/j.electacta.2019.04.178.

[94] A. Numan, N. Duraisamy, F. Saiha Omar, Y.K. Mahipal, K. Ramesh, S. Ramesh,

Enhanced electrochemical performance of cobalt oxide nanocube intercalated reduced graphene oxide for supercapacitor application, RSC Advances. 6 (2016) 34894–34902. https://doi.org/10.1039/c6ra00160b.

[95] S. Park, S. Kim, Effect of carbon blacks filler addition on electrochemical behaviors of Co3O4/graphene nanosheets as a supercapacitor electrodes, Electrochimica Acta. 89 (2013) 516–522. https://doi.org/10.1016/j.electacta.2012.11.075.

[96] H.J. Ahonen, J. Lukkari, J. Kankare, n- and p-doped poly(3,4-ethylenedioxythiophene): Two electronically conducting states of the polymer, Macromolecules. 33 (2000) 6787–6793. https://doi.org/10.1021/ma0004312.

[97] Y. Huang, H. Li, Z. Wang, M. Zhu, Z. Pei, Q. Xue, Y. Huang, C. Zhi, Nanostructured Polypyrrole as a flexible electrode material of supercapacitor, Nano Energy. 22 (2016) 422–438. https://doi.org/10.1016/j.nanoen.2016.02.047.

[98] K.S. Ryu, Y.G. Lee, Y.S. Hong, Y.J. Park, X. Wu, K.M. Kim, M.G. Kang, N.G. Park, S.H. Chang, Poly(ethylenedioxythiophene) (PEDOT) as polymer electrode in redox supercapacitor, Electrochimica Acta. 50 (2004) 843–847. https://doi.org/10.1016/j.electacta.2004.02.055.

[99] A. Laforgue, P. Simon, C. Sarrazin, J.F. Fauvarque, Polythiophene-based supercapacitors, Journal of Power Sources. 80 (1999) 142–148. https://doi.org/10.1016/S0378-7753(98)00258-4.

[100] X. Cao, H.Y. Zeng, S. Xu, J. Yuan, J. Han, G.F. Xiao, Facile fabrication of the polyaniline/layered double hydroxide nanosheet composite for supercapacitors, Applied Clay Science. 168 (2019) 175–183. https://doi.org/10.1016/j.clay.2018.11.011.

[101] M.A.A. Mohd Abdah, N.H.N. Azman, S. Kulandaivalu, Y. Sulaiman, Review of the use of transition-metal-oxide and conducting polymer-based fibres for high-

performance supercapacitors, Materials and Design. 186 (2020) 108199. https://doi.org/10.1016/j.matdes.2019.108199.

[102] H.W. Wang, Z.A. Hu, Y.Q. Chang, Y.L. Chen, Z.Y. Zhang, Y.Y. Yang, H.Y. Wu, Preparation of reduced graphene oxide/cobalt oxide composites and their enhanced capacitive behaviors by homogeneous incorporation of reduced graphene oxide sheets in cobalt oxide matrix, Materials Chemistry and Physics. 130 (2011) 672–679. https://doi.org/10.1016/j.matchemphys.2011.07.043.

[103] C. Zhong, Y. Deng, W. Hu, D. Sun, X. Han, J. Qiao, J. Zhang, Electrolytes for electrochemical supercapacitors, 2016. https://doi.org/10.1201/b21497-3.

[104] C. Zhong, Y. Deng, W. Hu, J. Qiao, L. Zhang, J. Zhang, A review of electrolyte materials and compositions for electrochemical supercapacitors, Chemical Society Reviews. 44 (2015) 7484–7539. https://doi.org/10.1039/c5cs00303b.

[105] L. Demarconnay, E. Raymundo-Piñero, F. Béguin, A symmetric carbon/carbon supercapacitor operating at 1.6 v by using a neutral aqueous solution, Electrochemistry Communications. 12 (2010) 1275–1278. https://doi.org/10.1016/j.elecom.2010.06.036.

[106] D. Jiménez-Cordero, F. Heras, M.A. Gilarranz, E. Raymundo-Piñero, Grape seed carbons for studying the influence of texture on supercapacitor behaviour in aqueous electrolytes, Carbon. 71 (2014) 127–138. https://doi.org/10.1016/j.carbon.2014.01.021.

[107] H. Wu, X. Wang, L. Jiang, C. Wu, Q. Zhao, X. Liu, B. Hu, L. Yi, The effects of electrolyte on the supercapacitive performance of activated calcium carbide-derived carbon, Journal of Power Sources. 226 (2013) 202–209. https://doi.org/10.1016/j.jpowsour.2012.11.014.

[108] K. Fic, G. Lota, M. Meller, E. Frackowiak, Novel insight into neutral medium as electrolyte for high-voltage supercapacitors, Energy and Environmental Science. 5 (2012) 5842–5850. https://doi.org/10.1039/c1ee02262h.

[109] K. Fic, G. Lota, E. Frackowiak, Effect of surfactants on capacitance properties of carbon electrodes, Electrochimica Acta. 60 (2012) 206–212. https://doi.org/10.1016/j.electacta.2011.11.059.

[110] P. Sun, Z. Li, L. Zhang, C. Dong, Z. Li, H. Yao, J. Wang, G. Li, Synthesis of cobalt-nickel pyrophosphates/N-doped graphene composites with high rate capability for asymmetric supercapacitor, Journal of Alloys and Compounds. 750 (2018) 607–616. https://doi.org/10.1016/j.jallcom.2018.04.024.

[111] A. Brandt, S. Pohlmann, A. Varzi, A. Balducci, S. Passerini, Ionic liquids in supercapacitors, MRS Bulletin. 38 (2013) 554–559. https://doi.org/10.1557/mrs.2013.151.

[112] J.S. Skyler, Ionic-liquid materials for the electrochemical challenges of the future, Endocrinologist. 3 (1993) 233–238. https://doi.org/10.1097/00019616-199307000-00001.

[113] P.W. Ruch, D. Cericola, A. Foelske-Schmitz, R. Kötz, A. Wokaun, Aging of electrochemical double layer capacitors with acetonitrile-based electrolyte at elevated voltages, Electrochimica Acta. 55 (2010) 4412–4420. https://doi.org/10.1016/j.electacta.2010.02.064.

[114] S. Vaquero, R. Díaz, M. Anderson, J. Palma, R. Marcilla, Insights into the influence of pore size distribution and surface functionalities in the behaviour of carbon supercapacitors, Electrochimica Acta. 86 (2012) 241–247. https://doi.org/10.1016/j.electacta.2012.08.006.

[115] E. Raymundo-Piñero, K. Kierzek, J. Machnikowski, F. Béguin, Relationship between the nanoporous texture of activated carbons and their capacitance properties in different electrolytes, Carbon. 44 (2006) 2498–2507. https://doi.org/10.1016/j.carbon.2006.05.022.

[116] Y.T. Pi, Y.T. Li, S.S. Xu, X.Y. Xing, H.K. Ma, Z.B. He, T.Z. Ren, Is the conductive agent useful in electrodes of graphitized activated carbon?, RSC Advances. 6 (2016) 100708–100712. https://doi.org/10.1039/c6ra18246a.

[117] S. Priyono, T.D. Sari, Ramlan, A. Subhan, B. Prihandoko, Effect of polymer binders on the electrochemical Performance of Al-doped lithium titanate electrode, Journal of Physics: Conference Series. 1282 (2019). https://doi.org/10.1088/1742-6596/1282/1/012056.

[118] M.D. Stoller, R.S. Ruoff, Best practice methods for determining an electrode material's performance for ultracapacitors, Energy and Environmental Science. 3 (2010) 1294–1301. https://doi.org/10.1039/c0ee00074d.

[119] N. Elgrishi, K.J. Rountree, B.D. McCarthy, E.S. Rountree, T.T. Eisenhart, J.L. Dempsey, A Practical Beginner's Guide to Cyclic Voltammetry, Journal of Chemical Education. 95 (2018) 197–206. https://doi.org/10.1021/acs.jchemed.7b00361.

[120] S. Zhang, N. Pan, Supercapacitors Performance Evaluation - Zhang - 2015 - Advanced Energy Materials - Wiley Online Library, Advanced Energy Materials. (2015). https://onlinelibrary.wiley.com/doi/pdf/10.1002/aenm.201401401.

[121] D.J. Tarimo, K.O. Oyedotun, A.A. Mirghni, N. Manyala, Sulphur-reduced graphene oxide composite with improved electrochemical performance for supercapacitor applications, International Journal of Hydrogen Energy. 45 (2020). https://doi.org/10.1016/j.ijhydene.2020.03.059.

[122] M. Lu, F. Beguin, E. Frackowiak, Supercapacitors : Materials, Systems, and Applications, Wiley VCH, Weinheim, 2013.

[123] D.J. Tarimo, K.O. Oyedotun, A.A. Mirghni, N.F. Sylla, N. Manyala, High energy and excellent stability asymmetric supercapacitor derived from sulphur-reduced graphene oxide/manganese dioxide composite and activated carbon from peanut shell,

Electrochimica Acta. 353 (2020) 136498.
https://doi.org/10.1016/j.electacta.2020.136498.

[124] A.A. Mirghni, K.O. Oyedotun, B.A. Mahmoud, A. Bello, S.C. Ray, N. Manyala, Nickel-cobalt phosphate/graphene foam as enhanced electrode for hybrid supercapacitor, Composites Part B: Engineering. 174 (2019) 106953. https://doi.org/10.1016/j.compositesb.2019.106953.

[125] J.H. Chae, G.Z. Chen, 1.9 V Aqueous Carbon-Carbon Supercapacitors With Unequal Electrode Capacitances, Electrochimica Acta. 86 (2012) 248–254. https://doi.org/10.1016/j.electacta.2012.07.033.

[126] F. Ochai-Ejeh, M.J. Madito, K. Makgopa, M.N. Rantho, O. Olaniyan, N. Manyala, Electrochemical performance of hybrid supercapacitor device based on birnessite-type manganese oxide decorated on uncapped carbon nanotubes and porous activated carbon nanostructures, Electrochimica Acta. 289 (2018) 363–375. https://doi.org/10.1016/j.electacta.2018.09.032.

[127] N. Aristov, A. Habekost, Cyclic Voltammetry - A Versatile Electrochemical Method Investigating Electron Transfer Processes, World Journal of Chemical Education, Vol. 3, 2015, Pages 115-119. 3 (2015) 115–119. https://doi.org/10.12691/WJCE-3-5-2.

[128] T.S. Mathis, N. Kurra, X. Wang, D. Pinto, P. Simon, Y. Gogotsi, Energy Storage Data Reporting in Perspective—Guidelines for Interpreting the Performance of Electrochemical Energy Storage Systems, Advanced Energy Materials. 9 (2019) 1–13. https://doi.org/10.1002/aenm.201902007.

[129] S. Alehashem, F. Chambers, J.W. Strojek, G.M. Swain, R. Ramesham, Cyclic Voltammetric Studies of Charge Transfer Reactions at Highly Boron-Doped Polycrystalline Diamond Thin-Film Electrodes, Analytical Chemistry. 67 (1995) 2812–2821. https://doi.org/10.1021/ac00113a014.

[130] W. Zhang, C. Ma, J. Fang, J. Cheng, X. Zhang, S. Dong, L. Zhang, Asymmetric electrochemical capacitors with high energy and power density based on graphene/CoAl-LDH and activated carbon electrodes, RSC Advances. 3 (2013) 2483–2490. https://doi.org/10.1039/c2ra23283a.

[131] Allen J. Bard and Larry R. Faulkner, Electrochemical Methods: Fundamentals and Applications, New York: Wiley, 2001, 2nd ed., Russian Journal of Electrochemistry. 38 (2002) 1364–1365. https://doi.org/10.1023/A:1021637209564.

[132] B. Akinwolemiwa, C. Peng, G.Z. Chen, Redox Electrolytes in Supercapacitors, Journal of The Electrochemical Society. 162 (2015) A5054–A5059. https://doi.org/10.1149/2.0111505jes.

[133] A.S. Ambrozevich, S.A. Ambrozevich, R.T. Sibatov, V. V. Uchaikin, Features of Charging–Discharging of Supercapacitors, Russian Electrical Engineering. 89 (2018) 64–70. https://doi.org/10.3103/S1068371218010029.

[134] S. Ban, J. Zhang, L. Zhang, K. Tsay, D. Song, X. Zou, Charging and discharging electrochemical supercapacitors in the presence of both parallel leakage process and electrochemical decomposition of solvent, Electrochimica Acta. 90 (2013) 542–549. https://doi.org/10.1016/j.electacta.2012.12.056.

[135] P.L. Taberna, P. Simon, J.F. Fauvarque, Electrochemical Characteristics and Impedance Spectroscopy Studies of Carbon-Carbon Supercapacitors, Journal of The Electrochemical Society. 150 (2003) A292. https://doi.org/10.1149/1.1543948.

[136] K. Hara, H. Arakawa, C. Dssc, S. Cell, D. Physics, K.M. Jeerage, R.D. Noble, C.A. Koval, M. Kouhnavard, N. Ahmad, L. Babak, V. Ghaffari, N. Chandra, D. Nath, H. Joon, W. Choi, J. Lee, Impedance Spectroscopy Theory, Experiment, and Applications, 2013. https://doi.org/10.1016/j.snb.2007.02.003.

[137] R. Negroiu, P. Svasta, C. Ionescu, A. Vasile, Investigation of Supercapacitor's

Impedance Based on Spectroscopic Measurements, (n.d.).

[138] F. Mansfeld, Analysis and Interpretation of EIS Data for Metals and Alloys - An Introduction to Electrochemical Impedance Measurement, (1999) 1–77.

[139] D.Y. Momodu, Investigation of metal hydroxides graphene composites as electrode materials for supercapacitor applications, (2015) 185. http://repository.up.ac.za/handle/2263/50281.

[140] B.A. Mei, O. Munteshari, J. Lau, B. Dunn, L. Pilon, Physical Interpretations of Nyquist Plots for EDLC Electrodes and Devices, Journal of Physical Chemistry C. 122 (2018) 194–206. https://doi.org/10.1021/acs.jpcc.7b10582.

[141] A. Allison, H.A. Andreas, Minimizing the Nyquist-plot semi-circle of pseudocapacitive manganese oxides through modification of the oxide-substrate interface resistance, Journal of Power Sources. 426 (2019) 93–96. https://doi.org/10.1016/j.jpowsour.2019.04.029.

[142] J. Bisquert, G. Garcia-Belmonte, P. Bueno, E. Longo, L.O.S. Bulhões, Impedance of constant phase element (CPE)-blocked diffusion in film electrodes, Journal of Electroanalytical Chemistry. 452 (1998) 229–234. https://doi.org/10.1016/S0022-0728(98)00115-6.

[143] H. Liu, M.G. George, N. Ge, D. Muirhead, P. Shrestha, J. Lee, R. Banerjee, R. Zeis, M. Messerschmidt, J. Scholta, P. Krolla, A. Bazylak, Microporous Layer Degradation in Polymer Electrolyte Membrane Fuel Cells, Journal of The Electrochemical Society. 165 (2018) F3271–F3280. https://doi.org/10.1149/2.0291806jes.

[144] A. Khosrozadeh, G. Singh, Q. Wang, G. Luo, M. Xing, Supercapacitor with extraordinary cycling stability and high rate from nano-architectured polyaniline/graphene on Janus nanofibrous film with shape memory, Journal of Materials Chemistry A. 6 (2018) 21064–21077. https://doi.org/10.1039/C8TA07426G.

[145] A. Laheäär, P. Przygocki, Q. Abbas, F. Béguin, Appropriate methods for evaluating the efficiency and capacitive behavior of different types of supercapacitors, Electrochemistry Communications. 60 (2015) 21–25. https://doi.org/10.1016/j.elecom.2015.07.022.

[146] A. Bello, F. Barzegar, M.J. Madito, D.Y. Momodu, A.A. Khaleed, T.M. Masikhwa, J.K. Dangbegnon, N. Manyala, Stability studies of polypyrole- derived carbon based symmetric supercapacitor via potentiostatic floating test, Electrochimica Acta. 213 (2016) 107–114. https://doi.org/10.1016/j.electacta.2016.06.151.

[147] D. Weingarth, A. Foelske-Schmitz, R. Kötz, Cycle versus voltage hold - Which is the better stability test for electrochemical double layer capacitors?, Journal of Power Sources. 225 (2013) 84–88. https://doi.org/10.1016/j.jpowsour.2012.10.019.

[148] J. Kowal, E. Avaroglu, F. Chamekh, A. Šenfelds, T. Thien, D. Wijaya, D.U. Sauer, Detailed analysis of the self-discharge of supercapacitors, Journal of Power Sources. 196 (2011) 573–579. https://doi.org/10.1016/j.jpowsour.2009.12.028.

[149] J. Niu, B.E. Conway, W.G. Pell, Comparative studies of self-discharge by potential decay and float-current measurements at C double-layer capacitor and battery electrodes, Journal of Power Sources. 135 (2004) 332–343. https://doi.org/10.1016/j.jpowsour.2004.03.068.

[150] L. Staudenmaier, Verfahren zur darstellung der graphitsäure, Berichte Der Deutschen Chemischen Gesellschaft. 31 (1898) 1481–1487.

[151] J. Chen, B. Yao, C. Li, G. Shi, An improved Hummers method for eco-friendly synthesis of graphene oxide, Carbon. 64 (2013) 225–229. https://doi.org/10.1016/j.carbon.2013.07.055.

[152] D.C. Marcano, D. V. Kosynkin, J.M. Berlin, A. Sinitskii, Z. Sun, A. Slesarev, L.B. Alemany, W. Lu, J.M. Tour, Improved synthesis of graphene oxide, ACS Nano. 4

(2010) 4806–4814. https://doi.org/10.1021/nn1006368.

[153] I.V.G. and A.A.F. K. S. Novoselov, A. K. Geim, S. V. Morozov, D. Jiang, Y. Zhang, S. V. Dubonos, Electric Field Effect in Atomically Thin Carbon Films, 306 (2016) 666–669.

[154] S.C. Tsinontides, P. Rajniak, D. Pham, W.A. Hunke, J. Placek, S.D. Reynolds, Freeze drying - Principles and practice for successful scale-up to manufacturing, International Journal of Pharmaceutics. 280 (2004) 1–16. https://doi.org/10.1016/j.ijpharm.2004.04.018.

[155] Lyophilization/Freeze Drying - An Review 7, (n.d.) 2700.

[156] Z. Ling, C. Yu, X. Fan, S. Liu, J. Yang, M. Zhang, G. Wang, N. Xiao, J. Qiu, Freeze-drying for sustainable synthesis of nitrogen doped porous carbon cryogel with enhanced supercapacitor and lithium ion storage performance, Nanotechnology. 26 (2015). https://doi.org/10.1088/0957-4484/26/37/374003.

[157] S. Singh, Lyophilization/Freeze drying - A review, Age. 20 (2015) 60yrs.

[158] J. Zhang, Z. Yang, X. Wang, T. Ren, Q. Qiao, Homogeneous sulphur-doped composites: Porous carbon materials with unique hierarchical porous nanostructure for super-capacitor application, RSC Advances. 6 (2016) 84847–84853. https://doi.org/10.1039/c6ra17231h.

[159] J. Li, Q. Wu, J. Wu, T.S. Division, O. Ridge, O. Ridge, C. Sciences, E. Division, Handbook of Nanoparticles, Handbook of Nanoparticles. (2015). https://doi.org/10.1007/978-3-319-13188-7.

[160] D. Rickard, G.W. Luther, Chemistry of iron sulfides, 2007. https://doi.org/10.1021/cr0503658.

[161] A.E. Lewis, Review of metal sulphide precipitation, Hydrometallurgy. 104 (2010) 222–234. https://doi.org/10.1016/j.hydromet.2010.06.010.

[162] J. Grandgirard, D. Poinsot, L. Krespi, J.P. Nénon, A.M. Cortesero, Conventional and Microwave Hydrothermal Synthesis and Application of Functional Materials: A Review, Entomologia Experimentalis et Applicata. 103 (2002) 239–248. https://doi.org/10.1023/A.

[163] Y.X. Gan, A.H. Jayatissa, Z. Yu, X. Chen, M. Li, Hydrothermal Synthesis of Nanomaterials, Journal of Nanomaterials. 2020 (2020). https://doi.org/10.1155/2020/8917013.

[164] G. Sharma, A. Kumar, S. Sharma, M. Naushad, R. Prakash Dwivedi, Z.A. ALOthman, G.T. Mola, Novel development of nanoparticles to bimetallic nanoparticles and their composites: A review, Journal of King Saud University - Science. 31 (2019) 257–269. https://doi.org/10.1016/j.jksus.2017.06.012.

[165] Y. Dahman, Chapter 6 - Nanopolymers**By Yaser Dahman, Kevin Deonanan, Timothy Dontsos, and Andrew Iammatteo., in: Y. Dahman (Ed.), Nanotechnology and Functional Materials for Engineers, Elsevier, 2017: pp. 121–144. https://doi.org/https://doi.org/10.1016/B978-0-323-51256-5.00006-X.

[166] B. Akturk, A.B. Kizilkanat, Improvement of durability and drying shrinkage of sodium carbonate activated slag through the incorporation of calcium hydroxide and sodium hydroxide, Construction and Building Materials. 243 (2020) 118260. https://doi.org/10.1016/j.conbuildmat.2020.118260.

[167] S. Barzgar, B. Lothenbach, M. Tarik, A. Di Giacomo, C. Ludwig, The effect of sodium hydroxide on Al uptake by calcium silicate hydrates (C[sbnd]S[sbnd]H), Journal of Colloid and Interface Science. 572 (2020) 246–256. https://doi.org/10.1016/j.jcis.2020.03.057.

[168] H.D. Alvarenga, T. Van De Putte, N. Van Steenberge, J. Sietsma, H. Terryn, Influence of Carbide Morphology and Microstructure on the Kinetics of Superficial

Decarburization of C-Mn Steels, Metallurgical and Materials Transactions A: Physical Metallurgy and Materials Science. 46 (2015) 123–133. https://doi.org/10.1007/s11661-014-2600-y.

[169] K. Xiao, H. Wu, H. Lv, X. Wu, H. Qian, The study of the effects of cooling conditions on high quality graphene growth by the APCVD method, Nanoscale. 5 (2013) 5524–5529. https://doi.org/10.1039/c3nr00524k.

[170] K.O. Oyedotun, M.J. Madito, D.Y. Momodu, A.A. Mirghni, T.M. Masikhwa, N. Manyala, Synthesis of ternary NiCo-MnO2 nanocomposite and its application as a novel high energy supercapattery device, Chemical Engineering Journal. 335 (2018) 416–433. https://doi.org/10.1016/j.cej.2017.10.169.

[171] J.D. Andrade, X-ray photoelectron spectroscopy (XPS), in: Surface and Interfacial Aspects of Biomedical Polymers, Springer, 1985: pp. 105–195.

[172] G. Greczynski, L. Hultman, X-ray photoelectron spectroscopy: Towards reliable binding energy referencing, Progress in Materials Science. 107 (2020) 100591. https://doi.org/10.1016/j.pmatsci.2019.100591.

[173] R. Kohli, K.L. Mittal, eds., Chapter 3 - Methods for Assessing Surface Cleanliness, in: Developments in Surface Contamination and Cleaning, Volume 12, Elsevier, 2019: pp. 23–105. https://doi.org/https://doi.org/10.1016/B978-0-12-816081-7.00003-6.

[174] J. Epp, X-ray diffraction (XRD) techniques for materials characterization, in: Materials Characterization Using Nondestructive Evaluation (NDE) Methods, Elsevier, 2016: pp. 81–124.

[175] J.P. Patel, P.H. Parsania, 3 - Characterization, testing, and reinforcing materials of biodegradable composites, in: N.G. Shimpi (Ed.), Biodegradable and Biocompatible Polymer Composites, Woodhead Publishing, 2018: pp. 55–79. https://doi.org/https://doi.org/10.1016/B978-0-08-100970-3.00003-1.

[176] O.I. Olubiyi, F.-K. Lu, D. Calligaris, F.A. Jolesz, N.Y. Agar, Advances in molecular imaging for surgery, in: Image-Guided Neurosurgery, Elsevier, 2015: pp. 407–439.

[177] P. Vandenabeele, Practical Raman spectroscopy: an introduction, John Wiley & Sons, 2013.

[178] K.S. Joya, X. Sala, In situ Raman and surface-enhanced Raman spectroscopy on working electrodes: Spectroelectrochemical characterization of water oxidation electrocatalysts, Physical Chemistry Chemical Physics. 17 (2015) 21094–21103. https://doi.org/10.1039/c4cp05053c.

[179] K. Kneipp, H. Kneipp, P. Corio, S.D.M. Brown, K. Shafer, J. Motz, L.T. Perelman, E.B. Hanlon, A. Marucci, G. Dresselhaus, M.S. Dresselhaus, Surface-enhanced and normal stokes and anti-stokes raman spectroscopy of single-walled carbon nanotubes, Physical Review Letters. 84 (2000) 3470–3473. https://doi.org/10.1103/PhysRevLett.84.3470.

[180] A.T. Ward, Raman spectroscopy of sulfur, sulfur-selenium, and sulfur-arsenic mixtures, Journal of Physical Chemistry. 72 (1968) 4133–4139. https://doi.org/10.1021/j100858a031.

[181] C. Nims, B. Cron, M. Wetherington, J. Macalady, J. Cosmidis, Low frequency Raman Spectroscopy for micron-scale and in vivo characterization of elemental sulfur in microbial samples, Scientific Reports. 9 (2019) 1–12. https://doi.org/10.1038/s41598-019-44353-6.

[182] G. Guimbretière, S. Duraipandian, T. Ricci, Field remote Stokes/anti-Stokes Raman characterization of sulfur in hydrothermal vents, Journal of Raman Spectroscopy. 49 (2018) 1385–1394. https://doi.org/10.1002/jrs.5378.

[183] G.S. Allan, Fourier Transform Infrared Spectroscopy (FTIR), Encyclopedia of Earth Sciences Series. (2017) 1046. https://doi.org/10.1007/978-1-4020-4409-0.

[184] P.M. Shameer, P.M. Nishath, Exploration and enhancement on fuel stability of biodiesel: A step forward in the track of global commercialization, in: Advanced Biofuels, Elsevier, 2019: pp. 181–213.

[185] D. Titus, E.J.J. Samuel, S.M. Roopan, Nanoparticle characterization techniques, in: Green Synthesis, Characterization and Applications of Nanoparticles, Elsevier, 2019: pp. 303–319.

[186] N.J. and D.R. Vij, FOURIER TRANSFORM INFRARED SPECTROSCOPY, 2006. https://doi.org/10.1007/0-387-37590-2.

[187] M. Salouti, F.K. Derakhshan, Chapter 3 - Phytosynthesis of Nanoscale Materials, in: M. Ghorbanpour, S.H. Wani (Eds.), Advances in Phytonanotechnology, Academic Press, 2019: pp. 45–121. https://doi.org/https://doi.org/10.1016/B978-0-12-815322-2.00003-1.

[188] J.I. Goldstein, D.E. Newbury, J.R. Michael, N.W.M. Ritchie, J.H.J. Scott, D.C. Joy, Scanning electron microscopy and X-ray microanalysis, Springer, 2017.

[189] A.K. Singh, Chapter 4 - Experimental Methodologies for the Characterization of Nanoparticles, in: A.K. Singh (Ed.), Engineered Nanoparticles, Academic Press, Boston, 2016: pp. 125–170. https://doi.org/https://doi.org/10.1016/B978-0-12-801406-6.00004-2.

[190] J. Telegdi, A. Shaban, G. Vastag, Biocorrosion-steel, in: Encyclopedia of Interfacial Chemistry: Surface Science and Electrochemistry, Elsevier, 2018: pp. 28–42.

[191] O.D. Neikov, N.A. Yefimov, Chapter 1 - Powder Characterization and Testing, in: O.D. Neikov, S.S. Naboychenko, N.A. Yefimov (Eds.), Handbook of Non-Ferrous Metal Powders (Second Edition), Second Edi, Elsevier, Oxford, 2019: pp. 3–62. https://doi.org/https://doi.org/10.1016/B978-0-08-100543-9.00001-4.

[192] J. Bergström, 2 - Experimental Characterization Techniques, in: J. Bergström (Ed.),

Mechanics of Solid Polymers, William Andrew Publishing, 2015: pp. 19–114. https://doi.org/https://doi.org/10.1016/B978-0-323-31150-2.00002-9.

[193] T. Walther, Chapter 4 - Transmission Electron Microscopy of Nanostructures, in: S. Thomas, R. Thomas, A.K. Zachariah, R.K. Mishra (Eds.), Microscopy Methods in Nanomaterials Characterization, Elsevier, 2017: pp. 105–134. https://doi.org/https://doi.org/10.1016/B978-0-323-46141-2.00004-3.

[194] C. Escalante, E. Sierra, Fundamentals of transmission electron microscopy, the technique with the best resolution in the world, (2019) 0–6.

[195] R.T. G, A.B. R, Review Article TRANSMISSION ELECTRON MICROSCOPY-AN OVERVIEW ISSN Online : - 2321-7855 International Research Journal for Inventions in TRANSMISSION ELECTRON MICROSCOPY- AN OVERVIEW, (2019).

[196] S. Brunauer, L.S. Deming, W.E. Deming, E. Teller, On a Theory of the van der Waals Adsorption of Gases, Journal of the American Chemical Society. 62 (1940) 1723–1732. https://doi.org/10.1021/ja01864a025.

[197] M. Thommes, K. Kaneko, A. V. Neimark, J.P. Olivier, F. Rodriguez-Reinoso, J. Rouquerol, K.S.W. Sing, Physisorption of gases, with special reference to the evaluation of surface area and pore size distribution (IUPAC Technical Report), Pure and Applied Chemistry. 87 (2015) 1051–1069. https://doi.org/10.1515/pac-2014-1117.

[198] C.D.H.E. (UK); R.A.W.H. (FRG); L.M. (Netherlands); R.A.P. (USA); J.R. (France); T.S. (Poland) K. S. W. SING (UK, *Membership, REPORTING PHYSISORPTION DATA FOR GAS/SOLID SYSTEMS with Special Reference to the Determination of Surface Area and Porosity, 81 (1998) 420–430.

[199] Bio-Logic, EC-Lab Software: Techniques and Applications, (2009) 1–175.

[200] F.-B. Wu, B. Yang, J.-L. Ye, eds., Chapter 2 - Technologies of energy storage systems, in: Grid-Scale Energy Storage Systems and Applications, Academic Press, 2019: pp.

17–56. https://doi.org/https://doi.org/10.1016/B978-0-12-815292-8.00002-2.

[201] L. Zhou, W. Utetiwabo, R. Chen, W. Yang, Layer by Layer Assemble of Colloid Nanomaterial and Functional Multilayer Films for Energy Storage and Conversion, (2019).

[202] E.Z. Kurmaev, A. V. Galakhov, A. Moewes, S. Moehlecke, Y. Kopelevich, Interlayer conduction band states in graphite-sulfur composites, Physical Review B - Condensed Matter and Materials Physics. 66 (2002) 1–3. https://doi.org/10.1103/PhysRevB.66.193402.

[203] Q. Cheng, J. Tang, J. Ma, H. Zhang, N. Shinya, L.C. Qin, Graphene and nanostructured MnO2 composite electrodes for supercapacitors, Carbon. 49 (2011) 2917–2925. https://doi.org/10.1016/j.carbon.2011.02.068.

[204] T. Chen, Y. Tang, Y. Qiao, Z. Liu, W. Guo, J. Song, S. Mu, S. Yu, Y. Zhao, F. Gao, All-solid-state high performance asymmetric supercapacitors based on novel MnS nanocrystal and activated carbon materials, Scientific Reports. 6 (2016) 1–9. https://doi.org/10.1038/srep23289.

[205] X. Zhao, H. Wang, G. Zhai, G. Wang, Facile Assembly of 3D Porous Reduced Graphene Oxide/Ultrathin MnO 2 Nanosheets-S Aerogels as Efficient Polysulfide Adsorption Sites for High-Performance Lithium–Sulfur Batteries, Chemistry - A European Journal. 23 (2017) 7037–7045. https://doi.org/10.1002/chem.201604828.

[206] C.W. Jones, Applications of hydrogen peroxide and derivatives, Royal Society of Chemistry, 2007.

[207] T.T. Nguyen, V.H. Nguyen, R.K. Deivasigamani, D. Kharismadewi, Y. Iwai, J.J. Shim, Facile synthesis of cobalt oxide/reduced graphene oxide composites for electrochemical capacitor and sensor applications, Solid State Sciences. 53 (2016) 71–77. https://doi.org/10.1016/j.solidstatesciences.2016.01.006.

[208] C. A reduced graphene oxide/Co3O4 composite for supercapacitor electrodeXiang, M. Li, M. Zhi, A. Manivannan, N. Wu, A reduced graphene oxide/Co3O4 composite for supercapacitor electrode, Journal of Power Sources. 226 (2013) 65–70. https://doi.org/10.1016/j.jpowsour.2012.10.064.

4.0 RESULTS AND DISCUSSION

This chapter presents the discussion of the results achieved from the synthesis, characterization and electrochemical measurements of all the materials synthesized through different methods. All the results presented in this chapter are author's original research work that have been published and some are still under review as articles in peer-reviewed journals.

4.1 Introduction

This study is motivated on developing sulphur-reduced graphene oxide composite materials for high performance in supercapacitor applications. Hummer's method, hydrothermal and precipitation method were employed in the synthesis of the materials. During synthesis, sodium sulphide and sulphur powder both act as a source of sulphur were introduced into reduced graphene oxide in order to enhance the overall electrochemical performance of the reduced graphene oxide (see section 4.2.1 and 4.2.2). Sulphur element is an appealing material for electrochemical energy storage devices due to its high theoretical capacity (1672 mAh g^{-1}) and specific energy (2600 Wh kg^{-1}), which can improve the whole reaction between sulphur and electrolyte ions to produce sulphide ions [200][201]. Furthermore, the comparatively small electronegativity (S - 2.58) that describe its capability to generate extra redox active sites, has been seen to improve capacity/capacitance of the material by forming strong bond between carbon/metallic surfaces [202]. Previously, only one precursor was used as a source of sulphur which limit the content of sulphur produced as most of them produced sulphide gases. In this study, a combination of two precursors (sodium sulphide and sulphur powder) were utilized so as to increase the sulphur amount. Thus, addition of sulphur content in this study facilitated more redox reaction leading to an increase in the overall capacity/capacitance. Moreover, sulphur is recognized for cost-effectiveness, non-corrosive, readily available and it has good

eco-friendly effect as an electrode material for supercapacitor [201]. Therefore, sulphur-comprising composite materials display reasonably high capacity and high charge/discharge cycle stability developing from the enhanced electrical conductivity, wettability and surface properties of the electrode materials [73]. In this chapter, the synthesis, characterization and the electrochemical results of RGO-S, RGO-S/MnO_2 and RGO-S/Co_3O_4 are discussed.

4.2: Sulphur-reduced graphene oxide composite with improved electrochemical performance for supercapacitor applications

4.2.1: Summary of the study

In this study, two materials were synthesized; reduced graphene oxide (RGO) and sulphur-reduced graphene oxide (RGO-S) by using a modified Hummer's method. First, RGO (pristine) sample was synthesized by using graphite powder as the main precursor, then, during synthesis sulphur (S) was introduced to enhance the electrochemical performance of RGO through forming a composite (RGO-S). The introduction of S to the composite material has demonstrated a huge effect on the overall performance of the composite compared to pristine (RGO) sample. The material was characterized by SEM, TEM, EDX, SPS, XRD, FTIR and Raman spectroscopy. A 6 M KOH was used as electrolyte to evaluate the electrochemical characterization. Attached below is the publication reporting the synthesis procedure, characterization and the electrochemical results for these materials.

INTERNATIONAL JOURNAL OF HYDROGEN ENERGY 45 (2020) 13189–13201

Available online at www.sciencedirect.com

ScienceDirect

journal homepage: www.elsevier.com/locate/he

Sulphur-reduced graphene oxide composite with improved electrochemical performance for supercapacitor applications

*Delvina Japhet Tarimo, Kabir O. Oyedotun, Abdulmajid A. Mirghni, Ncholu Manyala**

Department of Physics, Institute of Applied Materials, SARChI Chair in Carbon Technology and Materials, University of Pretoria, Pretoria 0028, South Africa

HIGHLIGHTS

- RGO-S was synthesized by a modified Hummers method.
- Combination of nanosheet, nanorods and nanofibers morphologies were observed.
- High specific capacity of about 113.8 mAh g^{-1} was recorded for the half cell.
- The material displayed specific energy and power of 35.2 Wh kg^{-1} and 375 W kg^{-1} at 0.5 Ag^{-1}, respectively.
- The fabricated material revealed good electrochemical performance for future supercapacitor applications.

GRAPHICAL ABSTRACT

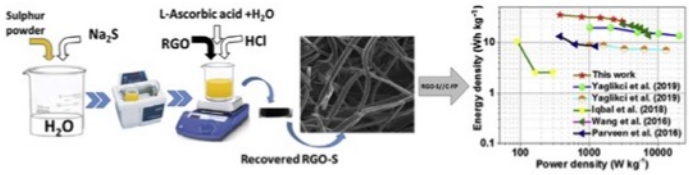

ARTICLE INFO

Article history:
Received 17 December 2019
Received in revised form
2 March 2020
Accepted 7 March 2020
Available online 31 March 2020

Keywords:
Carbon nanorods/fibers
Sulphur-reduced graphene oxide (RGO-S)

ABSTRACT

In this research, carbon nanorods/fibers materials were successfully synthesized from sulphur-reduced graphene oxide (RGO-S) composite by using an improved Hummers' method. Morphological, structural, compositional and textural characterization of the composite material were obtained via scanning electron microscope (SEM), energy dispersive x-ray spectroscopy (EDX), transmission electron microscopy (TEM), X-ray diffraction (XRD), Raman spectroscopy, Fourier transform infrared spectroscopy (FTIR) and X-ray photoelectron spectroscopy (XPS), respectively. The electrochemical performance of the composite sample as a promising supercapacitor electrode revealed a peak specific capacity of 113.8 mAh g^{-1} at 0.5 A g^{-1} estimated via GCD curves in 6 M KOH aqueous electrolyte. The half-cell could retain a columbic efficiency of about 98.7% with a corresponding energy efficiency of about 98.5% over 2000 constant charge/discharge cycle at a

* *Corresponding author.*
E-mail address: ncholu.manyala@up.ac.za (N. Manyala).
https://doi.org/10.1016/j.ijhydene.2020.03.059

Carbonized iron cations (C-FP)
Energy density
Capacity retention

specific current of 5 A g^{-1}. Remarkably, an assembled hybrid device with carbonized iron cations (C-FP) and the RGO-S composite delivered high energy and power densities of 35.2 Wh kg^{-1} and 375 W kg^{-1} at 0.5 A g^{-1} within a 1.5 V operating potential, respectively. A good cycling stability performance with an energy efficiency of 99% was observed for the device for up to 10,000 cycling at a specific current of 3 A g^{-1}.

Introduction

Sufficient resources of energy and their adequate effective usage are some major factors crucial to the growth of our socio-economical modern civilizations. The reliability on the fossil fuel as a main source of energy is heading to an extinction. In the light of this, there is an urgent call to source for alternative sources of energy. This challenge remains critical in our everyday life and thus, requires urgent solutions [1,2]. In order to address this problem, practicable energy storage technology is required to proffer solutions to the lingering energy problem for immediate future demand.

Due to massive effect caused by climatic change and high consumption of fossil fuels, there has been a great interest in developing alternative improved energy storage systems. Such systems include supercapacitors, batteries and other energy conversion system like fuel cells and solar cells [3–8]. Supercapacitor, a device that stores charges by electrochemical process has been considered a potential candidate for efficient energy storage due to its excellent cycling stability, high power density and fast charge/discharge ability [9,10].

Supercapacitors can be categorized into three types: I. Electric double-layer capacitor (EDLCs) which mechanism of charging/discharging is based on the electrostatic process whereby energy is stored by adsorption of ions on the surface of the electrode. II. Redox capacitor which employs faradic mechanism occurring on the surface of the electrode that involves charge-transfer from redox reactions. In redox capacitor the faradic phenomenon involves fast and reversible electrochemical reactions between the electrolyte and electrode materials. III. Hybrid supercapacitor combines faradic electrode material and EDLCs to make up hybrid system [4,10–12].

Normally, carbon based materials such as activated carbon, carbon fibres, graphene, conducting polymers and metal oxides has been categorized as some of the materials used for fabrications of supercapacitors [6,13,14]. However, conducting polymers and transition metal oxide has been faced with low charge discharge rate and cycling stability [15–18].

Graphene has attracted researchers' interest due to its worthy mechanical and chemical stability, high electrical conductivity, larger specific surface area and low cost [3,9,19]. In spite of these excellent properties of the material, when the graphene as electrode material employed in an energy storage devices such as supercapacitors, it is still plagued with low specific capacitance [4,14]. Thus modification of its surface chemistry such as by optimizing the oxygen-containing surface functionalities, as well as morphological properties can improve electrochemical performance of the material [3,8,18–20]. Besides, the introduction of heteroatoms such as sulphur (S), nitrogen (N), boron (B) and phosphorus (P) had been seen to improve the electrochemical performance of the material. Integration of heteroatom into carbon materials has improved electrical and surface properties, decreased charge transfer resistance and improved wettability of graphene-related materials [5,7,11,21].

Incorporation of these heteroatoms by either substitutions or replacement into graphene materials creates defects into graphene as a result of changes in the graphene properties [19,22]. Sulphur-reduced graphene composites are of specific interest due to charge transfer in C–S bond arising from the slight difference in electronegativity of S (2.58) and carbon (2.55) [7,23,24]. Also, sulphur can be easily polarized, thus increase chemical reactivity of the graphene. Yaglikci et al. reported on sulphur doped activated carbon prepared using microwave and activation at 850 °C and obtained a smaller pitted shapes with energy and power densities of 20.1 Wh kg^{-1} and 294.35 W kg^{-1} respectively, at 1 A g^{-1} in 6 M KOH electrolyte and, energy and power densities of 9.06 Wh kg^{-1} and 400.10 W kg^{-1} respectively, at 1 A g^{-1} in 1 M H_2SO_4 electrolyte [6]. Nitrogen and sulphur co-doped carbon nanosheets derived from willow catkin reported by Wang et al. was prepared by pyrolisis and activation at 850 °C displayed interconnected carbon nanosheets with energy and power densities of 21 Wh kg^{-1} and 180 W kg^{-1} respectively, at 50 A g^{-1} in 1 M Na_2SO_4 electrolyte [11]. Iqbal et al. prepared graphene oxide based strontium sulfide using hydrothermal method and obtain nanorods like morphology with few bunches indicating an incomplete growth of nanorods that exhibited energy and power densities of 10.55 Wh kg^{-1} and 294.35 Wh kg^{-1} respectively, at 0.5 $mAcm^{-2}$ in 2 M KOH electrolyte [13]. Parveen et al. obtained sulphur doped graphene using electrochemical exfoliation method and obtained a transparent sheets with a small black dots with energy density of 9.6 Wh kg^{-1} and power density of 375.7 Wh kg^{-1} at 5 A g^{-1} in 3 M KOH electrolyte [25]. These results show that heteroatom composite carbon materials demonstrated synergetic electrochemical properties due to high electron donating property and charge density enhancement of carbon materials. However, in most cases chemical and thermal treatment were used to prepare carbon-based material in which it requires high energy, longer reaction time and organic solvents in order to reduce functional groups in graphene oxide which become problems for mass production [7].

In this study, we report on the role of morphology control through the addition of sulphur in enhancing electrochemical performances of graphene-based supercapacitors via an environmentally friendly and cost-effective synthesis

method. The synthesized material was obtained from sulphur-reduced graphene oxide (RGO-S) composite by using an improved Hummers' method. The as-synthesized electrode was characterized by different techniques and the electrochemical performance was evaluated in both three and two-electrode systems using 6 M KOH electrolyte. In a three-electrode setup, the fabricated materials displayed a highest specific capacity of 113.8 mAh g^{-1} at 0.5 A g^{-1} evaluated from the galvanostatic charge-discharge (GCD) curve. Remarkably, an assembled hybrid device with carbonized iron cations (C-FP) and the RGO-S composite delivered high energy and power densities of 35.2 Wh kg^{-1} and 375 W kg^{-1} at 0.5 A g^{-1} at an operating potential of 1.5 V, respectively. The as-synthesized material revealed good electrochemical properties, which proves its promising potential as electrode material for supercapacitor applications.

Experimental details

Preparation of reduced graphene oxide (RGO) samples

Graphene oxide was prepared by a modified hummer's method using graphite powder [4,14,26]. Graphite powder (5 g) was added slowly to 100 mL of sulphuric acid (H_2SO_4) which serve as intercalated molecules for the penetrating oxidation of bulk graphite in an ice bath to cool the acid. Thereafter, 2.5 g each of potassium hydrogen sulphate ($KHSO_4$) and calcium chloride ($CaCl_2$) were added subsequently upon stirring. $KHSO_4$ was used to start up the reaction while $CaCl_2$ used as a water remover. Effervescence was noticed upon additional of $CaCl_2$. The resulting mixture was stirred (400 rev/min) for 40 min at 60 °C, followed by a further addition of 10 g of potassium permanganate ($KMnO_4$) as an oxidizing agent and additional 50 mL of H_2SO_4. The solution was further stirred (250 rev/min) for 2 h at 60 °C for homogeneity. The dark-grey resulting mixture was removed from the heating plate and left to cool down to room temperature. Thereafter, 20 mL of hydrogen peroxide (H_2O_2 - 30%) alongside 120 mL of deionized water (DI water) were added to stop the reaction, which caused a vigorous rise in temperature of the mixture and beard great potential hazard. Therefore, great caution must be taken during the synthesis of the material. The resulting mixture called graphene oxide (GO) was allowed to cool down naturally to room temperature, and thereafter was re-dispersed into a 100 mL of DI water and sonicated for 2 h for further reduction of GO. Sonication uses sound energy to agitate atoms in a solution whereby it converts an electrical signal into a physical vibration to break materials apart. These disturbances can mix solutions, accelerate the dissolution of GO into a liquid and remove dissolved gas from liquids. The mixture was left to settle down for 12 h, washed several times with DI water and then centrifuge and dried in a vacuum oven at 80 °C for 6 h to obtain the final sample named as reduced graphene oxide (RGO).

Preparation of sulphur-reduced graphene oxide (RGO-S) composite

1 g of sulphur powder together with 3 g of sodium sulphide (Na_2S) act as a sulphur source were added into 100 mL of DI water and sonicated until a homogenous solution named 'A' was formed. 50 g of L-Ascorbic acid used a reducing agent was liquefied in 12 g of DI water to form a solution named 'B'. Thereafter, 3 g of as-synthesized RGO was mixed into solution 'A' together with solution 'B' and the resulting mixture was named as solution 'C'. Subsequently, 2 mL of HCl was added to the mixture (solution 'C') and then stirred for 5 min. The little volume of HCl added to the mixture was not to cause a further reaction, but to alter the pH of the mixture as well as for the purpose of ion exchange, which resulted in effective polarity. Besides, H_2S that may be formed in the addition of the HCl is soluble in water and was not expected to be part of the sulphur in the RGO matrix. The mixture was sonicated for 2 h and then stirred (400 rev/min.) for 1 h at 40 °C, centrifuged for 10 min at 5000 rpm and dried at 80 °C for 12 h in a vacuum oven. The resulting as-synthesized sample was designated as sulphur-reduced graphene oxide (RGO-S) composite.

Preparation of polyaniline (PANI)

The PANI material employed in this study was synthesized as described in our previous publication [27]. In brief, 0.2 M aniline hydrochloride was added to 0.25 M of ammonium peroxydisulfate. The mixture was stirred for 10 min, and then left to stand overnight for polymerization. The supernatant was decanted away and the recovered precipitate was washed several times with deionized. The resulting sample was dried overnight in an electric oven at 60 °C under ambient condition.

Preparation of carbonized iron cations adsorbed onto PANI (C-FP) material

0.4 g iron (II) nitrate nonahydrate, 0.5 g of polyaniline (PANI), 0.25 g each of polyvinylidene fluoride (PVDF) and carbon acetylene black (CAB) were mixed together and then completely dispersed into 20 mL of 99.9% ethanol. PVDF was used as a binder to bind the material onto nickel foam while CAB was added as a conducting agent. The mixture was sonicated until it evaporated to slurry. The slurry was coated into nickel foam and then annealed at a ramping rate of 17 °C/min until 850 °C in nitrogen (500 cc flow rate) gas environment at a dwell time of 2 h to obtain iron cations (Fe^{2+}) adsorbed onto the PANI film (C-FP) directly grown onto the nickel foam. At this temperature of 850 °C, the PANI film decomposed into the nickel foam template on which the material was coated. The precursors' masses were carefully selected to ensure an approximate weight ratio of 80:10:10 for iron (II) nitrate salt and PANI, CB and PVDF respectively [27].

Characterization of the samples

The transmission electron microscope (TEM) and scanning electron microscope (SEM) equipped with an energy-dispersive X-ray (EDX) of the as-synthesized samples were obtained from a JEOL-2100F high resolution transmission electron microscope (HRTEM FEI Tecnai-F30) alongside 200 kV acceleration voltage and a Zeiss Ultra Plus 55 field emission scanning electron microscope (FE-SEM) operated at 1.0 kV and 2.0 kV, respectively. The material's phase structure was analyzed by a Bruker BV 2D PHASER Best Benchtop X-ray

diffraction (XRD) analyzer with reflection geometry at 2θ values (5–90°) with a step size of 0.005°, operating with a Cu $K\alpha_1$ radiation source ($\lambda = 0.15406$ nm) at 50 kV and 30 mA. A WITec alpha 300 RAS + Confocal micro-Raman microscope operated at 532 nm laser wavelength was used to characterize the as-prepared sample with a spectral acquisition time of 150 s and laser power of 5 mW on the sample to avoid sample heating. Fourier transform-infrared (FTIR) analysis was achieved via a Varian FT-IR spectroscopy in a range of 500–4000 cm^{-1} in wavenumber. An X-ray photoelectron spectroscopy (XPS) analyzer (Versa Probe 5000 spectrometer activated with a 100 μm monochromatic Al-Kα exciting source) was employed to analyze the electronic states of surface elements present in the composite sample.

Electrochemical characterization

The three- and two-electrode systems were used to carry out the electrochemical measurements. For the three-electrode system, the working electrode was prepared by mixing 80% of the active material with 10% each of conductive carbon acetylene black (CB) and Polyvinylidene fluoride (PVDF) as a binder to form a homogenous slurry by addition of few drops of 1-methyl 2-pyrollidone (NMP). The slurry was pasted onto a clean nickel foam cut into 1.0 × 1.0 cm^2 serving as current collector for three-electrode and then dried in an oven at 60 °C for 12 h. The capacitive performance of the electrodes was carried out with the aid of a Bio-Logic VMP300 potentiostat (Knoxville TN 37930, USA) controlled by EC-Lab V1.40 software in a three-electrode set-up. The electrochemical measurements in three electrode configuration were carried out using glassy carbon as a counter electrode, Ag/AgCl as a reference electrode, carbon nanorods/fibers as the working electrode in 6 M KOH aqueous electrolyte. The cyclic voltammetry (CV) of the as-prepared samples were performed at different scan rates ranging from 5 to 100 mVs^{-1} within a potential window ranging from 0.0 to 0.45 V vs. Ag/AgCl. The galvanostatic charge-discharge (GCD) was performed at various specific currents ranging from 0.5 to 20 A g^{-1} in a potential window range of 0.0 V to 0.45 V. The single electrode specific capacity, Q_s (mAh g^{-1}) was obtained via a GCD profiles using equation (1) below [4]:

$$Q_s = \frac{I_d \times \Delta t}{3.6} \tag{1}$$

where Q_s is the specific capacity, I_d is specific current in A g^{-1}, and Δt is time in seconds taken for a complete discharge cycle. The energy efficiency, η_E (%) was calculated from the following relations:

$$\eta_E = \frac{E_d}{E_c} \text{ x } 100\ \% \tag{2}$$

E_c, E_d and η_E are charge energy, discharge energy and energy efficiency from the integral of the area under the charge-discharge curve of the electrode respectively.

The columbic efficiency C_E was calculated according to the following relation [13]:

$$C_E = \frac{t_D}{t_c} \times 100\% \tag{3}$$

where t_c, t_D and C_E (%) are times for charging and discharging times with the same current, as well as the columbic efficiency respectively.

An open circuit potential of a frequency range from 10 mHz–100 kHz was used to measure the electrochemical impedance spectroscopy (EIS) of the samples.

The two electrode asymmetric hybrid device was assembled by using the as-synthesized RGO-S nanorods/fibres as positive electrode and C-FP material as negative electrode with a thickness and diameter of 0.2 and 16 mm, respectively in a standard 2032 grade coin cell using Watman Celgard paper-based separator and 6 M KOH as electrolyte. The charge balance $Q_+ = Q_-$ was used to balance the mass of each electrode. Since the RGO-S shows a Faradic behaviour the specific capacity (Q_s) was calculated by integrating the area under the GCD curve as shown in equation (1) above. The specific capacity Q_s was then written as a function of mass, specific current and discharge time as shown below [27,28]:

$$m_+ I_{d(+)} \Delta_{t(+)} = m_- I_{d(-)} \Delta_{t(-)} \tag{4}$$

Since the same specific current was used, equation (4) can be simplified as:

$$\frac{m_+}{m_-} = \frac{\Delta_{t(-)}}{\Delta_{t(+)}} \tag{5}$$

where, m_+ and m_- are the positive and negative electrode masses respectively, $I_{d(+)}$ and $I_{d(-)}$ are positive and negative electrode specific currents respectively and $\Delta_{t(+)}$ and $\Delta_{t(-)}$ are the discharge time for the positive and negative electrode respectively.

The fabricated cell could operate in a wider potential window of 1.5 V based on the operating potential of respective electrodes that made up the device. The specific capacity, Q_s of the hybrid device was calculated following equation (1), while energy and power densities of the device with respect to the specific current were calculated according to the following equations:

$$E_d = \frac{I}{3.6 * m} \int V dt \quad \left[\text{Wh kg}^{-1}\right] \tag{6}$$

$$P_d = \frac{E_d}{\Delta t} \times 3600 \quad \left[\text{W kg}^{-1}\right] \tag{7}$$

where, I is the applied current (mA), $\int V dt$ is the area under discharge curve of the device, m (mg) is the total mass of the active electrode, Δt is electrode discharge time in seconds, E_d and P_d are the energy and power densities, respectively, with their specified units [7,18,19,27].

Results and discussion

Morphological, structural and composition characterization

The surface morphology of the as-synthesized samples was characterized by SEM and the results are shown in Fig. 1. Reduced graphene oxide (RGO) was observed to have a sheet like structure (Fig. 1(a and b)). The RGO-S composite showed a morphology, which comprises a combination of nanorods and

nanofibers that is attributed to a chemical reaction that occurred between the RGO and sulphur (Fig. 1(c and d)). With an improved Hummers' method, nanorods/fibres of different nanometers in length of ~150 nm were formed. It was revealed that, the technique can attain a homogenous blend of the reactants in solution whilst maintaining the reaction condition like temperature and concentration [4,29]. The improved Hummer's method as narrated in the experimental section (section Preparation of Reduced Graphene Oxide (RGO) Samples) was completed by sonication and magnetic stirring, which resulted in nanorods/nanofibers formation without the use of external devices or apparatus. Throughout synthesis, the sonication and uniform stirring rate provide active sites for initiation of sulphur which act as a seed for the growth of nanorods/fibers which was not observed for RGO pristine sample. Similar morphology was obtained by Iqbal et al. and Oyedotun et al. whereby hydrothermal and refluxing method with the help of reflux set up was used to initiate the formation of nanorods [4,13]. Therefore, this study reveals that the same morphology can be obtained by addition of sulphur and constant stirring of the solution and sonication which prevents sedimentation and force the close mixing, thus ensuring the occurrence of a homogenous reaction for the growth of nanorods/fibers like structure without hydrothermal or reflux set up. The observed SEM images in Fig. 1(a–d) were further confirmed by the TEM micrographs in Fig. 1 (e and f) for both the RGO and RGO-S samples, respectively.

The phase-structure analysis of the as-synthesized samples was investigated by adopting XRD according to the matching card no. JCPDS N34-0941 [30]. Fig. 2 (a) represents the XRD spectra measured within the angular range $2\theta = 5^{\circ} - 90^{\circ}$,

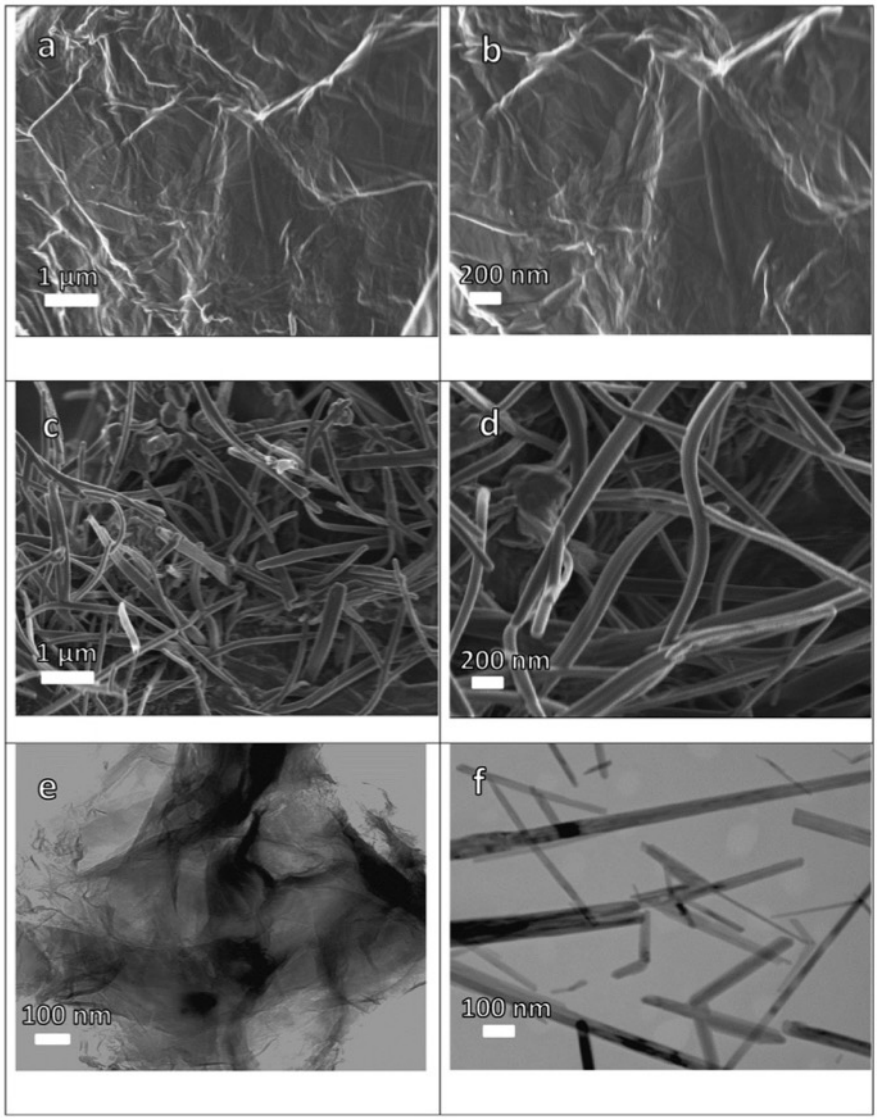

Fig. 1 – (a, b) SEM images of RGO and (c, d) RGO-S at low and high magnifications, respectively, (e, f) TEM images of RGO and RGO-S, respectively.

showing a crystalline structure for both samples. The appeared diffraction peaks at around 2θ = 15.3 °C, 23 °C and 31.1 °C and 34.3 °C are due to sulphur, while the rest of the peaks belong to RGO. The broadness of some peaks such as 25.8 °C and 42.7 °C may be caused by the formation of defects arising from the heteroatom doping [9].

Fig. 2(b) shows the Raman spectra of the materials, revealing four major distinct peaks at 1344 cm^{-1}, 1586 cm^{-1}, 2699 cm^{-1} and 2930 cm^{-1} corresponding to D, G, 2D and 2D′ bands, respectively. The appearance of D bands corresponds to A_{1g} lattice distortion mode. The G band was due to vibrational mode in the plane E_{2g} of the sp^2 hybridized carbon [31]. 2D and 2D' is a second-order two-phonon process that displays a strong frequency dependence on the excitation laser energy. This is due to double resonance transition resulting from generation of two opposite phonon momentum which indicates the number of layers in the graphene structure [32]. The degree of defects evaluated by intensity ratio of D and G band peaks (I_d/I_g) was estimated to be 0.97 and 1.1 for RGO and RGO-S, respectively. The former displayed low value owing to the reduction in the number of defects and functional groups while the latter indicated higher value which shows that sulphur atom create defects in the graphene sheet due to the larger atomic size of sulphur than carbon [15,33].

Fig. 2(c) represents the EDX spectrum for RGO-S composite sample. It was observed that the synthesized sample contains C, S and O as the major elements confirming the successful incorporation of sulphur into the matrix of RGO material. The inset to Fig. 2(c) shows a description of percentage weight composition of elements in the RGO-S material. The presence of Na (~6.6 wt %) in the EDX spectrum is ascribed to the Na_2S adopted during synthesis of the composite material.

Fig. 2(d) presents the FTIR analysis of both the RGO and RGO-S samples. The FTIR peak at C=S (1124 cm^{-1}) confirms the formation of carbon-sulphur covalent bond. The existence of characteristics bands around 823 cm^{-1} is assigned to the stretching mode of C–S bonds, showing that sulfides were successfully inserted within the graphite layers forming C–S bonds. Other stretching vibrations include 1424 cm^{-1}, 2363 cm^{-1} and 2682 cm^{-1} which correspond to C–H, CO_2 and ≡C–H bands, respectively [34–36].

Fig. 3(a–d) reveals the result of XPS analysis conducted to determine the types of oxygen, carbon and sulphur bonds that are present in the as-synthesized RGO-S sample. The XPS survey scans (Fig. 3(a)) of the RGO-S reveals a complete surface elemental composition with predominant peaks of O 1s, C 1s and S 2p. The Na observed in trace for the material is due to the Na_2S salt adopted in the synthesis of the RGO-S material [37]. As shown in Fig. 3(b) the strong peaks observed for O=S (530.1 eV), C=O (531.7 eV), C–OH (533.6 eV) and O=C (535.4 eV) were assigned to O 1s [38–41]. The high resolution C 1s spectra in Fig. 3(c) shows the formation of three peaks corresponding

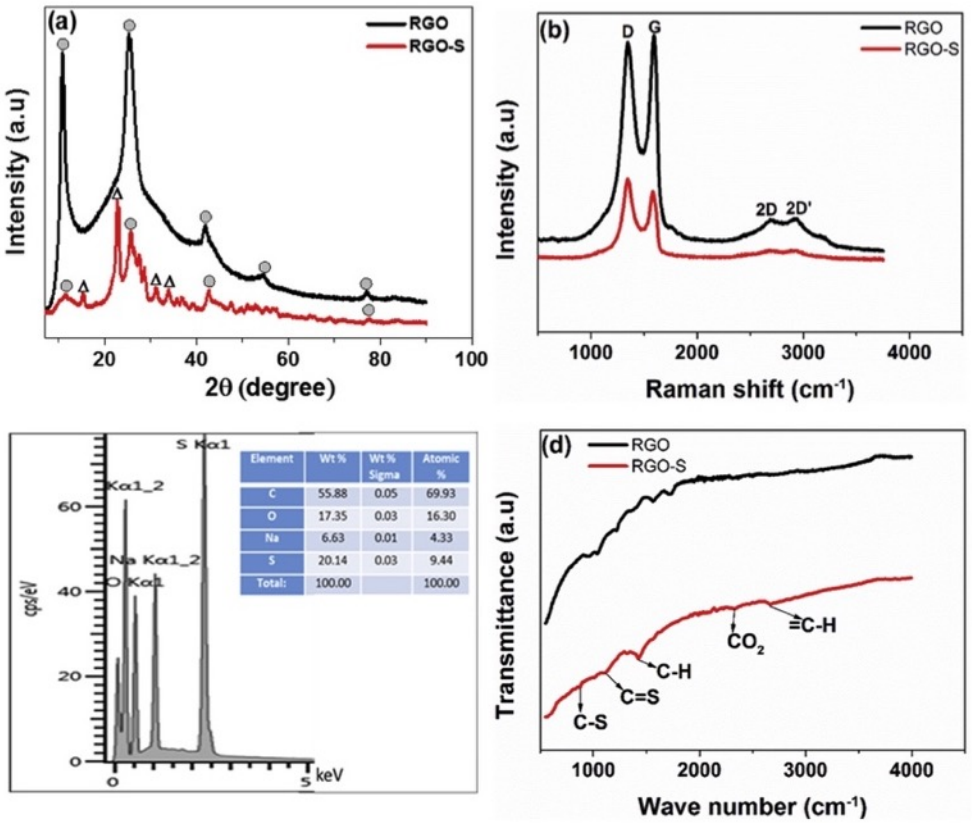

Fig. 2 – (a) XRD pattern with a matching card no. JCPDS N34-0941, (b) Raman spectrum, (c) EDX spectrum and (d) FTIR spectrum of RGO and RGO-S samples, respectively.

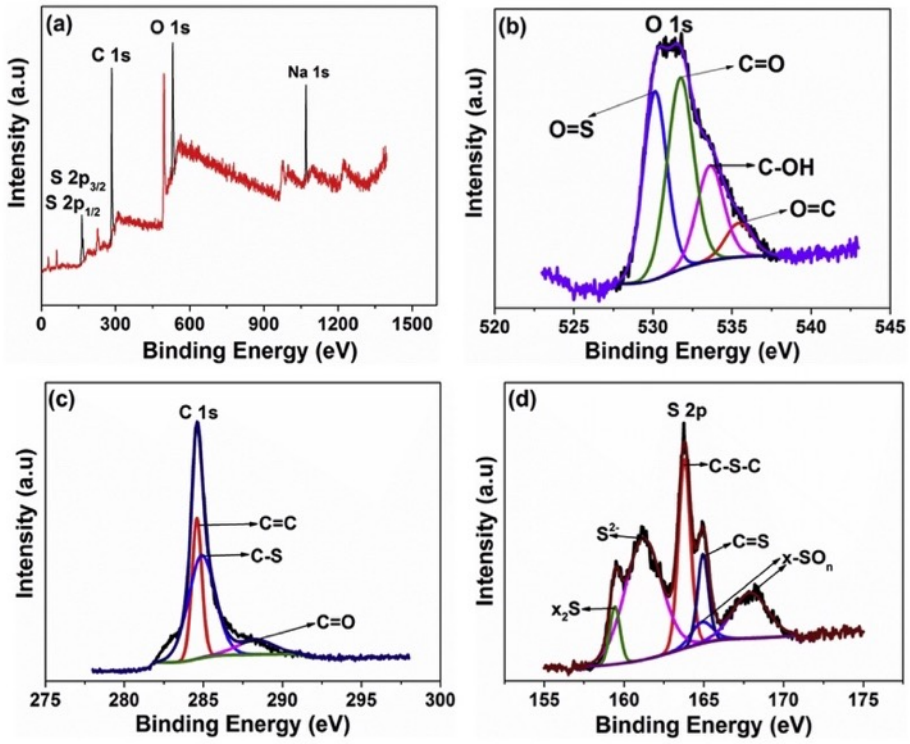

Fig. 3 – (a) XPS survey spectra, core level spectrum of (b) O 1s, (c) C 1s and (d) S 1s of RGO-S of as-synthesized sample, respectively.

to C=C (284.6 eV), C–S/C–H/C–O (284.9 eV) and C=O (288.3 eV) [7,39,42]. The presence of C=C and C–S bonds in the C 1s spectra reflect the reduction of graphene oxide and successful incorporation of sulphur atoms. According to Fig. 3(d) sulphur bonding peaks assigned to thiol S-2p3/2 (C–S–C, 163.8 eV) and S-2p1/2 (C=S, 164.9 eV) are due to spin – orbit coupling [5,43,44]. The presence of thiol 3/2 and 1/2 shows that sulphur atoms were directly bonded to carbon atoms and reveal the defects of graphene. Furthermore, the presence of metal sulfides X_2S (159.4 eV), S^{2-} (161.2 eV) and metal sulphate X-SO_n (165.0 and 167.9 eV) are due to the oxidation of S^{2-} which occurs in graphene oxide by the reduction and substitution reaction between the functional groups present in graphene oxide and sulphur atoms in Na_2S and S during synthesis [5,9,43]. The chemical compositions values were C 52%, O 26%, S 19% and Na 3% respectively. The compositions values were in a good agreement with EDX values in Fig. 2(c).

Electrochemical measurements

Three-electrode measurements

The electrochemical performance of the as-synthesized samples was first evaluated in a three-electrode system using 6 M KOH electrolyte. Fig. 4(a and b) shows the cyclic voltammetry (CV) curves at a scan rate of 50 mVs^{-1} in both positive and negative potential windows range of −0.45 to 0.0 V and 0.0–0.45 V for RGO and RGO-S samples, respectively. The CV curves in the positive potential window displayed a Faradaic behavior while in the negative potential window displayed pseudocapacitive behaviour. This might be linked to the presence of functional groups in the material and the concentration of KOH electrolyte which produces the OH^- in the positive potential window and K^+ in the negative potential window [45]. Fig. 4(c and d) represents the galvanostatic charge/discharge (GCD) curves at a current density of 0.5 Ag^{-1} in both positive and negative potential windows for RGO and RGO-S samples, respectively. It was observed that the GCD curve is nonlinear with a potential plateau in the positive potential window and semi-linear in the negative potential window for both samples, which corresponds well with the CV curves observed in Fig. 4(a and b). The observed oxidation peaks at 0.292 V and 0.285 V and reduction peaks at 0.180 V and 0.166 V for RGO and RGO-S, respectively in the CV curves in the positive potential window are due to the electrochemical redox reactions arising from the presence of functional groups which have high redox reactivity characteristics in the positive potential window [46]. From the results, it is observed that the current response and discharge time for the RGO-S in both the CV and GCD profiles were higher compare to that of RGO in both negative and positive operating potentials respectively. This is ascribed to addition of sulphur heteroatom into the matrix of the material [7,31] which increases electrochemical performance of RGO through increase in electrical conductivity of RGO and also plays important role in increasing capacity of RGO due to additional redox reactions. It is also clear that the positive potential window electrochemical performances are far higher than those in the negative potential window.

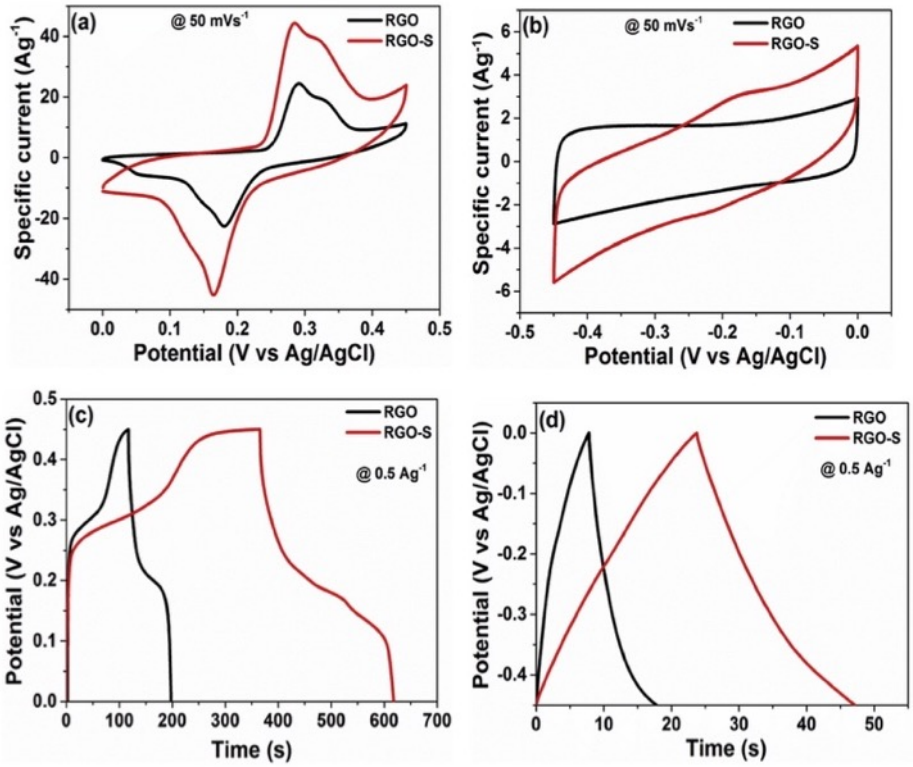

Fig. 4 – (a, b) CV curves at a scan rate of 50 mVs^{-1} in both positive and negative potential windows, (c, d) GCD curves at a current density of 0.5 Ag^{-1} in both positive and negative potential windows for RGO and RGO-S sample in 6 M KOH, respectively.

Fig. 5(a and b) reveals Columbic efficiency and energy efficiency for RGO and RGO-S electrode over a 2000 charge and discharge cycling test at 5 A g^{-1}. The half-cells could maintain 98.5% and 98.7% cycling stability with an energy efficiency of about 98.1% and 98.5% after 2000 cycles for both RGO and RGO-S respectively. It was revealed that RGO-S has high cycling stability and energy efficiency compared to RGO. This might be due to the redox reaction facilitated by incorporation of sulphur, which enhanced the electrochemical performance and stability of the sample.

Fig. 5 (c) is a representation of specific capacities against specific currents evaluated from GCD profiles using equation (1) for both RGO and RGO-S electrode materials in the positive potential window. A maximum value of 12.5 mAh g^{-1} and 113.8 mAh g^{-1} was recorded for RGO and RGO-S electrode, respectively at a specific current of 0.5 A g^{-1}. This better performance observed for the RGO-S was ascribed to the improved Hummers' method adopted in the material's synthesis as well as the introduction of heteroatom (sulphur nanoparticle) into the graphene-based material, which resulted in a unique morphology, improvement in electrical conductivity and additional redox reactions. The introduction of heteroatom can change the electronic state of graphene sheets and facilitate transportation of electrolyte's ions [3].

The EIS Nquist plots in Fig. 5(d) display characteristics frequency response of RGO and RGO-S corresponding to an AC impedance spectrum. Remarkably, low equivalent series resistance (R_s) value of about 0.43 Ω was observed for RGO-S compared to 0.65 Ω of RGO. This lower Rs value of RGO-S electrode accounts for the material's improved conductivity compared to the RGO. Also, RGO-S shows very short diffusion length compared to RGO which also indicates a great electrochemical improvement of RGO due to presence of S heteroatoms.

From the above discussion, it was revealed that RGO-S performed better than RGO in terms of CV, GCD, cycling performance, energy efficiency, specific capacity and EIS Nyquist impedance. Since it was further shown that CV and GCD of RGO-S displays higher specific current and discharge time in the positive potential window than in the negative potential window, therefore, RGO-S was selected as a positive electrode material for a full cell device. Fig. 6 (a) shows the CV curves of RGO-S at different scan rates ranging from 5 to 100 mV s^{-1} in a potential window range of 0.0–0.45 V. Fig. 6 (b) represents the GCD curves at different specific currents from 0.5 to 20 A g^{-1}. It was observed that the GCD curves agree well with the peaks displayed by the CV curves in Fig. 6 (a). The CV and GCD curves show the redox peaks contributed by the faradaic reaction which has resulted in enhanced specific capacity of the material as shown in Fig. 5 (c).

Two-electrode evaluations of asymmetric RGO-S//C-FP cell

The electrochemical performance of RGO-S nanorods/fibres electrode was evaluated further in a two-electrode system. For

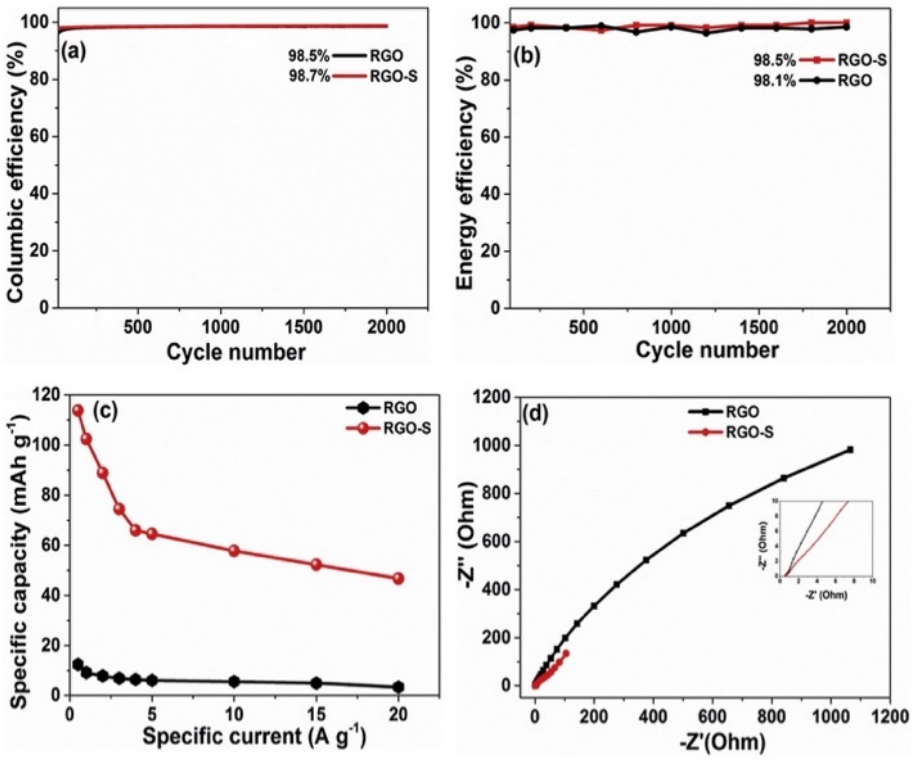

Fig. 5 – (a) Cycling performance, (b) energy efficiency, (c) specific capacity against specific current and (d) EIS Nyquist plot for RGO and RGO-S sample in 6 M KOH, respectively.

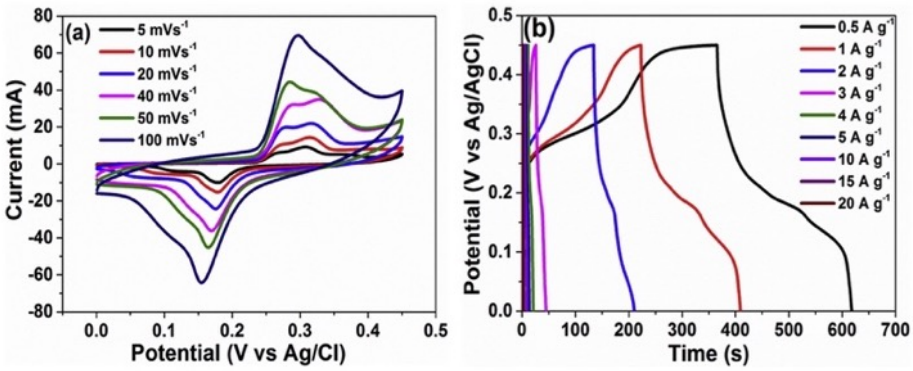

Fig. 6 – (a) CV curves and (b) GCD curves of RGO-S sample in 6 M KOH, respectively.

further electrochemical analysis, an asymmetric cell designated as **RGO-S//C-FP** was assembled using RGO-S and C-FP as positive and negative electrodes respectively. Using equation (5), a mass balance ratio of 1.0:1.6 was evaluated, corresponding to a mass of 2.0 and 3.2 mg for RGO-S and C-FP electrode, respectively, resulting in a total mass of 5.2 mg/cm^2 for the asymmetric cell. The set up was completed in a standard 2032 grade coin cell sandwiched with a filter paper as the separator and 6 M KOH as electrolyte.

Fig. 7 (a) presents the CV curves of C-FP and RGO-S nanorods/fibres materials employed as negative and positive electrodes, respectively. The C-FP electrode displayed an ideal rectangular shape, indicating a reversible capacitive behavior, while the RGO-S electrode displays presence of redox peaks attributed to ongoing electrochemical oxidation and reduction reaction arising from the presence of oxygen and sulphur [3,15].

The CV curves for the asymmetric RGO-S//C-FP evaluated at different scan rates from 5 to 100 mV s^{-1} displayed a nonlinear pseudocapacitive curve as shown in Fig. 7 (b). The fabricated asymmetric cell was able to operate in a higher potential window of about 1.5 V which is a result of synergy between the positive and negative electrode materials that made up the cell. This result shows that the combination of

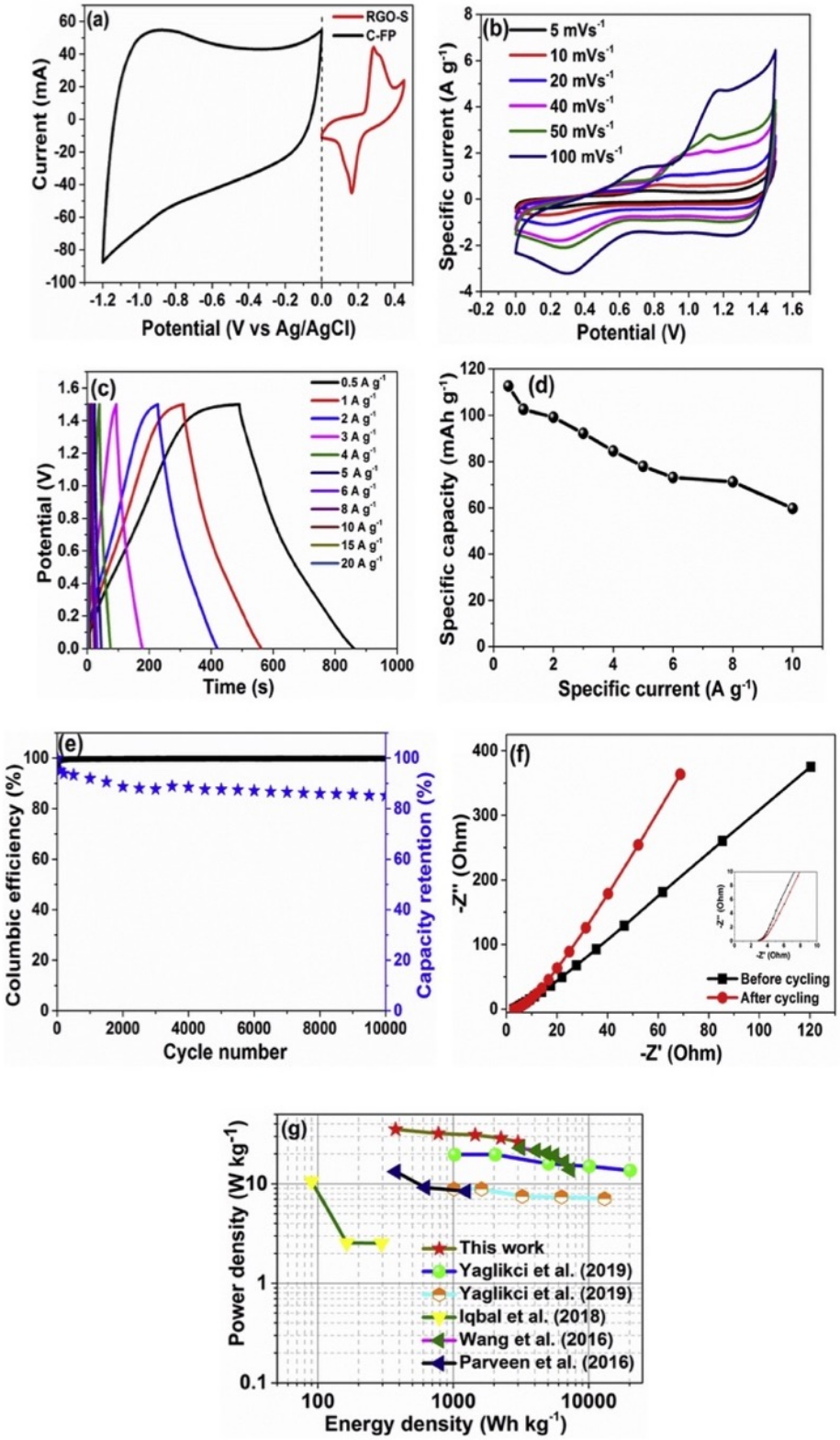

Fig. 7 – (a) CV curves in both negative and positive potential windows, (b) CV curves, (c) GCD curves, (d) specific capacity versus specific current (e) cycling performance versus capacity retention, (f) EIS Nyquist plot before and after cycling and (g) Ragone plot of RGO-S//C-FP, respectively.

RGO-S//C-FP improves the electrochemical performance by facilitating the charge carriers which improve the potential window and increases the current value at the same scan rate.

Fig. 7 (c) presents GCD profile of the fabricated asymmetric cell at different specific currents ranging from 0.5 to 20 A g^{-1}. The quasi linear GCD curves displayed the faradic contribution via redox reaction from RGO-S//C-FP which corresponds with the CV curves in Fig. 7 (b). This indicates that C-FP has rationalized the purely faradic behaviour of RGO-S to pseudocapacitive behaviour. This combined characteristics of faradic and EDLC is called supercapattery behavior [27,45]. Fig. 7 (d) displays the specific capacity versus specific currents of the RGO-S//C-FP cell obtained using equation (1) from GCD curves displayed in Fig. 7 (c). At a specific current of 0.5 A g^{-1}, the maximum specific capacity of about 112.7 mAh g^{-1} was recorded. Fig. 7 (e) shows a capacity retention of about 85.13% for the cell and a corresponding columbic efficiency of about 99% over 10, 000 cycles at 3 A g^{-1}, which proves an excellent long-term electrochemical stability of the asymmetric cell. Fig. 7 (f) displays the EIS before and after cycling. It was observed that an equivalent series resistance was reduced from 3 Ω to 2.5 Ω after 10, 000 cycling at 3 A g^{-1}. This could be due to wettability and also the material became more accessible to the ions after it has been exposed to a quite number of cycles [5,21].

The Ragone plot was shown in Fig. 7 (g) to compare the energy and power densities in this work and some other similar materials recently reported in the literature. From Fig. 7 (g) the energy and power densities of the fabricated cell were calculated using equations (6) and (7), respectively. Remarkably, a high energy density of 35.2 Wh kg^{-1} corresponding to a power density of 375 W kg^{-1} at a specific current of 0.5 A g^{-1} was recorded. These values were found to be in the same range and also superior to other works in the literature reporting the similar devices which have been stated in the introduction section [6,11,13,19,25].

Conclusion

Sulphur-reduced graphene oxide (RGO-S) was successfully synthesized using an improved Hummers' method. The characterization of the material revealed the formation of carbon nanorods/fibers material without an addition of any device or apparatus for influencing the formation/growth of nanorods/fibers like structure. This shows that sulphur was successfully incorporated into graphene oxide by the formation of C–S bond. This was further confirmed from the material's crystalline structure showing composition of S, C, O and Na. The fabricated three-electrode material displayed a highest specific capacity of 113.8 mAh g^{-1} at 0.5 A g^{-1}. The half-cell could retain a columbic efficiency of about 98.7% with corresponding energy efficiency of about 98.5% over 2000 constant charge/discharge cycle at a specific current of 5 A g^{-1}. Remarkably, the fabricated hybrid device with carbonized iron cations (C-FP) and the RGO-S composite delivered a specific capacity of 112.7 mAh g^{-1}, high energy and power densities of 35.2 Wh kg^{-1} and 375 W kg^{-1} at 0.5 A g^{-1} within a 1.5 V operating potential, respectively. A good cycling stability performance with an energy efficiency of 99% was observed for the device for up to 10,000 cycling at a specific current of 3 A g^{-1}. The fabricated sample revealed good electrochemical properties which offer the materials in question as for supercapacitor application.

Acknowledgements

This work is based on the research supported by the South African Research Chairs Initiative of the Department of Science and Technology and National Research Foundation of South Africa (Grant No. 61056). Any opinion, finding, and conclusion expressed in this material are that of the authors, and the NRF does not accept any liability in this regard. Delvina Japhet Tarimo acknowledges the financial support from NRF through SARChI chair in Carbon Technology and Materials. Patrick Urbankowski of the Department of Materials Science and Engineering, Drexel University, USA is acknowledged for performing XPS measurements.

REFERENCES

[1] Moriarty P, Honnery D. Hydrogen's role in an uncertain energy future. Int J Hydrogen Energy 2009;34:31–9. https://doi.org/10.1016/j.ijhydene.2008.10.060.

[2] Lin KS, Adhikari AK, Ku CN, Chiang CL, Kuo H. Synthesis and characterization of porous HKUST-1 metal organic frameworks for hydrogen storage. Int J Hydrogen Energy 2012;37:13865–71. https://doi.org/10.1016/j.ijhydene.2012.04.105.

[3] Yu X, Park HS. Sulfur-incorporated, porous graphene films for high performance flexible electrochemical capacitors. Carbon 2014;77:59–65. https://doi.org/10.1016/j.carbon.2014.05.002.

[4] Oyedotun KO, Madito MJ, Bello A, Momodu DY, Mirghni AA, Manyala N. Investigation of graphene oxide nanogel and carbon nanorods as electrode for electrochemical supercapacitor. Electrochim Acta 2017;245:268–78. https://doi.org/10.1016/j.electacta.2017.05.150.

[5] Yu X, Kang Y, Park HS. Sulfur and phosphorus co-doping of hierarchically porous graphene aerogels for enhancing supercapacitor performance. Carbon 2016;101:49–56. https://doi.org/10.1016/j.carbon.2016.01.073.

[6] Yaglikci S, Gokce Y, Yagmur E, Aktas Z. The performance of sulphur doped activated carbon supercapacitors prepared from waste tea. Environ Technol 2019:1–13. https://doi.org/10.1080/09593330.2019.1575480. 0.

[7] Duraivel M, Nagappan S, Balamuralitharan B, Selvam S, Karthick SN, Prabakar K, et al. Superior one-pot synthesis of a doped graphene oxide electrode for a high power density supercapacitor. New J Chem 2018;42:11093–101. https://doi.org/10.1039/c8nj01672k.

[8] Karthik N, Edison TNJI, Atchudan R, Xiong D, Lee YR. Electrosynthesis of sulfur doped nickel cobalt layered double hydroxide for electrocatalytic hydrogen evolution reaction and supercapacitor applications. J Electroanal Chem 2019;833:105–12. https://doi.org/10.1016/j.jelechem.2018.11.028.

[9] Zhang X, Yan P, Zhang R, Liu K, Liu Y, Liu T, et al. A novel approach of binary doping sulfur and nitrogen into graphene layers for enhancing electrochemical performances of supercapacitors. J Mater Chem 2016;4. https://doi.org/10.1039/c6ta08482f. 19053–9.

[10] Zhu J, Zhou W, Zhou Y, Cheng X, Yang J. Cobalt sulfide/reduced graphene oxide nanocomposite with enhanced performance for supercapacitors. J Electron Mater 2019;48:1531–9. https://doi.org/10.1007/s11664-018-06910-z.
[11] Li Y, Wang G, Wei T, Fan Z, Yan P. Nitrogen and sulfur co-doped porous carbon nanosheets derived from willow catkin for supercapacitors. Nano Energy 2016;19:165–75. https://doi.org/10.1016/j.nanoen.2015.10.038.
[12] Chen Q, Cai D, Zhan H. Construction of reduced graphene oxide nanofibers and cobalt sulfide nanocomposite for pseudocapacitors with enhanced performance. J Alloys Compd 2017;706:126–32. https://doi.org/10.1016/j.jallcom.2017.02.189.
[13] Iqbal MF, Ashiq MN, Razaq A, Saleem M, Parveen B, Hassan MU. Excellent electrochemical performance of graphene oxide based strontium sulfide nanorods for supercapacitor applications. Electrochim Acta 2018;273:136–44. https://doi.org/10.1016/j.electacta.2018.04.014.
[14] Yang J, Gunasekaran S. Electrochemically reduced graphene oxide sheets for use in high performance supercapacitors. Carbon 2013;51:36–44. https://doi.org/10.1016/j.carbon.2012.08.003.
[15] Yu X, Park SK, Yeon SH, Park HS. Three-dimensional, sulfur-incorporated graphene aerogels for the enhanced performances of pseudocapacitive electrodes. J Power Sources 2015;278:484–9. https://doi.org/10.1016/j.jpowsour.2014.12.102.
[16] Snook GA, Kao P, Best AS. Conducting-polymer-based supercapacitor devices and electrodes. J Power Sources 2011;196:1–12. https://doi.org/10.1016/j.jpowsour.2010.06.084.
[17] Barik R, Devi N, Perla VK, Ghosh SK, Mallick K. Stannous sulfide nanoparticles for supercapacitor application. Appl Surf Sci 2019;472:112–7. https://doi.org/10.1016/j.apsusc.2018.03.172.
[18] Yang Y, Liu L, Tang Y, Zhang Y, Jia D, Kong L. Bamboo-like carbon nanotubes containing sulfur for high performance supercapacitors. Electrochim Acta 2016;191:846–53. https://doi.org/10.1016/j.electacta.2016.01.149.
[19] Parveen N, Ansari MO, Ansari SA, Cho MH. Simultaneous sulfur doping and exfoliation of graphene from graphite using an electrochemical method for supercapacitor electrode materials. J Mater Chem 2015;4:233–40. https://doi.org/10.1039/c5ta07963b.
[20] Elmouwahidi A, Castelo-Quibén J, Vivo-Vilches JF, Pérez-Cadenas AF, Maldonado-Hódar FJ, Carrasco-Marín F. Activated carbons from agricultural waste solvothermally doped with sulphur as electrodes for supercapacitors. Chem Eng J 2018;334:1835–41. https://doi.org/10.1016/j.cej.2017.11.141.
[21] Han J, Zhang LL, Lee S, Oh J, Lee KS, Potts JR, et al. Generation of B-doped graphene nanoplatelets using a solution process and their supercapacitor applications. ACS Nano 2013;7:19–26. https://doi.org/10.1021/nn3034309.
[22] Khandelwal M, Li Y, Molla A, Hyun Hur S, Suk Chung J. Single precursor mediated one-step synthesis of ternary-doped and functionalized reduced graphene oxide by pH tuning for energy storage applications. Chem Eng J 2017;330:965–78. https://doi.org/10.1016/j.cej.2017.08.040.
[23] Kurmaev EZ, Galakhov AV, Moewes A, Moehlecke S, Kopelevich Y. Interlayer conduction band states in graphite-sulfur composites. Phys Rev B Condens Matter 2002;66:1–3. https://doi.org/10.1103/PhysRevB.66.193402.
[24] Zhang J, Yang Z, Wang X, Ren T, Qiao Q. Homogeneous sulphur-doped composites: porous carbon materials with unique hierarchical porous nanostructure for super-capacitor application. RSC Adv 2016;6:84847–53. https://doi.org/10.1039/c6ra17231h.
[25] Parveen N, Ansari MO, Ansari SA, Cho MH. Erratum: simultaneous sulfur doping and exfoliation of graphene from graphite using an electrochemical method for supercapacitor electrode materials (Journal of Materials Chemistry A. 4 (233-240) J Mater Chem 2016;4:12668–9. https://doi.org/10.1039/C6TA90155G. 2016.
[26] Kannappan S, Kaliyappan K, Manian RK, Pandian AS, Yang H, Lee YS, et al. Graphene based supercapacitors with improved specific capacitance and fast charging time at high current density. 2013.
[27] Oyedotun KO, Madito MJ, Momodu DY, Mirghni AA, Masikhwa TM, Manyala N. Synthesis of ternary NiCo-MnO2 nanocomposite and its application as a novel high energy supercapattery device. Chem Eng J 2018;335:416–33. https://doi.org/10.1016/j.cej.2017.10.169.
[28] Mirghni AA, Oyedotun KO, Mahmoud BA, Bello A, Ray SC, Manyala N. Nickel-cobalt phosphate/graphene foam as enhanced electrode for hybrid supercapacitor. Compos B Eng 2019;174:106953. https://doi.org/10.1016/j.compositesb.2019.106953.
[29] Tang Y, Zhang Y, Deng J, Wei J, Tam H Le, Chandran BK, et al. Mechanical force-driven growth of elongated bending Tio 2 -based nanotubular materials for ultrafast rechargeable lithium ion batteries. Adv Mater 2014;26:6111–8. https://doi.org/10.1002/adma.201402000.
[30] Guo Y, Zhao J, Yang S, Yu K, Wang Z, Zhang H. Preparation and characterization of monoclinic sulfur nanoparticles by water-in-oil microemulsions technique. Powder Technol 2006;162:83–6. https://doi.org/10.1016/j.powtec.2005.12.012.
[31] Yu X, Park HS. Sulfur-incorporated, porous graphene films for high performance flexible electrochemical capacitors. Carbon 2014. https://doi.org/10.1016/j.carbon.2014.05.002.
[32] Escobar-Alarcón L, Espinosa-Pesqueira ME, Solis-Casados DA, Gonzalo J, Solis J, Martinez-Orts M, et al. Two-dimensional carbon nanostructures obtained by laser ablation in liquid: effect of an ultrasonic field. Appl Phys Mater Sci Process 2018;124:1–7. https://doi.org/10.1007/s00339-018-1559-8.
[33] Zhang J, Jiang M, Xing L, Qin K, Liu T, Zhou J, et al. Three dimensional sulfur-doped graphene hydrogels with tetrathiafulvalene for high performance supercapacitors. Chin J Chem 2016;34:46–52. https://doi.org/10.1002/cjoc.201500656.
[34] Ouyang Z, Lei Y, Chen Y, Zhang Z, Jiang Z, Hu J, et al. Preparation and specific capacitance properties of sulfur, nitrogen Co-doped graphene quantum dots. Nanoscale Res Lett 2019;14:219. https://doi.org/10.1186/s11671-019-3045-4.
[35] Qu D, Zheng M, Du P, Zhou Y, Zhang L, Li D, et al. Highly luminescent S, N co-doped graphene quantum dots with broad visible absorption bands for visible light photocatalysts. Nanoscale 2013;5:12272–7. https://doi.org/10.1039/c3nr04402e.
[36] Compounds O, Rao CNR, Venkataraghavan R, Kasturi TR. Contribution to the infrared spectra of organosulphur compounds. Can J Chem 1964;42(1):36–42. Science 1964;42:36–42.
[37] Oyedotun KO, Masikhwa TM, Lindberg S, Matic A, Johansson P, Manyala N. Comparison of ionic liquid electrolyte to aqueous electrolytes on carbon nanofibres supercapacitor electrode derived from oxygen-functionalized graphene. Chem Eng J 2019;375:121906. https://doi.org/10.1016/j.cej.2019.121906.
[38] Longo A, Verucchi R, Aversa L, Tatti R, Ambrosio A, Orabona E, et al. Graphene oxide prepared by graphene nanoplatelets and reduced by laser treatment.

Nanotechnology 2017;28:224002. https://doi.org/10.1088/1361-6528/aa6c3c.
[39] Lin W, Chen Y, Li P, He J, Zhao Y, Wang Z, et al. Enhanced performance of lithium sulfur battery with a reduced graphene oxide coating separator. J Electrochem Soc 2015;162:A1624–9. https://doi.org/10.1149/2.0891508jes.
[40] Drewniak S, Muzyka R, Stolarczyk A, Pustelny T, Kotyczka-Morańska M, Setkiewicz M. Studies of reduced graphene oxide and graphite oxide in the aspect of their possible application in gas sensors. Sensors 2016;16. https://doi.org/10.3390/s16010103.
[41] Song X, Chen Q, Shen E, Liu H. Supercapacitive performances of few-layer MoS 2 on reduced graphene oxides. 2019. p. 911–23.
[42] Chu RX, Lin J, Wu CQ, Zheng J, Chen YL, Zhang J, et al. Reduced graphene oxide coated porous carbon-sulfur nanofiber as a flexible paper electrode for lithium-sulfur batteries. Nanoscale 2017;9:9129–38. https://doi.org/10.1039/c7nr02423a.
[43] Wang X, Gao T, Han F, Ma Z, Zhang Z, Li J, et al. Stabilizing high sulfur loading Li–S batteries by chemisorption of polysulfide on three-dimensional current collector. Nano Energy 2016;30:700–8. https://doi.org/10.1016/j.nanoen.2016.10.049.
[44] Chen L, Cui X, Wang Y, Wang M, Qiu R, Shu Z, et al. One-step synthesis of sulfur doped graphene foam for oxygen reduction reactions. 3420–3423, https://doi.org/10.1039/c3dt52253a; 2014.
[45] Rantho MN, Madito MJ, Manyala N. Symmetric supercapacitor with supercapattery behavior based on carbonized iron cations adsorbed onto polyaniline. Electrochim Acta 2018;262:82–96. https://doi.org/10.1016/j.electacta.2018.01.001.
[46] Conway BE, Ku JCH, Ho FC. The electrochemical surface reactivity of iron sulfide, FeS2. J Colloid Interface Sci 1980;75:357–72. https://doi.org/10.1016/0021-9797(80)90461-0.

4.2.2: Concluding remarks

The development of carbon nanorods/fibers material exclusive of any mechanism affecting their formation was noted by different characterization techniques for the composite sample. The formation of C-S bond confirm that sulphur was effectively integrated into graphene oxide. The highest specific capacity of 12.5 and 113.8 mAh g^{-1} at 0.5 A g^{-1} was noted for RGO and RGO-S in three-electrode measurement, respectively. Addition of S into RGO creates defects which modify its properties by increasing redox active sites, hence improved the capacity of RGO-S compared to RGO. The fabricated hybrid device with RGO-S composite as a positive electrode and carbonized iron cations (C-FP) as a negative electrode delivered a high specific energy of 35.2 Wh kg^{-1} and specific power of 375 W kg^{-1} at 0.5 A g^{-1} within a working voltage of 1.5 V. A good cycling stability performance with an energy efficiency of 99% was recorded for long terms stability up to 10,000 cycling at 3 A g^{-1}.

4.3: High energy and excellent stability asymmetric supercapacitor derived from sulphur-reduced graphene oxide/manganese dioxide composite and activated carbon from peanut shell

4.3.1: Summary of the study

In this work, RGO-S and RGO-S/MnO_2 composite were effectively produced via a modified Hummer's method followed by freeze drying process, and hydrothermal method. Graphite powder and potassium permanganate were utilized as the starting precursor. RGO-S/MnO_2 composite was formed by optimizing different mass loading by adding 50, 100 and 150 mg of MnO_2. The development of nanorods/fibers, nanosheets and nano-flower like morphology was witnessed by the analysis done on the samples depending on the mass loading of MnO_2. The aim of adding MnO_2 is to increase the capacitance and improve the stability over a long cycle [203]. This is because MnO_2 has the ability to serve as a sulphur host for different sulphide species [204]. It suppresses the polysulphide diffusion by preserving the stability of supercapacitor during long cycling through formation of strong chemical adsorption bond [205]. SEM, TEM, EDS, XRD and FTIR were applied to characterize the material, while the electrochemical evaluation was done using 2.5 M KNO_3 as electrolyte. The following attached publication presents a detailed synthesis procedures, characterization and electrochemical measurements of RGO-S/MnO_2 composite.

Electrochimica Acta 353 (2020) 136498

Contents lists available at ScienceDirect

Electrochimica Acta

journal homepage: www.elsevier.com/locate/electacta

High energy and excellent stability asymmetric supercapacitor derived from sulphur-reduced graphene oxide/manganese dioxide composite and activated carbon from peanut shell

Delvina Japhet Tarimo , Kabir O. Oyedotun , Abdulmajid A. Mirghni , Ndeye Fatou Sylla , Ncholu Manyala *

Department of Physics, Institute of Applied Materials, SARChI Chair in Carbon Technology and Materials, University of Pretoria, Pretoria, 0028, South Africa

ARTICLE INFO

Article history:
Received 18 March 2020
Received in revised form
13 May 2020
Accepted 20 May 2020
Available online 25 May 2020

Keywords:
Sulphur-reduced graphene oxide
Hybrid device
Energy density
Supercapacitor
Shuttle effects
Composite materials

ABSTRACT

Nanorods/fibers, nanosheet and nano-flower like structure were effectively synthesized from sulphur-reduced graphene oxide (RGO-S) and sulphur-reduced graphene oxide/manganese dioxide (RGO-S/MnO_2) composites for supercapacitor applications. Structural, chemical composition and morphological analysis reveal an effective synthesis of the RGO-S and RGO-S/MnO_2 composite. Electrochemical measurements of the optimized mass loading of MnO_2 on RGO-S in a three electrode configurations revealed a specific capacitance of 180.4 F g^{-1} compared to 75.2 F g^{-1} of the pristine sample at 1 A g^{-1} in 2.5 M KNO_3 electrolyte. An assembled asymmetric device consists of optimized RGO-S/MnO_2 as positive electrode and activated carbon from peanut shell (AC-PS) as a negative electrode delivered a high specific energy of 71.74 Wh kg^{-1} with its corresponding specific power of 850 W kg^{-1} at 1 A g^{-1}. It was observed that even at high specific current of 5 A g^{-1} the device was able to maintain a specific energy of 55.30 Wh kg^{-1}. An excellent stability with capacitance retention of 94.5% and columbic efficiency of 99.6% up to 10, 000 cycles was recorded for the device at 5 A g^{-1}. The device demonstrated a very good stability after being subjected to a voltage holding of up to 90 h and an outstanding self-discharge of about 1.45 V was recorded within the first 10 h and 1.00 V after 72 h from its maximum potential of 1.7 V.

1. Introduction

The variations in precipitation, sea level and rising temperature will affect how much energy is produced, delivered and consumed. Due to a huge effect caused by climate change and high consumption of fossil fuels which is limited and has environmental problems like green-house effect, there is a need to find an alternative energy source. Renewable energy is the energy harvested from natural resources such as geothermal energy, solar, hydropower and wind. However, energy harvested from these resources is not available all the time because it depends on the weather and time. For example, solar energy can only be harvested during the day time, so in order to have sufficient energy, energy storage devices like supercapacitors, battery and other energy conversion systems are required [1,2,4–6].

Recently, the supercapacitor has attracted most research community owing excellent cycling stability, high power density and fast charge/discharge ability [2,7–9]. By considering the charge storage mechanism, the supercapacitor is characterized as the electric double-layer capacitor (EDLC) and faradic/pseudo capacitor. EDLC store energy through the separation of charges in a Helmholtz double layer at the interface of electrode and electrolyte while pseudo/faradic capacitor its storage is achieved by a redox reaction between the electrode and the electrolyte [10–14].

For innovative energy storage devices (supercapacitor), microstructure has effect on the electrochemical performance of electrode materials [15–17]. This makes scientists focus on developing new materials which can meet energy demands. Mostly, carbonaceous materials such as activated carbon, carbon aerogel, graphene and carbon nanotube store energy through reversible adsorption-desorption of ions on the surface of the electrode leading to high power density and long cycle life but low energy density [4,18–22]. The use of dopants such as boron (B), phosphorus (P), sulphur (S) and nitrogen (N) has seen to enrich physical and chemical properties like wettability of the carbonaceous materials [2,10,23,24].

* Corresponding author.
E-mail address: ncholu.manyala@up.ac.za (N. Manyala).

https://doi.org/10.1016/j.electacta.2020.136498
0013-4686/

Precisely, the synthesis of sulphur carbonaceous materials for supercapacitor is of great importance due to its ability to create redox active sites by attracting the greater number of electrons which in turn increases the capacity/capacitance of the material [1,11,21,25]. However, shuttle effects occur during the conversion of sulphur to different sulphides products, makes supercapacitor to suffer from poor stability during a long cycling process [6,26–30]. Several approaches have been attempted to resolve the problem, which include binding the material onto conducting polymers [31], metal hydroxides [7], metal oxides [12] and metal sulphides [32] hosts which derives its capacitance from redox reaction that occurs between or on the surface of the electrode which proves to have a high energy density [16,27,33]. These material hosts offer high efficiency of chemisorption, which suppress polysulphide diffusion by improving the long term stability through the creation of strong chemical adsorption and immobilize the polysulphide species.

Recently, the varieties of d-block metals and their oxides such as cobalt oxide, manganese dioxide (MnO_2), tin oxide and nickel oxide, have been used as a well-established active electrode for supercapacitor due to several oxidation states and pseudocapacitive behaviour [4,20,33–35]. MnO_2 has been regarded as a high standard electrode material for supercapacitor applications, owing to high specific capacity/capacitance, variable oxidation state, abundant availability/low cost and non-toxicity. Since MnO_2 exits in different polymorphs, it can be tuned to produce different crystallography structure and morphological properties which in turn can change the electrochemical properties via doping or composites formation [9,29,36,37]. The material has the ability to grow within or around the carbon matrix, thus serves as a highly effective sulphur host which offers strong face-to-face entrapment, greatly maintaining the polysulphide and improves cycling stability over a long cycles.

In this study, sulphur-reduced graphene oxide/manganese dioxide composite was synthesized for supercapacitor applications. The electrochemical performance of the material was evaluated using both three- and two-electrode configurations in 2.5 M KNO_3 electrolyte. The RGO-S/100 mg MnO_2 composite measured as a half-cell revealed a peak specific capacitance of 180.4 F g^{-1} at 1 A g^{-1}. The fabricated RGO-S/100 mg MnO_2//AC-PS asymmetric hybrid device using RGO-S/100 mg MnO_2 and activated carbon from peanut shells (AC-PS) demonstrated high energy density of about 71.74 Wh kg^{-1} with its corresponding power density of 850 W kg^{-1} at a specific current of 1 A g^{-1}. The material was able to retain about 94.5% of its initial capacitance, with a columbic efficiency of 99.6% at 5 A g^{-1} for over 10, 000 cycles. Also, the device proved its stability in long cycling after being able to stand a voltage holding test for up to 90 h and preserving a 1.45 V of its maximum potential after a self-discharge test for the first 10 h, and a 1.00 V after 72 h in an open circuit.

2. Experimental

2.1. Synthesis of sulphur-reduced graphene oxide (RGO-S)

RGO-S was synthesized by mixing 1 g of sulphur and 3 g of sodium sulphide (Na_2S) into 100 mL of deionized (DI) water. The mixture was sonicated until a homogenous solution was formed labelled sample A. Then, sample B was formed by dissolving 50 mg of L-ascorbic acid into 12 g of DI water, followed by addition of 2 mL of hydrochloric acid (HCl). Thereafter, 3 g of as-prepared RGO (details in the supporting information, S1 [[38–40]]) and sample B were mixed and then added into sample A. The resulting mixture was sonicated for 2 h and then stirred at 40 °C for 1 h. Thereafter, the mixture was allowed to settle down naturally for about 12 h. It was washed several times with DI water, centrifuge three times at 10,000 rpm for 10 min and later freeze-dried for 24 h.

2.2. Synthesis of manganese dioxide (MnO_2)

0.5 g of $KMnO_4$ was liquefied into 60 mL of DI water and stirred at 150 revs/min for 10 min. Subsequently, 2 mL of HCl was added dropwise and stirred for 10 min in air. The solution was transferred into 100 mL autoclave and heated in the oven at 130 °C for 1 h. The procedures were repeated at different dwell times of 2 h, 5 h, 8 h and 11 h respectively. The solution was left to cool down naturally and then washed several times with the mixture of DI water and ethanol to remove the impurities. The sample was dried in the oven for 12 h at 60 °C.

2.3. Synthesis of the composite sample (RGO-S/MnO_2)

1 g of RGO-S was liquefied into 80 mL of DI water to form a solution which was stirred at 200 revs/min for 10 min for homogeneity. Thereafter, 50 mg of MnO_2 prepared for 1 h was added into the solution and then stirred for 5 min. The procedures were repeated by different masses of MnO_2 synthesized for 1 h (100 mg and 150 mg). The suspension was transferred into the autoclave and then heated in the oven at 150 °C for 1 h. The solution was left to cool down to room temperature, washed several times with DI water and then dried in the oven for 12 h.

2.4. Synthesis of activated carbon from peanut shell waste (AC-PS)

The activated carbon nanostructure employed in this study was synthesized as per our previous work [41]. Briefly, the material was synthesized using two steps at elevated temperature. First, pyrolysis of the raw material from peanut shell waste was done at 600 °C for 2 h under argon atmosphere. Thereafter, potassium hydroxide (KOH) as an activating agent and peanut shell waste as a raw material were mixed together in a mass ratio of 4:1 and activated at 850 °C for 1 h. The obtained product was named as AC-PS.

2.5. Characterization

The morphology and elemental composition of the as-synthesized material was examined by the scanning electron microscope (SEM-Zeiss Ultra Plus 55 field emission scanning electron microscope operated at 2.0 kV; Akishima-shi, Japan) equipped with an energy-dispersive X-ray (EDX) and a high resolution transmission electron microscope (HRTEM FEI Tecnai-F30 operated at 1.0 kV); (Akishima-shi, Japan). X-ray diffraction (XRD - Bruker BV 2D PHASER Best Benchtop); (PANalytical BV, Amsterdam, Netherland) with reflection geometry at 2θ values (5 - 90°) in a step size of 0.005° using Cu K_{α_1} radiation source ($\lambda = 0.15406\ nm$) at 50 kV and 30 mA, was used to analyse the phase structures of the material. The functional group of the material was determined by using a Fourier transmission-infrared (FTIR) achieved via Varian FT-IR spectroscopy ranging 400 - 4000 cm^{-1} in wavenumber.

2.6. Electrochemical characterization

Two- and three-electrode configuration measurements were performed by a Bio-Logic VMP300 potentiostat (Knoxville TN, USA) operating on the EC-Lab VI.41 software. The electrodes were prepared by mixing 80% of the sample as working material, 10% conductive carbon acetylene (CAB) and 10% of polyvinylidene (PVDF) as the binder. Few drops of 1-methyl 2-pyrollidone (NMP) was added to the mixture to form slurry, which was pasted onto a nickel form, 1.0 × 1.0 cm^2 and thickness-diameter of 0.2 by 16 mm

serving as current collector for three and two-electrode respectively. The electrodes were dried in the oven at 60 °C for 12 h. All electrochemical measurements were carried out using 2.5 M KNO_3 aqueous electrolyte. The 2.5 M KNO_3 was chosen as electrolyte because it is environmentally friendly, non-corrosive and has high conductivity hence revealed better electrochemical performance compared 1 M Na_2SO_4, 1 M KOH, 1 M H_2SO_4 and 1 M KNO_3 as shown in Fig. S6 in the supporting information. This performance might be contributed by the stability and pH of the electrolyte which makes it to operate in a wider potential window unlike acidic/alkaline electrolyte which is limited by oxygen evolution reaction (OER) and hydrogen evolution reaction (HER). The fabricated electrodes were tested using cyclic voltammetry (CV), galvanostatic charge discharge (GCD) and electrochemical impedance spectroscopy (EIS), respectively.

3. Results and discussion

The morphology and elemental analysis of the as-synthesized RGO-S (pristine sample) with its composites are shown in Figs. 1 and 2, respectively. Fig. 1 (a, b) shows low and high magnifications SEM images of RGO-S confirming the formation of nanorods/nanofibers and nanosheet morphologies. The formation of these morphologies were contributed by the addition of sulphur and the long-chained ascorbic acid [25,42,43]. Fig. 1 (c) shows a TEM image for RGO-S which confirms what was observed from the SEM analysis. Fig. 1 (d, e) shows low and high magnifications SEM images of MnO_2 flower like morphology synthesized for 1 h with its corresponding TEM image in Fig. 1 (f). Since integration of external additives is expected to affect chemical and physical properties of the composites, thus variation of masses of the MnO_2 sample become necessary. Besides, conductivity and the resultant capacitance of RGO-S and MnO_2 composites can be improved by investigating their ratio. Fig. 1 (g, h, j, k, m, and n) displays the SEM images of RGO-S/MnO_2 composites at different mass loading of MnO_2 with their corresponding TEM micrograph in Fig. 1 (i, l and o), respectively. It was observed that all the three composite samples (50, 100 and 150 mg) revealed similar morphologies comprising nanosheets, nanorods and nanoflowers like particles. The RGO-S/100 mg MnO_2 composite was noticed to be consisting of visible porous structure, which is expected to allow for more effective passage of electrolyte ions within the material as compared to the RGO-S/50 mg MnO_2 and RGO-S/150 mg MnO_2 samples. For RGO-S/150 mg MnO_2, the morphology looks non-porous hence the movement of ions from the electrolyte within the material is expected to be not so great which should lead to poor electrochemical performance. EDX analysis was used to determine the elemental composition of the as-synthesized RGO-S and RGO-S/MnO_2 composites with different mass loading of MnO_2. Fig. 2 (a) shows EDX analysis of RGO-S confirming the presence of individual elements C, S, O, while Fig. 2 (b) shows Mn and O in the MnO_2 sample. Fig. 2 (c – e) confirm the existence of C, S, O and Mn in the RGO-S/MnO_2 composites. The observed K in the spectrum of MnO_2 is due to the potassium per manganite ($KMnO_4$) chemical used during the sample synthesis.

Fig. S7 (a, b) in supporting document displays SEM images of pristine RGO at low and high magnifications, respectively. The RGO without sulphur doping reveals a sheet like morphology as already indicated and discussed in our previous work [40].

Fig. 3 (a) displayed the XRD spectrum for the as-synthesized RGO-S (pristine), MnO_2, RGO-S/50 mg MnO_2, RGO-S/100 mg MnO_2 and RGO-S/150 mg MnO_2 shown crystal structure and phase purity of the samples. Both samples revealed a crystallinity structure measured between the angular range $2\theta = 5° - 90°$. The monoclinic crystal structure of RGO-S corresponds to the matching card no. JCPDS N34-0941 [44] while that of MnO_2 are in line with the α-MnO_2 card no. JCPDS 00-044-0141 [18,45]. The XRD spectrum around 12.5°, 27.6°, 23.08° and 42.4° corresponds to (002), (331), (222) and (319) planes respectively, displaying the existence of C and S in the RGO-S matrix, respectively. The presence of peaks around 12.1°, 24.6°, 36.5° and 65.7° which corresponds to the α-MnO_2 (110), (220), (211) and (002), planes respectively, conforms to the successful incorporation of α-MnO_2 into RGO-S/MnO_2 composites. The FTIR analysis of the RGO-S (pristine), MnO_2, RGO-S/50 mg MnO_2, RGO-S/100 mg MnO_2 and RGO-S/150 mg MnO_2 is shown in Fig. 3 (b). Bending vibrations of hydroxyl groups and stretching vibrations of interlayer water molecules was observed around 1741 cm^{-1} bands. The peak around 1218 cm^{-1} was assigned to the interaction of Mn with the host species [15].

The as-synthesized sample was evaluated for electrochemical measurements in a three-electrode configuration using Ag/AgCl as reference electrode and glassy carbon as the counter electrode in 2.5 M KNO_3 aqueous electrolyte. Fig. S2 (a) indicates an electrochemical evaluation in a positive potential window range of 0.0−0.6 V vs Ag/AgCl through cyclic voltammetry (CV) for the RGO-S (pristine) sample at different scan rates, which shows a rectangular shape that reveals an electric double layer capacitor (EDLC) behaviour. This was further confirmed by a symmetric triangular shape possessed by the galvanostatic charge-discharge profile as shown in Fig. S2 (b). Furthermore, to make an evaluation of the composite material an additive manganese dioxide (MnO_2) was prepared by varying hydrothermal dwelling time. The electrochemical measurements in a positive potential window range of 0.0−0.6 V vs Ag/AgCl revealed that 1 h dwelling time performed better compared to the rest of the dwelling times as shown in Fig. S3 (a-c). Therefore, 1 h preparation of the additive MnO_2 was chosen to prepare RGO-S/MnO_2 composites by varying the mass of MnO_2. MnO_2 is one of the classic pseudocapacitive material which will possibly increase the capacitance of RGO-S, while the RGO-S is expected to provide or improve the conductivity of the material and at the same time contributed to the sample's pseudocapacitive behaviour. Sulphur is an attractive material for energy storage devices owing to its high theoretical capacity (1672 mAh g^{-1}) and specific energy (2600 Wh kg^{-1}), which could enhance complete reaction of electrolyte ions with sulphur to form sulphide of the ions. It is also known for its relatively low cost and environmental impact as an electrode material. Sulphur offers strong coordinate bonding with carbon/metallic surfaces due to its relatively low electronegativity. Its lower electronegativity S (2.58) accounts for capability to create more redox active sites, which improves capacity/capacitance of the electrode. Thus, sulphur-containing composite materials exhibit relatively high capacity retention and high charge/discharge cycle stability resulting from improved electrical and surface properties, and improved wettability of the electrode materials.

Fig. S8 in the supporting document shows the CV curves at a scan rate of 50 mV s^{-1} in a positive potential window for RGO and RGO-S samples, respectively. The current response in the CV curves for RGO is less compared to the RGO-S. Also, RGO-S has high potential window compared to RGO as observed from Fig. S8. Hence, RGO-S has better performance compared to RGO. Fig. 4 (a) shows a rectangular CV curves of RGO-S and RGO-S/MnO_2 composites at different MnO_2 mass loading in a positive potential window range of 0.0−0.6 V vs Ag/AgCl at a scan rates of 50 mV s^{-1}. The overall CV curves show rectangular shape with no obvious redox peaks as indicative of EDLC dominance in the materials. From the figure it was observed that, the 100 mg of MnO_2 loading into the RGO-S sample proves to have higher current response as compared to the rest of the composites which is the indication of higher specific capacitance [8].

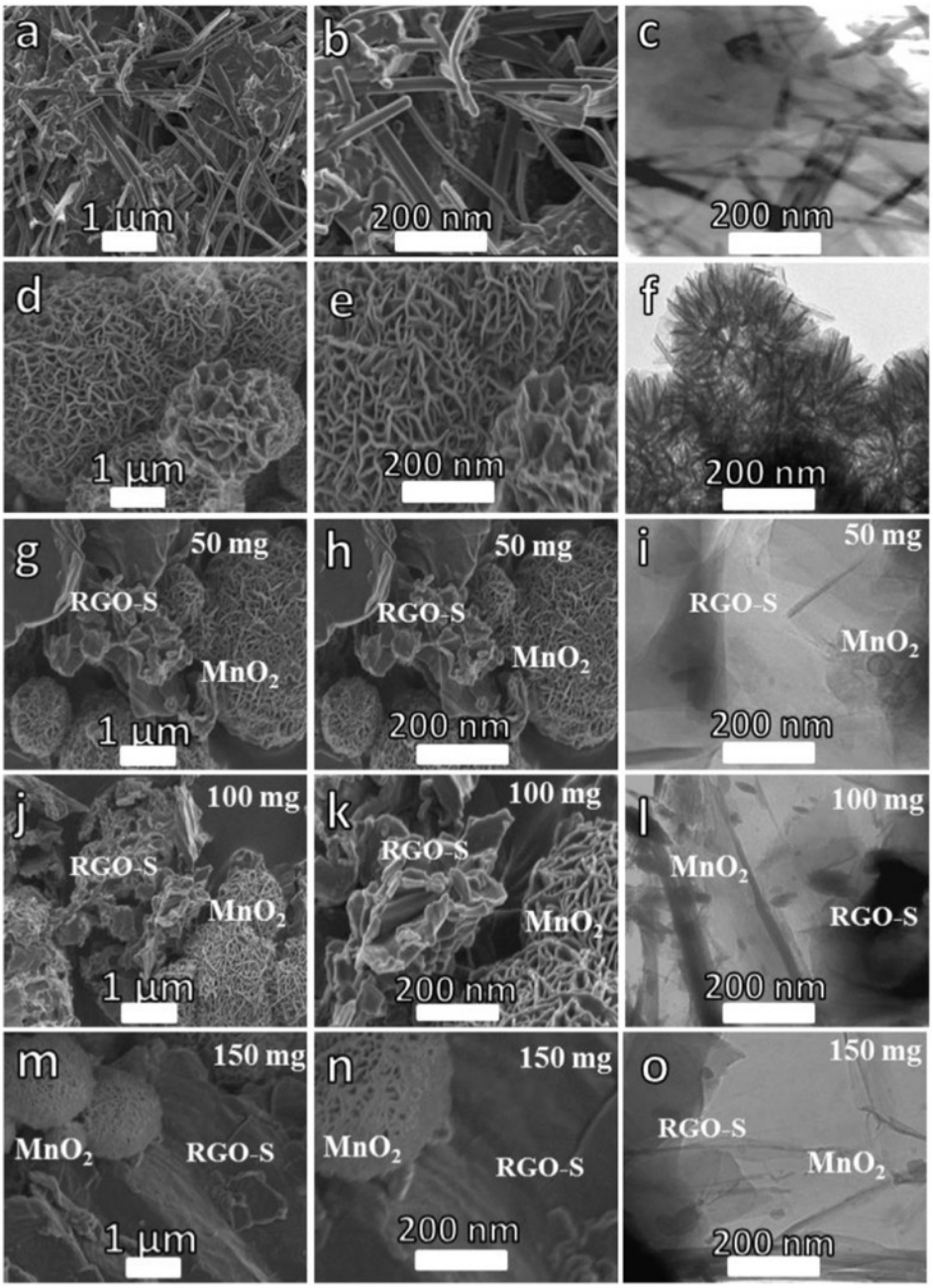

Fig. 1. (a, b), (d, e): SEM images of RGO-S and MnO_2 respectively and (g, h) (j, k) and (m, n): SEM images for RGO-S/50 mg MnO_2, RGO-S/100 mg MnO_2 and RGO-S/150 mg MnO_2 at low and high magnifications, respectively. (c, f, i, l and o) are TEM images for RGO-S, MnO_2, RGO-S/50 mg MnO_2, RGO-S/100 mg MnO_2 and RGO-S/150 mg MnO_2, respectively.

The electrochemical evaluation of the RGO-S and RGO-S/MnO_2 composites at different MnO_2 loading was further examined using the GCD curves at a specific current of 1 A g^{-1} in a positive potential range of 0.0−0.6 V as shown in Fig. 4 (b). The GCD behaviour corresponds well with the CV in Fig. 4 (a). The observed linear variation in the GCD curves shows that the constant charge-discharge rate reveals the features of EDLC behaviour within the material. Equation (1), was used to estimate the specific capacitance (C_s) of the RGO-S and RGO-S/MnO_2 composite with different mass loading of MnO_2, as shown below [14,37]:

$$C_s = \frac{I_d \times \Delta t}{m \times \Delta V}\left[F\ g^{-1}\right] \quad (1)$$

where, ΔV is the operating potential window in (V), I_d is the discharge current in (mA), m is the mass loading of the active

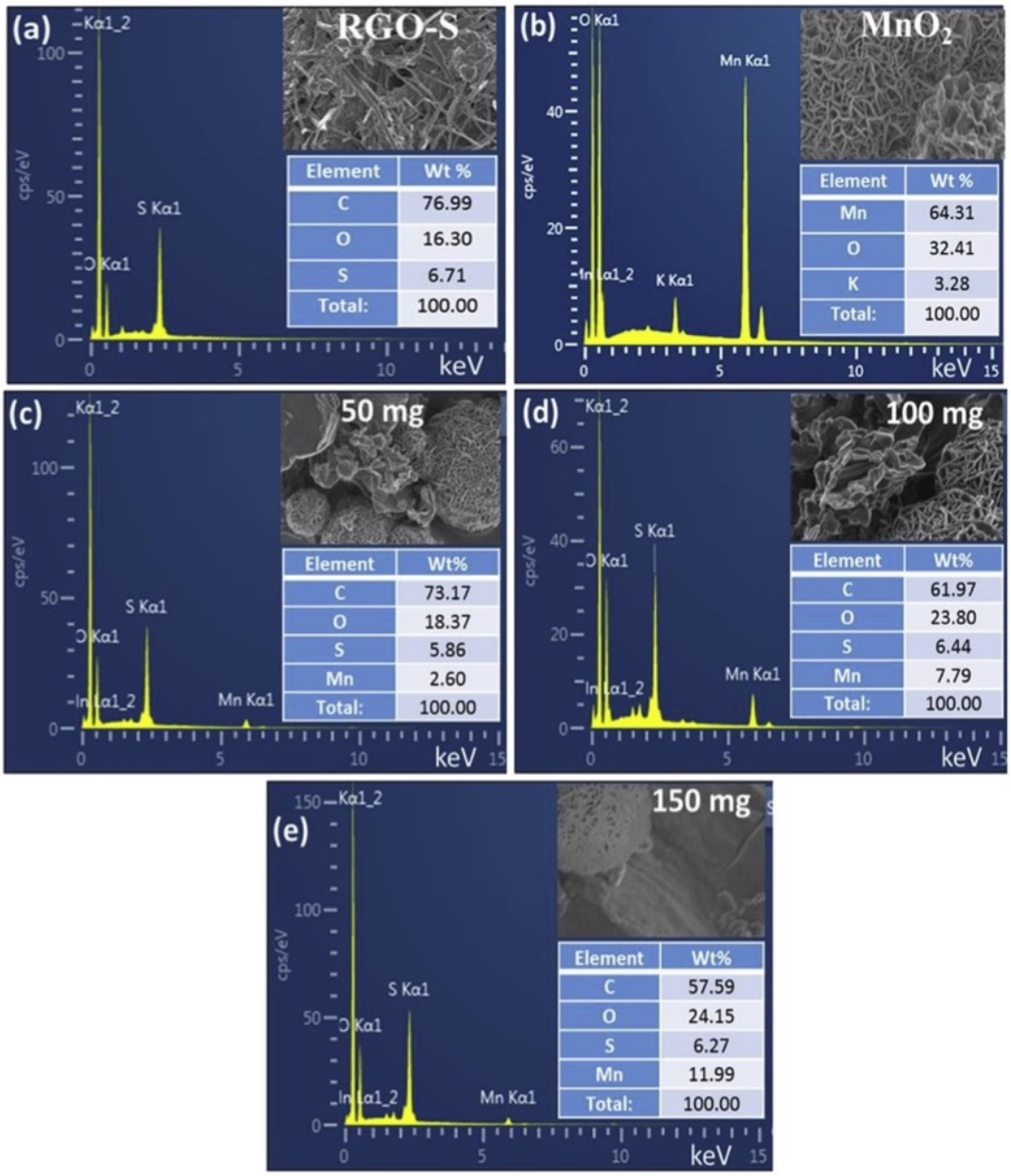

Fig. 2. EDX for (a) RGO-S, (b) MnO_2, (c) RGO-S/50 mg MnO_2, (d) RGO-S/100 mg MnO_2 and (e) RGO-S/150 mg MnO_2, respectively.

material in (mg), and Δt (s) is the electrode discharge time.

Evaluated C_s corresponding to RGO-S, RGO-S/50 mg MnO_2, RGO-S/100 mg MnO_2 and RGO-S/150 mg MnO_2 were 75.2 F g^{-1}, 63.7 F g^{-1}, 180.4 F g^{-1} and 169.5 F g^{-1}, respectively. The calculated C_s value (63.7 F g^{-1}) for RGO-S/50 mg MnO_2 was observed to be lower than that of pristine RGO-S and the other composites, which is attributed to the disparity between contributing capacitive properties of both the MnO_2 and RGO-S materials. In principle, the capacitive contribution of the respective materials in the composite is supposed to be equal or very close to each other to effect enhanced electrochemical performances. The added 50 mg of MnO_2 in the RGO-S/50 mg MnO_2 sample was not enough to facilitate effective interaction within the matrix of the composite material. This is also indicated by the sample's SEM/TEM morphology (Fig. 1(g, h and i)), which is observed to be agglomerated and inhomogenously distributed. The higher C_s observed for the RGO-S/100 mg MnO_2 composite indicates that the material responds better electrochemically as compared to the other samples. This is the indication of a good synergy between RGO-S and MnO_2 at this particular mass loading. This was also in agreement with SEM

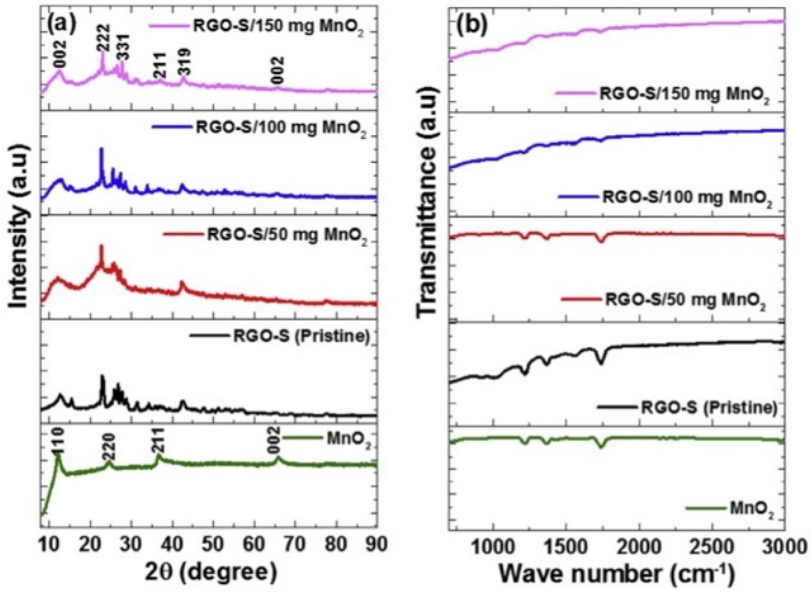

Fig. 3. (a) XRD and (b) FTIR for RGO-S (Pristine), MnO_2, RGO-S/50 mg MnO_2, RGO-S/100 mg MnO_2 and RGO-S/150 mg MnO_2, respectively.

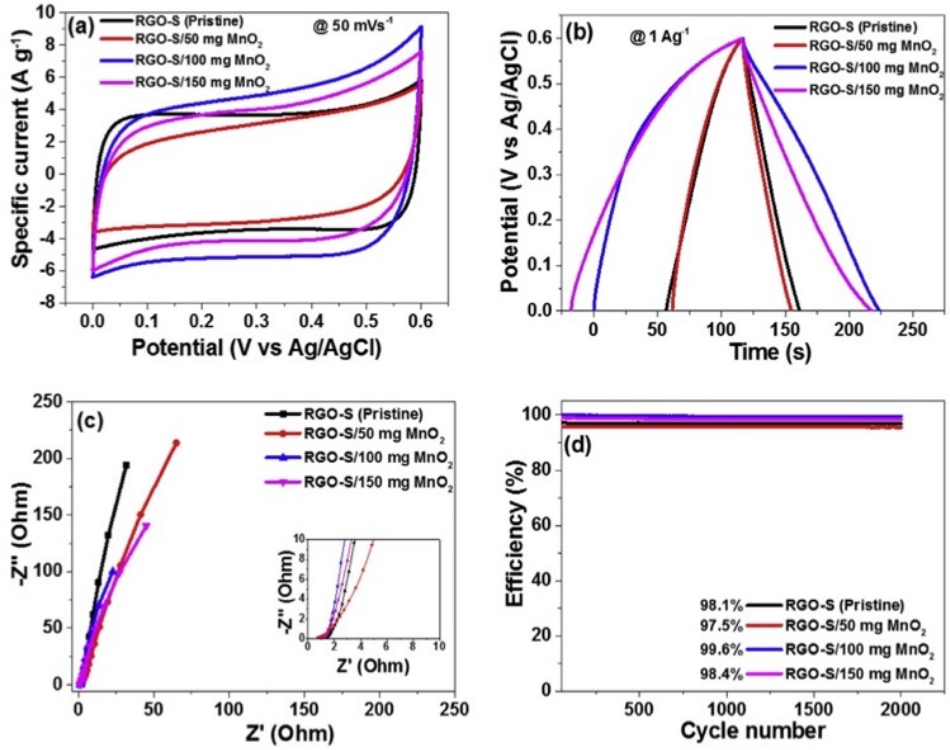

Fig. 4. (a, b) CV and GCD curves in a positive potential window for RGO-S/MnO_2 at different MnO_2 mass loading respectively and (c, d) EIS Nyquist plot and cycling stability for RGO-S/MnO_2 at different MnO_2 loading in 2.5 M KNO_3, respectively.

morphology for RGO-S/100 mg MnO_2 composite (Fig. 1 (j and k)) that showed well distributed porous structure. This shows that morphology plays a significant role in the electrochemical performance of the material.

The EIS technique through Nyquist plot with the frequency range 10 mHz–100 kHz in an open circuit potential 0.0 V was used to determine the electrical resistance of the as-synthesized material. The EIS of the RGO-S and RGO-S/MnO_2 composites is displayed

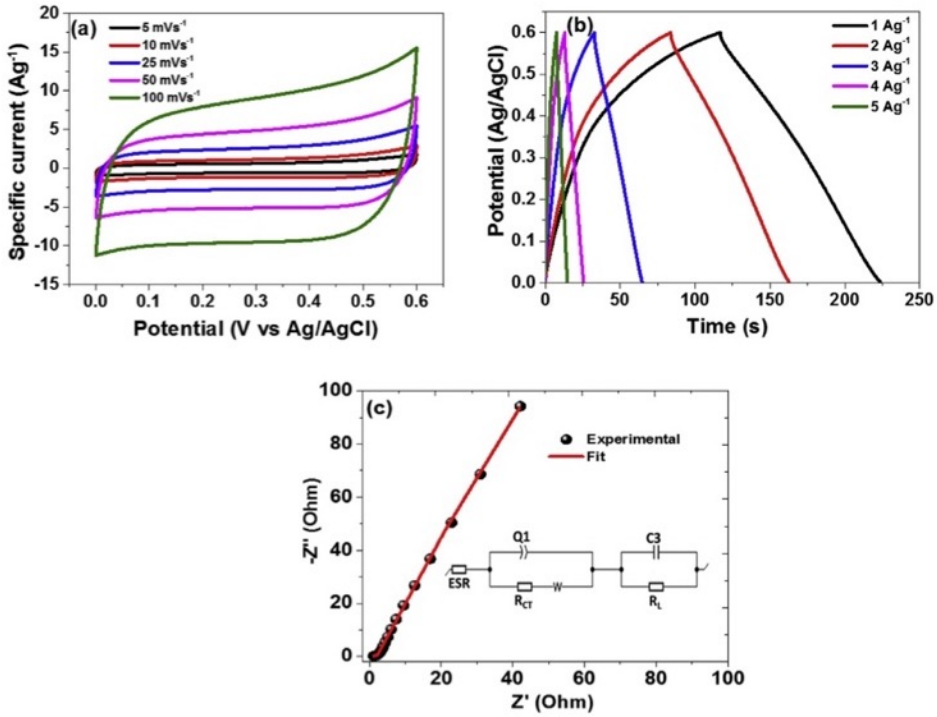

Fig. 5. (a, b) CV and GCD curves in a positive potential window at different scan rates and specific currents, respectively and (c) EIS Nyquist plot with an insert circuit for RGO-S/100 mg MnO_2 in 2.5 M KNO_3, respectively.

in Fig. 4 (c). The equivalence series resistance (ESR) which is intersect at Z' axis is a sum total of a contact resistance between the working electrode and the current collector, the interface resistance of the working electrode and ions from the electrolyte. Its values were found to be 1.5 Ω, 1.8 Ω, 0.9 Ω and 1.2 Ω for RGO-S, RGO-S/50 mg MnO_2, RGO-S/100 mg MnO_2 and RGO-S/150 mg MnO_2, respectively. It is clear that RGO-S/100 mg MnO_2 composite is having the smallest ESR value and smallest diffusion length as compared to the rest of the samples. These results still prove that RGO-S/100 mg MnO_2 composite is the best composite due to the effective incorporation of MnO_2 into RGO-S matrix.

The columbic efficiency versus cycle number is shown in Fig. 4 (d) for RGO-S, RGO-S/50 mg MnO_2, RGO-S/100 mg MnO_2 and RGO-S/150 mg MnO_2 at 5 A g^{-1}. The stability was carried out for 2000 charge-discharge cycles. The following equation was used to evaluate the columbic efficiency C_E (%) of the material:

$$C_E = \frac{t_D}{t_c} \times 100\% \quad (2)$$

where t_c and t_D are charging-discharging time with the same current respectively.

The three-electrode measurements reveal maximum cycling stability of about 99.6% for RGO-S/100 mg MnO_2 composite while 98.1%, 97.5% and 98.4% for RGO-S, RGO-S/50 mg MnO_2 and RGO-S/150 mg MnO_2, respectively. The unique morphology and low ESR value of about 0.9 Ω has contributed to the higher cycling stability of RGO-S/100 mg MnO_2 composite.

The electrochemical measurements of the RGO-S/100 mg MnO_2 composite was evaluated using CV curves at various scan rates starting from 5, 10, 25, 50 and 100 mV s^{-1} in a working potential range of 0.0−0.6 V vs Ag/AgCl displaying EDLC behaviour as shown in Fig. 5 (a). It was observed that as the scan rate increases, the current response increases as well, while the shape kept unchanged. Further evaluation of the GCD curves for RGO-S/100 mg MnO_2 at different specific currents is presented in Fig. 5 (b). The symmetric triangular curves at different specific currents with a small IR drop (at the beginning of the discharge curve) is observed and corresponds well with the CV curves in Fig. 5 (a). Fig. 5 (c) shows the EIS Nyquist plot for experimental and fitting, with the fitting circuit is shown as inset to the figure for RGO-S/100 mg MnO_2. The circuit shows ESR (equivalent series resistance) is in series with R_{CT} (charge transfer resistance) at high-frequency region and W (Warburg) is in parallel with Q1 (real capacitance). A mass capacitance (C3) is parallel with the leakage resistance (R_L) at low frequency region. R_{CT} represents the reactions that occurs at the interface of the electrode and electrolyte. The obtained values for ESR = 1.2 Ω and R_{CT} = 0.8 Ω from the fitting are comparable with the experimental values ESR = 0.9 Ω and R_{CT} = 0.6 Ω, respectively indicating good fitting of the Nyquist plot. The small R_{CT} = 0.8 Ω reveals fast ion transport and charge-transfer kinetics which describes good properties for capacitive material.

The as-synthesized RGO-S/100 mg MnO_2 composite material was further investigated using two-electrode measurements for the real application. The electrode was tested in both positive (as discussed above) and negative potential window and shows better performance in the positive potential window (in terms of current response) as shown in the supporting information Fig. S5 (a). Furthermore, based on CV curves in Fig. S5 (a, b), the asymmetric device could be pushed further to an extended operating potential of about 1.5 V. Therefore, the RGO-S/100 mg MnO_2 was selected as positive electrode while activated carbon from peanut shells (AC-

PS) was selected as negative electrode (see Fig. S4 in the supporting information for more details) to make up the device. The choice of AC-PS was due to its compatibility in the same electrolyte with positive electrode, high pore size which easy the passage of electrolyte ions and high conductivity and its detailed electrochemical properties had been discussed in our previous work [41].

The charge balance equation, $Q_+ = Q_-$ was used to balance the mass of each electrode with the charge stored on each electrode being stated as:

$$Q = C_s \times m\,\Delta V \tag{3}$$

where m (g) is the mass of active material, C_S (F g^{-1}) is the specific capacitance of the electrode based on the mass of active material, ΔV (V) is the potential window and Q (C) is the stored charge on the electrode.

The following equation (4) was used to determine the mass balance between positive and negative electrodes [46]:

$$\frac{m_+}{m_-} = \frac{C_{s-}\ \ \Delta V_-}{C_{s+}\ \ \Delta V_+} \tag{4}$$

The mass balance ratio of 1.0:2.0 obtained by using equation (4) for each electrode was 2.0 and 4.0 mg for RGO-S/100 mg MnO_2 and AC-PS, respectively making a total mass of 6.0 mg cm^{-2}. A filter paper soaked into 2.5 M KNO_3 was sandwiched between a mass of positive and negative electrode in a coin cell (Standard 2032 grade) setup.

Fig. 6 (a) shows the CV curves at 50 mV s^{-1} of RGO-S/100 mg MnO_2 composite and AC-PS (see Fig. S4 in supporting information

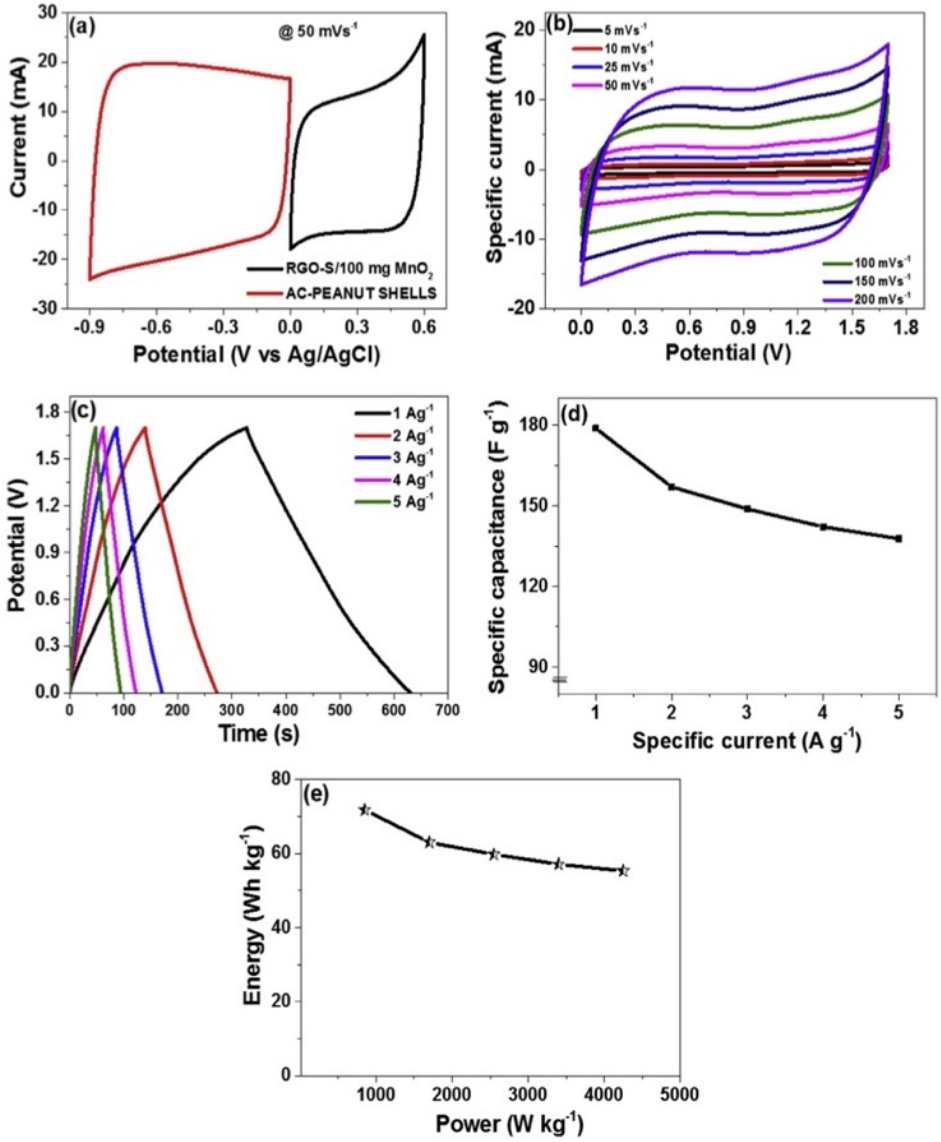

Fig. 6. RGO-S/MnO_2//AC-PS asymmetric device: (a) CV of positive and negative electrodes, (b) CV curves at different scan rates, (c) GCD curves at different specific currents, (f) Specific capacitance versus specific current and (e) Ragone plot in 2.5 M KNO_3, respectively.

for more on electrochemical properties of the AC-PS) materials used as positive and negative electrodes, respectively. Both electrodes display rectangular CV shapes revealing the properties of electric double layer capacitor (EDLC) in the 2.5 M KNO_3 neutral electrolyte. The fabricated hybrid device could run well at a much higher potential of up to 1.7 V, due to the synergetic effect between the two electrode materials and the use of neutral electrolyte which can still work on the high potential window. The CV curves of the asymmetric device at different scan rates are shown in Fig. 6 (b). It was observed that the synergetic effect of the combined material can be clearly revealed by the CV curves at different scan rates, showing the contribution from the negative and positive electrodes as depicted in Fig. 6 (a and b). Fig. 6 (c) shows the galvanostatic charge-discharge (GCD) of the asymmetric device at different specific currents of 1, 2, 3, 4 and 5 A g^{-1}. The GCD curves displays the symmetric triangular profiles which is in accordance with the CV curves in Fig. 6 (b).

Fig. 6 (d) shows specific capacitance (C_S) evaluated from the GCD curves of the device using Eqn (1) plotted against different specific currents. The evaluated specific capacitances for the asymmetric device were recorded as 178.74, 156.99, 148.84, 142.19 and 137.76 F g^{-1} at 1, 2, 3, 4 and 5 A g^{-1}, respectively. It was observed that as the specific current increases the specific capacitances decreased slowly indicating highly reversible capacitive nature of the material (ie there was no rapid reduction of the specific capacitance as the specific current increases). This indicates high rate capability of the material which was contributed by synergy between RGO-S/100 mg MnO_2 and AC-PS which allowed electrolytes ions to access the material during rapid charge/discharge process. The practical application of the device was pointed out by these values. The specific energy and power densities were evaluated using Eqns. (5) and (6) below [46,47].

$$E_d = \frac{1}{2} C_S V^2 = \frac{C_S V^2}{7.2} \left[\text{Wh kg}^{-1}\right] \quad (5)$$

$$P_d = \frac{E_d}{\Delta t} \times 3600 \left[\text{W kg}^{-1}\right] \quad (6)$$

where, C_S corresponds to the specific capacitance (F g^{-1}), V operating potential (V), Δt is discharge time (s), E_d and P_d are specific energy and power densities, respectively, with their specified units.

Fig. 6 (e) displays the so-called Ragone plot (specific energy versus specific power plot) and it found that specific energy of about 71.74 Wh kg^{-1} with its corresponding specific power of 850 W kg^{-1} was recorded for the device at 1 A g^{-1}. The fabricated asymmetric device displayed very state specific energy versus specific power to the extent that even at a high specific current of 5 A g^{-1}, the specific energy remains as 55.30 Wh kg^{-1} with its corresponding specific power of 4250 W kg^{-1}. The fabricated device revealed higher energy and power density compared to some similar materials previously reported in the literature as shown in Table 1.

The charge-discharge cycling test was carried out at 5 A g^{-1} to determine the stability of the device. Eqn. (2) was used to estimate the columbic efficiency of the device. It was found that, the device could maintain a 94.5% of its initial capacitance with an equivalent columbic efficiency of 99.6% for over 10, 000 cycles as presented in Fig. 7(a). The stability test of the device was further carried out through more practical stability test known as voltage holding or floating test. The degradation of an electrochemical performance for the device can be viewed straight using this phenomenon. Fig. 7 (b) displays a voltage holding for the device in a maximum working potential of 1.7 V for 90 h at 5 A g^{-1}. The device was charge-discharged for three cycles whereby the specific capacitance was monitored. The device was then held at a maximum potential of 1.7 V for 10 h intervals, then subjected to charge-discharge again for three cycles and left at that fixed potential for next 10 h. The process was repeated for up to 90 h. The capacitance decreased in the first 20 h but later became stable from 20 h to over 90 h of the aging test. This could be due to the fact that at initial stage, the electrode lacks wettability. A self-discharge (SD) test was conducted at room temperature to examine the shelve life of the asymmetric device. The device was fully charged to its peak potential of 1.7 V at 1 A g^{-1} and then left in an open circuit potential to undergo a SD. Fig. 7 (c, d) shows that within the first 10 h the device was able to maintain a potential of 1.45 V and 1.00 V after 72 h. The decrease in the device voltage was associated with the decomposition of water which was used as a solvent.

Fig. 8 (a) is a representation of the Nyquist plot of EIS test performed before cycling, after cycle stability and after voltage holding on the device. The noticed small semicircle at a high frequency region proves a low resistance and good ion diffusion at the electrode-electrolyte interface, which contributed to the supercapacitor's enhanced capacitive behaviour. It was also observed that after voltage holding test, the ESR and diffusion length reduced compared to before and after the cycling tests. This shows that after voltage holding test, the material becomes more accessible to the ions within the electrolyte. The ESR values before cycling, after cycle cycling and after voltage holding tests were recorded as ~5.7 Ω, 3.9 Ω and 3.7 Ω, respectively, which agree well with the observed diffusion lengths (Fig. 8 (a)). Moreover, the EIS Nyquist plot for RGO-S/MnO_2//AC-PS asymmetric supercapacitor was fitted as displayed in Fig. 8 (b) with the help of Z-FIT fitting program v11.02, with the matching electrical circuit shown as inset to the figure. The equivalent circuit shows that equivalent series resistance (ESR) is connected in series with two units. The constant phase element (Q2) is parallel with charge transfer resistance (R_{CT}) while another constant phase element (Q3) is parallel with the leakage resistance (R_L) at low frequency region. The obtained values for equivalent series resistance (ESR = 5.7 Ω–4.3 Ω (experimental)) and charge transfer resistance (R_{CT} = 2.5 Ω–2.0 Ω (experimental)) are comparable with experimental and fitting values, respectively. Moreover, Fig. 8 (c) shows the phase angle versus frequency curve with a phase angle value of about −80.4 for the device which is very close

Table 1
Comparisons of electrochemical performance (energy and power density) of some similar materials on RGO-S/MnO_2//AC-PS evaluated using two electrode cell configurations.

Electrodes (Device)	Electrolyte	Energy density	Power density	Ref.
GF/MnO_2//GF/MnO_2	1 M Na_2SO_4	34 Wh kg^{-1}	20 kW kg^{-1}	[20]
G-ϒ-MnO_2/CNT//G-ϒ-MnO_2/CNT	1 M KOH	43 Wh kg^{-1}	26 kW kg^{-1}	[17]
e-CMG/MnO_2//e-CMG	1 M Na_2SO_4	44 Wh kg^{-1}	25 kW kg^{-1}	[13]
GF/MnO_2//AC	1 M Na_2SO_4	51.1 Wh kg^{-1}	102.2 W kg^{-1}	[47]
MnO_2/rEGO//MnO_2/rEGO	6 M KOH	25.5 Wh kg^{-1}	45 W kg^{-1}	[48]
MnO_2/rGO//MnO_2/rGO	1 M Na_2SO_4	42.7 Wh kg^{-1}	22.5 kW kg^{-1}	[49]
MnO_2/CNT//AC	2 M KNO_3	21 Wh kg^{-1}	123 kW kg^{-1}	[50]
RGO-S/MnO_2//AC-PS	2.5 M KNO_3	71.74 Wh kg^{-1}	850 W kg^{-1}	This work

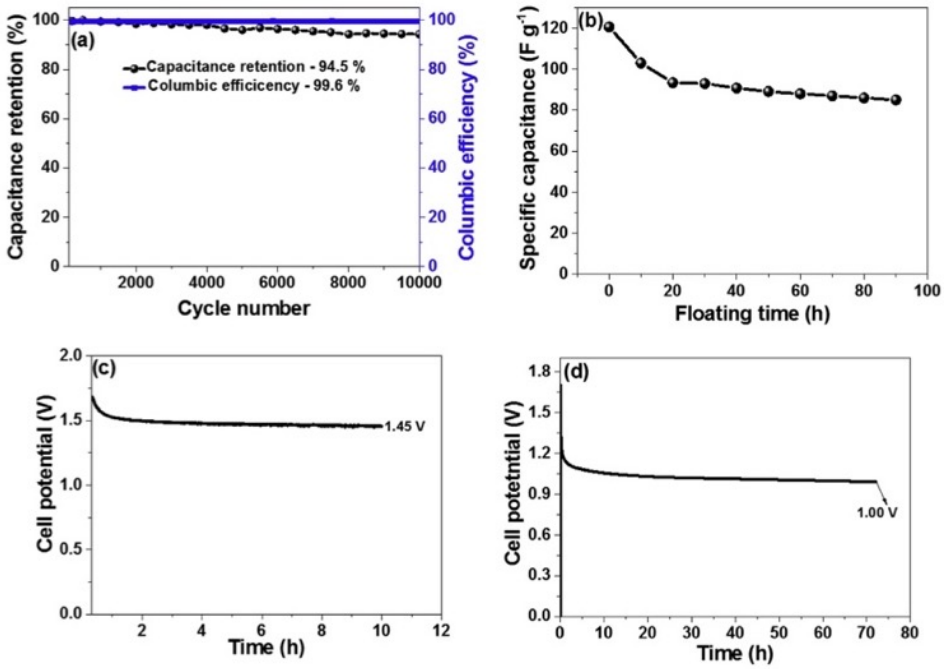

Fig. 7. (a) Capacitance retention and columbic efficiency versus cycling number, (b) Specific capacitance versus floating time, (c) Self-discharge after full charged to 1.70 V at 3 A g^{-1} within the first 10 h and (d) Self-discharge after 72 h for asymmetric device.

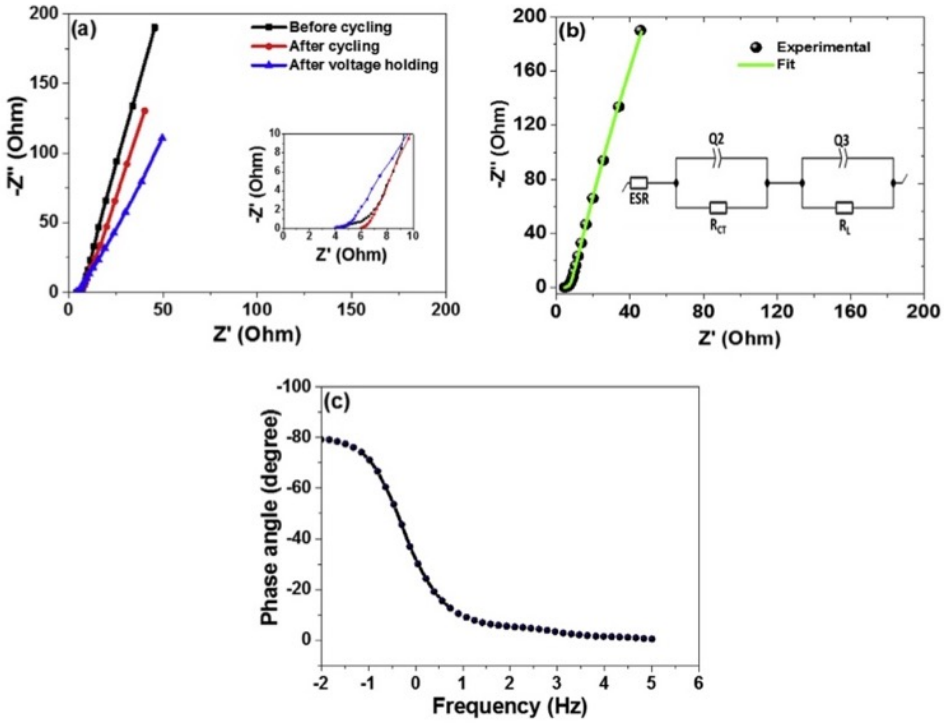

Fig. 8. (a) The EIS Nyquist plot before cycling, after cycle cycling and after voltage holding, (b) EIS Nyquist plot with an insert of equivalent electrical circuit and (c) Phase angle versus frequency for the device.

to the ideal value of −90. This result reveals that the fabricated device is performing closer to the ideal capacitive behaviour.

4. Conclusion

RGO-S and its MnO_2 composites were successfully synthesized in this study. The characterization of the samples revealed the formation of nanorods/fibers, nanosheets and nano-flower like morphology depending on the MnO_2 mass loading. The RGO-S/100 mg MnO_2 composite measured as a three electrode revealed a specific capacitance of 180. 4 F g^{-1} compared to 75.2 F g^{-1} of the RGO-S (pristine) sample at 1 A g^{-1} in 2.5 M KNO_3 electrolyte. The assembled RGO-S/MnO_2//AC-PS device delivered a high specific energy of 71.74 Wh kg^{-1} with its corresponding specific power of 850 W kg^{-1} at 1 A g^{-1}. An incredible observation was noted when the device was able to maintain a specific energy of 55.30 Wh kg^{-1} at a high specific current of 5 A g^{-1}. The capacitance retention of 94.5% and columbic efficiency of 99.6% up to 10, 000 cycles at 5 A g^{-1} was recorded showing outstanding stability for the device. These results show that the as-synthesized materials have great potential for supercapacitors applications.

Declaration of competing interest

The authors declare that they have no known competing financial interests or personal relationships that could have appeared to influence the work reported in this paper.

CRediT authorship contribution statement

Delvina Japhet Tarimo: Conceptualization, Methodology, Formal analysis, Data curation, Investigation, Writing - original draft. **Kabir O. Oyedotun:** Methodology, Validation, Writing - review & editing. **Abdulmajid A. Mirghni:** Formal analysis, Validation, Writing - review & editing. **Ndeye Fatou Sylla:** Methodology, Resources. **Ncholu Manyala:** Conceptualization, Methodology, Supervision, Writing - review & editing, Funding acquisition, Project administration, Resources, Validation.

Acknowledgements

This work is based on the research supported by the South African Research Chairs Initiative of the Department of Science and Technology and National Research Foundation of South Africa (Grant No. 61056). Any opinion, finding, and conclusion expressed in this material are that of the authors, and the NRF does not accept any liability in this regard. Delvina Japhet Tarimo acknowledges the financial support from NRF through SARChI chair in Carbon Technology and Materials.

Appendix A. Supplementary data

Supplementary data to this article can be found online at https://doi.org/10.1016/j.electacta.2020.136498.

References

[1] S. Sahoo, C.S. Rout, Facile electrochemical synthesis of porous manganese-cobalt-sulfide based ternary transition metal sulfide nanosheets architectures for high performance energy storage applications, Electrochim. Acta 220 (2016) 57–66, https://doi.org/10.1016/j.electacta.2016.10.043.

[2] R. Ramachandran, M. Saranya, A.N. Grace, F. Wang, MnS nanocomposites based on doped graphene: simple synthesis by a wet chemical route and improved electrochemical properties as an electrode material for supercapacitors, RSC Adv. 7 (2017) 2249–2257, https://doi.org/10.1039/c6ra25457h.

[4] C.Y. Chen, C.Y. Fan, M.T. Lee, J.K. Chang, Tightly connected MnO 2-graphene with tunable energy density and power density for supercapacitor applications, J. Mater. Chem. 22 (2012) 7697–7700, https://doi.org/10.1039/c2jm16707g.

[5] F. Barzegar, A. Bello, D. Momodu, M.J. Madito, J. Dangbegnon, N. Manyala, Preparation and characterization of porous carbon from expanded graphite for high energy density supercapacitor in aqueous electrolyte, J. Power Sources 309 (2016) 245–253, https://doi.org/10.1016/j.jpowsour.2016.01.097.

[6] J. Zhao, G. Wang, R. Hu, K. Zhu, K. Cheng, K. Ye, D. Cao, Z. Fan, Ultrasmall-sized SnS nanosheets vertically aligned on carbon microtubes for sodium-ion capacitors with high energy density, J. Mater. Chem. 7 (2019) 4047–4054, https://doi.org/10.1039/c9ta00141g.

[7] J.P. Cheng, J. Zhang, F. Liu, Recent development of metal hydroxides as electrode material of electrochemical capacitors, RSC Adv. 4 (2014) 38893–38917, https://doi.org/10.1039/c4ra06738j.

[8] J. Yan, Z. Fan, T. Wei, W. Qian, M. Zhang, F. Wei, Fast and reversible surface redox reaction of graphene-MnO2 composites as supercapacitor electrodes, Carbon 48 (2010) 3825–3833, https://doi.org/10.1016/j.carbon.2010.06.047.

[9] Q. Cheng, J. Tang, J. Ma, H. Zhang, N. Shinya, L.C. Qin, Graphene and nanostructured MnO2 composite electrodes for supercapacitors, Carbon 49 (2011) 2917–2925, https://doi.org/10.1016/j.carbon.2011.02.068.

[10] S. Ramesh, H.M. Yadav, K. Karuppasamy, D. Vikraman, H.S. Kim, J.H. Kim, H.S. Kim, Fabrication of manganese oxide@nitrogen doped graphene oxide/polypyrrole (MnO2@NGO/PPy) hybrid composite electrodes for energy storage devices, J. Mater. Res. Technol. 8 (2019) 4227–4238, https://doi.org/10.1016/j.jmrt.2019.07.033.

[11] H. Chen, F. Yu, G. Wang, L. Chen, B. Dai, S. Peng, Nitrogen and sulfur self-doped activated carbon directly derived from elm flower for high-performance supercapacitors, ACS Omega 3 (2018) 4724–4732, https://doi.org/10.1021/acsomega.8b00210.

[12] W. Zhang, F. Liu, Q. Li, Q. Shou, J. Cheng, L. Zhang, B.J. Nelson, X. Zhang, Transition metal oxide and graphene nanocomposites for high-performance electrochemical capacitors, Phys. Chem. Chem. Phys. 14 (2012) 16331–16337, https://doi.org/10.1039/c2cp43673f.

[13] B.G. Choi, M. Yang, W.H. Hong, J.W. Choi, Y.S. Huh, 3D macroporous graphene frameworks for supercapacitors with high energy and power densities, ACS Nano 6 (2012) 4020–4028, https://doi.org/10.1021/nn3003345.

[14] S. Ramesh, D. Vikraman, H.S. Kim, H.S. Kim, J.H. Kim, Electrochemical performance of MWCNT/GO/NiCo2O4 decorated hybrid nanocomposite for supercapacitor electrode materials, J. Alloys Compd. 765 (2018) 369–379, https://doi.org/10.1016/j.jallcom.2018.06.194.

[15] J. Zhu, J. He, Facile synthesis of graphene-wrapped honeycomb MnO 2 nanospheres and their application in supercapacitors, ACS Appl. Mater. Interfaces 4 (2012) 1770–1776, https://doi.org/10.1021/am3000165.

[16] L. Deng, G. Zhu, J. Wang, L. Kang, Z.H. Liu, Z. Yang, Z. Wang, Graphene-MnO2 and graphene asymmetrical electrochemical capacitor with a high energy density in aqueous electrolyte, J. Power Sources 196 (2011) 10782–10787, https://doi.org/10.1016/j.jpowsour.2011.09.005.

[17] R.B. Rakhi, W. Chen, D. Cha, H.N. Alshareef, Nanostructured ternary electrodes for energy-storage applications, Adv. Energy Mater. 2 (2012) 381–389, https://doi.org/10.1002/aenm.201100609.

[18] P.M. Shafi, R. Dhanabal, A. Chithambararaj, S. Velmathi, A.C. Bose, α-MnO2/h-MoO3 hybrid material for high performance supercapacitor electrode and photocatalyst, ACS Sustain. Chem. Eng. 5 (2017) 4757–4770, https://doi.org/10.1021/acssuschemeng.7b00143.

[19] H. Chen, M.Q. Wang, Y. Yu, H. Liu, S.Y. Lu, S.J. Bao, M. Xu, Assembling hollow cobalt sulfide nanocages array on graphene-like manganese dioxide nanosheets for superior electrochemical capacitors, ACS Appl. Mater. Interfaces 9 (2017) 35040–35047, https://doi.org/10.1021/acsami.7b12069.

[20] A. Bello, O.O. Fashedemi, J.N. Lekitima, M. Fabiane, D. Dodoo-Arhin, K.I. Ozoemena, Y. Gogotsi, A.T. Charlie Johnson, N. Manyala, High-performance symmetric electrochemical capacitor based on graphene foam and nanostructured manganese oxide, AIP Adv. 3 (2013), https://doi.org/10.1063/1.4819270.

[21] A. Elmouwahidi, J. Castelo-Quibén, J.F. Vivo-Vilches, A.F. Pérez-Cadenas, F.J. Maldonado-Hódar, F. Carrasco-Marín, Activated carbons from agricultural waste solvothermally doped with sulphur as electrodes for supercapacitors, Chem. Eng. J. 334 (2018) 1835–1841, https://doi.org/10.1016/j.cej.2017.11.141.

[22] J. Zhao, G. Wang, K. Cheng, K. Ye, K. Zhu, J. Yan, D. Cao, H.E. Wang, Growing NiS2 nanosheets on porous carbon microtubes for hybrid sodium-ion capacitors, J. Power Sources 451 (2020), https://doi.org/10.1016/j.jpowsour.2020.227737.

[23] J. Zhao, Y. Li, G. Wang, T. Wei, Z. Liu, K. Cheng, K. Ye, K. Zhu, D. Cao, Z. Fan, Enabling high-volumetric-energy-density supercapacitors: designing open, low-tortuosity heteroatom-doped porous carbon-tube bundle electrodes, J. Mater. Chem. 5 (2017) 23085–23093, https://doi.org/10.1039/c7ta07010a.

[24] C. Jing, X. Song, K. Li, Y. Zhang, X. Liu, B. Dong, F. Dong, S. Zhao, H. Yao, Y. Zhang, Optimizing the rate capability of nickel cobalt phosphide nanowires on graphene oxide by the outer/inter-component synergistic effects, J. Mater. Chem. 8 (2020) 1697–1708, https://doi.org/10.1039/c9ta12192g.

[25] T. Lin, Y. Tang, Y. Wang, H. Bi, Z. Liu, F. Huang, X. Xie, M. Jiang, Scotch-tape-like exfoliation of graphite assisted with elemental sulfur and graphene-sulfur composites for high-performance lithium-sulfur batteries, Energy Environ. Sci. 6 (2013) 1283–1290, https://doi.org/10.1039/c3ee24324a.

[26] M. Chen, Q. Lu, S. Jiang, C. Huang, X. Wang, B. Wu, K. Xiang, Y. Wu, MnO2

nanosheets grown on the internal/external surface of N-doped hollow porous carbon nanospheres as the sulfur host of advanced lithium-sulfur batteries, Chem. Eng. J. 335 (2018) 831–842, https://doi.org/10.1016/j.cej.2017.11.039.
[27] X. Zhao, H. Wang, G. Zhai, G. Wang, Facile assembly of 3D porous reduced graphene oxide/ultrathin MnO 2 nanosheets-S aerogels as efficient polysulfide adsorption sites for high-performance lithium–sulfur batteries, Chem. Eur J. 23 (2017) 7037–7045, https://doi.org/10.1002/chem.201604828.
[28] Z. Li, Y. Huang, L. Yuan, Z. Hao, Y. Huang, Status and prospects in sulfur-carbon composites as cathode materials for rechargeable lithium-sulfur batteries, Carbon 92 (2015) 41–63, https://doi.org/10.1016/j.carbon.2015.03.008.
[29] Q. Pang, D. Kundu, M. Cuisinier, L.F. Nazar, Surface-enhanced redox chemistry of polysulphides on a metallic and polar host for lithium-sulphur batteries, Nat. Commun. 5 (2014) 3–10, https://doi.org/10.1038/ncomms5759.
[30] C. Jing, X. Guo, L. Xia, Y. Chen, X. Wang, X. Liu, B. Dong, F. Dong, S. Li, Y. Zhang, Morphologically confined hybridization of tiny CoNi2S4 nanosheets into S, P co-doped graphene leading to enhanced pseudocapacitance and rate capability, Chem. Eng. J. 379 (2020) 122305, https://doi.org/10.1016/j.cej.2019.122305.
[31] X. Liang, C. Hart, Q. Pang, A. Garsuch, T. Weiss, L.F. Nazar, A highly efficient polysulfide mediator for lithium-sulfur batteries, Nat. Commun. 6 (2015) 1–8, https://doi.org/10.1038/ncomms6682.
[32] R.B. Pujari, A.C. Lokhande, A.A. Yadav, J.H. Kim, C.D. Lokhande, Synthesis of MnS microfibers for high performance flexible supercapacitors, Mater. Des. 108 (2016) 510–517, https://doi.org/10.1016/j.matdes.2016.07.038.
[33] Z. Li, J. Wang, S. Liu, X. Liu, S. Yang, Synthesis of hydrothermally reduced graphene/MnO2 composites and their electrochemical properties as supercapacitors, J. Power Sources 196 (2011) 8160–8165, https://doi.org/10.1016/j.jpowsour.2011.05.036.
[34] P. Simon, Y. Gogotsi, Materials for Electrochemical Capacitors, Materials for Sustainable Energy: A Collection of Peer-Reviewed Research and Review Articles from, Nature Publishing Group, 2010, pp. 138–147, https://doi.org/10.1142/9789814317665_0021.
[35] O. Sadak, W. Wang, J. Guan, A.K. Sundramoorthy, S. Gunasekaran, MnO2 nanoflowers deposited on graphene paper as electrode materials for supercapacitors, ACS Appl. Nano Mater. 2 (2019) 4386–4394, https://doi.org/10.1021/acsanm.9b00797.
[36] T. Chen, Y. Tang, Y. Qiao, Z. Liu, W. Guo, J. Song, S. Mu, S. Yu, Y. Zhao, F. Gao, All-solid-state high performance asymmetric supercapacitors based on novel MnS nanocrystal and activated carbon materials, Sci. Rep. 6 (2016) 1–9, https://doi.org/10.1038/srep23289.
[37] F. Ochai-Ejeh, M.J. Madito, K. Makgopa, M.N. Rantho, O. Olaniyan, N. Manyala, Electrochemical performance of hybrid supercapacitor device based on birnessite-type manganese oxide decorated on uncapped carbon nanotubes and porous activated carbon nanostructures, Electrochim. Acta 289 (2018) 363–375, https://doi.org/10.1016/j.electacta.2018.09.032.
[38] J. Yang, S. Gunasekaran, Electrochemically reduced graphene oxide sheets for use in high performance supercapacitors, Carbon 51 (2013) 36–44, https://doi.org/10.1016/j.carbon.2012.08.003.
[39] S. Kannappan, K. Kaliyappan, R.K. Manian, A.S. Pandian, H. Yang, Y.S. Lee, J.-H. Jang, W. Lu, Graphene Based Supercapacitors with Improved Specific Capacitance and Fast Charging Time at High Current Density, 2013. http://arxiv.org/abs/1311.1548.
[40] D.J. Tarimo, K.O. Oyedotun, A.A. Mirghni, ScienceDirect Sulphur-reduced graphene oxide composite with improved electrochemical performance for supercapacitor applications, Int. J. Hydrogen Energy (2020), https://doi.org/10.1016/j.ijhydene.2020.03.059.
[41] N.F. Sylla, N.M. Ndiaye, B.D. Ngom, D. Momodu, M.J. Madito, B.K. Mutuma, N. Manyala, Effect of porosity enhancing agents on the electrochemical performance of high-energy ultracapacitor electrodes derived from peanut shell waste, Sci. Rep. 9 (2019) 1–15, https://doi.org/10.1038/s41598-019-50189-x.
[42] H. Wang, Y. Yang, Y. Liang, J.T. Robinson, Y. Li, A. Jackson, Y. Cui, H. Dai, Graphene-wrapped sulfur particles as a rechargeable lithium-sulfur battery cathode material with high capacity and cycling stability, Nano Lett. 11 (2011) 2644–2647, https://doi.org/10.1021/nl200658a.
[43] X. Wang, T. Gao, F. Han, Z. Ma, Z. Zhang, J. Li, C. Wang, Stabilizing high sulfur loading Li–S batteries by chemisorption of polysulfide on three-dimensional current collector, Nanomater. Energy 30 (2016) 700–708, https://doi.org/10.1016/j.nanoen.2016.10.049.
[44] Y. Guo, J. Zhao, S. Yang, K. Yu, Z. Wang, H. Zhang, Preparation and characterization of monoclinic sulfur nanoparticles by water-in-oil microemulsions technique, Powder Technol. 162 (2006) 83–86, https://doi.org/10.1016/j.powtec.2005.12.012.
[45] J. Luo, H. Zhu, H. Fan, J. Liang, H. Shi, G. Rao, Synthesis of Single-Crystal Tetragonal Alpha-MnO 2 Nanotubes, vol. 3, 1996, p. 2005.
[46] T.M. Masikhwa, F. Barzegar, J.K. Dangbegnon, A. Bello, M.J. Madito, D. Momodu, N. Manyala, Asymmetric supercapacitor based on VS2 nanosheets and activated carbon materials, RSC Adv. 6 (2016) 38990–39000, https://doi.org/10.1039/c5ra27155j.
[47] Z. Fan, J. Yan, T. Wei, L. Zhi, G. Ning, T. Li, F. Wei, Asymmetric supercapacitors based on graphene/MnO2 and activated carbon nanofiber electrodes with high power and energy density, Adv. Funct. Mater. 21 (2011) 2366–2375, https://doi.org/10.1002/adfm.201100058.
[48] H. Wang, Q. Fu, C. Pan, Green mass synthesis of graphene oxide and its MnO2 composite for high performance supercapacitor, Electrochim. Acta 312 (2019) 11–21, https://doi.org/10.1016/j.electacta.2019.04.178.
[49] S. Jadhav, R.S. Kalubarme, C. Terashima, B.B. Kale, V. Godbole, A. Fujishima, S.W. Gosavi, Manganese dioxide/reduced graphene oxide composite an electrode material for high-performance solid state supercapacitor, Electrochim. Acta 299 (2019) 34–44, https://doi.org/10.1016/j.electacta.2018.12.182.
[50] V. Khomenko, E. Raymundo-Piñero, F. Béguin, Optimisation of an asymmetric manganese oxide/activated carbon capacitor working at 2 v in aqueous medium, J. Power Sources 153 (2006) 183–190, https://doi.org/10.1016/j.jpowsour.2005.03.210.

4.3.2: Concluding remarks

RGO-S and RGO-S/MnO_2 composites were effectively produced whereby RGO-S/100 mg MnO_2 presented better performance compared to pristine and the rest of the composites. The optimized RGO-S/100 mg MnO_2 composite presented a specific capacitance of 180. 4 F g^{-1} compared to 75.2, 63.7, and 169.5 F g^{-1} for RGO-S (pristine) sample, RGO-S/50 mg MnO_2 and RGO-S/150 mg MnO_2 composite at 1 A g^{-1} in 2.5 M KNO_3 electrolyte evaluated in three-electrode configurations. This particular mass loading has contributed to the excellent performance of RGO-S/100 mg MnO_2 composite which is understood to be due to the synergy effect between RGO-S and MnO_2. A high specific energy of 71.74 Wh kg^{-1} and specific power of 850 W kg^{-1} was recorded at 1 A g^{-1} for the device fabricated through utilizing RGO-S/MnO_2//AC-PS. Furthermore, the device displayed a remarkable performance after sustaining a specific energy of 55.30 Wh kg^{-1} at a high specific current of 5 A g^{-1}. The capacitance retention of 94.5 % and columbic efficiency of 99.6 % over 10, 000 cycles at 5 A g^{-1} was retained. An efficiency of 70.5 % was maintained by the device for a voltage holding of up to 90 h. A remarkable self-discharge of about 1.45 V was displayed within the first 10 h and 1.00 V after 72 h from the initial potential of 1.7 V. This reveals a great potential of this material for supercapacitors applications due to an outstanding stability of the device.

4.4: Enhanced electrochemical performance of supercapattery derived from sulphur-reduced graphene oxide/cobalt oxide composite and activated carbon from peanut shells

4.4.1: Summary of the study

In this study, RGO-S pristine sample was prepared by Hummers method followed by freeze drying process. It was followed by a separate preparation of Co_3O_4 through precipitation, then followed by annealing in air at 800 ^oC (5 ^oC/min) for 2 h to remove the OH group and any feasible contaminations. Thereafter, RGO-S/Co_3O_4 composite with various mass loading of Co_3O_4 was obtained through hydrothermal method. Graphene oxide is known for good conductivity; however, it suffers from low specific capacity/capacitance due to formation of large number of radical generations resulted from the synthesis method [206][68]. On the other side, Co_3O_4 has high redox behavior which contributes to high specific capacity/capacitance, but they are encountered with low ionic/electrical conductivity which cause dissolution and aggregation, hence result into rapid reduction of specific energy [207][208]. The challenge can be solved by making a composite of Co_3O_4 and an improved graphene oxide which is anticipated to have high conductivity in order to form a hybrid material that integrates both the advantage and disadvantage of the two materials [34]. The electrochemical performance of the combined effects of the two materials can be identified by the exact amount for each material in the formed composite. The optimized 200 mg of Co_3O_4 was added into RGO-S to make a composite. The morphological, elemental composition/mapping, structural, functional group and specific surface area/pore size distribution investigation were done using SEM, TEM, EDS, Raman spectroscopy, XRD, FTIR, XPS and BET techniques. The electrochemical evaluation of the material was conducted using 1 M KOH electrolyte. A detailed description of the synthesis procedures, characterization and electrochemical performance is stipulated in the article in press below.

ARTICLE IN PRESS

INTERNATIONAL JOURNAL OF HYDROGEN ENERGY XXX (XXXX) XXX

Available online at www.sciencedirect.com

ScienceDirect

journal homepage: www.elsevier.com/locate/he

Enhanced electrochemical performance of supercapattery derived from sulphur-reduced graphene oxide/cobalt oxide composite and activated carbon from peanut shells

*Delvina Japhet Tarimo, Kabir O. Oyedotun, Abdulmajid A. Mirghni, Bridget Mutuma, Ndeye Fatou Sylla, Phathutshedzo Murovhi, Ncholu Manyala**

Department of Physics, Institute of Applied Materials, SARChI Chair in Carbon Technology and Materials, University of Pretoria, Pretoria, 0028, South Africa

HIGHLIGHTS

- RGO-S and RGO-S/Co_3O_4 composites were successfully synthesized.
- Electrochemical performance of RGO-S has been improved by introduction of Co_3O_4.
- The RGO-S/Co_3O_4 was adopted as a positive electrode in a supercapattery device.
- The fabricated device demonstrate great potential for supercapacitors applications.

GRAPHICAL ABSTRACT

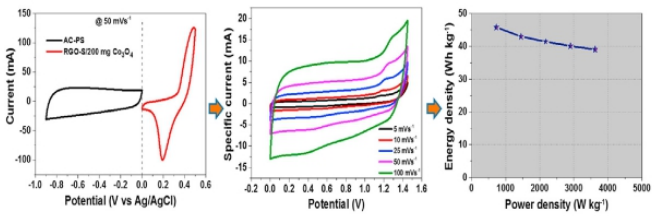

ARTICLE INFO

Article history:
Received 9 June 2020
Received in revised form
14 September 2020
Accepted 18 September 2020
Available online xxx

Keywords:
Supercapattery
Sulphur
Graphene oxide
Cobalt oxide composites

ABSTRACT

Sulphur-reduced graphene oxide/cobalt oxide composites (RGO-S/Co_3O_4) were successfully synthesized by varying mass loading of Co_3O_4 through a simple hydrothermal method. Structural, morphological, chemical compositional and surface area/pore-size distribution analysis of the materials were obtained by using XRD, Raman spectroscopy, SEM, TEM, EDX, FTIR, XPS and BET techniques, which reveal an effective synthesis of the RGO-S/Co_3O_4 composites. Electrochemical performance of the materials was evaluated using a three- and two-electrode system in 1 M KOH electrolyte. An optimized RGO-S/200 mg Co_3O_4 composite displayed the highest specific capacity of 171.8 mA h g^{-1} and superior cycling stability of 99.7% for over 5000 cycles at 1 and 5 A g^{-1}, respectively, in a three-electrode system. A fabricated supercapattery device utilizing RGO-S/200 mg Co_3O_4 (positive electrode) and activated carbon from peanut shells (AC-PS) (negative electrode), revealed a high specific energy and power of 45.8 W h kg^{-1} and 725 W kg^{-1}, respectively, at 1 A g^{-1}. The device retained 83.4% of its initial capacitance for over 10, 000 cycles with a columbic

* *Corresponding author.*
E-mail address: ncholu.manyala@up.ac.za (N. Manyala).
https://doi.org/10.1016/j.ijhydene.2020.09.142

Please cite this article as: Tarimo DJ et al., Enhanced electrochemical performance of supercapattery derived from sulphur-reduced graphene oxide/cobalt oxide composite and activated carbon from peanut shells, International Journal of Hydrogen Energy, https://doi.org/10.1016/j.ijhydene.2020.09.142

Cycling stability
Energy storage devices

efficiency of 99.5%. Also, a capacitance retention of 71.6% was preserved after being subjected to a voltage holding test of over 150 h at its maximum potential of 1.45 V.

Introduction

The increase in population and advancement in technology has resulted in the high demand for power consumption. Currently, the well-known deficiency of fossil fuels and increasing environmental distresses are pushing researchers to adventure on sustainable, clean and readily accessible technology to supply and store energy [1,2]. This increases an interest to develop and design an efficient energy storage device. Batteries, supercapacitors and other energy conversions systems like hydrogen cells, fuel cells have been categorized as energy storage devices that can meet up the demand for technological advancements [3–5]. Supercapacitors have gained a considerable attention due to their high specific power, low cost, fast charge-discharge rate, and excellent cycling stability compared to batteries and conventional capacitors [6–8]. However, the practical application is limited by low specific energy compared to rechargeable batteries. This drives scientists to develop and design novel electrode materials which possess high electrochemical performance so as to increase supercapacitors' specific energy [9–11].

Owing to different charge storage mechanism, pseudocapacitors (PCs) and electrical double-layer capacitors (EDLCs) demonstrate a distinguished benefits for supercapacitors. PCs store charges through redox reaction which has high specific capacitance, but its application is limited by poor charge transfer ability and shorter cycle life [12–14]. On the other hand, EDLCs store charges electrostatically on the surface of the electrode under constant potential, but, have low specific capacitance [1,15]. Therefore, by working with only one of them, it is difficult to manufacture a capacitor containing high energy and power densities. This challenge can be resolved by combining the advantages of both PCs and EDLCs through designing a hybrid electrode material with high capacitance and fast charge/discharge ability [9,16,17]. On the other hand, one can also form a hybrid device by combining a hybrid and an EDLC material working as a positive and negative electrode, respectively. The combination of these two materials with different charge-storage mechanisms and operating potentials could tailor the overall operating potential of the hybrid capacitor and hence improve its energy density [9,18–21]. Consequently, this type of energy storage device will be named as a hybrid or supercapattery device, depending on whether the final device shows mostly combination of pseudocapacitive and battery-type or pseudocapacitive behaviour, respectively. The charge to voltage ratio remains the same throughout the cyclic voltammetry and charge/discharge curve for a capacitive material. However, for metals oxides and hydroxides such as Fe_2O_3, $Ni(OH)_2$, $MnCo_2O_4$, NiO, Co_3O_4 and $Co(OH)_2$, the ratio does not follow the former trend due the formation of redox peaks and thus are classified as battery-type materials instead of pseudocapacitive materials [5,22,23].

On the other hand, due to low specific energy, supercapacitors are still struggling to meet the demand for commercial applications. Thus, the awareness of combining features of supercapacitor and battery-type material in a single device where the end product is pseudocapacitive devise called supercapattery, paved the approach for improvement in electrochemical energy storage devices [24]. This combination produces a supercapattery device with high specific energy and power, and satisfactory cycle life than the traditional carbon-based supercapacitors [25]. Therefore, supercapattery developed as an outstanding resolution intended for an electrochemical energy storage configuration which possesses the distinguishing features of advanced specific energy and power of batteries and supercapacitor, respectively. As a result, it decreases the specific energy gap between battery and supercapacitor [26,27]. Presently, most researchers are keen to improve the performance of supercapattery by merging together supercapacitors and batteries through designing a novel electrode materials with enhanced performance.

Mostly used electrode materials for supercapacitor applications include metal hydroxides, conducting polymers, metal oxides and carbon-based materials [13,28–30]. Recently, graphene and its derivatives namely, graphene oxide (GO) and reduced graphene oxide (RGO) have been used as electrode material for supercapacitor applications due to: 1) The properties of graphene can be enhanced by the addition of functional groups through utilizing the active sites contributed by the structural defects of graphene, 2) the electron transfer rate which can be promoted by electrical conductivity on the surface of graphene and 3) the agglomeration in graphene can be prevented by the flexibility of graphene nanosheets which offers sufficient space for the accommodation of different nanomaterials [4,31]. Despite these properties, the synthesis of graphene and its derivatives involve mostly chemical methods which consist of oxidation/reduction processes [32]. These methods affect the chemical structure of graphene due to the large number of radicals generated which in turn lower the electrochemical performance of the chemically modified graphene [21,33–36]. To overcome this drawback, heteroatom dopants such as sulphur can be incorporated into graphene matrix in order to increase the electrochemical performance of chemically modified graphene. Incorporation of S as a heteroatom by interstitials or substitutions create defects in graphene as a consequence of variations in graphene properties. It is known that C and S have small electronegativity variation of 0.03 (carbon (2.55) and S (2.58)), thus increase in redox-active sites and chemical reactivity of graphene.

Please cite this article as: Tarimo DJ et al., Enhanced electrochemical performance of supercapattery derived from sulphur-reduced graphene oxide/cobalt oxide composite and activated carbon from peanut shells, International Journal of Hydrogen Energy, https://doi.org/10.1016/j.ijhydene.2020.09.142

Therefore, incorporation of S into graphene materials has been known to enhance wettability, improve surface properties and decrease charge transfer resistance [21,32,37–40].

Additionally, the electrochemical performance of reduced graphene oxide can be enhanced via the generation of metal oxide/S-reduced graphene composites. Typically, due to multiple oxidation states, transition metal oxides like iron (Fe), manganese (Mn), nickel (Ni), and cobalt (Co) oxides display excellent chemical and physical properties that enrich the electrochemical properties of supercapacitors [8,29,35,41]. Also, at higher oxidation states of transition metals, transition metal oxides produce more powerful alkaline corrosion protection compared to other materials [31,42]. Specifically, cobalt oxide (Co_3O_4) has been examined as a promising electrode material due to its high redox reactivity, easily tunable surface properties, simple preparation method, higher stability and cost effectiveness [8,34]. Co_3O_4 has Co^{3+} and Co^{2+} oxidation states positioned at octahedral and interstitial tetrahedral sites formed by oxygen ions in a closed packed face centered cubic structure, respectively. Thus offers high surface to volume ratios and faster charge transfer kinetics [23,43]. The p-type semiconductor and cubic spinel structure found in Co_3O_4 displays enhanced electro-active sites which makes it suitable for different applications such as electrochemical capacitors, sensors, Li-ion batteries and solar selective absorbers [12,42,44]. Moreover, Co_3O_4 has high redox behaviour which contributes to high specific capacity/capacitance, but on the other hand, they are faced with low ionic/electrical conductivity. Also, during electrochemical reactions, they suffer from dissolution and aggregation resulting in a decrease in the number of active sites which hold back their capacitive behaviour especially during repeated cycling and at high scan rate, hence rapid reduction of specific energy at high specific power [18,29,45,46].

The shortcomings can be resolved by combining Co_3O_4 and an improved graphene oxide which is anticipated to have high conductivity. This shortens the diffusion length for charge carriers and produces an electrode material with better electrochemical properties [29,33,47]. The bond formed by the interaction between graphene oxide and Co_3O_4 support in decreasing particle aggregation and ultimately improving the cyclic stability of the material. Furthermore, it can ease diffusion rate and ionic mobility, and hence improve the overall electrochemical properties. Therefore, electrochemical performance is expected to improve via the combined effects of the two materials in a composite formation by identifying the exact amount for each material in the composite [9]. Moreover, previous reports have indicated an improvement in the capacitive performance of the composites of metal oxides than individual oxide materials [48,49]. Additionally, most of the studies have reported on graphene/reduced graphene oxide with Co_3O_4 composite by mixing the whole precursor with other constituents (impurity) whereby it is difficult to figure out the exact amount of pure individuals to be mixed to form a composite [3,8,14,45,46,50].

In this study, a simple hydrothermal method with easily controllable parameters like concentration of the reagent, pH, temperature and time was applied to synthesize sulphur-reduced graphene oxide/cobalt oxide composites (RGO-S/Co_3O_4) by varying the mass loading of Co_3O_4. Each material was synthesized separately in order to ensure the purity of each sample and the exact amount of each component used to form a composite. This method proved to improve the charge storage capacity of the composite material. To the best of our knowledge, the use of sulphur-reduced graphene oxide/cobalt oxide (RGO-S/Co_3O_4) composite as electrode material for supercapattery device and produced by a high degree of synthetic control during synthesis has been rarely reported.

The successful synthesis of RGO-S/Co_3O_4 composite was confirmed by different characterization techniques. An optimized RGO-S/200 mg Co_3O_4 composite in a half-cell using 1 M KOH electrolyte displayed the highest specific capacity of 171.8 mA h g^{-1} and superior stability of 99.7% for over 5000 cycles at 1 and 5 A g^{-1}, respectively. The fabricated supercapattery device demonstrated high specific energy of 45.8 W h kg^{-1} with a corresponding specific power of 725 W kg^{-1} at 1 A g^{-1}. This supercapattery device also demonstrated excellent stability from both cyclic and voltage holding stability tests. The synergetic effect of the two materials was observed to improve the specific capacity, cyclic stability and rate capability which eventually increased the electrochemical performance of the supercapattery device.

Experimental

Synthesis of sulphur-reduced graphene oxide (RGO-S)

Sulphur-reduced graphene oxide was synthesized using modified Hummer's method as explained in our previous work [51]. Briefly, a polysulphide solution was formed by mixing 1 g of sulphur and 3 g of sodium sulphide (Na_2S) in 100 mL of deionized (DI) water and sonicated for homogeneity. Then, 2 mL of hydrochloric acid (HCl) was added into a solution formed by dissolving 50 mg of L-ascorbic acid in 12 g of DI water. Thereafter, 3 g of RGO, the polysulphide solution and L-ascorbic acid solution were combined and sonicated for 2 h for homogeneity. The mixture was stirred at 40 °C for 1 h and allowed to settle down for separation. The sample was washed several times with DI water, centrifuged three times at 10,000 rpm for 10 min and later freeze-dried for 24 h.

Synthesis of cobalt oxide (Co_3O_4)

Precipitation method was acquired to produce Co_3O_4 sample. 8 g of $CoNO_3$ was added into 400 mL of DI water and stirred for 15 min. Thereafter, 56 mL of 1 M NaOH was added dropwise into the mixture which changed the color from pink to dark greenish color. $CoNO_3$ precursor was used as a source of cobalt while 1 M NaOH was used for polymerization and maintain the pH of 10 in the mixture while stirring for 2 h. The obtained mixture was decanted and washed several times with DI water, centrifuged at 10,000 rev/min for 10 min followed by drying in the oven at 60 °C for 12 h. The dried sample was later annealed in air for 2 h at 800 °C (5 °C/min) to remove the OH group and any possible impurities. Eqs (1) and (2) below shows a complete reaction for obtaining Co_3O_4.

Please cite this article as: Tarimo DJ et al., Enhanced electrochemical performance of supercapattery derived from sulphur-reduced graphene oxide/cobalt oxide composite and activated carbon from peanut shells, International Journal of Hydrogen Energy, https://doi.org/10.1016/j.ijhydene.2020.09.142

$$Co(NO_3)_{2(s)} + 2NaOH_{(l)} + H_2O_{(l)} \rightarrow Co(OH)_{2(s)} + 2NaNO_{3(aq)} + H_2O_{(l)} \quad (1)$$

$$3Co(OH)_{2(s)} \xrightarrow{annealed\ in\ air} Co_3O_{4(s)} + 2H_2O_{(g)} + H_{2(g)} \quad (2)$$

Synthesis of RGO-S/Co_3O_4 composite sample

The RGO-S/Co_3O_4 composite sample was prepared by adding 1 g of RGO-S and 100 mg of Co_3O_4 into 100 mL of DI water and sonicated for 1 h for homogeneity. Thereafter, the mixture was transferred into a Teflon-lined autoclave and heated in the oven at 150 °C for 1 h. The procedure was repeated by varying the mass of Co_3O_4 between 200 mg and 300 mg. The obtained mixture was allowed to settle down for easy separation. Later, it was washed several times with DI water and dried in the oven at 60 °C for 12 h.

Synthesis of activated carbon from peanut shell waste (AC-PS)

Activated carbon used in this study was produced from peanut shell waste as explained in our previous study [52]. In summary, two steps synthesis procedure was used to synthesize the material from peanut shell waste. Initially, the raw material from peanut shell waste was pyrolyzed using argon gas at 600 °C for 2 h. Then, the raw material (peanut shell waste) and activating agent (potassium hydroxide - KOH) were mixed in a mass ratio of 1:4. Thereafter, the mixture was activated at 850 °C for 1 h and the recovered sample was named as AC-PS.

Characterization

The micrographs of the pristine and composite material were obtained by using Zeiss Ultra Plus 55 field emission scanning electron microscope (FE-SEM; Akishima-shi, Japan) operated at 2.0 kV, equipped with an energy dispersive X-ray (EDX) and JEOL-2100 F transmission electron microscope (HRTEM FEI Tecnai-F30; Akishima-shi, Japan) operated at 200 kV. The phase structure of the as-synthesized materials was studied by X-ray diffraction (D8 ADVANCED Bruker; Gerulhe, Germany) with a reflection angle 2θ values ranging between 7 and 90° in a step size of 0.03 at 40 mA and 40 kV using Cu radiation source. A WITec Confocal Raman Microscope (WITec alpha 300 RAS+, Germany), Laser wavelength 532 nm, laser power 4 mW and spectral acquisition time 120-s was used for Raman analysis to determine the degree of defects in the material. Fourier transform-infrared spectroscopy (FT-IR) evaluation was obtained by a Varian FT-IR spectroscopy in a wavelength range 500–4000 cm^{-1}. An X-ray photoelectron spectroscopy (XPS) analyser (Versa Probe 5000 spectrometer initiated with a 100 μm monochromatic Al-Kα exciting source) was utilized to study the electronic states of the surface elements present within the composite sample. The Nitrogen adsorption and desorption isotherms were measured by NOVA Touch LX^6 version equipped with a quanta-chrome Touch-Win software analyser. All samples were degassed at 80 °C for 10 h under high vacuum environment. The specific surface area was evaluated using Brunauer-Emmett-Teller (BET) method from the absorption/adsorption isotherms in the relative pressure range (P/Po) of 0.01–0.2 and pore size distribution was calculated by using DFT method.

Electrochemical characterization

The EC-Lab V1.40 software in a BioLogic VMP300 potentiostat (Knoxville TN 37,930, USA), was used to evaluate the electrochemical measurements of the as-synthesize sample via three- and -two electrode systems. For three-electrode measurements, electrode was prepared by adding three drops of N-methyl-2-pyrrolidone (NMP) on a mixture containing 80% of the working material, and 10% each of carbon acetylene black (CB - conducting agent) and polyvinylidene fluoride (PVDF - binder) to make a slurry. The nickel foam 1 × 1 cm used as a current collector was coated with the slurry and then dried in the oven at 60 °C for 12 h. The mass of a single electrode was estimated as 2.4 mg/cm^2. The measurements were carried out by using Ag/AgCl as a reference electrode, material as a working electrode and glassy carbon as the counter electrode in 1 M KOH electrolyte. For three-electrode evaluation, the cyclic voltammetry (CV) and galvanostatic charge/discharge (GCD) measurements were done at various scan rates (5–100 mV s^{-1}) and specific currents (1–5 A g^{-1}), respectively within a working potential range 0.0 V–0.5 V and 0 V to −0.9 V for positive and negative electrodes, respectively. The electrochemical impedance spectroscopy (EIS) was assessed in an open circuit potential at a frequency range 10 mHz–100 kHz. The specific capacity (Q_s - mAh g^{-1}) and columbic efficiency (C_E - %) of a single positive electrode was evaluated using Eqs (3) and (4) from the GCD profiles, respectively [53,54]:

$$Q_s = \frac{\Delta t \times I_d}{3.6} \quad (3)$$

$$C_E = \frac{t_D}{t_C} \times 100\,\% \quad (4)$$

where; I_d stands for applied specific currents (A g^{-1}), Δt represents the discharge time (s), t_D and t_C - discharge and charge time with the same current, respectively.

For two-electrode evaluation, the RGO-S/200 mg Co_3O_4 composite was used as a positive electrode and activated carbon from peanut shells (AC-PS) which shows ELDC behaviour as a negative electrode in 1 M KOH electrolyte. The mass on each electrode was estimated via the charge balance equation, as shown below [23,53,54]:

$$Q_+ = Q_- \Rightarrow 3.6\, m_+ \times Q_{s+} = m_- \times \Delta V_- \times C_{s-} \Rightarrow \frac{m_-}{m_+} = \frac{3.6\, Q_{s+}}{\Delta V_- \times C_{s-}} \quad (5)$$

where;Q_{s+} - specific capacity for the positive electrode, C_{s-} specific capacitance for the negative electrode, ΔV_- - potential window for the negative electrode, Q_+ and Q_- are charge for positive and negative electrode while m_+ and m_- stands for masses (mg) for the positive and negative electrodes, respectively.

Please cite this article as: Tarimo DJ et al., Enhanced electrochemical performance of supercapattery derived from sulphur-reduced graphene oxide/cobalt oxide composite and activated carbon from peanut shells, International Journal of Hydrogen Energy, https://doi.org/10.1016/j.ijhydene.2020.09.142

The potential window of 1.45 V was reached by the fabricated supercapattery device. The following expressions were applied to evaluate the specific capacitance (C_s), specific energy (E_d) and specific power (P_d) of the device [20,50]:

$$C_s = \frac{\Delta t \times I_d}{\Delta V}\left[F\ g^{-1}\right] \quad (6)$$

$$E_d = \frac{1}{2}C_s\Delta V^2 = \frac{C_s \times \Delta V^2 \times 1000}{2 \times 3600} = \frac{C_s \times \Delta V^2}{7.2}\left[Wh\ kg^{-1}\right] \quad (7)$$

$$P_d = \frac{E_d}{\Delta t} \times 3600\left[W\ kg^{-1}\right] \quad (8)$$

where ΔV - operating potential (V), I_d - applied specific current (A g^{-1}), C_s- specific capacitance,Δt- discharge time (s), E_d - energy density and P_d - power density.

Results and discussion

Fig. 1 presents SEM and TEM micrographs acquired for the pristine and composite samples. Fig. 1 ((a, b), (d, e) and (g, h)) display the morphology of RGO-S, Co_3O_4 and RGO-S/200 mg Co_3O_4 composite (as an example of other composites which show similar morphology) in low and high magnification, respectively. The micrographs revealed that RGO-S comprises of nanorods/fibres and nanosheets like morphology (Fig. 1 (a, b)). Fig. 1 (d and e) displays a clear different morphology of Co_3O_4 with agglomerated nanograin-like structures, while RGO-S/200 mg Co_3O_4 (Fig. 1 (g and h)) show a combination of RGO-S and Co_3O_4 morphology. Fig. 1 (c, f and i) are TEM images of RGO-S, Co_3O_4 and RGO-S/200 mg Co_3O_4 composite, respectively at high magnification confirming the observations from SEM. It was also observed that the morphology of other RGO-S/Co_3O_4 composites remained the same regardless of the variation of mass loading 100 and 300 mg of Co_3O_4. However, with the introduction of Co_3O_4 into the active matrix of RGO-S, Co_3O_4 nanograins are seen to effectively attach themselves to the RGO-S nanorods/fibres and nanosheets, and formed a homogeneous and stable composite as shown in Fig. 1 (g and h). A uniform dispersion of the Co_3O_4 nanograins within the RGO-S nanorods/fibres and nanosheets is observed, which is vital for giving the essential surface required for effective electrochemical interactions. The uniform dispersion is contributed by the use of hydrothermal method which allows for an even distribution of Co_3O_4 in the RGO-S matrix, and hence the observed morphology.

As an example (Fig. 2), further EDX measurements on RGO-S/200 mg Co_3O_4 were performed to show the elemental mapping and percentage of elemental composition within the material. Fig. 2 (a, b, c and d) displays the elemental mapping distribution of C, O, S and Co, respectively within the RGO-S/200 mg Co_3O_4 composite. Fig. 2 (e) displays the percentage by

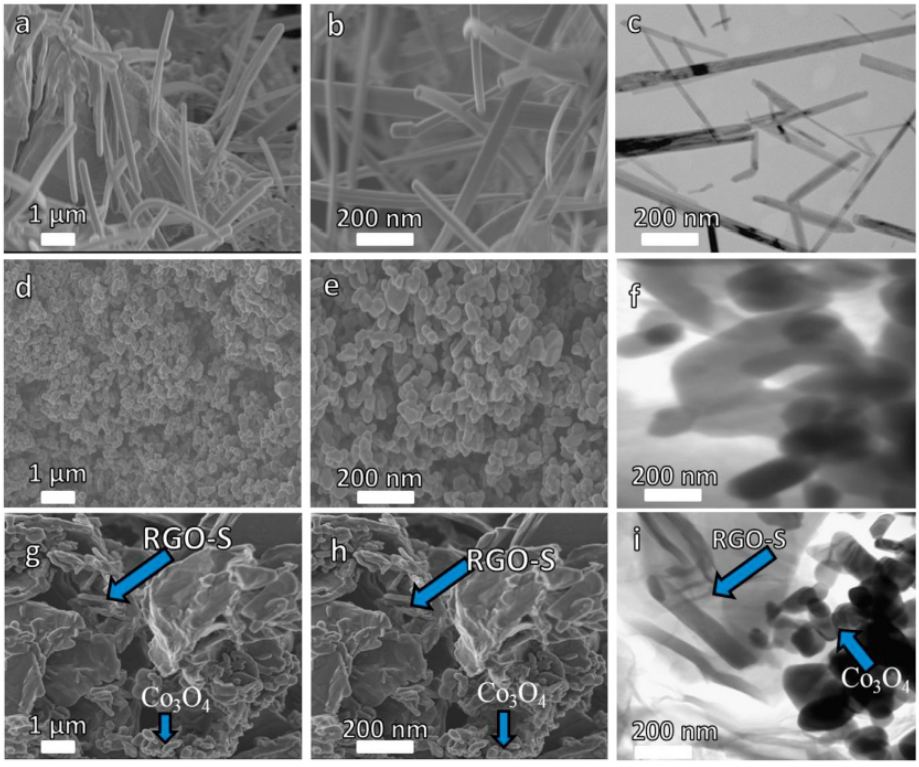

Fig. 1 – (a, b), (d, e) and (g, h) are SEM images for RGO-S, Co_3O_4 and RGO-S/200 mg Co_3O_4 at low and high magnifications, respectively. (c, f and i) are TEM images for RGO-S, Co_3O_4 and RGO-S/200 mg Co_3O_4, respectively.

Please cite this article as: Tarimo DJ et al., Enhanced electrochemical performance of supercapattery derived from sulphur-reduced graphene oxide/cobalt oxide composite and activated carbon from peanut shells, International Journal of Hydrogen Energy, https://doi.org/10.1016/j.ijhydene.2020.09.142

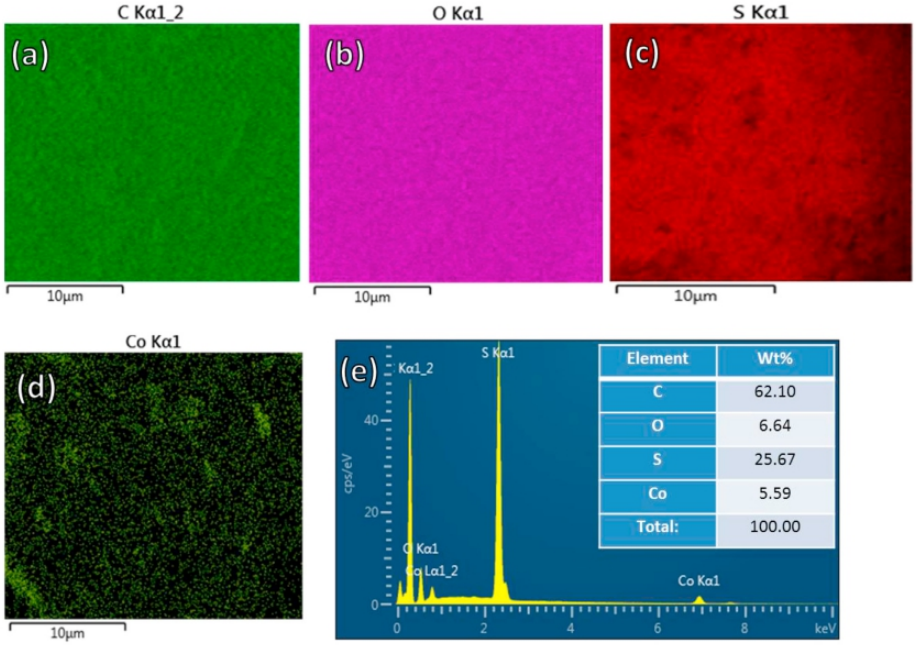

Fig. 2 – (a, b, c and d) indicates the elemental mapping for RGO-S/200 mg Co_3O_4 composite as example and (e) it's corresponding EDS showing the percentage composition of the element within the material.

weight of each element in the composite sample, whereby, 62.10, 6.64, 25.67 and 5.59 wt% was recorded for C, O, S and Co, respectively. Similar elemental distribution and composition were observed for RGO-S/100 mg Co_3O_4 and RGO-S/300 mg Co_3O_4 composites.

Rotational, vibrational and other low-frequency modes characterized by specific bonding in the materials were determined by Raman spectroscopy. Fig. 3 (a) displays the Raman spectra of the pristine sample (RGO-S) and all the composite samples (RGO-S/Co_3O_4 at various mass loading of Co_3O_4). The peaks observed at 1335 cm^{-1} and 1568 cm^{-1} correspond to D and G peaks of graphene, respectively, present in the pristine and the composites samples at different mass loading of Co_3O_4 [2]. The D peak indicates the existence of defects in the carbon matrix, while the G peak is a characteristic of sp^2 hybridized carbon in the graphene sheets. The I_d/I_g ratio signifies the level of defects in the material, which was estimated as 0.85 and 0.96 for RGO-S (pristine) and RGO-S/Co_3O_4 composites, respectively. This suggests a successful incorporation of Co_3O_4 within the RGO-S matrix and a good surface interaction of the two materials as confirmed by TEM morphology in Fig. 1 (i). The peak around 2674 cm^{-1} corresponds to 2D which developed from a second-order overtone due to a secondary inelastic scattering from a second phonon that distinguishes between monolayer and multilayer sheets of graphene within the material [3]. It was further observed that D, G and 2D band were able to maintain the same position for RGO-S and RGO-S/Co_3O_4 composites. However, the 2D intensity for the RGO-S/200 mg Co_3O_4 composite was noticed to have been reduced significantly as compared to the RGO-S and (100 and 300 mg) of Co_3O_4 composites revealing good interaction of Co_3O_4 nanograins with the RGO-S matrix because this band is very sensitive to the defects. It is also clear that D peak for this sample indicates more defective RGO-S where the intensity ratio of I_D to I_G is almost one as compared to the other samples. This is also the indication of a clear effect of good interaction of Co_3O_4 and RGO-S. The peaks around 486 and 653 cm^{-1} indicates E_g and $A1_g$ vibration modes of Co_3O_4, respectively [55]. These modes indicate coordination between Co and O atoms whereby cations and anions allocation on the spinel of Co_3O_4 is displayed as Co^{2+} $[Co_2^{3+}]$ O_4^{2-}. The cations in the brackets are octahedral and those outsides are coordinated with oxygen anions tetrahedrally [56]. These results show that Co_3O_4 was successfully incorporated into RGO-S matrix to form a composite material.

Fig. 3 (b) shows the phase structure analyzed by XRD displaying narrow and sharp peaks for the as-synthesized Co_3O_4, RGO-S, and RGO-S/Co_3O_4 composite with different mass loading of Co_3O_4 demonstrating high crystallinity of the material. The XRD spectrum at the bottom (black) is a clear indication of pure Co_3O_4 with the diffraction peaks around $2\theta = 18.9°$, 31.2°, 36.7°, 44.9°, 59.3° and 65.1° which corresponds to (111), (220), (311), (400), (511) and (440) planes, respectively. The XRD pattern of Co_3O_4 and its equivalent planes match well with the Joint Committee on Powder Diffraction Standards (JCPDS) card no. 42–1467 [12]. The observed diffraction peaks (red) around $2\theta = 11.4°$, 15.4°, 22.9°, 26.7°, 27.7°, 31.8°, 36.9° and 42.9° corresponding to (001), (113), (222), (002), (313), (044), (422) and (100) planes, respectively, suggest the existence of RGO-S in the material. The XRD spectra of RGO-S match well with the JCPDS card nos. 89–4307 and N34-0941 for RGO and S crystal structures, respectively [51,57]. The

Please cite this article as: Tarimo DJ et al., Enhanced electrochemical performance of supercapattery derived from sulphur-reduced graphene oxide/cobalt oxide composite and activated carbon from peanut shells, International Journal of Hydrogen Energy, https://doi.org/10.1016/j.ijhydene.2020.09.142

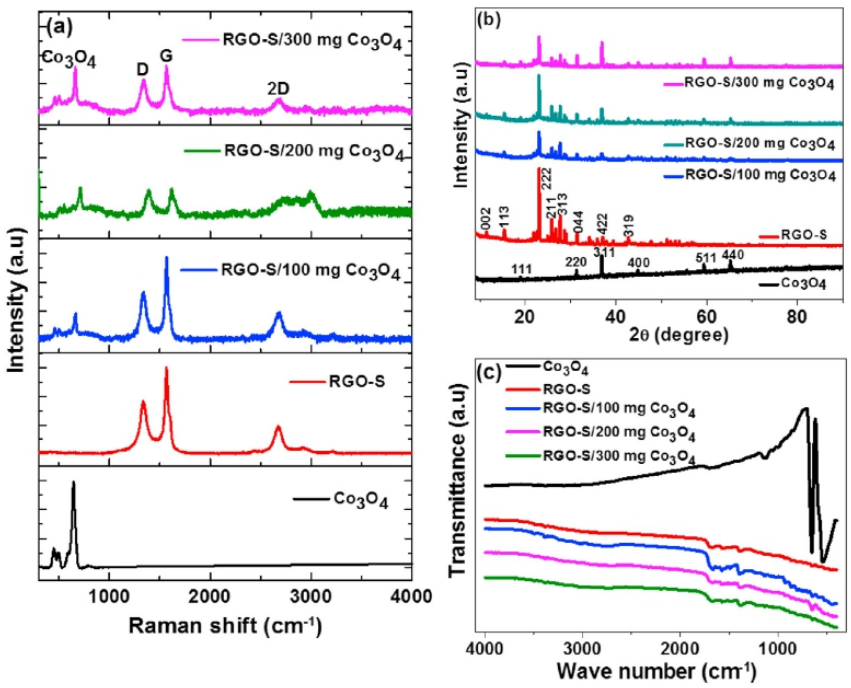

Fig. 3 – (a) Raman, (b) XRD and (c) FTIR spectrum for Co_3O_4, RGO-S, RGO-S/100 mg Co_3O_4, RGO-S/200 mg Co_3O_4 and RGO-S/300 mg Co_3O_4, respectively.

XRD patterns for RGO-S/100 mg Co_3O_4 (blue), RGO-S/200 mg Co_3O_4 (dark cyan) and RGO-S/300 mg Co_3O_4 (magenta) composites shows some sharp peaks arising from RGO-S and Co_3O_4 revealing the successful growth of Co_3O_4 on RGO-S as observed in SEM images in Fig. 1 (g and h). Furthermore, the analysis confirmed that the crystal structure of the RGO-S was maintained during the composites formation (RGO-S/Co_3O_4).

FTIR spectroscopy is a tool that provides a report concerning the phase composition of the material, behaviour regarding functional groups and how oxygen is attached to the metal ions. Fig. 3 (c) shows the FTIR spectra of the various samples as indicated in the figure, revealing surface functional groups of Co_3O_4, RGO-S, and RGO-S/Co_3O_4 composite materials. The –OH stretching vibration is ascribed to the absorption peak spotted at 3428 cm^{-1} presenting the hydroxyl group. The peak at 1396 cm^{-1} is linked to tertiary C–OH group while 1656 cm^{-1} is attributed to the O–H bending vibrations of absorbed water molecules. Stretching vibration of epoxy group (C–O) is observed at 998 cm^{-1} while the sp^2 vibration of the graphene sheets is confirmed by the peak marked at 1572 cm^{-1} (C=C). The Co_3O_4 spinel structure of the Co–O bond for ABO (A-Co^{2+} tetrahedral site) and OB_3 (B–Co^{3+} octahedral site) vibrations matches with the FTIR peaks around 542 and 652 cm^{-1}, respectively [28,48,58].

The XPS analysis was used to acquire the information about the chemical states of the as-synthesized RGO-S/200 mg Co_3O_4 composite sample. Generally, the spectrum (intensity versus binding energy) is being generated by a photoelectrons emitted from the surface of the tested sample by a monochromatic energies of Kα X-rays. The emitted lines are useful in determining the chemical states of the material through correlating the binding energy position and the intensity of each line in the material being analyzed [26]. Fig. 4 (a) shows a wide scan of RGO-S/200 mg Co_3O_4 composite presenting a comprehensive surface elemental composition with major peaks of C 1s, O 1s, S 2p and Co 2p indicating the presence of carbon, oxygen, sulphur and cobalt elements in the material. The single peak of C 1s (Fig. 4 (b)) was further deconvoluted into four sub-regions with their binding energies at 284.2, 284.9, 285.8 and 287.9 eV corresponding to C=C (sp^2), C–C (sp^3), C–O and C=O bonds, respectively. The former two peaks shows the existence of non-oxygenated carbon atoms corresponding to sp^2 and sp^3 hybridized carbon while the later presents the hydroxyl and carboxyl functional groups present within the material [59]. The deconvoluted O 1s in Fig. 4 (b) presents three peaks at 529.6, 531.2 and 533.0 eV, corresponding to metal oxides, C–O and C=O bonds, respectively. The first peak (529.6 eV) is related to the lattice oxygen in a Co_3O_4 spinel structure while the rest of the two peaks are linked to the oxygen bonded to carbon, oxygen in cobalt hydroxides ions, cobalt monoxide and water adsorbed on the surface of Co_3O_4 [10]. The high resolution S 2p spectra in Fig. 4 (c) shows the formation of C–S–C single bond and C=S double bond at a binding energies of 163.3 eV and 164.4 eV, respectively [4,32,60]. This shows that sulphur atom was successfully incorporated into the composite sample. Fig. 5 (e) displays two forms of cobalt oxide (CoO and Co_3O_4), which can be recognised by the shakeup satellites at 779.9 and 795 eV

Please cite this article as: Tarimo DJ et al., Enhanced electrochemical performance of supercapattery derived from sulphur-reduced graphene oxide/cobalt oxide composite and activated carbon from peanut shells, International Journal of Hydrogen Energy, https://doi.org/10.1016/j.ijhydene.2020.09.142

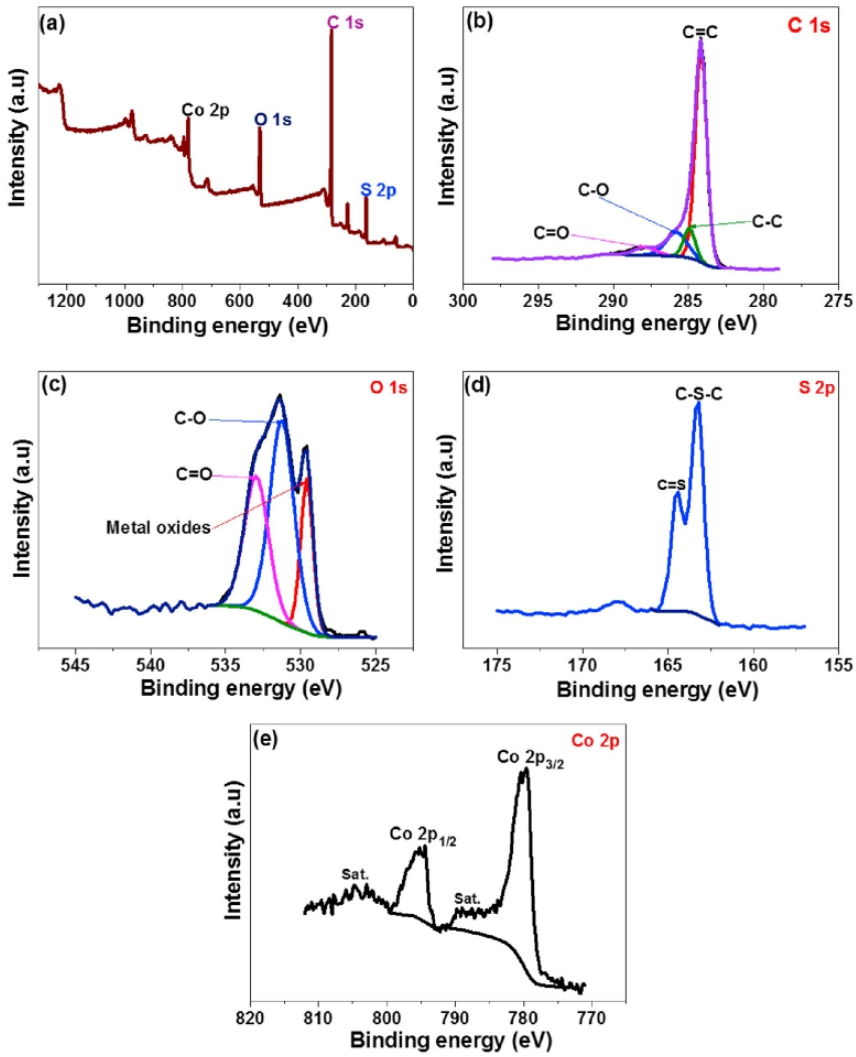

Fig. 4 – (a) XPS survey spectra, core level spectrum of (b) C 1s, (c) O 1s (d) S 2p and (e) Co 2p of RGO-S/200 mg Co_3O_4 composite, respectively.

which corresponds to Co $2p_{3/2}$ and Co $2p_{1/2}$, respectively. The gap between Co $2p_{3/2}$ and Co $2p_{1/2}$ is ~15.1 eV indicating the presence of standard Co_3O_4 spectra [59]. Additionally, there was existence of weak shake-up satellite peaks at 804.7 and 786.8 eV at higher binding energy. These specify that the composite is composed of Co_3O_4 and the oxygen connects between Co_3O_4 and RGO-S in the RGO-S/200 mg Co_3O_4 composite sample.

The nitrogen (N_2) gas adsorption/desorption investigation were conducted to evaluate the specific surface area and pore size distribution of the samples. Fig. 5 (a) and (b) displays the N_2 adsorption/desorption isotherms and pore size distribution calculated using DFT, respectively, of RGO-S, RGO-S/100 mg Co_3O_4, RGO-S/200 mg Co_3O_4 and RGO-S/300 mg Co_3O_4, respectively. From Fig. 5 (a), shows the N_2 adsorption/desorption isotherms whereby the specific surface areas recorded for RGO-S, RGO-S/100 mg Co_3O_4, RGO-S/200 mg Co_3O_4 and RGO-S/300 mg Co_3O_4 composite were found to be 11.66, 10.38, 14.68 and 9.71 m^2/g, respectively. It can be observed that RGO-S/200 mg Co_3O_4 composite displays a higher specific surface area (14.68 m^2/g) compared to the other samples. This is the clear indication that this the right composition that both materials synergize optimum composition which facilitated the interaction between the two materials [5]. Therefore, it is expected to enhance the electrochemical performance of RGO-S/200 mg Co_3O_4 composite. As displayed in Fig. 5 (b), all the samples present a type-III behaviour with an H3-type hysteresis loop signifying the existence of non-rigid aggregates of plate-like particles as it shown in the SEM images. Fig. 5 (b) shows the DFT pore size

Please cite this article as: Tarimo DJ et al., Enhanced electrochemical performance of supercapattery derived from sulphur-reduced graphene oxide/cobalt oxide composite and activated carbon from peanut shells, International Journal of Hydrogen Energy, https://doi.org/10.1016/j.ijhydene.2020.09.142

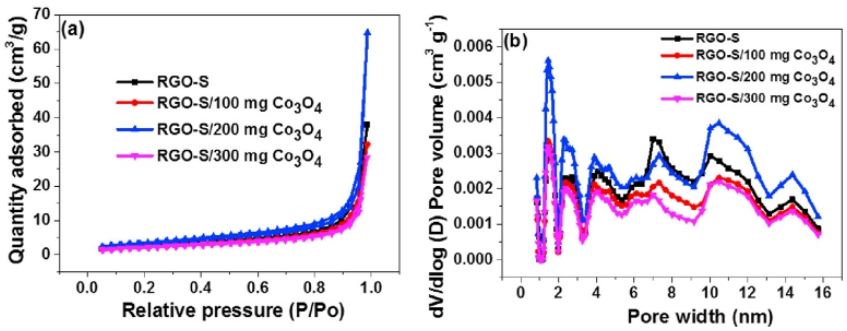

Fig. 5 – (a) N_2 adsorption/desorption isotherms and (b) DFT pore size distributions of RGO-S, RGO-S/100 mg Co_3O_4, RGO-S/200 mg Co_3O_4 and RGO-S/300 mg Co_3O_4, respectively.

distribution. It is also clear here that RGO-S/200 mg Co_3O_4 shows more pore volume as compare to the rest of the other samples and hence still showing better performance.

The cyclic voltammetry (CV) curves at 50 mV s^{-1} for RGO-S and RGO-S/Co_3O_4 composites at different mass loading of Co_3O_4 in a positive potential window range of 0.0–0.5 V vs Ag/AgCl is presented in Fig. 6 (a). The CV curves display a faradaic behaviour confirming the redox reaction within the material. It was further noted that the RGO-S/200 mg Co_3O_4 composite shows higher current response compared to the RGO-S (pristine), RGO-S/100 mg Co_3O_4 and RGO-S/300 mg Co_3O_4. The higher current response displayed by RGO-S/200 mg Co_3O_4 confirms the material's high specific capacity as a result of good synergy between 200 mg of Co_3O_4 and RGO-S. The galvanostatic charge-discharge (GCD) in Fig. 6 (b), was further used to analyse the electrochemical performance of the RGO-S (pristine) and RGO-S/Co_3O_4 composites at 1 A g^{-1} within a positive potential range of 0.0–0.5 V vs Ag/AgCl. The non-linear GCD curves with a potential plateau indicates a clear correspondence between features displayed by GCD curves in Fig. 6 (b) to that of CV curves in Fig. 6 (a). The specific capacity evaluated through the GCD curves using Eq. (3) at 1 A g^{-1}, was found to be 145.1, 79.7, 171.8, and 77.3 mA h g^{-1} for RGO-S, RGO-S/100 mg Co_3O_4, RGO-S/200 mg Co_3O_4 and RGO-S/300 mg Co_3O_4, respectively. Furthermore, the high specific capacity of RGO-S/200 mg Co_3O_4 was confirmed by the longest discharge time compared to other samples, as shown by the GCD curve in Fig. 6 (b), which corresponds with the high current response observed in the CV curve in Fig. 6 (a). This particular composition is the right amount of Co_3O_4 to have a positive impact on the RGO-S as compared with other mass loadings, which makes 200 mg mass loading the optimum amount.

Moreover, the charge-transfer resistance of the redox reactions, diffusive resistance of the electrolyte in the electrode, and ionic resistance of the electrolyte, was used to assess the capacitive performance of the as-synthesized materials by performing the EIS measurements. Fig. 6 (c) shows the EIS Nyquist plot of RGO-S and RGO-S/Co_3O_4 composites measured at a frequency range 10 mHz–100 kHz. From the EIS; the composites with 100 and 300 mg show long diffusion length with large deviation from the vertical line indicating more resistive behaviour and slow charge transport whereas the composite with 200 mg displays shorter diffusion length suggesting fast charge transport. The equivalent series resistance (ESR) value was experimentally determined from the x-axis intercept at high-frequency region as displayed in an inset to Fig. 6 (c). In the Nyquist plot, the intersection with the real Z′ axis is attributed to the equivalent series resistance (ESR) which is the total resistance of the ionic resistance of electrolyte, the electrolyte/electrode interface resistance and electrode/current collector interface resistance [40,54]. The ESR provides information about the contact resistance between the working electrode and the current collector, and the interface resistance of the working electrode and ions from the electrolyte [40,54]. An ESR value of ~1.54 Ω, 1.62 Ω, 1.43 Ω, and 1.81 Ω were recorded for RGO-S, RGO-S/100 mg Co_3O_4, RGO-S/200 mg Co_3O_4 and RGO-S/300 mg Co_3O_4, respectively. It was further observed that RGO-S/200 mg Co_3O_4 has the smallest ESR value compared to the RGO-S (pristine sample), RGO-S/100 mg Co_3O_4 and RGO-S/300 mg Co_3O_4. All these signify the good synergy between RGO-S and this particular mass loading of Co_3O_4 which performs the function of improving the electrochemical performance of the as-synthesized composite.

The charge-discharge cycles over 5000 cycles, were performed as shown in Fig. 6 (d) indicating an excellent columbic efficiency (C_E - %) versus cycle number for RGO-S and RGO-S/Co_3O_4 composites samples at 5 A g^{-1}, respectively. The C_E (%) calculated using Eq. (4) was found to be 99.2%, 98.8%, 99.7% and 98.5% for RGO-S, RGO-S/100 mg Co_3O_4, RGO-S/200 mg Co_3O_4 and RGO-S/300 mg Co_3O_4, respectively. From these results, a superior cycling stability of approximately 100% was demonstrated by RGO-S/200 mg Co_3O_4 compared to other samples. This performance is contributed by the combination of RGO-S and 200 mg Co_3O_4 which has been seen to enhance the accessibility and transport of OH^- ions during rapid charge-discharge process than an individual material. As a result, 200 mg Co_3O_4 was observed to act as a buffer for the volume change during charge-discharge and hence an improved stability in the RGO-S/200 mg Co_3O_4 composite [14,16,55,61].

In general, the RGO-S/200 mg Co_3O_4 composite was found to have high current response in the CV curve, longest discharge time in the GCD curve which shows high specific capacity, low ESR value and short diffusion length in the EIS

Please cite this article as: Tarimo DJ et al., Enhanced electrochemical performance of supercapattery derived from sulphur-reduced graphene oxide/cobalt oxide composite and activated carbon from peanut shells, International Journal of Hydrogen Energy, https://doi.org/10.1016/j.ijhydene.2020.09.142

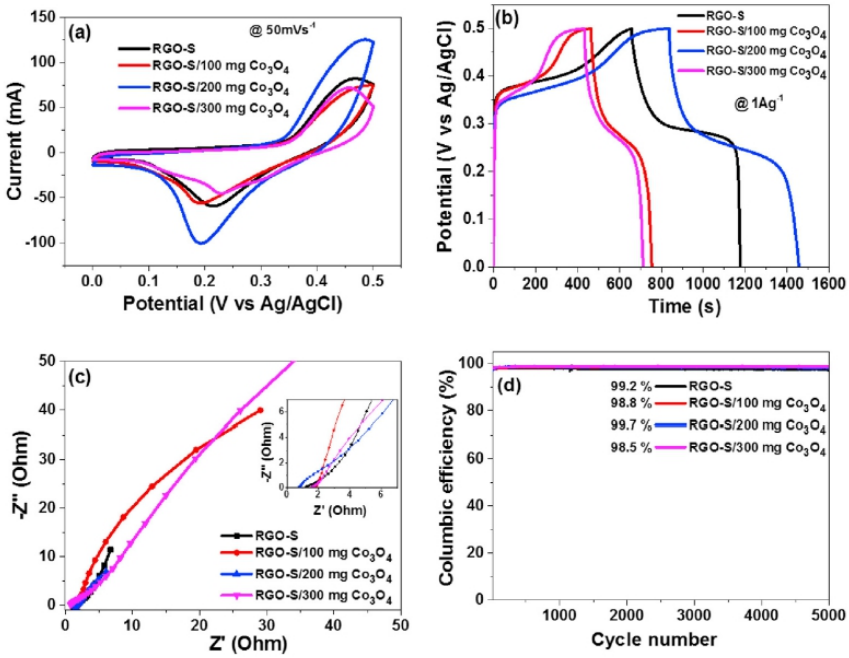

Fig. 6 – (a) CV curves at 50 mV s^{-1} in a positive potential window, (b) GCD curves at 1 A g^{-1} in a positive potential window, (c) EIS Nyquist plot with an insert as the enlarged high-frequency region and (d) Cycling performance for RGO-S and RGO-S/Co_3O_4 composites in 1 M KOH, respectively.

Nyquist impedance, and high cycling performance compared to pristine and other composites samples, respectively. These observed excellent performances might be associated with the synergy between RGO-S and 200 mg Co_3O_4 mass loading in particular as supported by SEM, Raman and BET measurements. The SEM showed well uniformly distributed nanograins of Co_3O_4 in the matrix of RGO-S nanorods/fibers (see Fig. 1 (g, h, i)). Raman spectra showed that 2D, which is very sensitive to defects is the most affected for this composite as compared to other samples, hence it's a clear indication of good interaction between the two materials (see Fig. 3 (a)). The BET measurements shows that this composite has much higher specific surface area and pore volume as compared to other samples (see Fig. 5). Therefore, these results shows that by controlling the amount of Co_3O_4 during the synthesis process has resulted into a composite with improved electrochemical performance. Hence, this study suggests that the easiest way of improving the performance of supercapattery electrode material is by focussing on the synthesis condition like the optimization of metal oxide mass loading ratio. From the above observations, RGO-S/200 mg Co_3O_4 was chosen as a positive electrode for device fabrication.

For further investigation on the electrochemical measurements of RGO-S/200 mg Co_3O_4 composite sample, the CV analysis (Fig. 7 (a)) was done at various scan rates from 5 to 100 mV s^{-1} in a positive potential window range 0.0–0.5 V vs Ag/AgCl. The anodic peak around 0.26 V and cathodic peak around 0.42 V were displayed by the CV curve at low scan rate. This might be contributed by the hydroxyl, carboxyl, and epoxy functional group from RGO-S and redox properties from Co_3O_4 sample [55]. The increase in scan rate shows oxidation and reduction peaks were shifted in the direction of higher and lower potential, respectively indicating the development of charge diffusion polarization in a battery-type material [54]. The CV curves of RGO-S/200 mg Co_3O_4 using 1 M KOH electrolyte shows a pair of broad peaks at about 0.26 V and 0.46 V, respectively. These peaks are due to the electron transfer between Co^{2+} and Co^{3+} ($Co^{2+} \leftrightarrow Co^{3+}$) and also S^{2+} and S^{4+} ($S^{2+} \leftrightarrow S^{4+}$) through the following redox reaction processes [18]:

$$Co_3O_4 + OH^- + H_2O \leftrightarrow 3CoOOH + e^- \quad (9)$$

$$CoOOH + OH^- \leftrightarrow CoO_2 + H_2O + e^- \quad (10)$$

$$S \leftrightarrow S^{2-} + 2e^- \quad (11)$$

The GCD curves (Fig. 7 (b)) of RGO-S/200 mg Co_3O_4 composite sample at various specific currents from 1 to 5 A g^{-1} corresponds well with the CV curves in Fig. 7 (a). The electrochemical redox reactions occur as a result of the interaction between the electrode and electrolyte in the material which produces redox peaks shown by the CV and GCD curves. In addition, a detailed analysis was conducted on EIS Nyquist plot. A representative EIS Nyquist plot comprises of two regions; a semicircle at high frequency and a straight line at low frequency region corresponding to charge transfer

Please cite this article as: Tarimo DJ et al., Enhanced electrochemical performance of supercapattery derived from sulphur-reduced graphene oxide/cobalt oxide composite and activated carbon from peanut shells, International Journal of Hydrogen Energy, https://doi.org/10.1016/j.ijhydene.2020.09.142

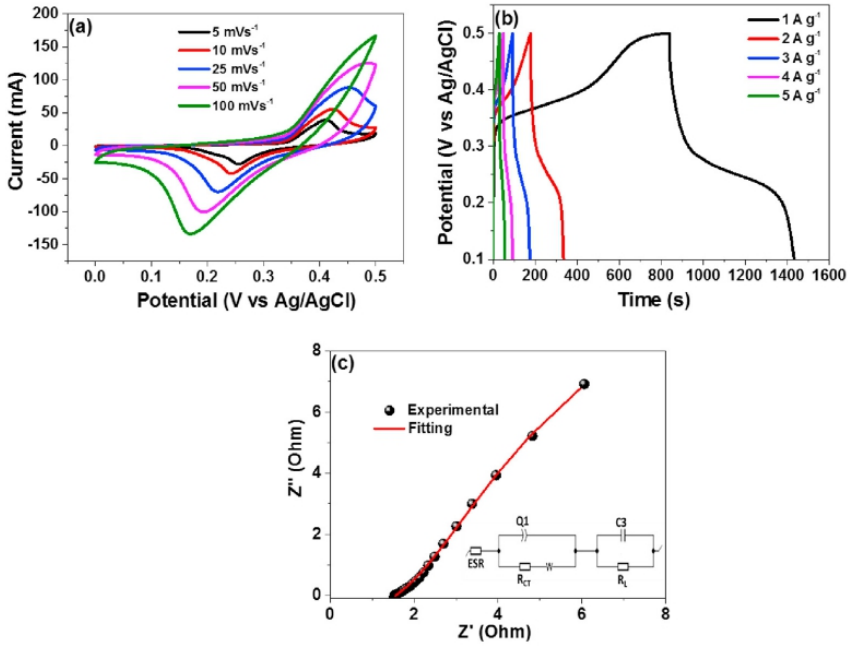

Fig. 7 – (a) CV curves at different scan rates, (b) GCD curves at different specific current and (c) EIS Nyquist plot with an insert circuit for RGO-S/200 mg Co_3O_4 sample in 1 M KOH, respectively.

resistance (R_{CT}) and ion diffusion characteristics, respectively. Fig. 7 (c) displays the fitted EIS Nyquist plot of the composite material, with its corresponding circuit as the insert. The circuit is adopted for fitting the data and illustrates an equivalent series resistance (ESR), which is in series with charge transfer resistance (R_{CT}) at high-frequency region, and a Warburg (W) element that is in parallel with real capacitance (Q1). A mass capacitance (C3) is in parallel with the leakage resistance (R_L) at low frequency region. R_{CT} provides information about the reactions occurring between the interface of the electrode and electrolyte while R_L describes the Faradaic charge transfer processes. The attained values of ESR = 1.56 Ω and R_{CT} = 0.07 Ω for the electrode are comparable with the experimental values of ESR = 1.43 Ω and R_{CT} = 0.04 Ω, respectively, indicating perfect fitting of the Nyquist plot. The obtained small R_{CT} = 0.04 Ω shows low internal resistance and good electrical conductivity of the material. It is known that, the highest specific power is inversely proportional to the ESR. Thus, reducing internal resistance is an important target in development of supercapattery with enhanced performances [1].

Since RGO-S/200 mg Co_3O_4 composite sample has shown superior electrochemical measurements compared to pristine and other composites samples, it was selected to investigate the practical applications of the material in supercapattery. The supercapattery device was designed using 1 M KOH electrolyte, RGO-S/200 mg Co_3O_4 composite as a positive electrode and activated carbon from peanut shell (AC-PS) as the negative electrode. AC-PS was selected as a negative electrode because it was found to have excellent electrochemical properties as detailed in our previous study [52]. Because of the variation in specific capacity/capacitance and the discharge time between the positive and negative electrode, Eq. (5) was utilized to balance the mass of the electrodes by applying the charge balance as $Q_+ = Q_-$. The total mass of 5.4 mg/cm^2 corresponds to 2.0 mg and 3.4 mg, resulted from a mass balance ratio of 1.0:1.7 was estimated for RGO-S/200 mg Co_3O_4 and AC-PS, respectively. The assembled device was labelled as RGO-S/200 mg Co_3O_4//AC-PS.

Fig. 8 (a)show the CV curves at 50 mV s^{-1} for RGO-S/200 mg Co_3O_4 as a positive electrode in a positive potential window (0.0–0.5 V) displaying a faradaic behaviour due to ongoing redox reaction, and AC-PS as a negative electrode showing EDLC shape indicating the capacitive behaviour of the material in a negative potential window (−0.9 - 0.0 V). The measurements performed at various scan rates from 5 to 100 mV s^{-1} in Fig. 8 (b) shows the CV curves of the device (RGO-S/200 mg Co_3O_4//AC-PS). The results confirm that the device is more of pseudocapacitive behaviour whereby in terms of the current response still the Faradaic positive electrode is pronounced, however, EDLC negative electrode has more influence because of the wide potential window. This kind of behaviour occurs when there is a good charge balancing signifying that electrode where charging and discharging at the same time regardless of their capacitive ability individually. A maximum cell potential window of 1.45 V, was produced by the assembled RGO-S/200 mg Co_3O_4//AC-PS device. The high rate capability of the material was confirmed by the current response in the CV curve which increases linearly as the scan rate increases without shape distortion [48]. Fig. 8 (c) presents the GCD curves of RGO-S/200 mg Co_3O_4//AC-PS at different specific currents. The GCD curves in Fig. 8 (b) are

Please cite this article as: Tarimo DJ et al., Enhanced electrochemical performance of supercapattery derived from sulphur-reduced graphene oxide/cobalt oxide composite and activated carbon from peanut shells, International Journal of Hydrogen Energy, https://doi.org/10.1016/j.ijhydene.2020.09.142

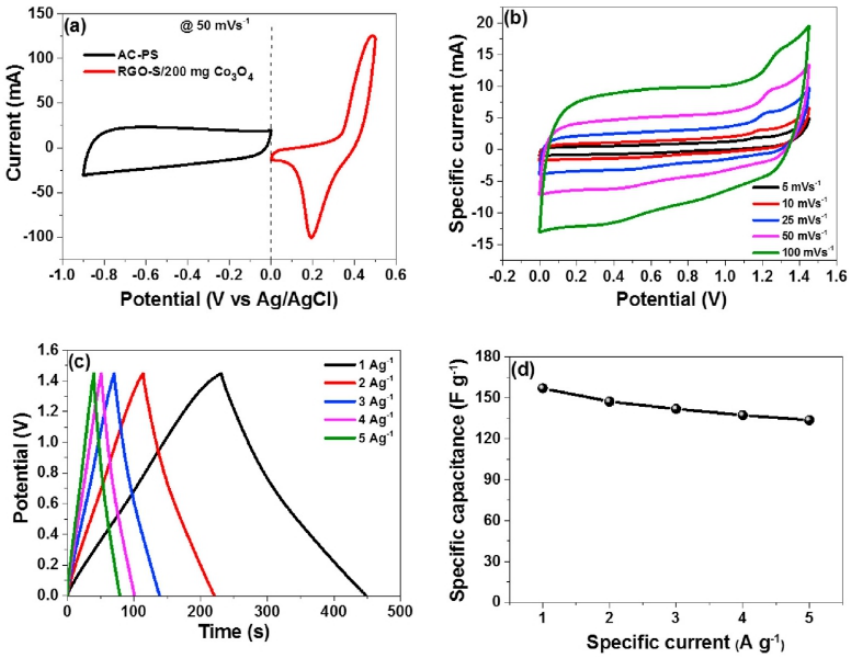

Fig. 8 – (a) CV curves of RGO-S/200 mg Co_3O_4 and AC-PS electrodes in a positive and negative potential windows, respectively, (b) CV curves, (c) GCD curves and (d) Specific capacitance versus specific current for RGO-S/200 mg Co_3O_4//AC-PS in 1 M KOH, respectively.

clearly pseudocapacitive with semi-linear curves confirming the two electrodes ended up with the so-called supercapattery device. It was further observed that the purely RGO-S/200 mg Co_3O_4 Faradaic behaviour was transformed into pseudocapacitive behaviour by utilizing AC-PS as an EDLC material. This indicates that the synergetic effect of the EDLC (capacitive) and the Faradaic (battery-type) material has resulted in a hybrid device with combined features, with the EDLC behaviour dominating because it had lower capacitance. Since the total capacitance of the device is the sum of the two capacitance in series as $C_T = 1/C_1 + 1/C_2$ then the material with lower capacitance will dominate and is termed as supercapattery. This is an emerging electrochemical energy storage devices, whereby a device is made up by combining the capacitive materials which store energy via adsorptions of ions and battery materials which store energy via faradaic redox reactions to produce the final capacitive device [5,15,22,49]. The specific capacitance versus specific current for the RGO-S/200 mg Co_3O_4//AC-PS supercapattery device evaluated from the GCD profiles in Fig. 8 (c) using Eq. (6) is presented in Fig. 8 (d). It was observed that the supercapattery device was able to preserve the specific capacitance as the specific current increases because there was no fast loss of the specific capacitance. Consequently, a rate capability of 85.1% was preserved by the supercapattery device.

Fig. 9 (a) display long cycling performance of up to 10, 000 cycles applied to evaluate the stability of the RGO-S/200 mg Co_3O_4//AC-PS supercapattery device. The RGO-S/200 mg Co_3O_4//AC-PS supercapattery device revealed a capacitance retention and columbic efficiency of 83.4% and 99.5%, respectively at 8 A g^{-1} over 10, 000 cycles. This good cycling performance could be due to the good synergy between Co_3O_4 and RGO-S, which resulted in a repeated contraction and expansion of the electrodes during charging-discharging cycles. Therefore, this shows that there was an improvement in wettability which allows accessibility of ions within the material [61]. Eqs (7) and (8) were employed to evaluate the specific energy and power for RGO-S/200 mg Co_3O_4//AC-PS supercapattery device and results are presented in Fig. 9 (b) as a Ragone plot. The highest specific energy recorded at 1 A g^{-1} was 45.8 W h kg^{-1} with its corresponding specific power of 725 W kg^{-1}. The fabricated RGO-S/200 mg Co_3O_4//AC-PS supercapattery device revealed higher value of specific energy and power compared to some similar materials reported recently in the literature as shown in Table 1 below.

Fig. 9 (c) display Nyquist plot showing fitting and experimental data plotted together for RGO-S/200 mg Co_3O_4//AC-PS supercapattery device. The EIS fitting circuit obtained by the Z fit software from the EC-lab 10.40 is displayed by the insert to Fig. 9 (c) presenting a linear line close to be parallel to y-axis at low-frequency region and a small semicircle at high-frequency region. From the circuit, R1, R2 and R3 present equivalent series resistance (ESR), charge transfer resistance and leakage resistance, respectively. Whereas, C2 and C3 indicate real and mass capacitance, respectively. R2 and C2 provides information about the resistance rate and Faradaic electrochemical activity which takes place between the electrode and electrolyte while R3 and C3 gives information about

Please cite this article as: Tarimo DJ et al., Enhanced electrochemical performance of supercapattery derived from sulphur-reduced graphene oxide/cobalt oxide composite and activated carbon from peanut shells, International Journal of Hydrogen Energy, https://doi.org/10.1016/j.ijhydene.2020.09.142

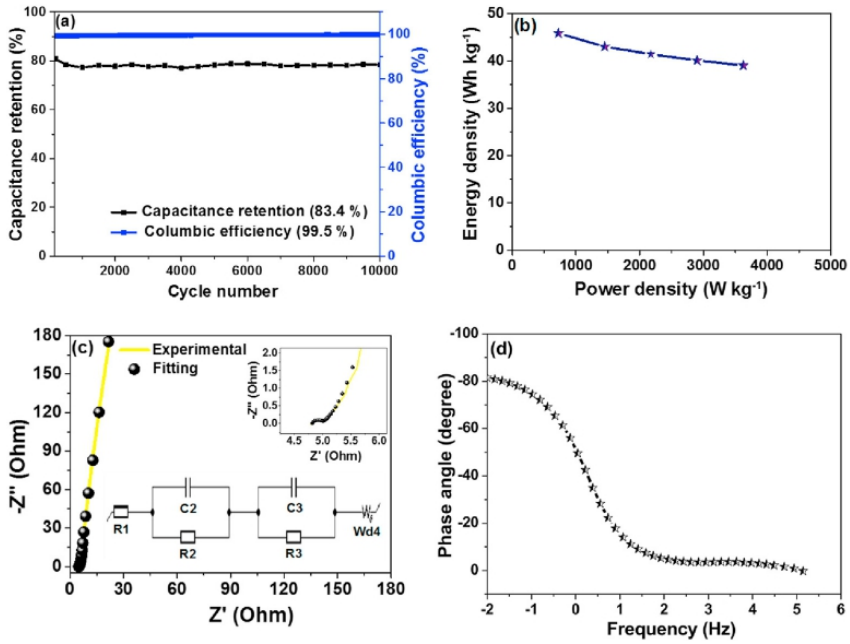

Fig. 9 – (a) Capacitance retention and columbic efficiency versus cycle number (b) Ragone plot (c) EIS Nyquist plot (the insert shows an equivalent circuit applied for EIS fitting) and (d) Bode impedance of RGO-S/200 mg Co_3O_4//AC-PS sample, respectively in 1 M KOH.

Table 1 – Comparisons of electrochemical performance (cycle life, energy and power density) of some similar materials from the literature calculated from two electrode systems.

Electrodes (Device)	Electrolyte	Energy density	Power density	Cycle life	Ref.
Co_3O_4/C//Co_3O_4/C	2 M KOH	23.4 W h kg^{-1}	162.5 W kg^{-1}	–	[50]
Co_3O_4-rGO//AC	6 M KOH	35.7 W h kg^{-1}	225 W kg^{-1}	1000	[20]
MWCNT-Co_3O_4–Ag//AC	1 M KOH	16.5 W h kg^{-1}	297.5 W kg^{-1}	3000	[22]
Co_3O_4//Co_3O_4	2 M KOH	25.5 W h kg^{-1}	11 kW kg^{-1}	4000	[46]
Co_3O_4-T//AC	6 M KOH	42.81 W h kg^{-1}	1.69 kW kg^{-1}	1000	[28]
MOF/PANI/AC	1 M KOH	23.2 W h kg^{-1}	1600 W h kg^{-1}	3000	[62]
Co_3O_4//rGO	1 M KOH	40 W h kg^{-1}	742 W kg^{-1}	5000	[27]
$MnCo_2O_4$//AC	6 M KOH	33.8 W h kg^{-1}	318.9 W kg^{-1}	10,000	[25]
rGO-Co_3O_4–Ag//AC	1 M KOH	23.63 W h kg^{-1}	440 W kg^{-1}	3000	[26]
Co_3O_4 nano flakes//AC	1 M KOH	23.7 W h kg^{-1}	307 W kg^{-1}	2500	[24]
RGO-S/200 mg Co_3O_4//AC-PS	**1 M KOH**	**45.8 W h kg^{-1}**	**725 W kg^{-1}**	**10,000**	**This work**

the resistance and capacitance associated with EDLC. The ESR (represented as R1 in the circuit) was estimated experimentally at high-frequency region while the lower charge transfer resistance is confirmed by a very small semicircle at higher frequency region as presented by the inset to Fig. 9 (c). The experimental values for the equivalent series resistance (R1) and charge transfer resistance (R2) were 4.78 and 0.16 Ω, respectively, which were comparable to the values obtained through fitting as 4.82 and 0.19 Ω, respectively. Other parameters recorded from the fitting circuit were R3, C2, C3 and Wd4 with 0.16 Ω, 0.092 F, 0.054 F and 5.9 Ω values, respectively. Furthermore, the response recorded from the Nyquist plot shows the curve is almost parallel to the imaginary impedance (-Z'') axis, which is evidence that the device is very close to the ideal capacitance behaviour. Fig. 8 (d) illustrates the phase angle versus frequency profile with an ideal value of −90 in which the RGO-S/200 mg Co_3O_4//AC-PS supercapattery device is at −81.60.

Fig. 10 (a) shows a specific capacitance versus floating time for the supercapattery device exposed to the highest voltage of 1.45 V for over 150 h at 10 A g^{-1}. After every 10 h the specific capacitance was monitored and the device was able to withstand a stability of 71.6% after 150 h. This superior cycling achievement could be associated with the chemically stable structure of the combined features of RGO-S and Co_3O_4. Also, Co_3O_4 act as a spacer to stabilize RGO-S whose interlayer spacing are extended when Co_3O_4 is incorporated [55]. The CV and GCD curves of RGO-S/200 mg Co_3O_4//AC-PS

Please cite this article as: Tarimo DJ et al., Enhanced electrochemical performance of supercapattery derived from sulphur-reduced graphene oxide/cobalt oxide composite and activated carbon from peanut shells, International Journal of Hydrogen Energy, https://doi.org/10.1016/j.ijhydene.2020.09.142

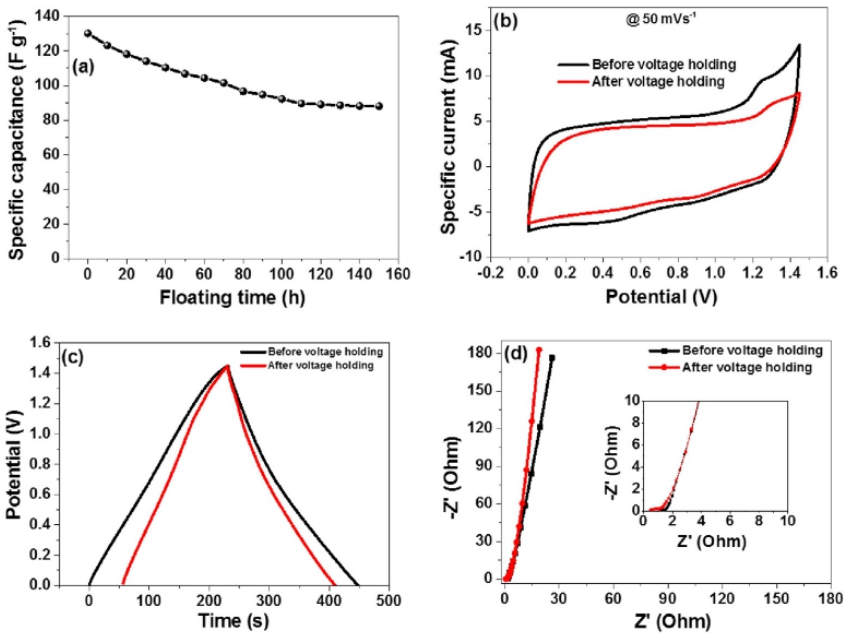

Fig. 10 – (a) Floating time versus specific capacitance, (b) CV curves before and after voltage holding at 50 mV s^{-1}, (c) CD curves before and after voltage holding at 1 A g^{-1} and (d) EIS Nyquist plot before and after voltage holding for RGO-S/200 mg Co_3O_4//AC-PS sample in 1 M KOH, respectively.

supercapattery device before and after voltage holding, respectively, are displayed in Fig. 10 (b and c). It was observed that after 150 h of cycling the shape was maintained, however, the current response in the CV curve and discharge time in the GCD curve slightly decreased after the device being subjected to many cycles. This proves good stability of the device which is attributed to the synergetic effect of the two materials. The RGO-S/200 mg Co_3O_4//AC-PS supercapattery device displayed an EIS Nyquist plot before and after voltage holding as observed in Fig. 10 (d). The figure revealed that after voltage holding there was an improvement in the equivalent series resistance from 1.04 Ω to 0.52 Ω. Also, the vertical line is considerably closer to the y-axis indicating an improvement in the capacitive behaviour of the device. This shows that more ions managed to access more pores of the material. Furthermore, the interaction of Co_3O_4 and RGO-S allows the insertion and de-insertion of the electrolyte ions within the material, thus inhibit its aggregation and minimize the charge transfer resistance of the device [55].

Conclusion

Sulphur-reduced graphene oxide/cobalt oxide composites (RGO-S/Co_3O_4) were successfully synthesized via a simple hydrothermal method. The micrographs, structural, chemical composition, and functional group analysis indicated the successful synthesis of RGO-S and RGO-S/Co_3O_4 composite samples. An optimized RGO-S/200 mg Co_3O_4 composite presented the highest specific capacity of 171.8 mA h g^{-1} and superior stability of 99.7% over 5000 cycles at 1 and 5 A g^{-1}, respectively, using 1 M KOH electrolyte in a three-electrode system. The fabricated supercapattery device, RGO-S/200 mg Co_3O_4//AC-PS demonstrated a high specific energy and power of 45.8 W h kg^{-1} and 725 W kg^{-1}, respectively, at 1 A g^{-1}. The device was able to retain about 83.4% of its initial capacitance and 99.5% of the columbic efficiency for over 10, 000 cycles. An outstanding cycling performance of 71.6% was sustained from the voltage holding test performed for over 150 h at 10 A g^{-1}. The results demonstrated excellent synergy between optimized Co_3O_4 and RGO-S which led to the supercapattery device when combined with activated carbon from the peanut shell.

Declaration of competing interest

The authors declare that they have no known competing financial interests or personal relationships that could have appeared to influence the work reported in this paper.

Acknowledgements

This work is based on the research supported by the South African Research Chairs Initiative of the Department of Science and Technology (DST) and National Research Foundation (NRF) of South Africa (Grant No. 61056). Any opinion, finding,

Please cite this article as: Tarimo DJ et al., Enhanced electrochemical performance of supercapattery derived from sulphur-reduced graphene oxide/cobalt oxide composite and activated carbon from peanut shells, International Journal of Hydrogen Energy, https://doi.org/10.1016/j.ijhydene.2020.09.142

and conclusion expressed in this material are that of the authors, and the DST and NRF do not accept any liability in this regard. Delvina Japhet Tarimo acknowledges the financial support from NRF through SARChI chair in Carbon Technology and Materials. Delvina Japhet Tarimo thanks the African-German Network of Excellence in Science (AGNES) for granting a Mobility Grant in 2019; the Grant is generously sponsored by German Federal Ministry of Education and Research and supported by the Alexander von Humboldt Foundation. Dr Cosmas Muiva of the Department of Physics, Botswana International University of Science and Technology, Botswana is acknowledged as a host supervisor during the visit.

REFERENCES

[1] Yin JL, Park JY. Electrochemical investigation of copper/nickel oxide composites for supercapacitor applications. Int J Hydrogen Energy 2014;39:16562–8. https://doi.org/10.1016/j.ijhydene.2014.04.202.
[2] Krishnamoorthy K, Thangavel S, Chelora Veetil J, Raju N, Venugopal G, Kim SJ. Graphdiyne nanostructures as a new electrode material for electrochemical supercapacitors. Int J Hydrogen Energy 2016;41:1672–8. https://doi.org/10.1016/j.ijhydene.2015.10.118.
[3] Numan A, Duraisamy N, Saiha Omar F, Mahipal YK, Ramesh K, Ramesh S. Enhanced electrochemical performance of cobalt oxide nanocube intercalated reduced graphene oxide for supercapacitor application. RSC Adv 2016;6:34894–902. https://doi.org/10.1039/c6ra00160b.
[4] Huo J, Zheng P, Wang X, Guo S. Three-dimensional sulphur/nitrogen co-doped reduced graphene oxide as high-performance supercapacitor binder-free electrodes. Appl Surf Sci 2018;442:575–80. https://doi.org/10.1016/j.apsusc.2018.01.221.
[5] Chen GZ. Supercapacitor and supercapattery as emerging electrochemical energy stores. Int Mater Rev 2017;62:173–202. https://doi.org/10.1080/09506608.2016.1240914.
[6] Wang JP, Wang SL, Huang ZC, Yu YM, Liu JL. Synthesis of long chain-like nickel cobalt oxide nanoneedles-reduced graphene oxide composite material for high-performance supercapacitors. Ceram Int 2014;40:12751–8. https://doi.org/10.1016/j.ceramint.2014.04.128.
[7] Lamiel C, Lee YR, Cho MH, Tuma D, Shim JJ. Enhanced electrochemical performance of nickel-cobalt-oxide@reduced graphene oxide//activated carbon asymmetric supercapacitors by the addition of a redox-active electrolyte. J Colloid Interface Sci 2017;507:300–9. https://doi.org/10.1016/j.jcis.2017.08.003.
[8] Ke Q, Tang C, Yang ZC, Zheng M, Mao L, Liu H, et al. 3D nanostructure of carbon nanotubes decorated Co_3O_4 nanowire arrays for high performance supercapacitor electrode. Electrochim Acta 2015;163:9–15. https://doi.org/10.1016/j.electacta.2015.02.136.
[9] Chen YY, Dhaiveegan P, Michalska M, Lin JY. Morphology-controlled synthesis of nanosphere-like $NiCo_2S_4$ as cathode materials for high-rate asymmetric supercapacitors. Electrochim Acta 2018;274:208–16. https://doi.org/10.1016/j.electacta.2018.04.086.
[10] García-Gómez A, Eugénio S, Duarte RG, Silva TM, Carmezim MJ, Montemor MF. Electrodeposited reduced-graphene oxide/cobalt oxide electrodes for charge storage applications. Appl Surf Sci 2016;382:34–40. https://doi.org/10.1016/j.apsusc.2016.04.113.
[11] García-Gómez A, Duarte RG, Eugénio S, Silva TM, Carmezim MJ, Montemor MF. Fabrication of electrochemically reduced graphene oxide/cobalt oxide composite for charge storage electrodes. J Electroanal Chem 2015;755:151–7. https://doi.org/10.1016/j.jelechem.2015.07.053.
[12] Ramesh S, Karuppasamy K, Kim HS, Kim HS, Kim JH. Hierarchical Flowerlike 3D nanostructure of Co3O4@MnO2/N-doped Graphene oxide (NGO) hybrid composite for a high-performance supercapacitor. Sci Rep 2018;8:1. https://doi.org/10.1038/s41598-018-34905-7.
[13] García-Gómez A, Eugénio S, Duarte RG, Silva TM, Carmezim MJ, Montemor MF. Electrodeposited reduced-graphene oxide/cobalt oxide electrodes for charge storage applications. Appl Surf Sci 2016;382:34–40. https://doi.org/10.1016/j.apsusc.2016.04.113.
[14] Wang HW, Hu ZA, Chang YQ, Chen YL, Zhang ZY, Yang YY, et al. Preparation of reduced graphene oxide/cobalt oxide composites and their enhanced capacitive behaviors by homogeneous incorporation of reduced graphene oxide sheets in cobalt oxide matrix. Mater Chem Phys 2011;130:672–9. https://doi.org/10.1016/j.matchemphys.2011.07.043.
[15] Omar FS, Numan A, Bashir S, Duraisamy N, Vikneswaran R, Loo YL, et al. Enhancing rate capability of amorphous nickel phosphate supercapattery electrode via composition with crystalline silver phosphate. Electrochim Acta 2018;273:216–28. https://doi.org/10.1016/j.electacta.2018.03.136.
[16] Jokar E, Iraji zad A, Shahrokhian S. Growth control of cobalt oxide nanoparticles on reduced graphene oxide for enhancement of electrochemical capacitance. Int J Hydrogen Energy 2014;39:21068–75. https://doi.org/10.1016/j.ijhydene.2014.10.061.
[17] García-Gómez A, Duarte RG, Eugénio S, Silva TM, Carmezim MJ, Montemor MF. Fabrication of electrochemically reduced graphene oxide/cobalt oxide composite for charge storage electrodes. J Electroanal Chem 2015;755:151–7. https://doi.org/10.1016/j.jelechem.2015.07.053.
[18] Xiang C, Li M, Zhi M, Manivannan A, Wu N. A reduced graphene oxide/Co3O4 composite for supercapacitor electrode. J Power Sources 2013;226:65–70. https://doi.org/10.1016/j.jpowsour.2012.10.064.
[19] Song Z, Zhang Y, Liu W, Zhang S, Liu G, Chen H, et al. Hydrothermal synthesis and electrochemical performance of Co 3O4/reduced graphene oxide nanosheet composites for supercapacitors. Electrochim Acta 2013;112:120–6. https://doi.org/10.1016/j.electacta.2013.08.155.
[20] Xie LJ, Wu JF, Chen CM, Zhang CM, Wan L, Wang JL, et al. A novel asymmetric supercapacitor with an activated carbon cathode and a reduced graphene oxide-cobalt oxide nanocomposite anode. J Power Sources 2013;242:148–56. https://doi.org/10.1016/j.jpowsour.2013.05.081.
[21] Huo J, Zheng P, Wang X, Guo S. Three-dimensional sulphur/nitrogen co-doped reduced graphene oxide as high-performance supercapacitor binder-free electrodes. Appl Surf Sci 2018;442:575–80. https://doi.org/10.1016/j.apsusc.2018.01.221.
[22] Iqbal J, Numan A, Rafique S, Jafer R, Mohamad S, Ramesh K, et al. High performance supercapattery incorporating ternary nanocomposite of multiwalled carbon nanotubes decorated with Co3O4 nanograins and silver nanoparticles as electrode material. Electrochim Acta 2018;278:72–82. https://doi.org/10.1016/j.electacta.2018.05.040.
[23] Noori A, El-Kady MF, Rahmanifar MS, Kaner RB, Mousavi MF. Towards establishing standard performance metrics for

Please cite this article as: Tarimo DJ et al., Enhanced electrochemical performance of supercapattery derived from sulphur-reduced graphene oxide/cobalt oxide composite and activated carbon from peanut shells, International Journal of Hydrogen Energy, https://doi.org/10.1016/j.ijhydene.2020.09.142

batteries, supercapacitors and beyond. Chem Soc Rev 2019;48:1272–341. https://doi.org/10.1039/c8cs00581h.
[24] Numan A, Ramesh kumar P, Khalid M, Ramesh S, Ramesh K, Shamsudin EM, et al. Facile sonochemical synthesis of 2D porous Co3O4 nanoflake for supercapattery. J Alloys Compd 2020;819:153019. https://doi.org/10.1016/j.jallcom.2019.153019.
[25] Saravanakumar B, Wang X, Zhang W, Xing L, Li W. Holey two dimensional manganese cobalt oxide nanosheets as a high-performance electrode for supercapattery. Chem Eng J 2019;373:547–55. https://doi.org/10.1016/j.cej.2019.05.080.
[26] Iqbal J, Numan A, Jafer R, Bashir S, Jilani A, Mohammad S, et al. Ternary nanocomposite of cobalt oxide nanograins and silver nanoparticles grown on reduced graphene oxide conducting platform for high-performance supercapattery electrode material. J Alloys Compd 2020;821:153452. https://doi.org/10.1016/j.jallcom.2019.153452.
[27] Sankar Devi V, Athika M, Duraisamy E, Prasath A, Selva Sharma A, Elumalai P. Facile sol-gel derived nanostructured spinel Co3O4 as electrode material for high-performance supercapattery and lithium-ion storage. J Energy Storage 2019;25:100815. https://doi.org/10.1016/j.est.2019.100815.
[28] Meng T, Xu QQ, Wang ZH, Li YT, Gao ZM, Xing XY, et al. Co3O4 nanorods with self-assembled nanoparticles in queue for supercapacitor. Electrochim Acta 2015;180:104–11. https://doi.org/10.1016/j.electacta.2015.08.085.
[29] Lamiel C, Lee YR, Cho MH, Tuma D, Shim JJ. Enhanced electrochemical performance of nickel-cobalt-oxide@reduced graphene oxide//activated carbon asymmetric supercapacitors by the addition of a redox-active electrolyte. J Colloid Interface Sci 2017;507:300–9. https://doi.org/10.1016/j.jcis.2017.08.003.
[30] Liu H, Gou X, Wang Y, Du X, Quan C, Qi T. Cauliflower-like Co3O4/three-dimensional graphene composite for high performance supercapacitor applications. J Nanomater 2015;2015. https://doi.org/10.1155/2015/874245.
[31] Halder A, Zhang M, Chi Q. Electrocatalytic applications of graphene–metal oxide nanohybrid materials. Adv Catal Mater - Photocatal Other Curr Trends 2016. https://doi.org/10.5772/61808.
[32] Kiciński W, Szala M, Bystrzejewski M. Sulfur-doped porous carbons: synthesis and applications. Carbon N Y 2014;68:1–32. https://doi.org/10.1016/j.carbon.2013.11.004.
[33] Bai Y, Lu L, Bao J, Sun G, Zhang B, Zeng J, et al. The preparation and electrochemical performance of nitrogen-doped graphene/Co(OH)2 composite. Int J Electrochem Sci 2019;14:606–17. https://doi.org/10.20964/2019.01.48.
[34] Xie LJ, Wu JF, Chen CM, Zhang CM, Wan L, Wang JL, et al. A novel asymmetric supercapacitor with an activated carbon cathode and a reduced graphene oxide-cobalt oxide nanocomposite anode. J Power Sources 2013;242:148–56. https://doi.org/10.1016/j.jpowsour.2013.05.081.
[35] Jokar E, Iraji zad A, Shahrokhian S. Growth control of cobalt oxide nanoparticles on reduced graphene oxide for enhancement of electrochemical capacitance. Int J Hydrogen Energy 2014;39:21068–75. https://doi.org/10.1016/j.ijhydene.2014.10.061.
[36] Yoo MJ, Park HB. Effect of hydrogen peroxide on properties of graphene oxide in Hummers method. Carbon N Y 2019;141:515–22. https://doi.org/10.1016/j.carbon.2018.10.009.
[37] Li Z, Li C, Ge X, Ma J, Zhang Z, Li Q, et al. Reduced graphene oxide wrapped MOFs-derived cobalt-doped porous carbon polyhedrons as sulfur immobilizers as cathodes for high performance lithium sulfur batteries. Nano Energy 2016;23:15–26. https://doi.org/10.1016/j.nanoen.2016.02.049.
[38] Yu X, Park SK, Yeon SH, Park HS. Three-dimensional, sulfur-incorporated graphene aerogels for the enhanced performances of pseudocapacitive electrodes. J Power Sources 2015;278:484–9. https://doi.org/10.1016/j.jpowsour.2014.12.102.
[39] Tian Z, Li J, Zhu G, Lu J, Wang Y, Shi Z, et al. Facile synthesis of highly conductive sulfur-doped reduced graphene oxide sheets. Phys Chem Chem Phys 2015;18:1125–30. https://doi.org/10.1039/c5cp05475c.
[40] Tarimo DJ, Oyedotun KO, Mirghni AA, Sylla NF, Manyala N. High energy and excellent stability asymmetric supercapacitor derived from sulphur-reduced graphene oxide/manganese dioxide composite and activated carbon from peanut shell. Electrochim Acta 2020;353:136498. https://doi.org/10.1016/j.electacta.2020.136498.
[41] Wang JP, Wang SL, Huang ZC, Yu YM, Liu JL. Synthesis of long chain-like nickel cobalt oxide nanoneedles-reduced graphene oxide composite material for high-performance supercapacitors. Ceram Int 2014;40:12751–8. https://doi.org/10.1016/j.ceramint.2014.04.128.
[42] Edison TNJI, Atchudan R, Sethuraman MG, Lee YR. Supercapacitor performance of carbon supported Co3O4 nanoparticles synthesized using Terminalia chebula fruit. J Taiwan Inst Chem Eng 2016;68:489–95. https://doi.org/10.1016/j.jtice.2016.09.021.
[43] Numan A, Shahid MM, Omar FS, Ramesh K, Ramesh S. Facile fabrication of cobalt oxide nanograin-decorated reduced graphene oxide composite as ultrasensitive platform for dopamine detection. Sensor Actuator B Chem 2017;238:1043–51. https://doi.org/10.1016/j.snb.2016.07.111.
[44] Song Z, Zhang Y, Liu W, Zhang S, Liu G, Chen H, et al. Hydrothermal synthesis and electrochemical performance of Co 3O4/reduced graphene oxide nanosheet composites for supercapacitors. Electrochim Acta 2013;112:120–6. https://doi.org/10.1016/j.electacta.2013.08.155.
[45] Nguyen TT, Nguyen VH, Deivasigamani RK, Kharismadewi D, Iwai Y, Shim JJ. Facile synthesis of cobalt oxide/reduced graphene oxide composites for electrochemical capacitor and sensor applications. Solid State Sci 2016;53:71–7. https://doi.org/10.1016/j.solidstatesciences.2016.01.006.
[46] Xia XH, Tu JP, Zhang YQ, Mai YJ, Wang XL, Gu CD, et al. Freestanding Co 3O 4 nanowire array for high performance supercapacitors. RSC Adv 2012;2:1835–41. https://doi.org/10.1039/c1ra00771h.
[47] Li Z, Li C, Ge X, Ma J, Zhang Z, Li Q, et al. Reduced graphene oxide wrapped MOFs-derived cobalt-doped porous carbon polyhedrons as sulfur immobilizers as cathodes for high performance lithium sulfur batteries. Nano Energy 2016;23:15–26. https://doi.org/10.1016/j.nanoen.2016.02.049.
[48] Naveen AN, Manimaran P, Selladurai S. Cobalt oxide (Co3O4)/graphene nanosheets (GNS) composite prepared by novel route for supercapacitor application. J Mater Sci Mater Electron 2015;26:8988–9000. https://doi.org/10.1007/s10854-015-3582-2.
[49] William JJ, Babu IM, Muralidharan G. Spongy structured α-Ni(OH)2: facile and rapid synthesis for supercapattery applications. Mater Lett 2019;238:35–7. https://doi.org/10.1016/j.matlet.2018.11.136.
[50] Balasubramanian S, Kamatchi Kamaraj P. Fabrication of natural polymer assisted mesoporous Co3O4/carbon composites for supercapacitors. Electrochim Acta 2015;168:50–8. https://doi.org/10.1016/j.electacta.2015.04.019.
[51] Tarimo DJ, Oyedotun KO, Mirghni AA, Manyala N. Sulphur-reduced graphene oxide composite with improved electrochemical performance for supercapacitor applications. Int J Hydrogen Energy 2020;45:13189–201. https://doi.org/10.1016/j.ijhydene.2020.03.059.
[52] Sylla NF, Ndiaye NM, Ngom BD, Momodu D, Madito MJ, Mutuma BK, et al. Effect of porosity enhancing agents on the

Please cite this article as: Tarimo DJ et al., Enhanced electrochemical performance of supercapattery derived from sulphur-reduced graphene oxide/cobalt oxide composite and activated carbon from peanut shells, International Journal of Hydrogen Energy, https://doi.org/10.1016/j.ijhydene.2020.09.142

electrochemical performance of high-energy ultracapacitor electrodes derived from peanut shell waste. Sci Rep 2019;9:1–15. https://doi.org/10.1038/s41598-019-50189-x.
[53] Mirghni AA, Oyedotun KO, Mahmoud BA, Bello A, Ray SC, Manyala N. Nickel-cobalt phosphate/graphene foam as enhanced electrode for hybrid supercapacitor. Compos B Eng 2019;174:106953. https://doi.org/10.1016/j.compositesb.2019.106953.
[54] Oyedotun KO, Madito MJ, Momodu DY, Mirghni AA, Masikhwa TM, Manyala N. Synthesis of ternary NiCo-MnO2 nanocomposite and its application as a novel high energy supercapattery device. Chem Eng J 2018;335:416–33. https://doi.org/10.1016/j.cej.2017.10.169.
[55] Wang B, Wang Y, Park J, Ahn H, Wang G. In situ synthesis of Co3O4/graphene nanocomposite material for lithium-ion batteries and supercapacitors with high capacity and supercapacitance. J Alloys Compd 2011;509:7778–83. https://doi.org/10.1016/j.jallcom.2011.04.152.
[56] Tang CW, Wang C Bin, Chien SH. Characterization of cobalt oxides studied by FT-IR, Raman, TPR and TG-MS. Thermochim Acta 2008;473:68–73. https://doi.org/10.1016/j.tca.2008.04.015.
[57] Guo Y, Zhao J, Yang S, Yu K, Wang Z, Zhang H. Preparation and characterization of monoclinic sulfur nanoparticles by water-in-oil microemulsions technique. Powder Technol 2006;162:83–6. https://doi.org/10.1016/j.powtec.2005.12.012.
[58] Nguyen TT, Nguyen VH, Deivasigamani RK, Kharismadewi D, Iwai Y, Shim JJ. Facile synthesis of cobalt oxide/reduced graphene oxide composites for electrochemical capacitor and sensor applications. Solid State Sci 2016;53:71–7. https://doi.org/10.1016/j.solidstatesciences.2016.01.006.
[59] Tan Y, Gao Q, Yang C, Yang K, Tian W, Zhu L. One-dimensional porous nanofibers of Co3O4 on the carbon matrix from human hair with superior lithium ion storage performance. Sci Rep 2015;5:15–7. https://doi.org/10.1038/srep12382.
[60] Tarimo DJ, Oyedotun KO, Mirghni AA, Manyala N. Sulphur-reduced graphene oxide composite with improved electrochemical performance for supercapacitor applications. Int J Hydrogen Energy 2020;45. https://doi.org/10.1016/j.ijhydene.2020.03.059.
[61] Li Q, Hu X, Yang Q, Yan Z, Kang L, Lei Z, et al. Electrocapacitive performance of graphene/Co3O4 hybrid material prepared by a nanosheet assembly route. Electrochim Acta 2014;119:184–91. https://doi.org/10.1016/j.electacta.2013.12.066.
[62] Iqbal MZ, Faisal MM, Ali SR, Farid S, Afzal AM. Co-MOF/polyaniline-based electrode material for high performance supercapattery devices. Electrochim Acta 2020;346:136039. https://doi.org/10.1016/j.electacta.2020.136039.

Please cite this article as: Tarimo DJ et al., Enhanced electrochemical performance of supercapattery derived from sulphur-reduced graphene oxide/cobalt oxide composite and activated carbon from peanut shells, International Journal of Hydrogen Energy, https://doi.org/10.1016/j.ijhydene.2020.09.142

4.4.2: Concluding remarks

RGO-S and RGO-S/Co_3O_4 composite was successfully studied; in which RGO-S/Co_3O_4 revealed better electrochemical performance indicating the synergy effects resulted in the combined materials. RGO-S/Co_3O_4 composite was formed by optimizing different mass loading (100, 200 and 300 mg) of Co_3O_4. The optimized RGO-S/200 mg Co_3O_4 composite at 1 A g^{-1} in 1 M KOH electrolyte presented the uppermost specific capacity of 171.8 mAh g^{-1}. Furthermore, an outstanding stability of about 99.7 % for over 5000 cycles was recorded at 5 A g^{-1} for RGO-S/200 mg Co_3O_4 in a three-electrode set-up. The assembled supercapattery device using RGO-S/200 mg Co_3O_4 and activated carbon from peanut shells (AC-PS) as a positive and negative electrode, respectively, presented high specific energy of 45.8 Wh kg^{-1} and power of 725 W kg^{-1} at 1 A g^{-1} in a working potential of 1.45 V. The stated device was found to be superior to other similar devices reported in the literature using the same electrolyte. The fabricated device was able to retain about 83.4 % of its initial capacitance for over 10, 000 cycles, with a columbic efficiency of 99.5 % at 8 A g^{-1}. A voltage holding for over 150 h at 10 A g^{-1} was recorded from the highest voltage of 1.45 V, revealing an outstanding cycling performance of the device by retaining an efficiency of 71.6 %. The results established that RGO-S/200 mg Co_3O_4 is a good candidate for supercapacitor applications.

REFERENCES

[1] J.W. Lund, 100 Years of Geothermal Power Product, Proceedings. (2005) 1–10.

[2] T. Ma, H. Yang, L. Lu, Development of hybrid battery-supercapacitor energy storage for remote area renewable energy systems, Applied Energy. 153 (2015) 56–62. https://doi.org/10.1016/j.apenergy.2014.12.008.

[3] G. Kayakutlu, E. Mercier-Laurent, 3 - Intelligence for Energy, in: G. Kayakutlu, E. Mercier-Laurent (Eds.), Intelligence in Energy, Elsevier, 2017: pp. 79–116. https://doi.org/https://doi.org/10.1016/B978-1-78548-039-3.50003-1.

[4] A.R. Dehghani-Sanij, E. Tharumalingam, M.B. Dusseault, R. Fraser, Study of energy storage systems and environmental challenges of batteries, Renewable and Sustainable Energy Reviews. 104 (2019) 192–208. https://doi.org/10.1016/j.rser.2019.01.023.

[5] X. Zhang, L. Hou, A. Ciesielski, P. Samorì, 2D Materials Beyond Graphene for High-Performance Energy Storage Applications, Advanced Energy Materials. 6 (2016) 21. https://doi.org/10.1002/aenm.201600671.

[6] R.B. Rakhi, H.N. Alshareef, Enhancement of the energy storage properties of supercapacitors using graphene nanosheets dispersed with metal oxide-loaded carbon nanotubes, Journal of Power Sources. 196 (2011) 8858–8865. https://doi.org/10.1016/j.jpowsour.2011.06.038.

[7] A. Eftekhari, Metrics for Fast Supercapacitors as Energy Storage Devices, ACS Sustainable Chemistry and Engineering. 7 (2019) 3688–3691. https://doi.org/10.1021/acssuschemeng.7b04532.

[8] K.W. Nam, C.W. Lee, X.Q. Yang, B.W. Cho, W.S. Yoon, K.B. Kim, Electrodeposited manganese oxides on three-dimensional carbon nanotube substrate: Supercapacitive behaviour in aqueous and organic electrolytes, Journal of Power Sources. 188 (2009) 323–331. https://doi.org/10.1016/j.jpowsour.2008.11.133.

[9] P. Simon, Y. Gogotsi, P. Simon, Y. Gogotsi, N. Materials, Materials for electrochemical capacitors To cite this version : HAL Id : hal-02417326, 7 (2019) 845–854.

[10] M. Vangari, T. Pryor, L. Jiang, Supercapacitors: Review of materials and fabrication methods, Journal of Energy Engineering. 139 (2013) 72–79. https://doi.org/10.1061/(ASCE)EY.1943-7897.0000102.

[11] M. Hahn, O. Barbieri, R. Gallay, R. Kötz, A dilatometric study of the voltage limitation of carbonaceous electrodes in aprotic EDLC type electrolytes by charge-induced strain, Carbon. 44 (2006) 2523–2533. https://doi.org/10.1016/j.carbon.2006.05.002.

[12] M. Jayalakshmi, K. Balasubramanian, Simple capacitors to supercapacitors - An overview, International Journal of Electrochemical Science. 3 (2008) 1196–1217.

[13] Xian Jian, Shiyu Liu, Yuqi Gao, Wei Tian, Zhicheng Jiang, Xiangyun Xiao, Hui Tang, Liangjun Yin, Carbon-Based Electrode Materials for Supercapacitor: Progress, Challenges and Prospective Solutions, J. of Electrical Engineering. 4 (2016) 75–87. https://doi.org/10.17265/2328-2223/2016.02.004.

[14] S. Najib, E. Erdem, Current progress achieved in novel materials for supercapacitor electrodes: Mini review, Nanoscale Advances. 1 (2019) 2817–2827. https://doi.org/10.1039/c9na00345b.

[15] A. Noori, M.F. El-Kady, M.S. Rahmanifar, R.B. Kaner, M.F. Mousavi, Towards establishing standard performance metrics for batteries, supercapacitors and beyond, Chemical Society Reviews. 48 (2019) 1272–1341. https://doi.org/10.1039/c8cs00581h.

[16] B. Viswanathan, Chapter 13 - Supercapacitors, in: B. Viswanathan (Ed.), Energy Sources, Elsevier, Amsterdam, 2017: pp. 315–328. https://doi.org/https://doi.org/10.1016/B978-0-444-56353-8.00013-7.

[17] G.Z. Chen, Supercapacitor and supercapattery as emerging electrochemical energy stores, International Materials Reviews. 62 (2017) 173–202. https://doi.org/10.1080/09506608.2016.1240914.

[18] A.S. Lemine, M.M. Zagho, T.M. Altahtamouni, N. Bensalah, Graphene a promising electrode material for supercapacitors—A review, International Journal of Energy Research. 42 (2018) 4284–4300. https://doi.org/10.1002/er.4170.

[19] M.E. Uddin, T. Kuila, G.C. Nayak, N.H. Kim, B.C. Ku, J.H. Lee, Effects of various surfactants on the dispersion stability and electrical conductivity of surface modified graphene, Journal of Alloys and Compounds. 562 (2013) 134–142. https://doi.org/10.1016/j.jallcom.2013.01.127.

[20] Y. Bai, L. Lu, J. Bao, G. Sun, B. Zhang, J. Zeng, S. Chen, The preparation and electrochemical performance of nitrogen-doped graphene/Co(OH)2 composite, International Journal of Electrochemical Science. 14 (2019) 606–617. https://doi.org/10.20964/2019.01.48.

[21] Z. Lin, Y. Liu, Y. Yao, O.J. Hildreth, Z. Li, K. Moon, C.P. Wong, Superior capacitance of functionalized graphene, Journal of Physical Chemistry C. 115 (2011) 7120–7125. https://doi.org/10.1021/jp2007073.

[22] N.A. Kumar, J.B. Baek, Doped graphene supercapacitors, Nanotechnology. 26 (2015). https://doi.org/10.1088/0957-4484/26/49/492001.

[23] S. Verma, B. Verma, Synthesis of sulfur / phosphorous-doped graphene aerogel as a modified super capacitor electrode, (2018).

[24] S. Yaglikci, Y. Gokce, E. Yagmur, Z. Aktas, The performance of sulphur doped activated carbon supercapacitors prepared from waste tea, Environmental Technology. 0 (2019) 1–13. https://doi.org/10.1080/09593330.2019.1575480.

[25] X. Yu, S.K. Park, S.H. Yeon, H.S. Park, Three-dimensional, sulfur-incorporated

graphene aerogels for the enhanced performances of pseudocapacitive electrodes, Journal of Power Sources. 278 (2015) 484–489. https://doi.org/10.1016/j.jpowsour.2014.12.102.

[26] W. Zhang, F. Liu, Q. Li, Q. Shou, J. Cheng, L. Zhang, B.J. Nelson, X. Zhang, Transition metal oxide and graphene nanocomposites for high-performance electrochemical capacitors, Physical Chemistry Chemical Physics. 14 (2012) 16331–16337. https://doi.org/10.1039/c2cp43673f.

[27] Y. Wang, J. Guo, T. Wang, J. Shao, D. Wang, Y.W. Yang, Mesoporous transition metal oxides for supercapacitors, Nanomaterials. 5 (2015) 1667–1689. https://doi.org/10.3390/nano5041667.

[28] Y.T. Wang, A.H. Lu, H.L. Zhang, W.C. Li, Synthesis of Nanostructured mesoporous manganese oxides with three-dimensional frameworks and their application in supercapacitors, Journal of Physical Chemistry C. 115 (2011) 5413–5421. https://doi.org/10.1021/jp110938x.

[29] M. Pang, G. Long, S. Jiang, Y. Ji, W. Han, B. Wang, X. Liu, Y. Xi, D. Wang, F. Xu, Ethanol-assisted solvothermal synthesis of porous nanostructured cobalt oxides (CoO/Co3O4) for high-performance supercapacitors, Chemical Engineering Journal. 280 (2015) 377–384. https://doi.org/10.1016/j.cej.2015.06.053.

[30] P. Simon, Y. Gogotsi, Materials for electrochemical capacitors, Materials for Sustainable Energy: A Collection of Peer-Reviewed Research and Review Articles from Nature Publishing Group. (2010) 138–147. https://doi.org/10.1142/9789814317665_0021.

[31] Z. Song, Y. Zhang, W. Liu, S. Zhang, G. Liu, H. Chen, J. Qiu, Hydrothermal synthesis and electrochemical performance of Co 3O4/reduced graphene oxide nanosheet composites for supercapacitors, Electrochimica Acta. 112 (2013) 120–126.

https://doi.org/10.1016/j.electacta.2013.08.155.

[32] Q. Yang, Z. Li, R. Zhang, L. Zhou, M. Shao, M. Wei, Carbon modified transition metal oxides/hydroxides nanoarrays toward high-performance flexible all-solid-state supercapacitors, Nano Energy. 41 (2017) 408–416. https://doi.org/10.1016/j.nanoen.2017.09.049.

[33] Y. Chiang, Electrochemical Energy Storage for the Grid, World. (2010).

[34] M.S. Whittingham, History, evolution, and future status of energy storage, Proceedings of the IEEE. 100 (2012) 1518–1534. https://doi.org/10.1109/JPROC.2012.2190170.

[35] O. Razbani, M. Assadi, Artificial neural network model of a short stack solid oxide fuel cell based on experimental data, Journal of Power Sources. 246 (2014) 581–586. https://doi.org/10.1016/j.jpowsour.2013.08.018.

[36] P.N. Kanani, The Parthian Battery: Electric current 2000 years ago?, Fachzeitschrift Des VINI. (2004) 38.

[37] D.S. Ginley, D. Cahen, Fundamentals of materials for energy and environmental sustainability, Fundamentals of Materials for Energy and Environmental Sustainability. (2011) 1–753. https://doi.org/10.1017/CBO9780511718786.

[38] J. Ho, T.R. Jow, S. Boggs, Historical introduction to capacitor technology, IEEE Electrical Insulation Magazine. 26 (2010) 20–25. https://doi.org/10.1109/MEI.2010.5383924.

[39] J. Hedesan, J. Tendler, The structure of scientific revolutions, 2017. https://doi.org/10.4324/9781912281589.

[40] M.J. Ratcliff, Abraham Trembley's strategy of generosity and the scope of celebrity in the mid-eighteenth century., Isis; an International Review Devoted to the History of Science and Its Cultural Influences. 95 (2004) 555–575. https://doi.org/10.1086/430649.

[41] A. Allerhand, Who Invented the Earliest Capacitor Bank ("Battery" of Leyden Jars)? It's Complicated, Proceedings of the IEEE. 106 (2018) 496–503. https://doi.org/10.1109/JPROC.2018.2795846.

[42] J. Both, Electrolytic capacitors, 1890 to 1925: Early history and basic principle, IEEE Electrical Insulation Magazine. 31 (2015) 22–29. https://doi.org/10.1109/MEI.2015.6996675.

[43] M. Yassine, D. Fabris, Performance of commercially available supercapacitors, Energies. 10 (2017). https://doi.org/10.3390/en10091340.

[44] M. Hepel, High Energy-Density Electric Double-Layer and Hybrid Supercapacitors Based on Graphene Composites, Encyclopedia of Surface and Colloid Science, Third Edition. 1 (2015) 1–22. https://doi.org/10.1081/e-escs3-120051485.

[45] L. Zhang, High-Power Energy Storage: Ultracapacitors, Elsevier Inc., 2018. https://doi.org/10.1016/B978-0-12-812786-5.00002-1.

[46] H. Ji, X. Zhao, Z. Qiao, J. Jung, Y. Zhu, Y. Lu, L.L. Zhang, A.H. MacDonald, R.S. Ruoff, Capacitance of carbon-based electrical double-layer capacitors, Nature Communications. 5 (2014). https://doi.org/10.1038/ncomms4317.

[47] A. González, E. Goikolea, J.A. Barrena, R. Mysyk, Review on supercapacitors: Technologies and materials, Renewable and Sustainable Energy Reviews. 58 (2016) 1189–1206. https://doi.org/10.1016/j.rser.2015.12.249.

[48] M.M.M. Ahmed, T. Imae, Graphene-Based Nanolayers Toward Energy Storage Device, Elsevier B.V., 2017. https://doi.org/10.1016/B978-0-444-63739-0.00010-4.

[49] K.B. Oldham, A Gouy-Chapman-Stern model of the double layer at a (metal)/(ionic liquid) interface, Journal of Electroanalytical Chemistry. 613 (2008) 131–138. https://doi.org/10.1016/j.jelechem.2007.10.017.

[50] V.L. Shapovalov, G. Brezesinski, Breakdown of the Gouy - Chapman model for

highly charged Langmuir monolayers: Counterion size effect, Journal of Physical Chemistry B. 110 (2006) 10032–10040. https://doi.org/10.1021/jp056801b.

[51] M.A. Brown, G.V. Bossa, S. May, Emergence of a Stern Layer from the Incorporation of Hydration Interactions into the Gouy-Chapman Model of the Electrical Double Layer, Langmuir. 31 (2015) 11477–11483. https://doi.org/10.1021/acs.langmuir.5b02389.

[52] Y. Jiang, J. Liu, Definitions of Pseudocapacitive Materials: A Brief Review, Energy & Environmental Materials. 2 (2019) 30–37. https://doi.org/10.1002/eem2.12028.

[53] D. Majumdar, M. Mandal, S.K. Bhattacharya, Journey from supercapacitors to supercapatteries: recent advancements in electrochemical energy storage systems, Emergent Materials. (2020). https://doi.org/10.1007/s42247-020-00090-5.

[54] A. Muzaffar, M.B. Ahamed, K. Deshmukh, J. Thirumalai, A review on recent advances in hybrid supercapacitors: Design, fabrication and applications, Renewable and Sustainable Energy Reviews. 101 (2019) 123–145. https://doi.org/10.1016/j.rser.2018.10.026.

[55] X. Li, B. Wei, Supercapacitors based on nanostructured carbon, Nano Energy. 2 (2013) 159–173. https://doi.org/10.1016/j.nanoen.2012.09.008.

[56] J.P. Cheng, J. Zhang, F. Liu, Recent development of metal hydroxides as electrode material of electrochemical capacitors, RSC Advances. 4 (2014) 38893–38917. https://doi.org/10.1039/c4ra06738j.

[57] G.A. Snook, P. Kao, A.S. Best, Conducting-polymer-based supercapacitor devices and electrodes, Journal of Power Sources. 196 (2011) 1–12. https://doi.org/10.1016/j.jpowsour.2010.06.084.

[58] Y. Lu, G. Long, L. Zhang, T. Zhang, M. Zhang, F. Zhang, Y. Yang, Y. Ma, Y. Chen, What are the practical limits for the specific surface area and capacitance of bulk sp2

carbon materials?, Science China Chemistry. 59 (2016) 225–230. https://doi.org/10.1007/s11426-015-5474-y.

[59] A. Bianco, H.M. Cheng, T. Enoki, Y. Gogotsi, R.H. Hurt, N. Koratkar, T. Kyotani, M. Monthioux, C.R. Park, J.M.D. Tascon, J. Zhang, All in the graphene family - A recommended nomenclature for two-dimensional carbon materials, Carbon. 65 (2013) 1–6. https://doi.org/10.1016/j.carbon.2013.08.038.

[60] A. Benítez, A. Caballero, J. Morales, J. Hassoun, E. Rodríguez-Castellón, J. Canales-Vázquez, Physical activation of graphene: An effective, simple and clean procedure for obtaining microporous graphene for high-performance Li/S batteries, Nano Research. 12 (2019) 759–766. https://doi.org/10.1007/s12274-019-2282-2.

[61] H. Nguyen Bich, H. Nguyen Van, Promising applications of graphene and graphene-based nanostructures, Advances in Natural Sciences: Nanoscience and Nanotechnology. 7 (2016). https://doi.org/10.1088/2043-6262/7/2/023002.

[62] J. Yang, S. Gunasekaran, Electrochemically reduced graphene oxide sheets for use in high performance supercapacitors, Carbon. 51 (2013) 36–44. https://doi.org/10.1016/j.carbon.2012.08.003.

[63] W.S. Hummers, R.E. Offeman, Preparation of Graphitic Oxide, Journal of the American Chemical Society. 80 (1958) 1339. https://doi.org/10.1021/ja01539a017.

[64] P.L. Chiu, D.D.T. Mastrogiovanni, D. Wei, C. Louis, M. Jeong, G. Yu, P. Saad, C.R. Flach, R. Mendelsohn, E. Garfunkel, H. He, Microwave- and nitronium ion-enabled rapid and direct production of highly conductive low-oxygen graphene, Journal of the American Chemical Society. 134 (2012) 5850–5856. https://doi.org/10.1021/ja210725p.

[65] C.N.R. Rao, K.S. Subrahmanyam, H.S.S.R. Matte, B. Abdulhakeem, A. Govindaraj, B. Das, P. Kumar, A. Ghosh, D.J. Late, A study of the synthetic methods and

properties of graphenes, Science and Technology of Advanced Materials. 11 (2010). https://doi.org/10.1088/1468-6996/11/5/054502.

[66] F. Bonaccorso, A. Lombardo, T. Hasan, Z. Sun, L. Colombo, A.C. Ferrari, Production and processing of graphene and 2d crystals, Materials Today. 15 (2012) 564–589. https://doi.org/10.1016/S1369-7021(13)70014-2.

[67] K. Parvez, S. Yang, X. Feng, K. Müllen, Exfoliation of graphene via wet chemical routes, Synthetic Metals. 210 (2015) 123–132. https://doi.org/10.1016/j.synthmet.2015.07.014.

[68] M.J. Yoo, H.B. Park, Effect of hydrogen peroxide on properties of graphene oxide in Hummers method, Carbon. 141 (2019) 515–522. https://doi.org/10.1016/j.carbon.2018.10.009.

[69] Z. Tian, J. Li, G. Zhu, J. Lu, Y. Wang, Z. Shi, C. Xu, Facile synthesis of highly conductive sulfur-doped reduced graphene oxide sheets, Physical Chemistry Chemical Physics. 18 (2015) 1125–1130. https://doi.org/10.1039/c5cp05475c.

[70] Y. Li, G. Wang, T. Wei, Z. Fan, P. Yan, Nitrogen and sulfur co-doped porous carbon nanosheets derived from willow catkin for supercapacitors, Nano Energy. 19 (2016) 165–175. https://doi.org/10.1016/j.nanoen.2015.10.038.

[71] J. Han, L.L. Zhang, S. Lee, J. Oh, K.S. Lee, J.R. Potts, J. Ji, X. Zhao, R.S. Ruoff, S. Park, Generation of B-doped graphene nanoplatelets using a solution process and their supercapacitor applications, ACS Nano. 7 (2013) 19–26. https://doi.org/10.1021/nn3034309.

[72] F. Alvi, M.K. Ram, P.A. Basnayaka, E. Stefanakos, Y. Goswami, A. Kumar, Graphene-polyethylenedioxythiophene conducting polymer nanocomposite based supercapacitor, Electrochimica Acta. 56 (2011) 9406–9412. https://doi.org/10.1016/j.electacta.2011.08.024.

[73] M. Duraivel, S. Nagappan, B. Balamuralitharan, S. Selvam, S.N. Karthick, K. Prabakar, C.S. Ha, H.J. Kim, Superior one-pot synthesis of a doped graphene oxide electrode for a high power density supercapacitor, New Journal of Chemistry. 42 (2018) 11093–11101. https://doi.org/10.1039/c8nj01672k.

[74] A.K. Geim, K.S. Novoselov, The rise of graphene, Nature Materials. 6 (2007) 183–191. https://doi.org/10.1038/nmat1849.

[75] B. Quan, S.H. Yu, D.Y. Chung, A. Jin, J.H. Park, Y.E. Sung, Y. Piao, Single source precursor-based solvothermal synthesis of heteroatom-doped graphene and its energy storage and conversion applications, Scientific Reports. 4 (2014) 23–25. https://doi.org/10.1038/srep05639.

[76] P.Z. Guo, Q.Q. Ji, L.L. Zhang, S.Y. Zhao, X.S. Zhao, Preparation and characterization of peanut shell-based microporous carbons as electrode materials for supercapacitors, Wuli Huaxue Xuebao/ Acta Physico - Chimica Sinica. 27 (2011) 2836–2840. https://doi.org/10.3866/PKU.WHXB20112836.

[77] N.F. Sylla, N.M. Ndiaye, B.D. Ngom, D. Momodu, M.J. Madito, B.K. Mutuma, N. Manyala, Effect of porosity enhancing agents on the electrochemical performance of high-energy ultracapacitor electrodes derived from peanut shell waste, Scientific Reports. 9 (2019) 1–15. https://doi.org/10.1038/s41598-019-50189-x.

[78] K. Yang, J. Peng, C. Srinivasakannan, L. Zhang, H. Xia, X. Duan, Preparation of high surface area activated carbon from coconut shells using microwave heating, Bioresource Technology. 101 (2010) 6163–6169. https://doi.org/10.1016/j.biortech.2010.03.001.

[79] L. Khezami, A. Chetouani, B. Taouk, R. Capart, Production and characterisation of activated carbon from wood components in powder: Cellulose, lignin, xylan, Powder Technology. 157 (2005) 48–56. https://doi.org/10.1016/j.powtec.2005.05.009.

[80] I.I.G. Inal, S.M. Holmes, A. Banford, Z. Aktas, The performance of supercapacitor electrodes developed from chemically activated carbon produced from waste tea, Applied Surface Science. 357 (2015) 696–703. https://doi.org/10.1016/j.apsusc.2015.09.067.

[81] H. Pan, J. Li, Y.P. Feng, Carbon nanotubes for supercapacitor, Nanoscale Research Letters. 5 (2010) 654–668. https://doi.org/10.1007/s11671-009-9508-2.

[82] J. Kong, A.M. Cassell, H. Dai, Chemical vapor deposition of methane for single-walled carbon nanotubes, Chemical Physics Letters. 292 (1998) 567–574. https://doi.org/10.1016/S0009-2614(98)00745-3.

[83] C.D. Scott, S. Arepalli, P. Nikolaev, R.E. Smalley, Growth mechanisms for single-wall carbon nanotubes in a laser-ablation process, Applied Physics A: Materials Science and Processing. 72 (2001) 573–580. https://doi.org/10.1007/s003390100761.

[84] J.L. Hutchison, N.A. Kiselev, E.P. Krinichnaya, A. V. Krestinin, R.O. Loutfy, A.P. Morawsky, V.E. Muradyan, E.D. Obraztsova, J. Sloan, S. V. Terekhov, D.N. Zakharov, Double-walled carbon nanotubes fabricated by a hydrogen arc discharge method, Carbon. 39 (2001) 761–770. https://doi.org/10.1016/S0008-6223(00)00187-1.

[85] C. qi YI, J. peng ZOU, H. zhi YANG, X. LENG, Recent advances in pseudocapacitor electrode materials: Transition metal oxides and nitrides, Transactions of Nonferrous Metals Society of China (English Edition). 28 (2018) 1980–2001. https://doi.org/10.1016/S1003-6326(18)64843-5.

[86] A.N. Naveen, P. Manimaran, S. Selladurai, Cobalt oxide (Co3O4)/graphene nanosheets (GNS) composite prepared by novel route for supercapacitor application, Journal of Materials Science: Materials in Electronics. 26 (2015) 8988–9000. https://doi.org/10.1007/s10854-015-3582-2.

[87] M. Toupin, T. Brousse, D. Bélanger, Charge storage mechanism of MnO2 electrode

used in aqueous electrochemical capacitor, Chemistry of Materials. 16 (2004) 3184–3190. https://doi.org/10.1021/cm049649j.

[88] L.-B. Kong, M. Liu, J.-W. Lang, Y.-C. Luo, L. Kang, Asymmetric Supercapacitor Based on Loose-Packed Cobalt Hydroxide Nanoflake Materials and Activated Carbon, Journal of The Electrochemical Society. 156 (2009) A1000. https://doi.org/10.1149/1.3236500.

[89] A. Bello, K. Makgopa, M. Fabiane, D. Dodoo-Ahrin, K.I. Ozoemena, N. Manyala, Chemical adsorption of NiO nanostructures on nickel foam-graphene for supercapacitor applications, Journal of Materials Science. 48 (2013) 6707–6712. https://doi.org/10.1007/s10853-013-7471-x.

[90] H. Kelly-Holmes, Principles and applications of electrochemical capacitors, Electrochimica Acta 45. 45 (2000) 2483–2498. https://doi.org/10.1057/9780230503014.

[91] F. Zhang, D. Zhu, X. Chen, X. Xu, Z. Yang, C. Zou, K. Yang, S. Huang, A nickel hydroxide-coated 3D porous graphene hollow sphere framework as a high performance electrode material for supercapacitors, Physical Chemistry Chemical Physics. 16 (2014) 4186–4192. https://doi.org/10.1039/c3cp54334j.

[92] F. Li, J. Song, H. Yang, S. Gan, Q. Zhang, D. Han, A. Ivaska, L. Niu, One-step synthesis of graphene/{SnO}2nanocomposites and its application in electrochemical supercapacitors, Nanotechnology. 20 (2009) 455602. https://doi.org/10.1088/0957-4484/20/45/455602.

[93] H. Wang, Q. Fu, C. Pan, Green mass synthesis of graphene oxide and its MnO2 composite for high performance supercapacitor, Electrochimica Acta. 312 (2019) 11–21. https://doi.org/10.1016/j.electacta.2019.04.178.

[94] A. Numan, N. Duraisamy, F. Saiha Omar, Y.K. Mahipal, K. Ramesh, S. Ramesh,

Enhanced electrochemical performance of cobalt oxide nanocube intercalated reduced graphene oxide for supercapacitor application, RSC Advances. 6 (2016) 34894–34902. https://doi.org/10.1039/c6ra00160b.

[95] S. Park, S. Kim, Effect of carbon blacks filler addition on electrochemical behaviors of Co3O4/graphene nanosheets as a supercapacitor electrodes, Electrochimica Acta. 89 (2013) 516–522. https://doi.org/10.1016/j.electacta.2012.11.075.

[96] H.J. Ahonen, J. Lukkari, J. Kankare, n- and p-doped poly(3,4-ethylenedioxythiophene): Two electronically conducting states of the polymer, Macromolecules. 33 (2000) 6787–6793. https://doi.org/10.1021/ma0004312.

[97] Y. Huang, H. Li, Z. Wang, M. Zhu, Z. Pei, Q. Xue, Y. Huang, C. Zhi, Nanostructured Polypyrrole as a flexible electrode material of supercapacitor, Nano Energy. 22 (2016) 422–438. https://doi.org/10.1016/j.nanoen.2016.02.047.

[98] K.S. Ryu, Y.G. Lee, Y.S. Hong, Y.J. Park, X. Wu, K.M. Kim, M.G. Kang, N.G. Park, S.H. Chang, Poly(ethylenedioxythiophene) (PEDOT) as polymer electrode in redox supercapacitor, Electrochimica Acta. 50 (2004) 843–847. https://doi.org/10.1016/j.electacta.2004.02.055.

[99] A. Laforgue, P. Simon, C. Sarrazin, J.F. Fauvarque, Polythiophene-based supercapacitors, Journal of Power Sources. 80 (1999) 142–148. https://doi.org/10.1016/S0378-7753(98)00258-4.

[100] X. Cao, H.Y. Zeng, S. Xu, J. Yuan, J. Han, G.F. Xiao, Facile fabrication of the polyaniline/layered double hydroxide nanosheet composite for supercapacitors, Applied Clay Science. 168 (2019) 175–183. https://doi.org/10.1016/j.clay.2018.11.011.

[101] M.A.A. Mohd Abdah, N.H.N. Azman, S. Kulandaivalu, Y. Sulaiman, Review of the use of transition-metal-oxide and conducting polymer-based fibres for high-

performance supercapacitors, Materials and Design. 186 (2020) 108199. https://doi.org/10.1016/j.matdes.2019.108199.

[102] H.W. Wang, Z.A. Hu, Y.Q. Chang, Y.L. Chen, Z.Y. Zhang, Y.Y. Yang, H.Y. Wu, Preparation of reduced graphene oxide/cobalt oxide composites and their enhanced capacitive behaviors by homogeneous incorporation of reduced graphene oxide sheets in cobalt oxide matrix, Materials Chemistry and Physics. 130 (2011) 672–679. https://doi.org/10.1016/j.matchemphys.2011.07.043.

[103] C. Zhong, Y. Deng, W. Hu, D. Sun, X. Han, J. Qiao, J. Zhang, Electrolytes for electrochemical supercapacitors, 2016. https://doi.org/10.1201/b21497-3.

[104] C. Zhong, Y. Deng, W. Hu, J. Qiao, L. Zhang, J. Zhang, A review of electrolyte materials and compositions for electrochemical supercapacitors, Chemical Society Reviews. 44 (2015) 7484–7539. https://doi.org/10.1039/c5cs00303b.

[105] L. Demarconnay, E. Raymundo-Piñero, F. Béguin, A symmetric carbon/carbon supercapacitor operating at 1.6 v by using a neutral aqueous solution, Electrochemistry Communications. 12 (2010) 1275–1278. https://doi.org/10.1016/j.elecom.2010.06.036.

[106] D. Jiménez-Cordero, F. Heras, M.A. Gilarranz, E. Raymundo-Piñero, Grape seed carbons for studying the influence of texture on supercapacitor behaviour in aqueous electrolytes, Carbon. 71 (2014) 127–138. https://doi.org/10.1016/j.carbon.2014.01.021.

[107] H. Wu, X. Wang, L. Jiang, C. Wu, Q. Zhao, X. Liu, B. Hu, L. Yi, The effects of electrolyte on the supercapacitive performance of activated calcium carbide-derived carbon, Journal of Power Sources. 226 (2013) 202–209. https://doi.org/10.1016/j.jpowsour.2012.11.014.

[108] K. Fic, G. Lota, M. Meller, E. Frackowiak, Novel insight into neutral medium as electrolyte for high-voltage supercapacitors, Energy and Environmental Science. 5 (2012) 5842–5850. https://doi.org/10.1039/c1ee02262h.

[109] K. Fic, G. Lota, E. Frackowiak, Effect of surfactants on capacitance properties of carbon electrodes, Electrochimica Acta. 60 (2012) 206–212. https://doi.org/10.1016/j.electacta.2011.11.059.

[110] P. Sun, Z. Li, L. Zhang, C. Dong, Z. Li, H. Yao, J. Wang, G. Li, Synthesis of cobalt-nickel pyrophosphates/N-doped graphene composites with high rate capability for asymmetric supercapacitor, Journal of Alloys and Compounds. 750 (2018) 607–616. https://doi.org/10.1016/j.jallcom.2018.04.024.

[111] A. Brandt, S. Pohlmann, A. Varzi, A. Balducci, S. Passerini, Ionic liquids in supercapacitors, MRS Bulletin. 38 (2013) 554–559. https://doi.org/10.1557/mrs.2013.151.

[112] J.S. Skyler, Ionic-liquid materials for the electrochemical challenges of the future, Endocrinologist. 3 (1993) 233–238. https://doi.org/10.1097/00019616-199307000-00001.

[113] P.W. Ruch, D. Cericola, A. Foelske-Schmitz, R. Kötz, A. Wokaun, Aging of electrochemical double layer capacitors with acetonitrile-based electrolyte at elevated voltages, Electrochimica Acta. 55 (2010) 4412–4420. https://doi.org/10.1016/j.electacta.2010.02.064.

[114] S. Vaquero, R. Díaz, M. Anderson, J. Palma, R. Marcilla, Insights into the influence of pore size distribution and surface functionalities in the behaviour of carbon supercapacitors, Electrochimica Acta. 86 (2012) 241–247. https://doi.org/10.1016/j.electacta.2012.08.006.

[115] E. Raymundo-Piñero, K. Kierzek, J. Machnikowski, F. Béguin, Relationship between the nanoporous texture of activated carbons and their capacitance properties in different electrolytes, Carbon. 44 (2006) 2498–2507. https://doi.org/10.1016/j.carbon.2006.05.022.

[116] Y.T. Pi, Y.T. Li, S.S. Xu, X.Y. Xing, H.K. Ma, Z.B. He, T.Z. Ren, Is the conductive agent useful in electrodes of graphitized activated carbon?, RSC Advances. 6 (2016) 100708–100712. https://doi.org/10.1039/c6ra18246a.

[117] S. Priyono, T.D. Sari, Ramlan, A. Subhan, B. Prihandoko, Effect of polymer binders on the electrochemical Performance of Al-doped lithium titanate electrode, Journal of Physics: Conference Series. 1282 (2019). https://doi.org/10.1088/1742-6596/1282/1/012056.

[118] M.D. Stoller, R.S. Ruoff, Best practice methods for determining an electrode material's performance for ultracapacitors, Energy and Environmental Science. 3 (2010) 1294–1301. https://doi.org/10.1039/c0ee00074d.

[119] N. Elgrishi, K.J. Rountree, B.D. McCarthy, E.S. Rountree, T.T. Eisenhart, J.L. Dempsey, A Practical Beginner's Guide to Cyclic Voltammetry, Journal of Chemical Education. 95 (2018) 197–206. https://doi.org/10.1021/acs.jchemed.7b00361.

[120] S. Zhang, N. Pan, Supercapacitors Performance Evaluation - Zhang - 2015 - Advanced Energy Materials - Wiley Online Library, Advanced Energy Materials. (2015). https://onlinelibrary.wiley.com/doi/pdf/10.1002/aenm.201401401.

[121] D.J. Tarimo, K.O. Oyedotun, A.A. Mirghni, N. Manyala, Sulphur-reduced graphene oxide composite with improved electrochemical performance for supercapacitor applications, International Journal of Hydrogen Energy. 45 (2020). https://doi.org/10.1016/j.ijhydene.2020.03.059.

[122] M. Lu, F. Beguin, E. Frackowiak, Supercapacitors : Materials, Systems, and Applications, Wiley VCH, Weinheim, 2013.

[123] D.J. Tarimo, K.O. Oyedotun, A.A. Mirghni, N.F. Sylla, N. Manyala, High energy and excellent stability asymmetric supercapacitor derived from sulphur-reduced graphene oxide/manganese dioxide composite and activated carbon from peanut shell,

Electrochimica Acta. 353 (2020) 136498. https://doi.org/10.1016/j.electacta.2020.136498.

[124] A.A. Mirghni, K.O. Oyedotun, B.A. Mahmoud, A. Bello, S.C. Ray, N. Manyala, Nickel-cobalt phosphate/graphene foam as enhanced electrode for hybrid supercapacitor, Composites Part B: Engineering. 174 (2019) 106953. https://doi.org/10.1016/j.compositesb.2019.106953.

[125] J.H. Chae, G.Z. Chen, 1.9 V Aqueous Carbon-Carbon Supercapacitors With Unequal Electrode Capacitances, Electrochimica Acta. 86 (2012) 248–254. https://doi.org/10.1016/j.electacta.2012.07.033.

[126] F. Ochai-Ejeh, M.J. Madito, K. Makgopa, M.N. Rantho, O. Olaniyan, N. Manyala, Electrochemical performance of hybrid supercapacitor device based on birnessite-type manganese oxide decorated on uncapped carbon nanotubes and porous activated carbon nanostructures, Electrochimica Acta. 289 (2018) 363–375. https://doi.org/10.1016/j.electacta.2018.09.032.

[127] N. Aristov, A. Habekost, Cyclic Voltammetry - A Versatile Electrochemical Method Investigating Electron Transfer Processes, World Journal of Chemical Education, Vol. 3, 2015, Pages 115-119. 3 (2015) 115–119. https://doi.org/10.12691/WJCE-3-5-2.

[128] T.S. Mathis, N. Kurra, X. Wang, D. Pinto, P. Simon, Y. Gogotsi, Energy Storage Data Reporting in Perspective—Guidelines for Interpreting the Performance of Electrochemical Energy Storage Systems, Advanced Energy Materials. 9 (2019) 1–13. https://doi.org/10.1002/aenm.201902007.

[129] S. Alehashem, F. Chambers, J.W. Strojek, G.M. Swain, R. Ramesham, Cyclic Voltammetric Studies of Charge Transfer Reactions at Highly Boron-Doped Polycrystalline Diamond Thin-Film Electrodes, Analytical Chemistry. 67 (1995) 2812–2821. https://doi.org/10.1021/ac00113a014.

[130] W. Zhang, C. Ma, J. Fang, J. Cheng, X. Zhang, S. Dong, L. Zhang, Asymmetric electrochemical capacitors with high energy and power density based on graphene/CoAl-LDH and activated carbon electrodes, RSC Advances. 3 (2013) 2483–2490. https://doi.org/10.1039/c2ra23283a.

[131] Allen J. Bard and Larry R. Faulkner, Electrochemical Methods: Fundamentals and Applications, New York: Wiley, 2001, 2nd ed., Russian Journal of Electrochemistry. 38 (2002) 1364–1365. https://doi.org/10.1023/A:1021637209564.

[132] B. Akinwolemiwa, C. Peng, G.Z. Chen, Redox Electrolytes in Supercapacitors, Journal of The Electrochemical Society. 162 (2015) A5054–A5059. https://doi.org/10.1149/2.0111505jes.

[133] A.S. Ambrozevich, S.A. Ambrozevich, R.T. Sibatov, V. V. Uchaikin, Features of Charging–Discharging of Supercapacitors, Russian Electrical Engineering. 89 (2018) 64–70. https://doi.org/10.3103/S1068371218010029.

[134] S. Ban, J. Zhang, L. Zhang, K. Tsay, D. Song, X. Zou, Charging and discharging electrochemical supercapacitors in the presence of both parallel leakage process and electrochemical decomposition of solvent, Electrochimica Acta. 90 (2013) 542–549. https://doi.org/10.1016/j.electacta.2012.12.056.

[135] P.L. Taberna, P. Simon, J.F. Fauvarque, Electrochemical Characteristics and Impedance Spectroscopy Studies of Carbon-Carbon Supercapacitors, Journal of The Electrochemical Society. 150 (2003) A292. https://doi.org/10.1149/1.1543948.

[136] K. Hara, H. Arakawa, C. Dssc, S. Cell, D. Physics, K.M. Jeerage, R.D. Noble, C.A. Koval, M. Kouhnavard, N. Ahmad, L. Babak, V. Ghaffari, N. Chandra, D. Nath, H. Joon, W. Choi, J. Lee, Impedance Spectroscopy Theory, Experiment, and Applications, 2013. https://doi.org/10.1016/j.snb.2007.02.003.

[137] R. Negroiu, P. Svasta, C. Ionescu, A. Vasile, Investigation of Supercapacitor's

Impedance Based on Spectroscopic Measurements, (n.d.).

[138] F. Mansfeld, Analysis and Interpretation of EIS Data for Metals and Alloys - An Introduction to Electrochemical Impedance Measurement, (1999) 1–77.

[139] D.Y. Momodu, Investigation of metal hydroxides graphene composites as electrode materials for supercapacitor applications, (2015) 185. http://repository.up.ac.za/handle/2263/50281.

[140] B.A. Mei, O. Munteshari, J. Lau, B. Dunn, L. Pilon, Physical Interpretations of Nyquist Plots for EDLC Electrodes and Devices, Journal of Physical Chemistry C. 122 (2018) 194–206. https://doi.org/10.1021/acs.jpcc.7b10582.

[141] A. Allison, H.A. Andreas, Minimizing the Nyquist-plot semi-circle of pseudocapacitive manganese oxides through modification of the oxide-substrate interface resistance, Journal of Power Sources. 426 (2019) 93–96. https://doi.org/10.1016/j.jpowsour.2019.04.029.

[142] J. Bisquert, G. Garcia-Belmonte, P. Bueno, E. Longo, L.O.S. Bulhões, Impedance of constant phase element (CPE)-blocked diffusion in film electrodes, Journal of Electroanalytical Chemistry. 452 (1998) 229–234. https://doi.org/10.1016/S0022-0728(98)00115-6.

[143] H. Liu, M.G. George, N. Ge, D. Muirhead, P. Shrestha, J. Lee, R. Banerjee, R. Zeis, M. Messerschmidt, J. Scholta, P. Krolla, A. Bazylak, Microporous Layer Degradation in Polymer Electrolyte Membrane Fuel Cells, Journal of The Electrochemical Society. 165 (2018) F3271–F3280. https://doi.org/10.1149/2.0291806jes.

[144] A. Khosrozadeh, G. Singh, Q. Wang, G. Luo, M. Xing, Supercapacitor with extraordinary cycling stability and high rate from nano-architectured polyaniline/graphene on Janus nanofibrous film with shape memory, Journal of Materials Chemistry A. 6 (2018) 21064–21077. https://doi.org/10.1039/C8TA07426G.

[145] A. Laheäär, P. Przygocki, Q. Abbas, F. Béguin, Appropriate methods for evaluating the efficiency and capacitive behavior of different types of supercapacitors, Electrochemistry Communications. 60 (2015) 21–25. https://doi.org/10.1016/j.elecom.2015.07.022.

[146] A. Bello, F. Barzegar, M.J. Madito, D.Y. Momodu, A.A. Khaleed, T.M. Masikhwa, J.K. Dangbegnon, N. Manyala, Stability studies of polypyrole- derived carbon based symmetric supercapacitor via potentiostatic floating test, Electrochimica Acta. 213 (2016) 107–114. https://doi.org/10.1016/j.electacta.2016.06.151.

[147] D. Weingarth, A. Foelske-Schmitz, R. Kötz, Cycle versus voltage hold - Which is the better stability test for electrochemical double layer capacitors?, Journal of Power Sources. 225 (2013) 84–88. https://doi.org/10.1016/j.jpowsour.2012.10.019.

[148] J. Kowal, E. Avaroglu, F. Chamekh, A. Šenfelds, T. Thien, D. Wijaya, D.U. Sauer, Detailed analysis of the self-discharge of supercapacitors, Journal of Power Sources. 196 (2011) 573–579. https://doi.org/10.1016/j.jpowsour.2009.12.028.

[149] J. Niu, B.E. Conway, W.G. Pell, Comparative studies of self-discharge by potential decay and float-current measurements at C double-layer capacitor and battery electrodes, Journal of Power Sources. 135 (2004) 332–343. https://doi.org/10.1016/j.jpowsour.2004.03.068.

[150] L. Staudenmaier, Verfahren zur darstellung der graphitsäure, Berichte Der Deutschen Chemischen Gesellschaft. 31 (1898) 1481–1487.

[151] J. Chen, B. Yao, C. Li, G. Shi, An improved Hummers method for eco-friendly synthesis of graphene oxide, Carbon. 64 (2013) 225–229. https://doi.org/10.1016/j.carbon.2013.07.055.

[152] D.C. Marcano, D. V. Kosynkin, J.M. Berlin, A. Sinitskii, Z. Sun, A. Slesarev, L.B. Alemany, W. Lu, J.M. Tour, Improved synthesis of graphene oxide, ACS Nano. 4

(2010) 4806–4814. https://doi.org/10.1021/nn1006368.

[153] I.V.G. and A.A.F. K. S. Novoselov, A. K. Geim, S. V. Morozov, D. Jiang, Y. Zhang, S. V. Dubonos, Electric Field Effect in Atomically Thin Carbon Films, 306 (2016) 666–669.

[154] S.C. Tsinontides, P. Rajniak, D. Pham, W.A. Hunke, J. Placek, S.D. Reynolds, Freeze drying - Principles and practice for successful scale-up to manufacturing, International Journal of Pharmaceutics. 280 (2004) 1–16. https://doi.org/10.1016/j.ijpharm.2004.04.018.

[155] Lyophilization/Freeze Drying - An Review 7, (n.d.) 2700.

[156] Z. Ling, C. Yu, X. Fan, S. Liu, J. Yang, M. Zhang, G. Wang, N. Xiao, J. Qiu, Freeze-drying for sustainable synthesis of nitrogen doped porous carbon cryogel with enhanced supercapacitor and lithium ion storage performance, Nanotechnology. 26 (2015). https://doi.org/10.1088/0957-4484/26/37/374003.

[157] S. Singh, Lyophilization/Freeze drying - A review, Age. 20 (2015) 60yrs.

[158] J. Zhang, Z. Yang, X. Wang, T. Ren, Q. Qiao, Homogeneous sulphur-doped composites: Porous carbon materials with unique hierarchical porous nanostructure for super-capacitor application, RSC Advances. 6 (2016) 84847–84853. https://doi.org/10.1039/c6ra17231h.

[159] J. Li, Q. Wu, J. Wu, T.S. Division, O. Ridge, O. Ridge, C. Sciences, E. Division, Handbook of Nanoparticles, Handbook of Nanoparticles. (2015). https://doi.org/10.1007/978-3-319-13188-7.

[160] D. Rickard, G.W. Luther, Chemistry of iron sulfides, 2007. https://doi.org/10.1021/cr0503658.

[161] A.E. Lewis, Review of metal sulphide precipitation, Hydrometallurgy. 104 (2010) 222–234. https://doi.org/10.1016/j.hydromet.2010.06.010.

[162] J. Grandgirard, D. Poinsot, L. Krespi, J.P. Nénon, A.M. Cortesero, Conventional and Microwave Hydrothermal Synthesis and Application of Functional Materials: A Review, Entomologia Experimentalis et Applicata. 103 (2002) 239–248. https://doi.org/10.1023/A.

[163] Y.X. Gan, A.H. Jayatissa, Z. Yu, X. Chen, M. Li, Hydrothermal Synthesis of Nanomaterials, Journal of Nanomaterials. 2020 (2020). https://doi.org/10.1155/2020/8917013.

[164] G. Sharma, A. Kumar, S. Sharma, M. Naushad, R. Prakash Dwivedi, Z.A. ALOthman, G.T. Mola, Novel development of nanoparticles to bimetallic nanoparticles and their composites: A review, Journal of King Saud University - Science. 31 (2019) 257–269. https://doi.org/10.1016/j.jksus.2017.06.012.

[165] Y. Dahman, Chapter 6 - Nanopolymers**By Yaser Dahman, Kevin Deonanan, Timothy Dontsos, and Andrew Iammatteo., in: Y. Dahman (Ed.), Nanotechnology and Functional Materials for Engineers, Elsevier, 2017: pp. 121–144. https://doi.org/https://doi.org/10.1016/B978-0-323-51256-5.00006-X.

[166] B. Akturk, A.B. Kizilkanat, Improvement of durability and drying shrinkage of sodium carbonate activated slag through the incorporation of calcium hydroxide and sodium hydroxide, Construction and Building Materials. 243 (2020) 118260. https://doi.org/10.1016/j.conbuildmat.2020.118260.

[167] S. Barzgar, B. Lothenbach, M. Tarik, A. Di Giacomo, C. Ludwig, The effect of sodium hydroxide on Al uptake by calcium silicate hydrates (C[sbnd]S[sbnd]H), Journal of Colloid and Interface Science. 572 (2020) 246–256. https://doi.org/10.1016/j.jcis.2020.03.057.

[168] H.D. Alvarenga, T. Van De Putte, N. Van Steenberge, J. Sietsma, H. Terryn, Influence of Carbide Morphology and Microstructure on the Kinetics of Superficial

Decarburization of C-Mn Steels, Metallurgical and Materials Transactions A: Physical Metallurgy and Materials Science. 46 (2015) 123–133. https://doi.org/10.1007/s11661-014-2600-y.

[169] K. Xiao, H. Wu, H. Lv, X. Wu, H. Qian, The study of the effects of cooling conditions on high quality graphene growth by the APCVD method, Nanoscale. 5 (2013) 5524–5529. https://doi.org/10.1039/c3nr00524k.

[170] K.O. Oyedotun, M.J. Madito, D.Y. Momodu, A.A. Mirghni, T.M. Masikhwa, N. Manyala, Synthesis of ternary NiCo-MnO2 nanocomposite and its application as a novel high energy supercapattery device, Chemical Engineering Journal. 335 (2018) 416–433. https://doi.org/10.1016/j.cej.2017.10.169.

[171] J.D. Andrade, X-ray photoelectron spectroscopy (XPS), in: Surface and Interfacial Aspects of Biomedical Polymers, Springer, 1985: pp. 105–195.

[172] G. Greczynski, L. Hultman, X-ray photoelectron spectroscopy: Towards reliable binding energy referencing, Progress in Materials Science. 107 (2020) 100591. https://doi.org/10.1016/j.pmatsci.2019.100591.

[173] R. Kohli, K.L. Mittal, eds., Chapter 3 - Methods for Assessing Surface Cleanliness, in: Developments in Surface Contamination and Cleaning, Volume 12, Elsevier, 2019: pp. 23–105. https://doi.org/https://doi.org/10.1016/B978-0-12-816081-7.00003-6.

[174] J. Epp, X-ray diffraction (XRD) techniques for materials characterization, in: Materials Characterization Using Nondestructive Evaluation (NDE) Methods, Elsevier, 2016: pp. 81–124.

[175] J.P. Patel, P.H. Parsania, 3 - Characterization, testing, and reinforcing materials of biodegradable composites, in: N.G. Shimpi (Ed.), Biodegradable and Biocompatible Polymer Composites, Woodhead Publishing, 2018: pp. 55–79. https://doi.org/https://doi.org/10.1016/B978-0-08-100970-3.00003-1.

[176] O.I. Olubiyi, F.-K. Lu, D. Calligaris, F.A. Jolesz, N.Y. Agar, Advances in molecular imaging for surgery, in: Image-Guided Neurosurgery, Elsevier, 2015: pp. 407–439.

[177] P. Vandenabeele, Practical Raman spectroscopy: an introduction, John Wiley & Sons, 2013.

[178] K.S. Joya, X. Sala, In situ Raman and surface-enhanced Raman spectroscopy on working electrodes: Spectroelectrochemical characterization of water oxidation electrocatalysts, Physical Chemistry Chemical Physics. 17 (2015) 21094–21103. https://doi.org/10.1039/c4cp05053c.

[179] K. Kneipp, H. Kneipp, P. Corio, S.D.M. Brown, K. Shafer, J. Motz, L.T. Perelman, E.B. Hanlon, A. Marucci, G. Dresselhaus, M.S. Dresselhaus, Surface-enhanced and normal stokes and anti-stokes raman spectroscopy of single-walled carbon nanotubes, Physical Review Letters. 84 (2000) 3470–3473. https://doi.org/10.1103/PhysRevLett.84.3470.

[180] A.T. Ward, Raman spectroscopy of sulfur, sulfur-selenium, and sulfur-arsenic mixtures, Journal of Physical Chemistry. 72 (1968) 4133–4139. https://doi.org/10.1021/j100858a031.

[181] C. Nims, B. Cron, M. Wetherington, J. Macalady, J. Cosmidis, Low frequency Raman Spectroscopy for micron-scale and in vivo characterization of elemental sulfur in microbial samples, Scientific Reports. 9 (2019) 1–12. https://doi.org/10.1038/s41598-019-44353-6.

[182] G. Guimbretière, S. Duraipandian, T. Ricci, Field remote Stokes/anti-Stokes Raman characterization of sulfur in hydrothermal vents, Journal of Raman Spectroscopy. 49 (2018) 1385–1394. https://doi.org/10.1002/jrs.5378.

[183] G.S. Allan, Fourier Transform Infrared Spectroscopy (FTIR), Encyclopedia of Earth Sciences Series. (2017) 1046. https://doi.org/10.1007/978-1-4020-4409-0.

[184] P.M. Shameer, P.M. Nishath, Exploration and enhancement on fuel stability of biodiesel: A step forward in the track of global commercialization, in: Advanced Biofuels, Elsevier, 2019: pp. 181–213.

[185] D. Titus, E.J.J. Samuel, S.M. Roopan, Nanoparticle characterization techniques, in: Green Synthesis, Characterization and Applications of Nanoparticles, Elsevier, 2019: pp. 303–319.

[186] N.J. and D.R. Vij, FOURIER TRANSFORM INFRARED SPECTROSCOPY, 2006. https://doi.org/10.1007/0-387-37590-2.

[187] M. Salouti, F.K. Derakhshan, Chapter 3 - Phytosynthesis of Nanoscale Materials, in: M. Ghorbanpour, S.H. Wani (Eds.), Advances in Phytonanotechnology, Academic Press, 2019: pp. 45–121. https://doi.org/https://doi.org/10.1016/B978-0-12-815322-2.00003-1.

[188] J.I. Goldstein, D.E. Newbury, J.R. Michael, N.W.M. Ritchie, J.H.J. Scott, D.C. Joy, Scanning electron microscopy and X-ray microanalysis, Springer, 2017.

[189] A.K. Singh, Chapter 4 - Experimental Methodologies for the Characterization of Nanoparticles, in: A.K. Singh (Ed.), Engineered Nanoparticles, Academic Press, Boston, 2016: pp. 125–170. https://doi.org/https://doi.org/10.1016/B978-0-12-801406-6.00004-2.

[190] J. Telegdi, A. Shaban, G. Vastag, Biocorrosion-steel, in: Encyclopedia of Interfacial Chemistry: Surface Science and Electrochemistry, Elsevier, 2018: pp. 28–42.

[191] O.D. Neikov, N.A. Yefimov, Chapter 1 - Powder Characterization and Testing, in: O.D. Neikov, S.S. Naboychenko, N.A. Yefimov (Eds.), Handbook of Non-Ferrous Metal Powders (Second Edition), Second Edi, Elsevier, Oxford, 2019: pp. 3–62. https://doi.org/https://doi.org/10.1016/B978-0-08-100543-9.00001-4.

[192] J. Bergström, 2 - Experimental Characterization Techniques, in: J. Bergström (Ed.),

Mechanics of Solid Polymers, William Andrew Publishing, 2015: pp. 19–114. https://doi.org/https://doi.org/10.1016/B978-0-323-31150-2.00002-9.

[193] T. Walther, Chapter 4 - Transmission Electron Microscopy of Nanostructures, in: S. Thomas, R. Thomas, A.K. Zachariah, R.K. Mishra (Eds.), Microscopy Methods in Nanomaterials Characterization, Elsevier, 2017: pp. 105–134. https://doi.org/https://doi.org/10.1016/B978-0-323-46141-2.00004-3.

[194] C. Escalante, E. Sierra, Fundamentals of transmission electron microscopy, the technique with the best resolution in the world, (2019) 0–6.

[195] R.T. G, A.B. R, Review Article TRANSMISSION ELECTRON MICROSCOPY-AN OVERVIEW ISSN Online : - 2321-7855 International Research Journal for Inventions in TRANSMISSION ELECTRON MICROSCOPY- AN OVERVIEW, (2019).

[196] S. Brunauer, L.S. Deming, W.E. Deming, E. Teller, On a Theory of the van der Waals Adsorption of Gases, Journal of the American Chemical Society. 62 (1940) 1723–1732. https://doi.org/10.1021/ja01864a025.

[197] M. Thommes, K. Kaneko, A. V. Neimark, J.P. Olivier, F. Rodriguez-Reinoso, J. Rouquerol, K.S.W. Sing, Physisorption of gases, with special reference to the evaluation of surface area and pore size distribution (IUPAC Technical Report), Pure and Applied Chemistry. 87 (2015) 1051–1069. https://doi.org/10.1515/pac-2014-1117.

[198] C.D.H.E. (UK); R.A.W.H. (FRG); L.M. (Netherlands); R.A.P. (USA); J.R. (France); T.S. (Poland) K. S. W. SING (UK, *Membership, REPORTING PHYSISORPTION DATA FOR GAS/SOLID SYSTEMS with Special Reference to the Determination of Surface Area and Porosity, 81 (1998) 420–430.

[199] Bio-Logic, EC-Lab Software: Techniques and Applications, (2009) 1–175.

[200] F.-B. Wu, B. Yang, J.-L. Ye, eds., Chapter 2 - Technologies of energy storage systems, in: Grid-Scale Energy Storage Systems and Applications, Academic Press, 2019: pp.

17–56. https://doi.org/https://doi.org/10.1016/B978-0-12-815292-8.00002-2.

[201] L. Zhou, W. Utetiwabo, R. Chen, W. Yang, Layer by Layer Assemble of Colloid Nanomaterial and Functional Multilayer Films for Energy Storage and Conversion, (2019).

[202] E.Z. Kurmaev, A. V. Galakhov, A. Moewes, S. Moehlecke, Y. Kopelevich, Interlayer conduction band states in graphite-sulfur composites, Physical Review B - Condensed Matter and Materials Physics. 66 (2002) 1–3. https://doi.org/10.1103/PhysRevB.66.193402.

[203] Q. Cheng, J. Tang, J. Ma, H. Zhang, N. Shinya, L.C. Qin, Graphene and nanostructured MnO2 composite electrodes for supercapacitors, Carbon. 49 (2011) 2917–2925. https://doi.org/10.1016/j.carbon.2011.02.068.

[204] T. Chen, Y. Tang, Y. Qiao, Z. Liu, W. Guo, J. Song, S. Mu, S. Yu, Y. Zhao, F. Gao, All-solid-state high performance asymmetric supercapacitors based on novel MnS nanocrystal and activated carbon materials, Scientific Reports. 6 (2016) 1–9. https://doi.org/10.1038/srep23289.

[205] X. Zhao, H. Wang, G. Zhai, G. Wang, Facile Assembly of 3D Porous Reduced Graphene Oxide/Ultrathin MnO 2 Nanosheets-S Aerogels as Efficient Polysulfide Adsorption Sites for High-Performance Lithium–Sulfur Batteries, Chemistry - A European Journal. 23 (2017) 7037–7045. https://doi.org/10.1002/chem.201604828.

[206] C.W. Jones, Applications of hydrogen peroxide and derivatives, Royal Society of Chemistry, 2007.

[207] T.T. Nguyen, V.H. Nguyen, R.K. Deivasigamani, D. Kharismadewi, Y. Iwai, J.J. Shim, Facile synthesis of cobalt oxide/reduced graphene oxide composites for electrochemical capacitor and sensor applications, Solid State Sciences. 53 (2016) 71–77. https://doi.org/10.1016/j.solidstatesciences.2016.01.006.

[208] C. A reduced graphene oxide/Co3O4 composite for supercapacitor electrodeXiang, M. Li, M. Zhi, A. Manivannan, N. Wu, A reduced graphene oxide/Co3O4 composite for supercapacitor electrode, Journal of Power Sources. 226 (2013) 65–70. https://doi.org/10.1016/j.jpowsour.2012.10.064.

CHAPTER 5

5.0 GENERAL CONCLUSION AND FUTURE WORK

This chapter presents the overall conclusion of the results and discussion of the previous chapters together with the suggestion for future work.

5.1 General conclusion

Graphene oxide, sulphur-reduced graphene oxide and graphene-based transition metal oxides composites were successfully synthesized using different methods. The micrographs, chemical composition, specific surface area/pore size distribution and structural properties of the materials were conducted by scanning electron microscope (SEM) linked with energy-dispersive X-ray spectroscopy (EDX), transmission electron microscopy (TEM), X-ray photoelectron spectroscopy (XPS), Brunauer-Emmett-Teller (BET), X-ray powdered diffraction (XRD), Fourie transform infrared (FTIR) spectroscopy and Raman spectroscopy. The electrochemical evaluation was done in three- and two-electrode configurations. The electrochemical performance of the synthesized RGO-S, RGO-S/100 mg MnO_2 and RGO-S/200 mg Co_3O_4 revealed major contribution of the materials for supercapacitor applications.

Graphene oxide (GO) and sulphur-reduced graphene oxide (RGO-S) were produced through a modified Hummer's method. GO displayed sheet like morphology while RGO-S display a morphology compromises of nanorods/fibers. The formation of nanorods/fibers morphology has shown an improvement in the electrochemical performance of RGO-S compared to RGO. The electrochemical evaluations were performed in 6 M KOH electrolyte. The specific capacity of 113.8 mAh g^{-1} was obtained for RGO-S at 0.5 A g^{-1} which is much higher compared to RGO with a specific capacity of 12.5 mAh g^{-1} at the same specific current. The fabricated hybrid device (RGO-S//C-FP) presented a high specific energy and specific power of 35.2 Wh kg^{-1} and 375 W kg^{-1} at 0.5 A g^{-1} in an working voltage of 1.5 V, respectively. A good cycling stability performance with an energy efficiency of 99% was recorded for the hybrid device for up to 10,000 cycling at 3 A g^{-1}.

Nanorods/fibers, nanosheet and nano-flower like morphology were successfully synthesized for RGO-S/MnO_2 composites with various mass loading of MnO_2 through an improved Hummer's method followed by freeze drying process, and hydrothermal method. An optimization was done by varying mass loading of MnO_2 (50, 100 and 150 mg) into the pristine sample (RGO-S). The electrochemical measurements were carried out in 2.5 M KNO_3 electrolyte. The superior electrochemical performance displayed by RGO-S/100 mg MnO_2 composite shows that the 100 mg MnO_2 can be considered as the precise composition to have good synergy between RGO-S and MnO_2. The RGO-S/100 mg MnO_2 composite presented a specific capacitance of 180. 4 F g^{-1} at 1 A g^{-1}, with good stability up to 2000 charge-discharge cycles for three electrode configurations. The assembled device (RGO-S/MnO_2//AC-PS) presented an outstanding specific energy of 71.74 Wh kg^{-1} with its corresponding specific power of 850 W kg^{-1} at 1 A g^{-1}. An incredible performance was recorded when the device was

able to withstand a specific energy of 55.30 Wh kg^{-1} at a high specific current of 5 A g^{-1}. The capacitance retention of 94.5 % and columbic efficiency of 99.6 % up to 10,000 cycles at 5 A g^{-1} was recorded. A voltage holding of up to 90 h was attained with an efficiency of 70.5 %. An exceptional self-discharge of about 1.45 V was recorded within the first 10 h, and 1.00 V after 72 h out of the initial potential of 1.7 V.

In additional, different metal oxide (Co_3O_4) which is stable because of its spinel structure and p-type semiconductor was introduced to improve the electrochemical properties of RGO-S. The mass loading (100, 200 and 300 mg) was carried out to determine the optimum composition of Co_3O_4 into RGO-S via hydrothermal method. The electrochemical evaluations were done in 1 M KOH electrolyte whereby RGO-S/200 mg Co_3O_4 revealed the best results indicating the optimal composition to have good synergy between RGO-S and Co_3O_4. An optimized RGO-S/200 mg Co_3O_4 composite material showed the uppermost specific capacity of 171.8 mAh g^{-1} at 1 A g^{-1} and an excellent stability of 99.7 % for over 5000 cycles at 5 A g^{-1} in three-electrode measurements. The constructed supercapattery device (RGO-S/200 mg Co_3O_4//AC-PS) demonstrated high specific energy of 45.8 Wh kg^{-1} and specific power of 725 W kg^{-1} at 1 A g^{-1} in an operating potential of 1.45 V. The fabricated device was capable to maintain 83.4 % of its initial capacitance for over 10,000 cycles, with a columbic efficiency of 99.5 % at 8 A g^{-1}. The device maintained an efficiency of 71.6 % over an outstanding floating time of 150 h at 10 A g^{-1}.

Capacitance/capacity retention, cycle stability, specific energy and specific power are the most essential parameters in evaluating the practical performance of supercapacitor. The following section provides a brief conclusion of the devices derived from the pristine and the composite

with different oxides (RGO-S//C-FP, RGO-S/100 mg MnO_2//AC-PS and RGO-S/200 mg Co_3O_4//AC-PS).

Figure 5.1 displays the capacity/capacitance retention of RGO-S//C-FP, RGO-S/100 mg MnO_2//AC-PS and RGO-S/200 mg Co_3O_4//AC-PS devices. It can be observed that RGO-S/100 mg MnO_2//AC-PS and RGO-S/200 mg Co_3O_4//AC-PS devices demonstrated an improved capacity/capacitance retention compared to RGO-S//C-FP. This could be due to the pseudocapacitive nature of the MnO_2 and Co_3O_4 materials and also as result of the synergy between RGO-S, 100 mg MnO_2 and 200 mg Co_3O_4 which were significantly reflected in the devices' performances.

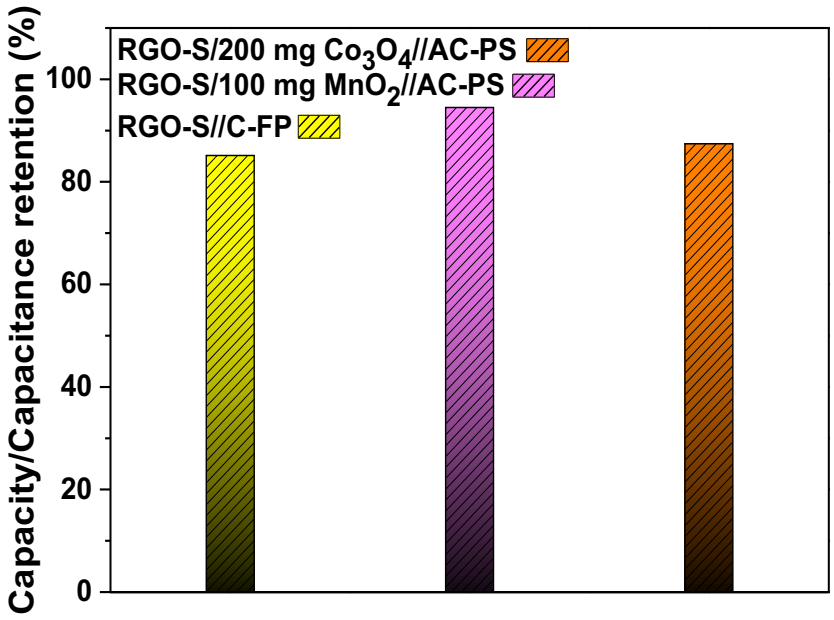

Figure 5.1: Capacity/capacitance retention of RGO-S//C-FP, RGO-S/100 mg MnO_2//AC-PS and RGO-S/200 mg Co_3O_4//AC-PS devices.

Figure 5.2 display a Ragone plot of RGO-S//C-FP, RGO-S/100 mg MnO_2//AC-PS and RGO-S/200 mg Co_3O_4//AC-PS devices. These results confirm that RGO-S/100 mg MnO_2//AC-PS and RGO-S/200 mg Co_3O_4//AC-PS hybrid device show higher specific energy and specific

power than RGO-S, in agreement with the capacity/capacitance retention revealed in Figure 5.1. This still demonstrates the good synergy between the optimized metal oxides with RGO-S to give such improved electrochemical properties. The better performance of RGO-S/100 mg MnO_2//AC-PS compared to RGO-S//C-FP and RGO-S/200 mg Co_3O_4//AC-PS hybrid devices could also be influenced by the use of neutral electrolyte (2.5 M KNO_3) which recognized to work in a wider voltage window of 1.7 V than alkaline electrolyte which is restricted by hydrogen evolution reaction (HER) and oxygen evolution reaction (OER).

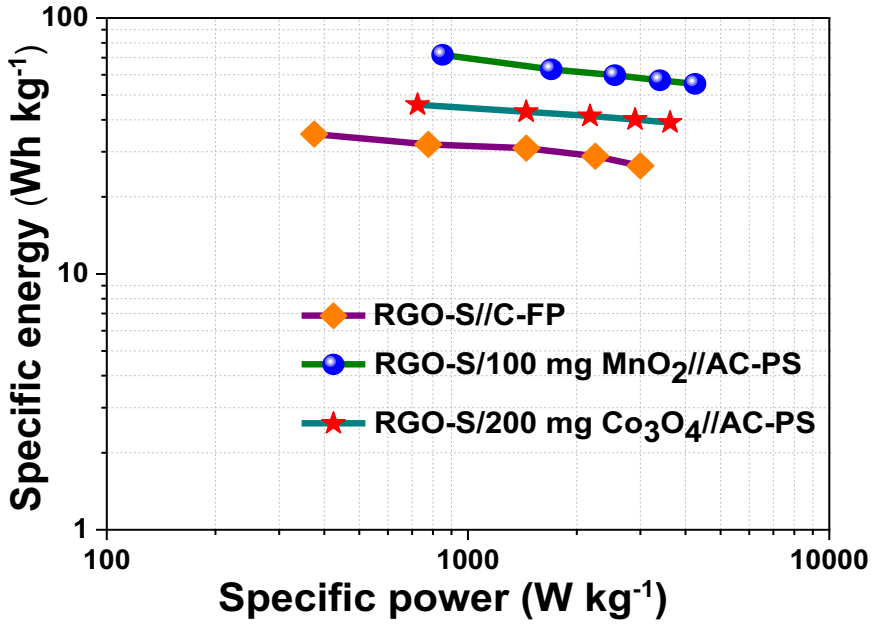

Figure 5.2: Ragone plot for RGO-S//C-FP, RGO-S/100 mg MnO_2//AC-PS and RGO-S/200 mg Co_3O_4//AC-PS devices.

In general, sulphur-reduced graphene oxide composite and graphene oxide-based transition metal oxides composites have demonstrated a significant potential as crucial materials for supercapacitor applications. Also, this research proved a significant addition to the energy storage through a supercapattery device fabricated by incorporating the advantages of supercapacitor and battery-type materials.

5.2 Future work

Each material in this study will undergo further evaluation by utilizing organic and ionic electrolytes. The advantage and disadvantage of different electrolytes will be assessed and compared for choosing the best electrolyte for supercapacitor and supercapattery applications. Also, all materials will be investigated as ex-situ and in-situ electrodes and Lithium-sulphur batteries electrodes. Additionally, the effect of temperature on both materials will be studied.